EFFECT OF PISTON BOWL GEOMETRY ON COMBUSTION AND EMISSIONS OF A DIRECT INJECTED DIESEL ENGINE

A thesis submitted for the degree of Doctor of Philosophy

by

Mark Robert Ellis

Department of Mechanical Engineering

Brunel University

Middlesex, England

October 1999

Brunel University
Department of Mechanical Engineering
Middlesex, England

Mark Robert Ellis
Effect of piston bowl geometry on combustion and emissions of a direct-injected diesel engine
October 1999, Ph.D.

Abstract

The effect of piston bowl geometry on the performance and exhaust emissions from a modern, high-speed direct-injection (HSDI) diesel engine was investigated. Four piston bowl geometry's (shapes) were designed, manufactured and tested in a pre-production HSDI diesel engine installed on an eddy-current dynamometer.

A series of experimental tests were performed to determine the optimum injector configuration for each piston bowl shape, the best bowl shape for minimum drive-cycle simulated emissions, and the effect of in-cylinder swirl ratio at various engine operating conditions. Results from computational fluid dynamics (CFD) combustion simulation of extreme injector configurations, correlated well with the experimental trends observed.

Full-load testing to determine the optimum injector configuration for each piston bowl shape, indicated that exhaust emissions were very sensitive to the point of fuel impingement on the piston bowl walls. In particular, the trend in the emission of particulates and NOx was explained in relation to the point of fuel impingement, and supported by CFD combustion simulation. The emission of smoke and particulates was found to be dependant on wall wetting and late combustion.

Key features for the successful design of future HSDI piston bowl shapes were identified, based on the results from piston bowl comparison tests at a selection of the European drive cycle simulation conditions.

The effect in-cylinder swirl ratio on engine performance and emissions was determined. An increase in the rate of mixing and heat release from higher swirl generally raised the emission of NOx, but reduced smoke formation at low engine speeds. Benefits of an increase in swirl on emissions was negated at high engine speeds due to throttling of the intake charge.

Acknowledgements

Brunel University provided the ideal environment in which to undertake combustion engine research. Many years of dedicated and focused work, closely linked with industry, have evolved the combustion engines group at Brunel University into the well resourced and staffed centre that it is today.

My special thanks are due to Professor Nicos Ladommatos, my 1st supervisor, for his support (both technical and moral) and conviction throughout the project. Thanks are also due to my second supervisor, Dr Hua Zhao for his support and opinion at numerous progress meetings.

In undertaking a predominately experimental research project, I have spent the majority of my time in the engine Laboratory. I would like to express my sincere thanks to Mr Andy Selway, the chief engine technician for his help throughout engine testing, maintenance and rebuilding. I am also indebted to Andy, and Mr Peter Tarrent for taking the time to develop my machining skills. My thanks are also due to Mr Bob Webb and Mr John Langdon, for their help with commissioning and development of the test cell, and Mr John Williams, for his help with my computing systems.

Last but not least, I would like to thank the Ford motor company for their technical and financial support. In particular, my sincere thanks are due to Mr Roy Horrocks and Mr Mike Watts for their technical input and overall project direction, and Dr Evangelos Karvounis for his CFD input which made this project complete.

Nomenclature

General notation

α_d	power correction factor
λ	air/fuel ratio
θ	equivalence ratio
ρ	density
ω	angular velocity
Ω_s	spray divergence angle
a	radius from the piston centre-line to bowl lip
A_c	cross-sectional area of cylinder
A_n	nozzle area
B	cylinder bore
C_D	discharge coefficient
D	maximum bowl diameter, differentiating component
f_a	atmospheric factor
f_m	characteristic parameter for each engine type
I	integrating component
k	turbulent wave number
L_i	Integral scale of turbulence
L_k	Kolmogorov scale of turbulence
L_m	Taylor microscale of turbulence
m	mode test
$\dot{m}$	mass flow rate
$\dot{m}$, Q_f	fuel mass flow rate
M	dynamometer torque, moment of momentum
N_e, n,	engine speed
n_t	frequency of turbulent fluctuation
p	pressure ratio across nozzle
P	cylinder pressure, gain component, engine power
P_b	combustion bomb pressure
P_0	overall particulate emission

S_p	instantaneous piston speed
t	time
t_i	integral timescale
t_k	Taylor timescale
t_m	Kolmogorov timescale
T	temperature, torque
u, u'	turbulent velocity fluctuation
$\overline{U}$	mean velocity
$\hat{U}$	cycle-by-cycle variation in mean velocity
V	cylinder volume, valve
V_B	volume of piston bowl
$\overline{V}_p$	mean piston speed
w_m	mode weight
W	sum of relative weights
Z	distance between piston crown top and cylinder head

Abbreviations

ABDC	after bottom dead centre
AFR	air/fuel ratio
ATDC	after top dead centre
BBDC	before bottom dead centre
BDC	bottom dead centre
BMEP	brake mean effective pressure
BSFC	brake specific fuel consumption
BSN, BSU,	Bosch smoke number
BTDC	before top dead centre
CA	crank angle
CAD	computer aided design
CAM	computer aided manufacture

cc, cm^3	centimetre cubed (= mm^3 x 10^3)
CCT	circuit
CFD	computational fluid dynamics
CNC	computer numerically controlled
CR	compression ratio
deg	degrees
DI	direct injection
DRG	drawing
ECE	European urban drive cycle
ECU	electronic control unit
EEC	European economic community
EGR	exhaust gas re-circulation
EOI	end of injection
EPROM	eraseable, programmable, read only memory
EUDC	extra urban drive cycle
FID	flame ionisation detection
FIE	fuel injection equipment
FIP	fuel injection pump
FM	frequency modulated
HMMS	Hino micro mixing system
HWA	hot wire anemometry
HSDI	high-speed direct injection
IDI	indirect injection
INCA	integrated calibration and application tools
LDA	laser doppler anemometry
LDV	laser doppler velocimetry
LH	left-hand

MAX	maximum
MIN	minimum
MVEG	combined ECE & EUDC drive cycle test
NA	normally aspirated
NTS	not to scale
ppm	parts per million
PC	personal computer
PCU	pump control unit
PID	proportional, integral, differential control
PIV	particle image velocimetry
R	radius
RH	right-hand
SFC	specific fuel consumption
SOI / IT	start of injection / injection timing
STD	standard
STP	standard temperature and pressure
TC	turbo-charged
TCI	turbo-charged and intercooled
TDC	top dead centre

Chemical symbols

C	carbon atom
CO	carbon monoxide
CO_2	carbon dioxide
H	hydrogen atom
H_2O	water
HC	hydrocarbon
N	nitrogen atom

N_2	nitrogen molecule
NO	nitric oxide
NO_2	nitrogen dioxide
NOx	oxides of nitrogen (NO and NO_2)
O	oxygen atom
O_2	oxygen molecule
OH	hydroxide radical
PM	particulate matter
SO_2	sulphur dioxide
SO_3	sulphur trioxide
SO_4	sulphuric acid
UHC	un-burnt hydrocarbons

Contents

Chapter 1:

Introduction

Chapter 1: Introduction

1.1 Overview of project

This project investigates the effect of piston bowl shape, on modern high-speed direct-injection (HSDI) diesel engine combustion and emissions. The project was initiated in response to demand from the Ford motor company, for an increase in the fundamental understanding of this area of engine design. Future tightening of legislated exhaust emissions, and an increasingly shorter design and gestation period for each new engine upgrade, require a more fundamental approach to engine design, rather than testing numerous variations.

The project was mainly experimental, supported by CFD combustion simulation. Testing was performed on a prototype, HSDI diesel engine designed for application to passenger car sized vehicles. A dedicated test cell at Brunel University, containing a fully electronic, eddy-current dynamometer was used for engine testing. Four different design piston bowl shapes were tested, sharing the same bowl volume but significant dimensional variations. CFD combustion simulation was performed using the KIVA-2 simulation code, at Ford in Aachen, Germany, with participation by the author, and with further analysis and post processing by the author at Brunel University. Experimental and CFD results showed good correlation, and allowed significant advances in the understanding of the effect of piston bowl shape on combustion and emissions to be made.

1.2 Philosophy of work and research method

It was decided from initiation of the project that a complete and systematic parametric study of piston bowl parameters was not feasible within the time-scale and resources available. The methodology adopted was one of learning from each piston bowl shape tested, and implementing the knowledge gained in the subsequent bowl design, with a view to a further reduction in exhaust emissions.

Following optimisation and testing of each new piston bowl shape, the results were analysed, and conclusions drawn from the understanding gained of the effect of piston bowl shape. The next piston bowl shape was then designed using AutoCAD, and produced from blank pistons using a CNC lathe. Following piston installation and run-in, the process of piston bowl testing and analysis was then repeated.

The performance of each piston bowl shape was assessed by its quantity of exhaust emissions, at various test conditions. Test conditions were primarily chosen from the 14-mode drive cycle simulation, designed to replicate vehicle engine speed and load requirements through a typical range of driving conditions. Particular emphasis was placed on the emission of particulates and NOx, as a good assessment of the overall piston bowl performance, and tolerance to EGR. Reducing the overall value of the particulates verses NOx trade-off was fundamental to successful piston bowl design. However, the introduction of particulate traps or de-NOx catalysts may change the desired operating characteristics of a given piston bowl shape in the future.

1.3 Objectives of project

The objectives of the project were to:

(i) improve the fundamental understanding of the effect of piston bowl geometry on HSDI diesel engine combustion, exhaust emissions, and other performance parameters,

(ii) design, manufacture, and test a number of bowl geometry's, which would improve exhaust emissions and fuel economy of a pre-production HSDI diesel engine,

(iii) determine the effect of the position of the fuel injector in the combustion chamber (and thus the point of fuel impingement on the bowl walls) on HSDI performance and emissions,

(iv) apply CFD analysis in order to gain further insights into the effects of bowl geometry on in-cylinder airflow, air/fuel mixture distribution and soot formation,

(v) relate CFD results with the experimental test results,

(vi) examine the effect of a variation in the intake-generated air-swirl, and in-bowl swirl ratio, on combustion and exhaust emissions.

1.4 Outline of thesis

Following this introduction, chapter two describes the literature review, which was performed prior to, and during the project duration. The literature review is broadly split into three main sections; the first describes an overview of HSDI diesel engine combustion, based on the different stages of heat release; the second section details airflow and fuel impingement within the piston bowl; and the last section gives an overview of the formation of exhaust emissions and legislative control.

Chapter three describes the experimental test facility and prototype engine used for testing of different piston bowl shapes. Operation of the engine dynamometer was discussed, as well as the engine fluid systems, instrumentation and data acquisition, and an overview of the method of operation of the exhaust emissions measuring equipment.

Piston bowl design and development is the subject of chapter four. Critical parameters which were thought to be most influential in the design of the bowl shape are described. The four different bowl designs are presented in this chapter, and an overview of the bowl development progress is given. Practical aspects of piston machining, bowl volume checking, and installation are also described. Manufacturing drawings for each piston bowl shape are presented in a later appendix.

Chapter five details the results and discussion from injector optimisation tests. These tests were required to optimise the fuel spray origin, and cone angle, within the combustion chamber for each new piston bowl shape. Results and discussion are

presented from each piston bowl shape in chronological order. A separate section is included that discusses the effect of the point of fuel impingement on combustion and emissions, from which some of the most important findings of this work were identified.

CFD simulation of in-cylinder combustion is presented in chapter six. Special emphasis is placed on the effect of the point of impingement on the emission of smoke from piston bowl shape TWO. This bowl had been identified as particularly sensitive to impingement point, from injector optimisation in the previous chapter. Close correlation between the results of CFD combustion simulation, and the experimental results of injector optimisation from chapter five were observed.

Chapter seven compares results from overall piston bowl comparison testing. Results from the seven selected EGR-loop test conditions are discussed separately, enabling direct comparison between each piston bowl shape at a particular test condition. Overall bowl comparison is made possible by calculating a weighted sum of particulates and NOx emissions from each test condition, corresponding to the relative importance of that test condition to the total drive cycle emissions.

An investigation into the variation of the effect of swirl on combustion and emissions is presented in chapter eight. Two different bowl designs having different in-bowl swirl levels were compared at various test conditions taken from the drive cycle test, with and without EGR.

Conclusions and recommendations from each set of results are summarised in chapter nine. The main areas of progress made in the understanding of the effect of piston bowl shape on combustion and emissions are stated here. A more detailed set of conclusions is included at the end of each chapter.

1.5 Benefits of project and contribution to knowledge

This project has provided substantial insights into the effect of piston bowl shape on combustion and emissions from a modern HSDI diesel engine. In particular, a clear link between fuel impingement on the sides of the piston bowl walls, and emissions of particulates and smoke was established. When combined with the results from CFD combustion simulation, the most likely reasons for the trends in emissions observed were determined.

The effect of a number of different piston bowl shapes on the overall exhaust emission performance was determined. Unlike previous piston bowl shape studies, this work focused on reducing drive cycle test emissions. Differences between bowl design requirements for good full-load performance, and minimum drive cycle emissions were evident.

The study of how in-cylinder swirl affects combustion and emissions performance identified benefits from increased swirl at low engine speed. However, it also showed that higher swirl could be detrimental at high engine speed, because of a trade-off with engine volumetric efficiency. Testing with different piston bowl designs has also identified the need to re-optimise swirl for optimum performance for different bowl shapes having different aspect ratios.

Chapter 2:

Literature review

Chapter 2: Literature review

2.1 Introduction

Diesel combustion is inherently complex. Fuel injection into hot, moving air creates a highly non-uniform, three-dimensional fuel distribution, which is modified by combustion chamber boundaries. Injected fuel must mix with the intake air and combust within a few milliseconds. Not only must the engine produce the required torque and power, and at low cost to compete in the commercial market, but environmental pressures mean its exhaust must be cleaner than ever.

This chapter reviews the current level of understanding of the effect of piston bowl shape and airflow, on high-speed direct-injection (HSDI) diesel engine combustion and emissions. Firstly, an insight into the complexities of HSDI diesel engine combustion is given. The rate of heat release is used as a basis for discussion of the different stages of combustion.

The main section of this chapter considers in detail the effect of piston bowl shape and airflow (which is largely controlled by bowl shape) on diesel combustion and emissions. Swirl, squish, turbulence and fuel impingement on the bowl walls are discussed as the main parameters affecting diesel combustion. Particular emphasis is given to their relation with piston bowl shape.

Finally, a review of the mechanisms and formation of the main exhaust emissions which affect diesel engine design are given. The influence of engine design and operating conditions on emissions is discussed, and a summary of past, present and future emission legislation is given. Special consideration is given to the trade-off between the emission of particulates and NOx, as it is one of the major challenges facing diesel engineers of today.

2.2 Direct-injection (DI) diesel combustion

Diesel combustion can be considered as several distinct phases during the heat release process. Heat release 'drives' cylinder pressure changes. A clear understanding of the phases of heat release is essential for successful diesel engine combustion analysis.

2.2.1 Heat release

The rate of heat release is defined as the rate at which heat is released during the combustion process, predominately by releasing chemical energy of the burning fuel. Heat release can be calculated from engine data by predicting (using the 1st law of thermodynamics) how much heat would have to be added to the working fluid to produce a given cylinder pressure change, taking into account changes in the combustion chamber volume. Heat release can also be predicted using engine modelling techniques. When heat release rate is calculated from measured cylinder pressure, it is termed the 'net heat release rate'. This is because it includes heat transfer to the cylinder walls, and other losses which are inherent in the cylinder pressure data (typically 10-25% of the available chemical fuel energy is lost to the cylinder walls [Heywood, 1988]). The net heat release rate is given by equation 2.1 below.

Net heat release rate = gross heat release rate – heat transfer to the walls
= rate at which work is done on piston + change of sensible internal energy of the working fluid

Equation 2.1 Calculation of the net heat release rate [Heywood, 1988].

Piston bowl design can affect the rate of heat release, and the different phases of heat release in many ways. It affects the shape and magnitude of the heat release rate profile, by affecting bulk airflow and turbulence, thus affecting air/fuel mixing rates. Effective control and manipulation of the heat release rate is important to limit peak

cylinder pressure, combustion noise, and emissions, whilst increasing or maintaining efficiency. Figure 2.1 shows the different phases of heat release, starting from mid-compression stroke [Heywood, 1988].

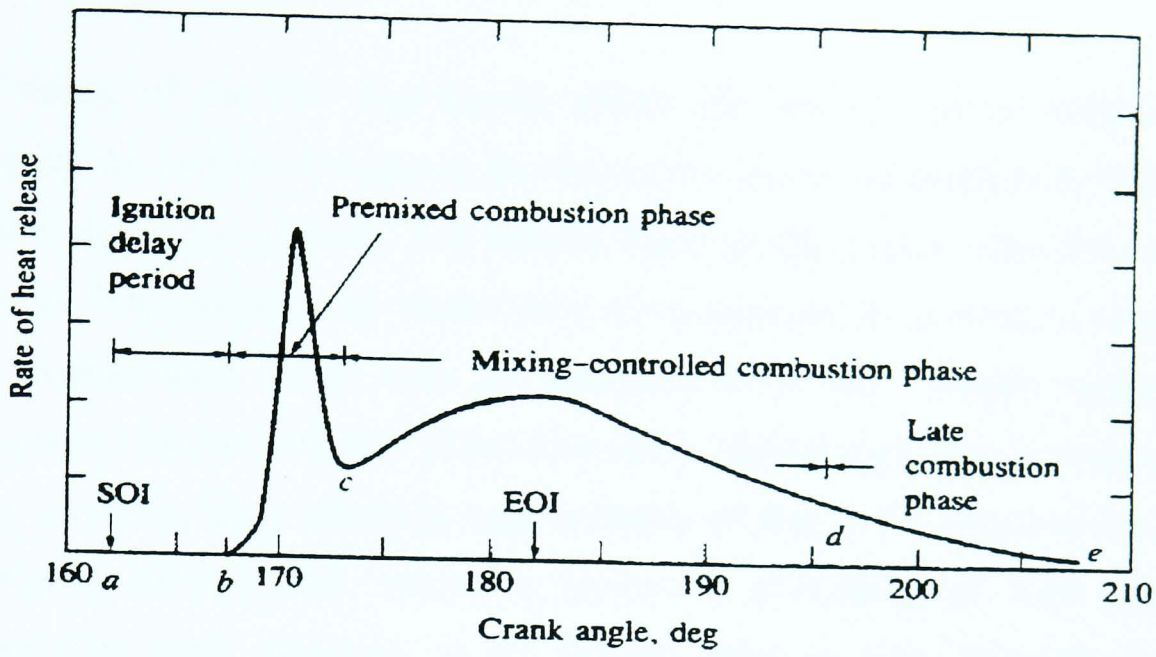

KEY: (a) Start of injection (SOI), (a-b) Delay period, (b-c) Pre-mixed combustion, (c-d) Diffusion burning, (d-e) Late heat release

Figure 2.1 Rate of heat release as a function of crank angle, for typical DI diesel combustion from late compression to late expansion [Heywood, 1988]. Letters on the lower axis indicate key stages in the combustion process.

2.2.2 Start Of Injection (SOI)

At a predetermined crank-angle (CA), at the end of the compression stroke (around TDC), high pressure fuel is injected into the combustion chamber. The duration of fuel injection is proportional to the engine load required. The fuel injector needle has inertia, and the pressure force on the needle must overcome the spring seating loads to open. The fuel injection pressure at nozzle exit ramps up as needle lift increases, during the finite time it takes for the fuel injector to open. Early injected fuel leaving the nozzle is at a lower pressure than the main injection event; thus, early injected fuel will be poorly prepared for combustion, exiting as large droplets with little velocity to aid mixing. Some injectors increase the rate of nozzle opening by using two springs of different spring rates mounted in series. Unit injectors and common rail fuel systems

also reduce the rise time of injected fuel pressure, and allow more control over the start of injection. Common rail fuel injection systems may allow the introduction of pilot and post fuel injection, to reduce emissions and noise on production high-speed DI diesel engines [Abe et al, 1994; Minami et al, 1995].

The timing of the SOI significantly affects the rate of cylinder pressure rise, by changing the cylinder volume at the time of pre-mixed combustion, and affecting the ignition delay period itself. The shortest delay period occurs when the delay period includes TDC (because the temperature of compressed air is close to its maximum). The longest delay occurs with late injection, when both cylinder temperature and pressure are lowest. The rate of pressure rise is highest with early injection, when the delay period is long, allowing large amounts of fuel to be prepared for pre-mixed combustion, and cylinder volume at ignition is at a minimum. Late injection also creates high peak pressures, as the ignition delay is long, although the effect is reduced by increased cylinder volume [Taylor, 1968].

2.2.3 Ignition delay period

Fuel injected into the cylinder does not combust instantaneously, even though the temperature and pressure of air into which fuel is injected will be above that required for self-ignition. The time period between the start of fuel injection (usually defined as the start of injector needle lift, or a small fraction of the total needle lift), and combustion (usually defined as when the rate of heat release becomes positive or the first luminous flame [Ladommatos et al, 1994]), is called the delay period.

At the end of the compression stroke, and during the delay period, a small amount of heat is transferred from the hot compressed air to the cylinder walls, cylinder head, piston and other combustion chamber surfaces. Further heat transfer from the working fluid (compressed air) occurs, to heat and evaporate the injected fuel prior to ignition. These two effects result in the initial heat release rate being negative, as heat is given up by the working fluid.

The delay period changes considerably with air temperature, but is only slightly affected by the air pressure [Taylor, 1968; Wang et al, 1995]. Figure 2.2 below, shows the variation of ignition delay period with air pressure and temperature. The results have been obtained by experiments performed in a constant volume bomb, using a fuel with a low cetane number and, hence, poor ignition quality, so as to highlight the ignition delay period.

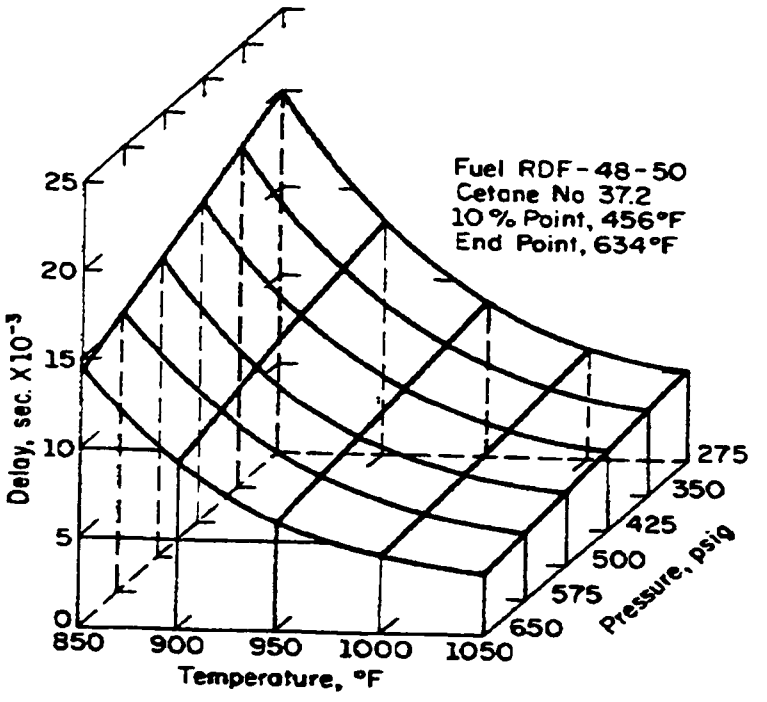

Figure 2.2 Ignition delay period shown as a function of air temperature and pressure prior to fuel injection. Results have been obtained with a fuel of low cetane number in a constant volume bomb, to simulate in-cylinder conditions at engine TDC [Taylor, 1968].

Turbocharging of DI diesel engines produces high air temperatures and increased pressure at the end of compression. This significantly reduces combustion noise, as less fuel is prepared for pre-mixed combustion during the shorter delay period.

In small high-speed DI diesel engines, injected fuel will impinge on the walls of the piston bowl. As temperature is the most significant factor affecting ignition delay, the temperature of the wall upon which fuel impinges will affect the ignition delay period. Increasing wall temperature reduces the ignition delay period [Werlberger and Cartellieri, 1987].

Unlike diffusion burning, which is mixing controlled and thus independent of speed on a crank-angle basis, ignition delay period is controlled primarily by chemical reactions (preliminary reactions in the ignitable mixture and self-ignition) and not mixing (atomisation and vaporisation). Mixing is not a significant factor affecting the delay period in modern, well mixed systems, as it is the local air-fuel ratio which affects self-ignition, and not the amount of fuel mixed within combustible limits (although this will affect the subsequent peak heat release rate from pre-mixed combustion). Ignition delay does not scale with engine speed, resulting in an increase in duration on a crank angle basis, with increasing engine speed.

2.2.4 Pre-mixed combustion

Fuel prepared to within combustible limits during the delay period, burns in a pre-mixed combustion mode. Early ignition sites within the cylinder compress the remaining mixture already prepared to within combustible limits, raising its temperature and promoting more rapid combustion.

Fuel prepared for combustion during the ignition delay period causes a very high initial heat release rate spike. This is caused by significant quantities of fuel burning in a pre-mixed condition, at high temperature and from multiple ignition sites. The magnitude of heat release depends on the amount of fuel prepared for pre-mixed combustion before ignition, and thus on the delay period, fuel injection characteristics and air-flow. Piston bowl shape affects the airflow and turbulence level, and, thereby, changes the amount of fuel prepared for pre-mixed combustion [Rao et al, 1992].

The heat release spike caused by pre-mixed combustion is not desirable. It creates high peak cylinder pressures, requiring increased cylinder strength, and contributes significantly to diesel combustion noise and knock. Emissions of NOx also increase, because of the high peak local temperatures. Modern high-speed DI diesel engines aim to reduce the magnitude of pre-mixed combustion heat release, by reducing the amount fuel prepared during the delay period, and by reducing the duration of the delay period.

2.2.5 Diffusion burning

The bulk of the heat released during DI diesel combustion occurs during the diffusion burning phase. A second heat release rate peak occurs during this phase, its magnitude being dependant on engine load, and boost pressure if turbocharged. In fact, in modern high-speed DI diesel engines that are turbocharged, the conventional description of combustion phases is less distinct than implied here. At full load, air density and temperature at the end of compression are high. This reduces the ignition delay period, and the amount of fuel prepared for pre-mixed combustion is small.

Upon combustion, the high temperature and density of charge air, coupled with vigorous in-cylinder motion, cause the rate of diffusion burning to be very rapid. The result is that separate pre-mixed and diffusion burning phases are not obvious; rather, a smooth rapid heat release from the start of combustion to the end of the diffusion process exists. This more closely approximates the ideal, limited-pressure fuel-air cycle for the diesel engine, shown in figure 2.3.

For ideal cycle approximation, the pressure rise during the period corresponding to constant volume combustion should be as rapid as possible, up to a limiting value. Subsequent injected fuel should be burned at a rate necessary to sustain the cylinder pressure constant throughout the expansion stroke, or until all the fuel is burned.

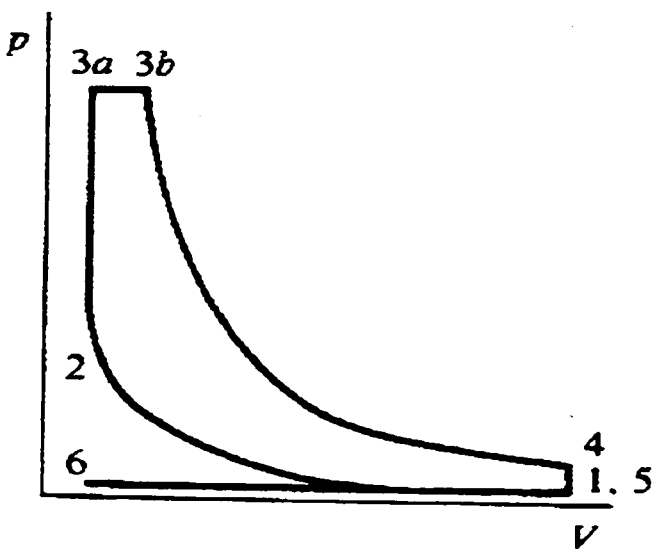

Figure 2.3 Ideal cycle for limited-pressure combustion. This cycle is the most applicable to practical diesel combustion.

1-2 corresponds to compression of air. Stage 2-3a corresponds to pre-mixed burning, up to the limiting cylinder pressure. Subsequent diffusion burning, until the desired quantity of fuel has been burnt, is represented by the line 3a-3b. Expansion along 3b-4 completes the expansion stroke in this ideal cycle [Heywood, 1988].

The rate of heat release during diffusion burning is predominately mixing controlled. This is because the characteristic times for turbulent fuel jet mixing (comparable to burning times) are much longer than the characteristic times for evaporation and combustion kinetics [Kuo et al, 1983; Plee and Ahmad, 1983]. The rate of heat release during diffusion burning is essentially proportional to engine speed, because mixing rate also scales with engine speed. Combustion at full load, typically, occupies a crank angle of 40 degrees. By the end of the diffusion burning process, approximately 80% of the injected fuel energy for that cycle will have been released.

2.2.6 Late heat release

The last distinct phase of heat release consists of a small but steady 'tail' which continues well into the expansion stroke. It accounts for around 20% of the injected fuel heat release [Heywood, 1988]. Combustion late in the expansion stroke will be much cooler and less vigorous, because the air motion, availability of oxygen, and mixing rates are all reduced. Late combustion significantly affects engine-out smoke emissions, and to a lesser extent emission of unburned HC. Late combustion is the main factor that determines the minimum air/fuel ratio (maximum engine load) in production engines, due to the production of smoke. All modern passenger car diesel engines are 'smoke limited' in torque production.

2.3 Piston bowl shape and airflow: effect of swirl

2.3.1 Description and definition of swirl

Swirl is the ordered rotation of air about the cylinder axis, and is the most important air motion in high-speed DI diesel engines. It is created by introducing the intake air into the cylinder with an initial swirling motion, or angular momentum. For comparison between different engine designs, a swirl ratio is defined as [Stone, 1992]:

$$\text{Swirl ratio} = \text{swirl speed (rpm)} / \text{engine speed (rpm)}$$

Equation 2.2 Definition of in-cylinder swirl ratio [Stone, 1992]

Alternatively 'swirl density ratio' (swirl ratio x density at any CA / density at STP) can be used as it is believed to be more important in fuel-air mixing situations [Khan et al, 1972].

It is the geometry of bowl–in–piston combustion chambers that governs the extent to which induction-generated swirl velocity is amplified and modified during the compression and combustion strokes.

2.3.2 Benefits of in-cylinder swirl

Swirl is used to promote more rapid mixing between the inducted charge air and fuel injected at the end of the compression stroke. Fuel/air mixing is predominantly governed by the fuel injection characteristics and air-swirl. Rapid mixing is essential, because small DI diesel engines operating at high speed have a very short 'time-window' over which combustion must occur. This is necessary in order to limit formation of soot late in the expansion phase, and to minimize BSFC.

2.3.3 Trade-offs in swirl production

There exist two main trade-offs, which tend to limit the amount of swirl that is desirable in practice for rapid combustion:

(1) Design changes necessary to introduce the intake air with an initial angular momentum, also tend to reduce engine volumetric efficiency. Although methods of inducing swirl vary, there is a balance between generating swirl necessary for rapid combustion and the reduction in BMEP and BSFC, resulting from a lower volumetric efficiency [Stone, 1992].

(2) Increasing swirl increases the convective heat transfer from the working fluid to the cylinder walls. This manifests itself as a reduction in exhaust gas temperature (particularly important for turbo-charged engines), and an increase in heat transfer to the coolant, reducing BSFC [Stone, 1992]. Ricardo and Hempson (1968), showed clearly (see figure 2.4) the loss of efficiency due to reduction in volumetric efficiency, and increased heat transfer at high swirl levels.

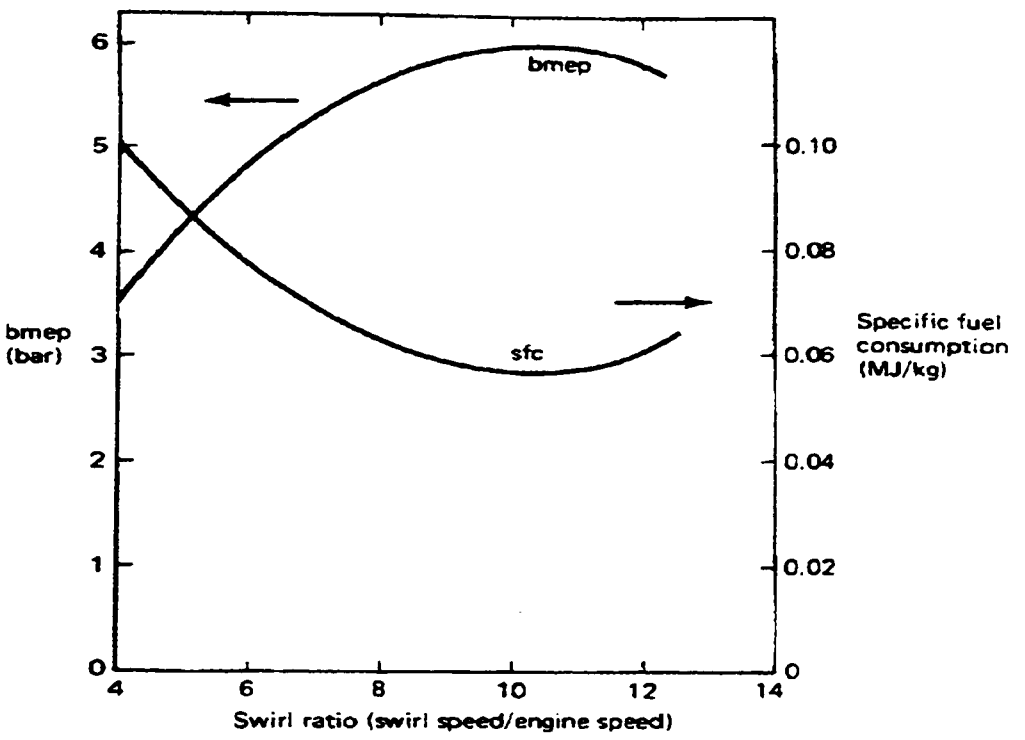

Figure 2.4 Effect of an increase of swirl ratio on BMEP and SFC, from a DI diesel engine [adapted from Ricardo and Hempson, 1968, by Stone, 1992].

2.3.4 Methods of swirl production

There are many methods of swirl generation. The most common method uses a helical port shape in which the intake air is forced to rotate about the intake-valve stem axis, prior to entering the cylinder during the intake stroke. A typical example is shown in figure 2.5, of a two valve per cylinder DI diesel engine.

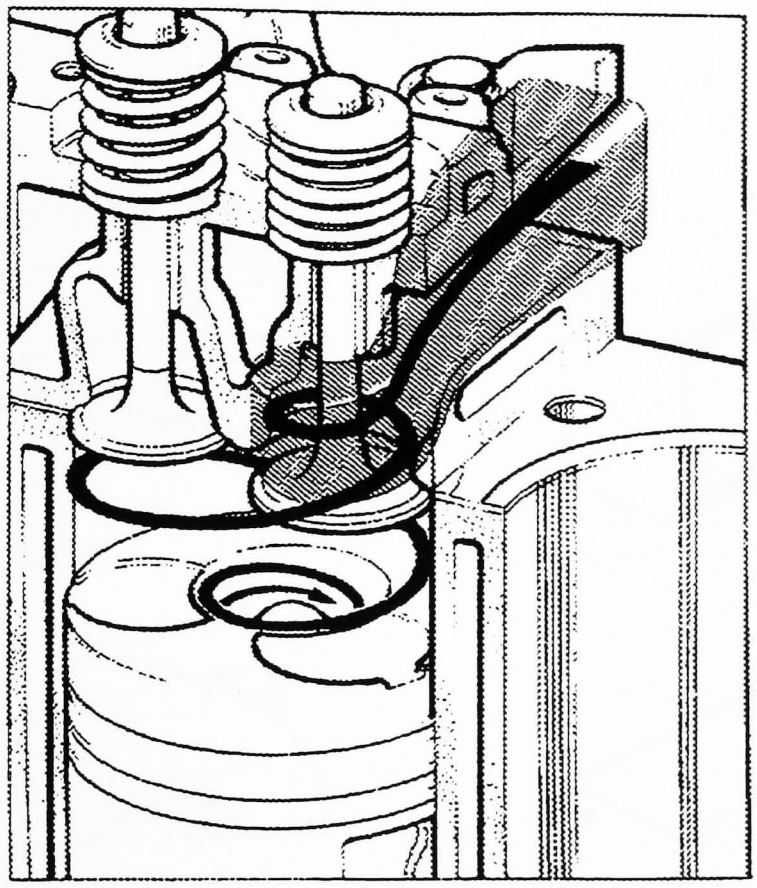

Figure 2.5 Swirl generation using a helical port design in the Ford 2.5ltr DI Diesel engine [Stone, 1992].

Helical ports offer the best compromise between swirl generation and a high flow coefficient, as no part of the valve opening area is shrouded to induce swirl (maintaining good volumetric efficiency) [Heywood, 1988]. Other methods include directed ports, where the intake flow discharges into the cylinder tangentially toward the cylinder wall. However, this suffers from highly non-uniform flow around the periphery of the valve giving poor discharge coefficients, and sensitivity to sand core position during manufacture.

Masked/shrouded valves (where part of the periphery of the intake valve is covered), can also be used to generate swirl. Although used as a research swirl tool, masked/shrouded valves are not a practical solution for production engines, because of high cost and weight, reduced volumetric efficiency, and the need to prevent valve rotation [Heywood, 1988].

Some examples of swirl producing port and valve designs are shown below in figures 2.6 a, b, c, d and figure 2.7.

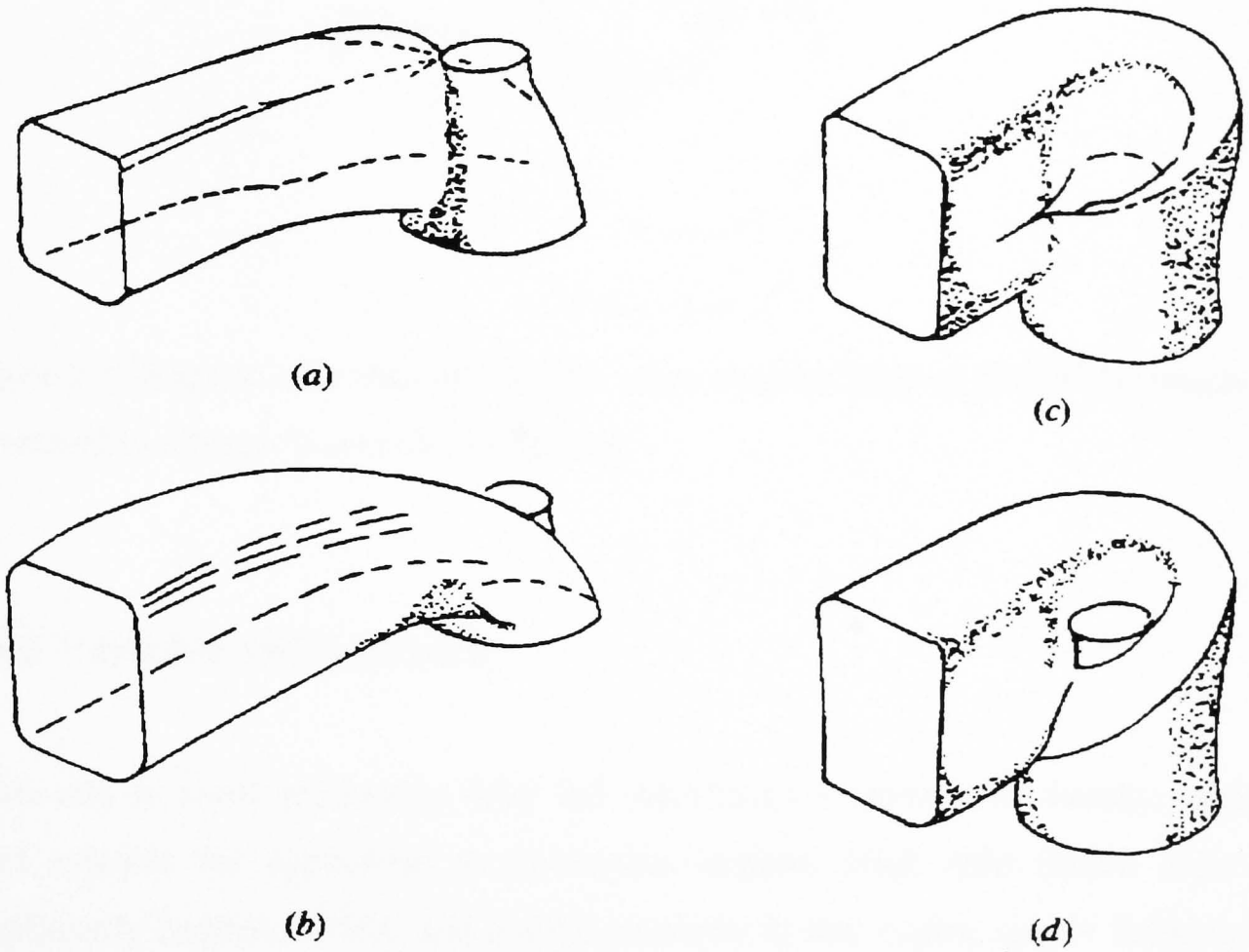

Figure 2.6 Different designs of swirl-generating port include (a) deflector wall; (b) directed; (c) shallow ramp helical; (d) steep ramp helical [Heywood, 1988].

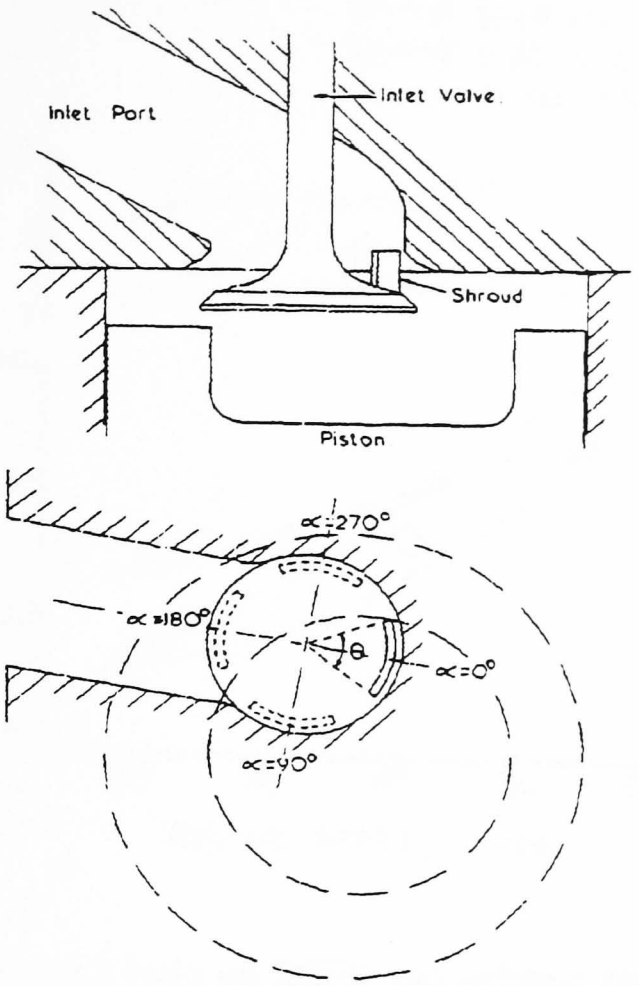

Figure 2.7 Diagram of a shrouded intake valve used by Khan et al (1972), which can be rotated to change in-cylinder swirl level.

2.3.5 Variable swirl systems

Trade-offs in swirl production have led researchers to attempt to develop variable swirl systems for application to production engines. High swirl intake ports can significantly improve BSFC and smoke emission at low engine speeds (although at the expense of increased NOx emission), but at high engine speeds low swirl is desirable to maintain the inlet air flow coefficient and reduce BSFC and Smoke emission. Hino Motors development of a light duty DI diesel engine illustrates the difficulty of finding an optimum swirl ratio for all engine conditions (see figure 2.8).

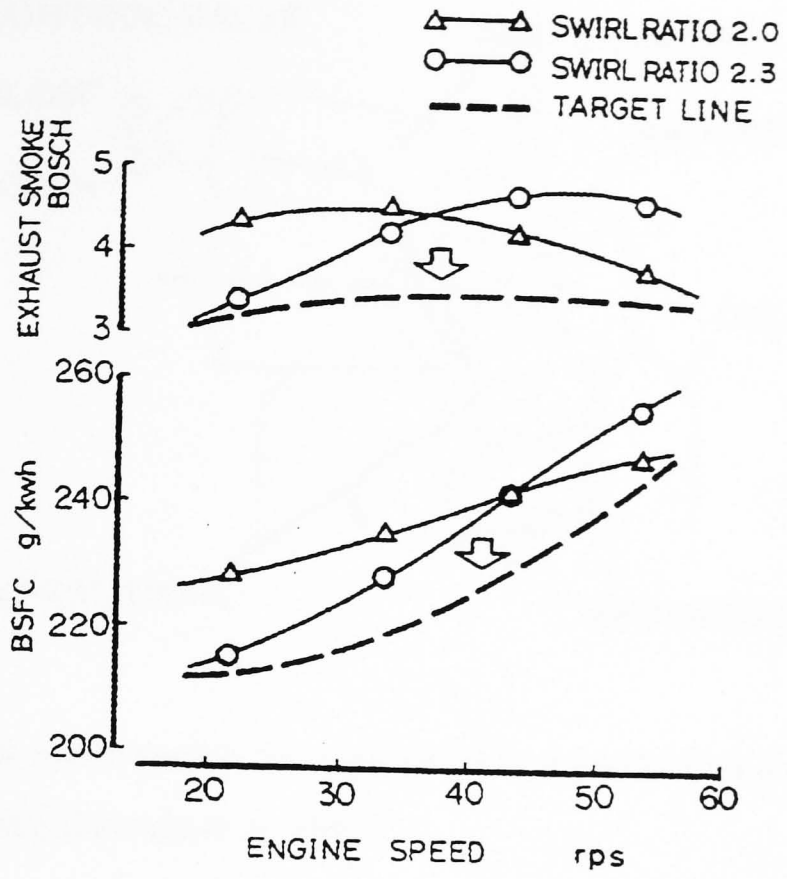

Figure 2.8 The effect of swirl ratio on BSFC and exhaust smoke at various engine speeds [Shigemori et al, 1983].

Figure 2.8 shows experimentation by Shigemori et al (1983), illustrating that a different swirl ratio is desirable at different engine speeds and full-load. Development of a variable swirl system would allow engine operation nearer the target line.

Mitsubishi Motors Corporation [Shimada et al, 1986] developed a variable swirl intake system typical of the industry solution to this problem. They determined that the resultant swirl in the cylinder was dependent on the sum of the positive swirl and reverse swirl, produced by a classical helical port design (see figure 2.9). By introducing a second supplementary port to produce reverse swirl, the resultant in-cylinder swirl ratio could be controlled. Figure 2.10 shows an engine map of optimum swirl, depending on engine speed and load, which was developed by Shimada et al (1986), to achieve up to a 15% torque increase at low engine speeds and improved BSFC.

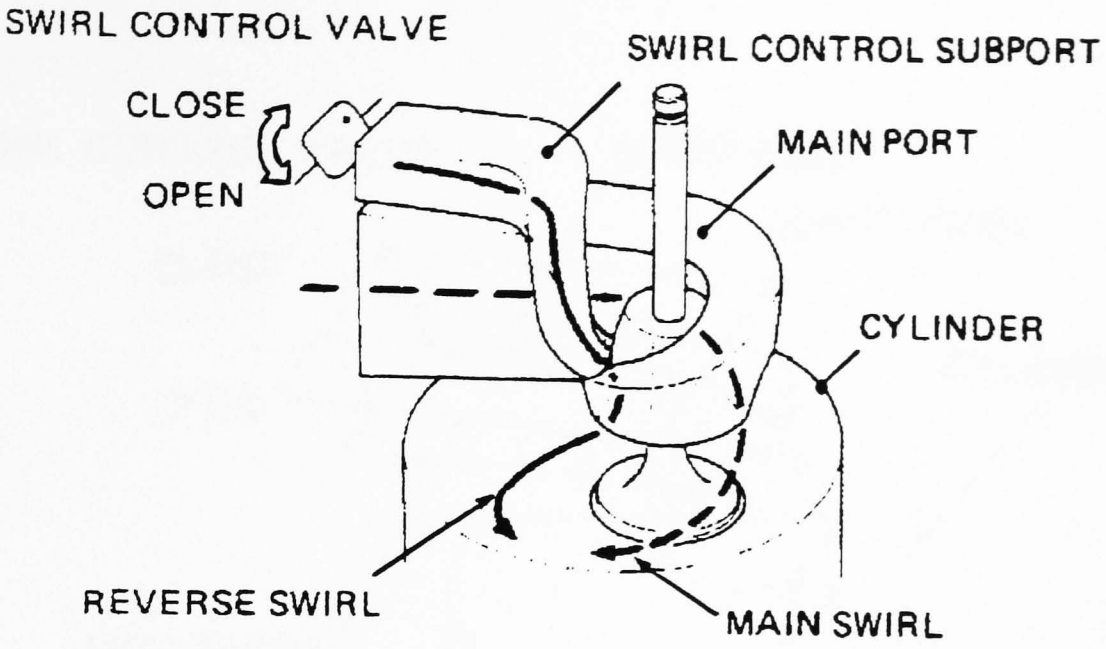

Figure 2.9 Variable swirl system for application to a production engine by Mitsubishi Motors Corporation [Shimada et al, 1986].

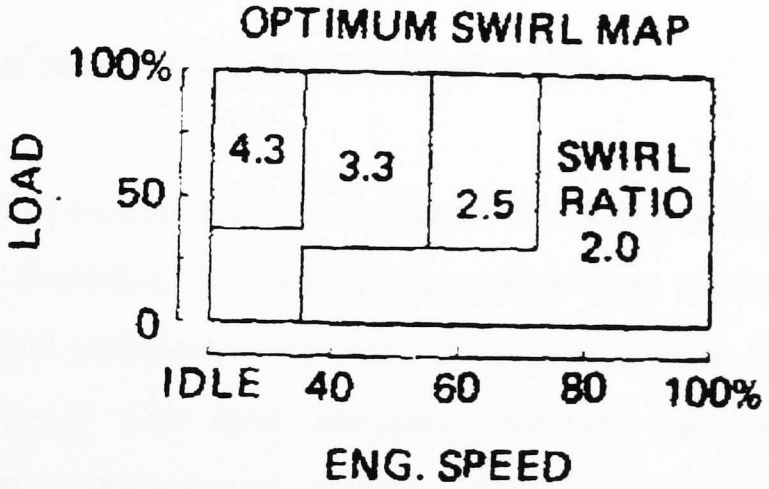

Figure 2.10 Optimum swirl ratio map at various speed/load combinations [Shimada et al, 1986].

Another way of controlling swirl is by using a separated helical port system, in which the helical intake port is split vertically into two sections. Airflow velocity through the bottom half of the port is increased by progressively closing off the upper port section, as shown in figure 2.11. The swirl ratio increases with the airflow velocity, although the port flow coefficient decreases sharply [Shimada et al, 1986; Ishida et al, 1985].

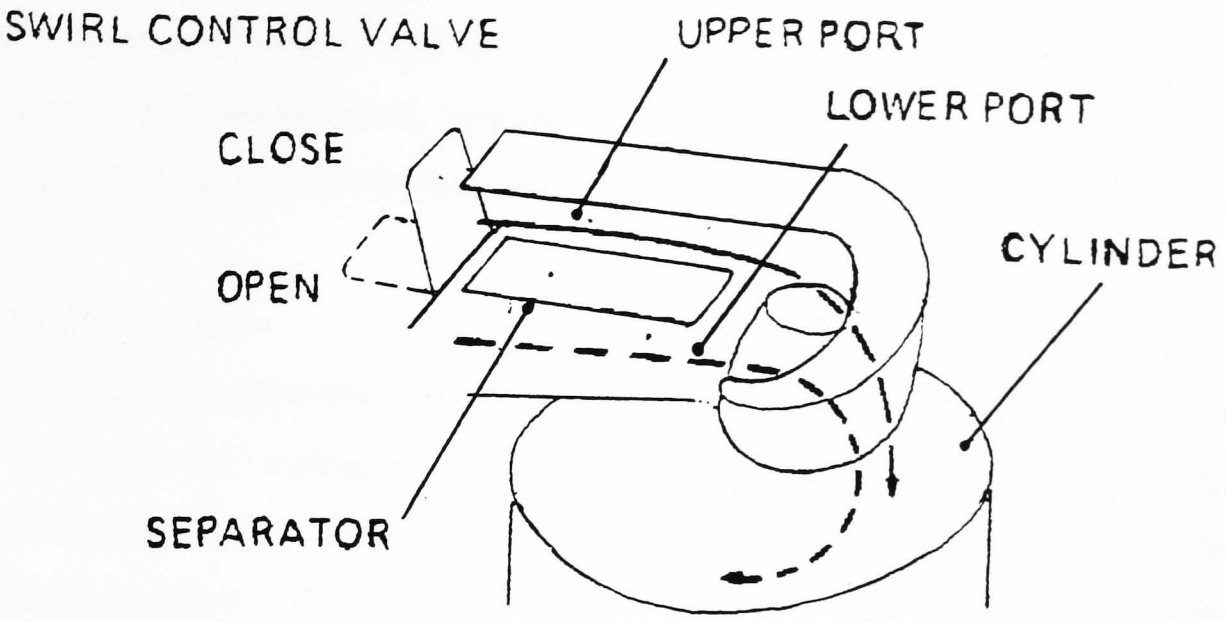

Figure 2.11 Separated port system used for varying the in-cylinder swirl ratio [Shimada et al, 1986].

2.3.6 Methods of measuring in-cylinder swirl

The nature of swirling airflow within the cylinder of a firing or even a motored engine is very difficult to determine. For this reason, steady flow tests are most often used during the design and optimisation of swirl producing devices. However, it must be remembered that steady flow tests adequately describe only the swirl generating characteristics of the intake port and valve (at a fixed valve lift). The swirling flow set up in the cylinder during the intake stroke is substantially modified during compression, and varies with crank angle as a result.

There are various methods of measuring air-swirl. These include:

(1) Paddle wheel (or vane) anemometer.

A multiple vane wheel is suspended or supported at the centerline of the bore on low friction bearings. Air is drawn in through the intake valve at a steady flow rate, and the rotational speed of the vane wheel is measured and taken as an approximation of the swirl speed. However, the vanes disturb airflow if sampling is performed near the

cylinder head, and the wheel speed cannot accurately account for spatial variations of flow velocity and direction across the cylinder bore [Fitzgeorge and Allison, 1962-63]. Slip between the vanes and air-flow, and friction in the bearings further reduces the accuracy of measurements, and means that the vane wheel must under-estimate the true swirl speed [Stone and Ladommatos, 1992].

(2) Flow straightener.

A honeycomb type structure is used, which allows easy passage of air in-line with its cells. The structure, having small mass and supported on low friction bearings, is inserted some distance down an experimental cylinder where the flow is to be measured (see figure 2.12). The flow does not have to be fully developed into a forced vortex, as the flow straightener measures the total momentum of the flow (ie, spacial integral), and automatically accounts for any spatial variations. The cylinder head and port design to be tested are secured on top of the cylinder, as shown in figure 2.12, and air is either blown or sucked through the intake port at various valve lifts. The swirling airflow is straightened (and therefore its momentum reduced to zero) by the honeycomb cells. Thus the torque on the honeycomb cells, resulting from the straightening of the airflow, is a measure of the swirling air momentum, and it can be related to swirl velocity using:

$$M = \tfrac{1}{8}\dot{m}\omega B^2$$

Equation 2.3 Calculation of swirling air momentum, where M = moment of momentum flux (Nm), $\dot{m}$ = mass flow rate (kg/s), ω = swirl angular velocity (rad/s), and B = cylinder bore.

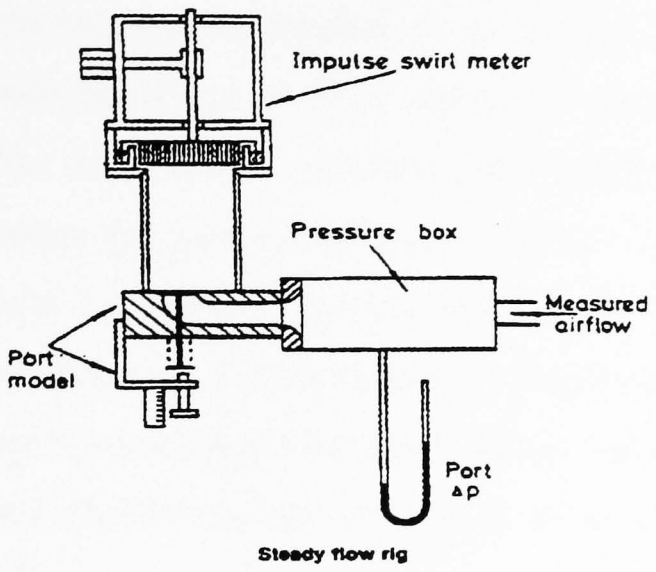

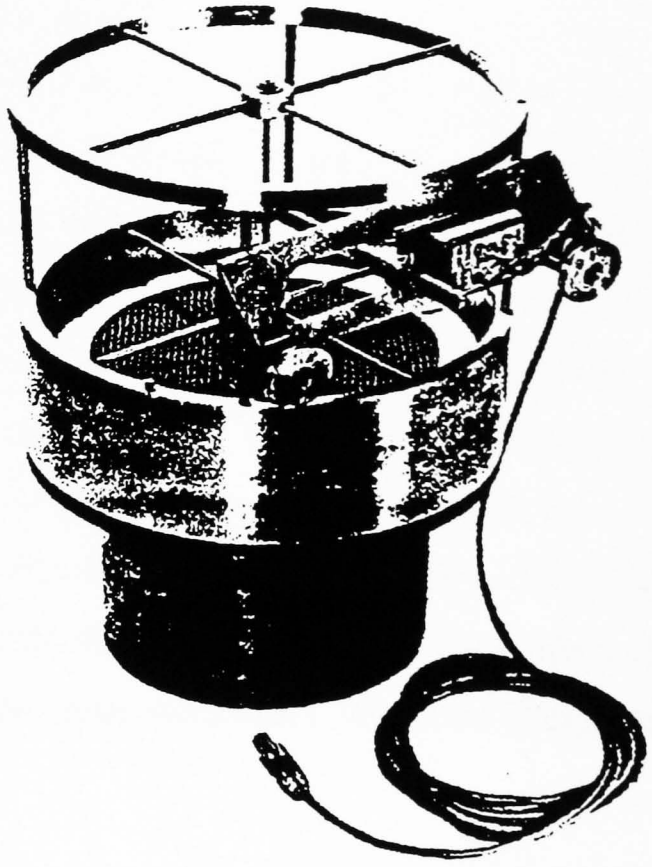

Figure 2.12 Schematic representation and photograph of a honeycomb flow straightening apparatus [Ricado, Advertising brochure].

(3) Hot wire anemometry (HWA).

A short wire held in a small metal fork is heated to a temperature slightly above that of the airflow, and placed perpendicular to the airflow at the desired measuring point, where velocity levels might directly influence combustion characteristics [Khan et al, 1972]. For example, one wire can be orientated radially (with respect to the cylinder bore) to detect swirl flow, and another tangentially to detect squish flow. HWA is much cheaper than laser doppler anemometry (LDA) / velocimetry (LDV), and provides continuous results. However the output must be linearised, corrected for temperature and pressure, and is not directionally sensitive [Stone and Ladommatos, 1992]. For these reasons, HWA tends to be less accurate than LDA, although it can provide significant information about the flow field.

(4) Laser doppler anemometry (LDA) / velocimetry (LDV).

Measurement of instantaneous air velocity at any point within the combustion chamber, without disturbing or influencing the flow in anyway, is possible with LDA/LDV, which provides discontinuous, high frequency results [Stone and

Ladommatos, 1992]. However, optical access must be provided from two (preferably orthogonal) directions, and the signal processing requirements are considerable. A beam from an argon laser is divided, and then refocused on the area of interest within the combustion chamber, so as to form a series of interference fringes. Small particles introduced into the flow scatter the laser light as they pass through the control area, and some of this scattered light is collected and focused onto a photomultiplier to detect the presence of scattered light (see figure 2.13). The frequency of scattered light is dependent on the velocity of the tracer particles as they pass through the control area, and the change in frequency being due to the Doppler effect. Electronic post-processing of the signal allows calculation of air velocity in one plane. The laser and photomultiplier are rotated to obtain all three component velocities [Ferguson, 1986].

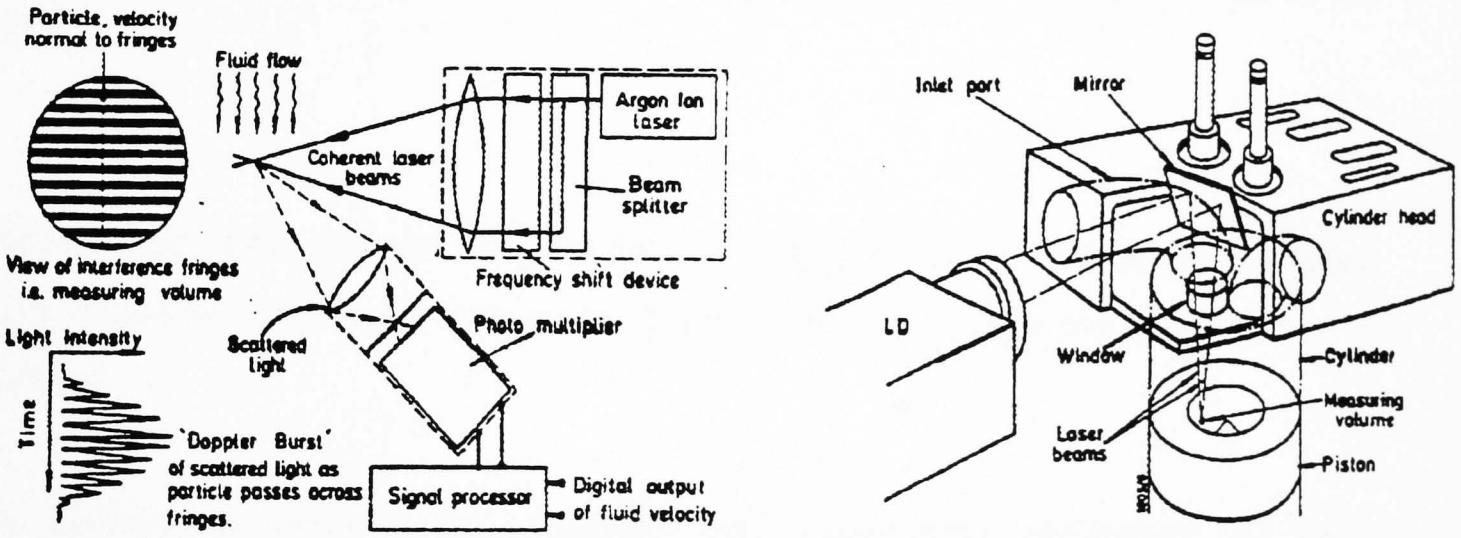

Figure 2.13 Schematic diagram and perspective view illustrating the operation and optical access of LDA/LDV in engine cylinders [Ferguson, 1986].

Arcoumanis et al (1994) used LDV to characterise the steady intake flow of an optically accessed engine. The results provide a much clearer picture of the flow field affecting combustion than is possible with bulk flow measurement techniques. Figure 2.14 below shows the 3D flow field generated from a series of LDV measurements taken in planes down the cylinder bore, just prior to inlet valve closure in a real engine.

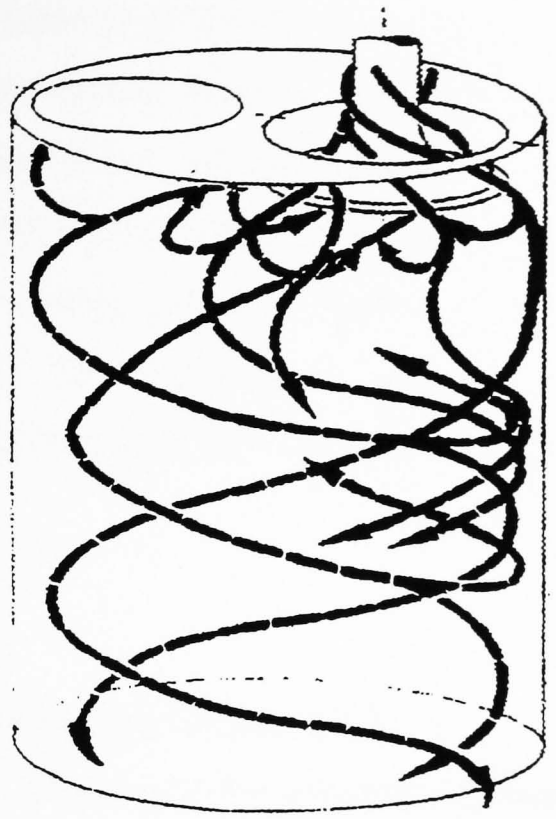

Figure 2.14 Three-dimensional flow field obtained using 2-D LDV [Arcoumanis et al, 1994].

Results from these methods can give different absolute velocity values, so published data should be treated on a comparative basis unless the experimental method is fully defined.

In addition to methods for qualitative and quantitative description of swirl summarised above, in-cylinder flow can be visualised using smoke, cotton tuffs , water flow rigs, steak lines in dissimilar fluids, light sheets, and hollow phenolic spheres (micro balloons). A dynamic model and video camera/PC can be used to view in-cylinder flow, perhaps using Freon as the working fluid to enable the model engine to be run at slower speeds whilst maintaining similar fluid dynamic properties.

2.3.7 Nature of in-cylinder swirl

Approximation to solid-body rotation

The bulk air motion of swirl approximates to a forced vortex about the cylinder axis (solid body rotation – constant angular velocity) [Schapertons and Thiele, 1986;

Arcoumanis et al, 1994; Arold et al, 1990]. Superimposed within this bulk motion is turbulence. However, flow patterns close to the cylinder head during induction are comparatively disorganised, and do not approximate to a forced vortex [Tindal et al, 1982]. This is due to a system of vorticies and high levels of shear created by the jet-like intake flow of air oozing past the intake valve [Heywood, 1987]. Some researchers have reported the existence of a primary swirl component, and a secondary counter-rotating jet giving rise to high turbulence levels during induction [Arcoumanis et al, 1994].

Swirl modification during the compression stroke

Rotational motion induced during intake is substantially modified during compression to aid complete combustion of the diesel fuel spray. Results from an engine model developed by Morel and Keribar (1985), indicate that air remaining above the piston during compression near TDC loses angular momentum rapidly because of losses associated with wall friction. Intake generated swirl also decays due to turbulent dissipation within the fluid. However, typically 66-75% of the initial angular momentum about the cylinder axis will persist throughout the compression stroke [Heywood, 1988].

Air inside and above the cup-type bowl-in-piston significantly increases its angular momentum, in-line with mass transfer of air into the bowl during compression [Morel and Keribar, 1985]. Re-entrant design bowl shapes produce more complicated modification of the angular air momentum during compression, with less communication between the various volumes within the combustion chamber [Morel and Keribar, 1985].

A compact bowl-in-piston combustion chamber substantially increases the swirl velocity. Assuming no losses, as the moment of momentum is conserved, but the radius of air rotation (and moment of inertia) is reduced, the angular velocity must increase. It can be shown that in the absence of friction, the swirl angular velocity for solid body rotation would increase by $(B/D)^2$ [Heywood, 1988] for simple bowl-in-piston combustion chambers (B is the cylinder bore, D is the bowl diameter). At current HSDI engine compression ratio's, this is typically a factor of 4 increase in air

angular velocity. In reality, due to energy dissipation in an operating engine the angular velocity increases by a factor of about 2 [Heywood (1988)].

Figure 2.15 shows swirl amplification, as a function of crank angle, during induction and compression of a motored engine, for various swirl configurations [Dent and Suliamam, 1977].

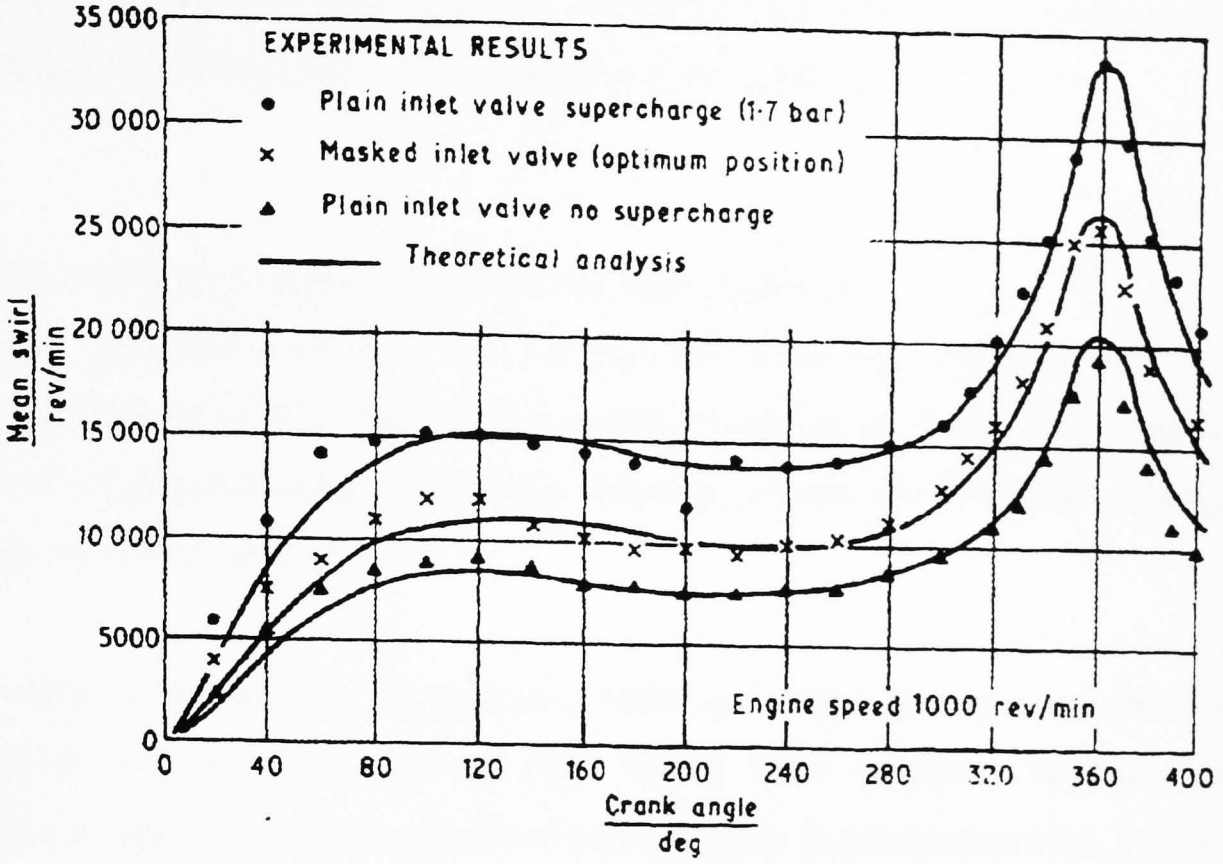

Figure 2.15 Swirl amplification during compression [Dent and Suliamam, 1977].

Air forced into the piston bowl during compression adds a radial component to the intake generated swirl. This is most profound near TDC, where the rate of change in volume of the region between the piston face and cylinder head is most rapid. A high velocity blanket jet of air – known as squish – can substantially modify the swirl velocity distribution and magnitude, and subsequent combustion characteristics. The influence of squish is more profound at lower swirl levels, and care is required to maintain tight tolerances on bump-height to avoid airflow anomalies between cylinders [Schapertons and Thiele, 1986].

Piston bowl shapes with a large squish area relative to the maximum bowl diameter (very re-entrant type bowl shapes), are less sensitive to swirl levels than open bowl

shapes. This is because the high squish velocities generated with re-entrant designs promote better mixing [Saito et al, 1986]. However, piston bowls offset from the cylinder center-line can destroy or at best reduce intake generated swirl by the end of compression [Naber and Reitz, 1988].

Once combustion has started, the hot, expanding gases increase the swirl velocity by many times in bowl-in-piston designs, enhancing air motion and mixing processes, according to the individual bowl design [Dent and Suliamam, 1977].

Effect of engine operating parameters on swirl generation

Typically, induction-generated swirl velocity will scale with engine speed, the swirl ratio therefore remaining essentially constant [Bopp et al, 1986]. This results in a relatively constant duration of diffusion burning, as the rate of fuel/air mixing also roughly scales with engine speed.

Swirl ratio increases with compression ratio and boost pressure, as more air is transferred into the bowl-in-piston than would have otherwise remained in the clearance volume, and the air mass flow rate increases [Ladommatos et al, 1992].

2.3.8 Effect of swirl on combustion

Effect of swirl on combustion efficiency

Increasing swirl results in a reduction in brake specific fuel consumption (BSFC), as the rate of heat release and mixing rates are increased [Hiroyasu et al, 1986]. The swirl desirable for minimum BSFC at high-speeds and loads is significantly less than the optimum for low-speed operating points, although at low-speed and part-load conditions the benefit of swirl on BSFC is offset by increased heat transfer to the coolant [Shimada et al, 1986]. Injection timing giving minimum BSFC shifts towards TDC as the swirl ratio increases, due to reduced combustion duration (however, very high swirl mixing rates are offset by increased heat transfer and reduced volumetric efficiency).

Spicher and Dresen-Rausch (1990), and Spicher et al (1987) have reported a small decrease in ignition delay as swirl is increased, although Van Gerpen et al (1985) have shown an increase in ignition delay and pre-mixed fraction of burned fuel. In reality, swirl has little effect on the ignition delay because ignition delay is predominantly determined by chemical reaction rates, and not the rate of mixing in modern HSDI diesel engines.

Effect of swirl on heat release

The rate of heat release increases with increasing swirl, regardless of engine speed and load because swirl increases the rate of fuel/air entrainment. Increased rate of burning causes a higher peak pressure (also increasing noise), and shorter initial combustion duration. However, at high speeds, increasing swirl has been shown to increase total combustion duration due to over-mixing [Shimada et al, 1986]. Research undertaken by Ricardo and Hempson (1968), shown in figure 2.16, illustrates the effect of increasing swirl ratio on peak cylinder pressure, and therefore engine harshness and noise.

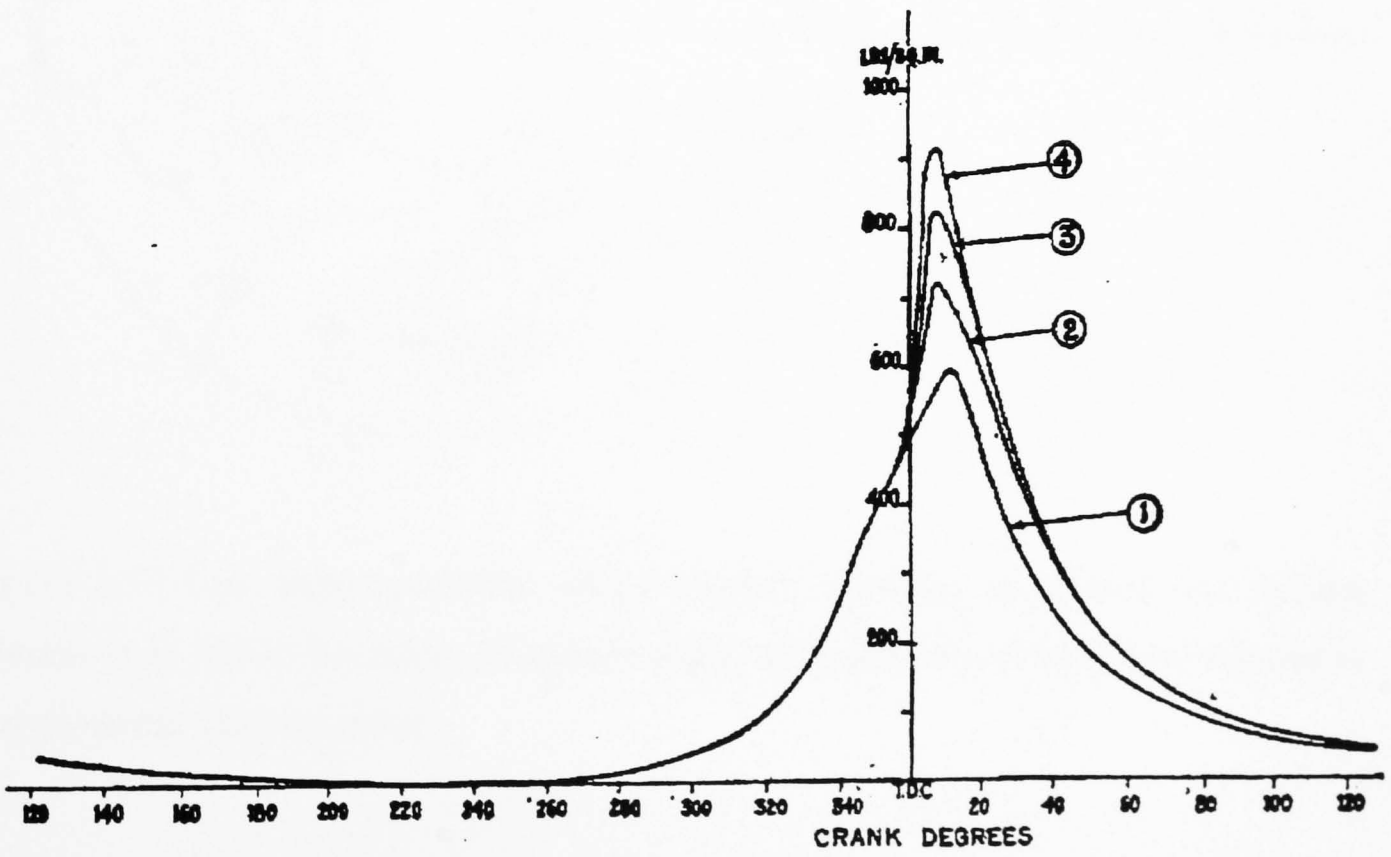

Figure 2.16 Indicator diagrams showing effect of swirl on peak cylinder pressure (numerically higher numbered pressure traces have higher swirl intensity) [Ricardo and Hempson, 1968].

Effect of swirl on fuel spray penetration

The mixing patterns of injected fuel jets and swirling air change considerably with different swirl levels. One important change is a reduction of spray jet penetration with increasing swirl [Packer et al, 1983 and 1985; Arold et al, 1990].

Water rig simulation of gas-into-gas injection (see figures 2.17 and 2.18), clearly shows that under similar conditions jet penetration and growth reduce with increasing swirl. Numbers in the figures 2.17 and 2.18 below show successive frame photographs, spaced 0.0157seconds apart, of jet entrainment within the swirling flow at two different swirl ratio's.

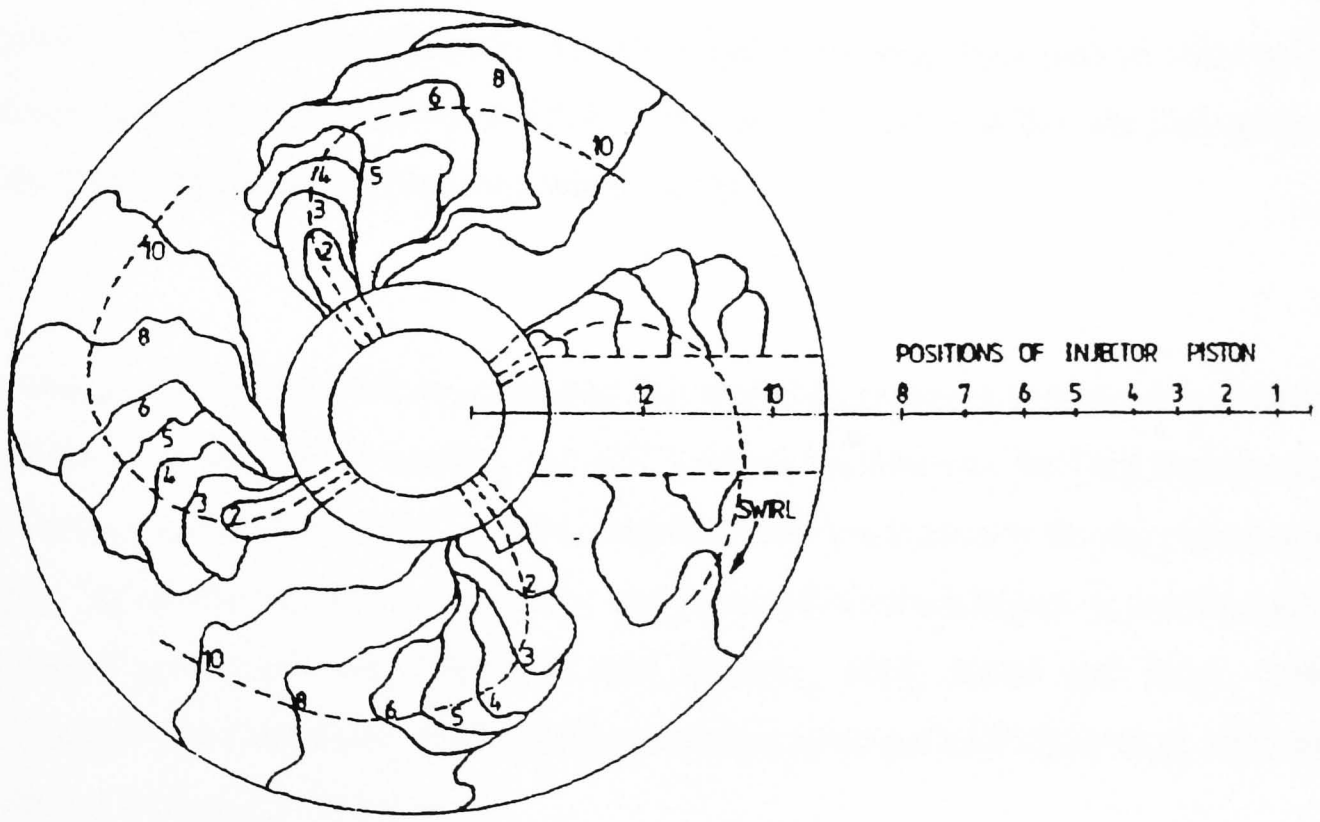

Figure 2.17 Low swirl condition (40 rev/minute) showing jet growth and mixing [Packer et al, 1983]. Positions of injector piston are indicative of total fluid injected at any particular frame number.

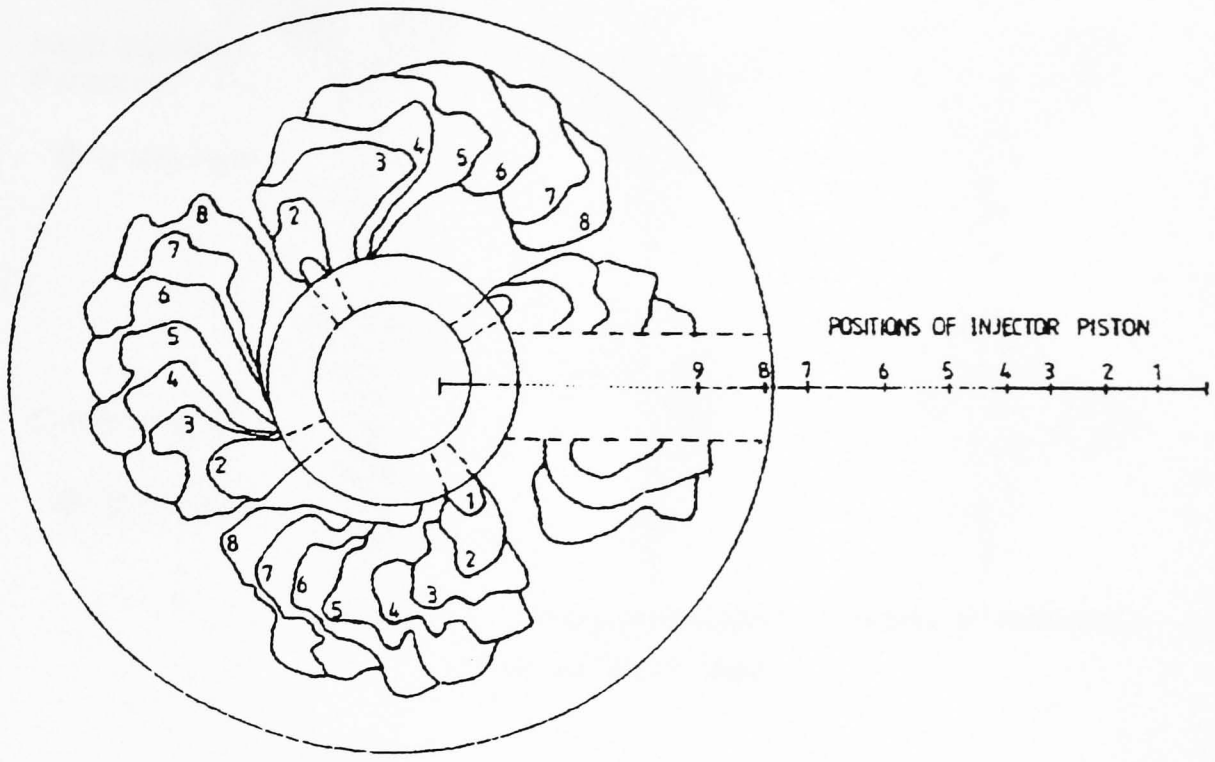

Figure 2.18 High swirl condition (50 rev/minute) showing increased jet mixing but reduced penitration [Packer et al, 1983]. Positions of injector piston are indicative of total fluid injected at any particular frame number.

However, with modern DI diesel engine fuel injection pressures (which are increasing continually to aid fuel/air mixing, and will increase significantly with the introduction of common rail fuel injection systems), injected fuel heads directly for the piston bowl edges. Hence the liquid core trajectory and penetration time/distance is unaffected by induction generated swirl [Hiroyasu and Nishida, 1989; Naber and Reitz, 1988; Werlberger and Cartellieri, 1987] and combustion enhanced swirl [Rao et al 1992(b)], as shown in figure 2.19 below.

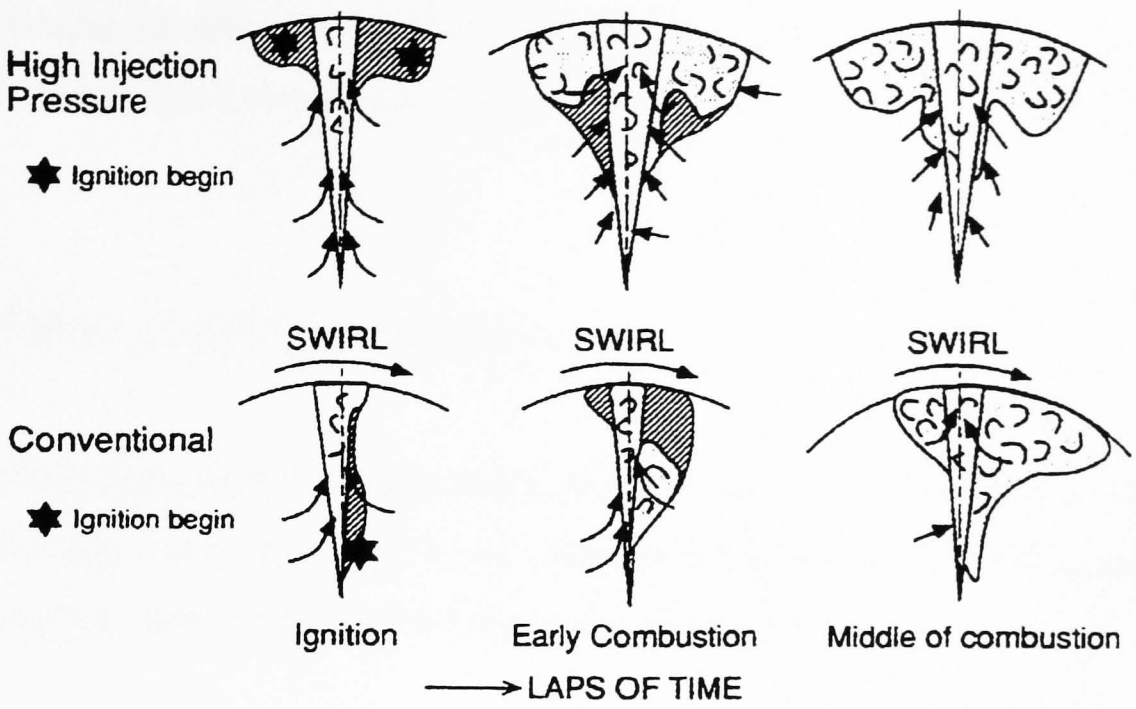

Figure 2.19 Comparision between the effect of high-pressure and convention fuel injection systems on fuel jet impingement [Suzuki, 1997].

Effect of swirl on combustion after fuel impingement

Less fuel reaches the bowl in high swirl cases due to increased evaporation rates, and because small drops are deflected away from the wall by high air velocities. However, once the jet has impinged on the wall, swirl controls the rate of air entrainment with fuel vapour, as it does for fuel vapour surrounding the liquid jet core during injection [Zhang et al, 1993].

Swirl also controls the wall jet development – fuel films caused by impinged fuel are dragged around in high swirl cases, leading to increased re-entrainment of fuel into the main air-stream and subsequent combustion [Werlberger and Cartellieri, 1987]. Fuel impinging in a low swirl environment will travel down the bowl sides and may even start to be swept up towards the central pip [Naber and Reitz (1988)]

Increasing swirl may also concentrate the close-to-stoichiometric mixture strengths (and thus combustion) near the piston wall. Ignition kernels tend to increase near the vicinity of the wall as swirl is increased, and are most likely in the direction of swirl behind the spray axis [Spicher and Dresen-Rausch, 1990].

The optimum amount of swirl for any particular engine is very system specific, and dependent on engine operating condition as well.

2.3.9 Effect of swirl on emissions

Many researchers have investigated the effect of swirl on combustion and emissions. Swirl is a major tool used by DI diesel research engineers to control these parameters. Some general conclusions can be drawn from their results.

Effect of swirl on air utilisation

Given that air swirl increases the fuel-air mixing and evaporation rates, one would expect combustion duration to shorten as swirl is increased. Also, emissions that depend on the rate of combustion can also be expected to be swirl dependant. Increasing swirl results in a decrease in the concentration of fuel-rich zones, which produce smoke, and of lean regions where NOx is expected to form. However, combustion temperatures are increased due to the faster rate of burning [Khan et al, 1972], and this results in an overall net rise in NOx.

For a particular combination of injection and combustion system design, and engine load, the optimum swirl ratio is closely linked to air utilisation. Consider for example, a bowl-in-piston combustion chamber utilising a four hole injector. Its theoretical optimum swirl ratio for best air utilisation would result in the swirling air sweeping around an angle of about 90 degrees during the injection period. Any increase in swirl at this fuelling level would allow over-mixing between fuel vapour of individual sprays, creating rich and lean regions. Conversely, a reduction in swirl might under-utilise the air available [Schapertons and Thiele, 1986; Wakuri et al, 1989].

Figure 2.20 shows in-cylinder photographic analysis by Wakuri et al (1989), illustrating how swirl substantially increases mixing rates and sweeps fuel vapour around the cylinder.

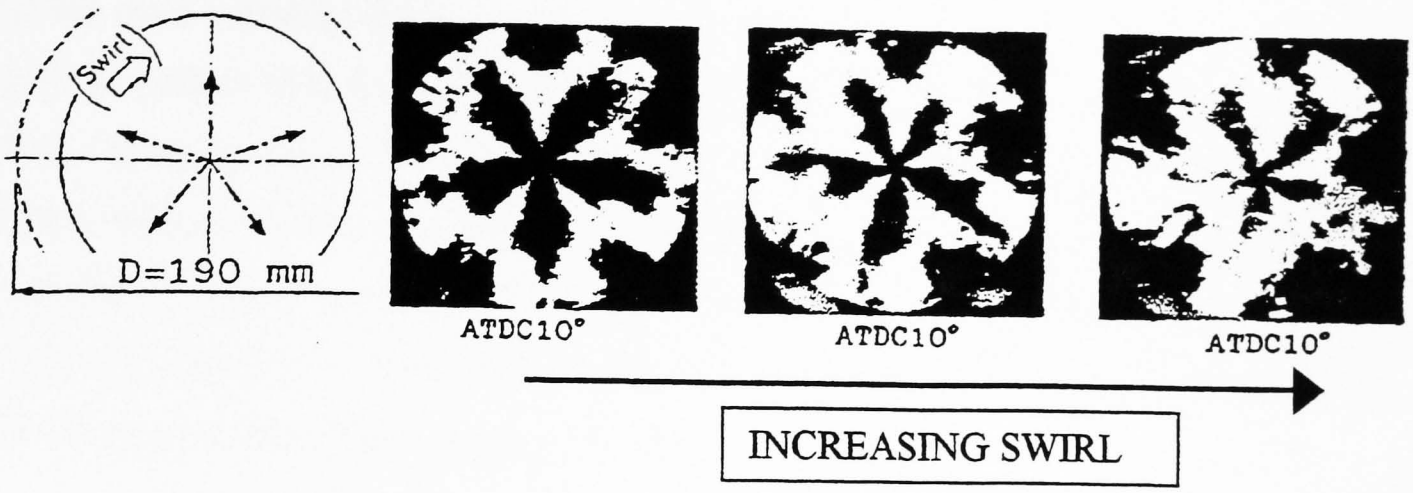

Figure 2.20 The effect of swirl intensity on combustion in a DI diesel engine [Wakuri et al, 1989]. Swirl intensity increases from left to right in these photographs of combustion in a shallow piston bowl, 10 degrees ATDC.

Effect of swirl on smoke and particulate emission

Smoke emissions decrease with an increase in swirl ratio, unless over mixing allows local rich regions to form as individual spray vapour clouds mix and overlap with each other [Hiroyasu et al, 1986]. The emission of smoke is affected by swirl more than any other gaseous emission.

Particulate (and CO) emissions decrease as swirl ratio increases due to more rapid fuel-air mixing, and improved transfer of clean air to rich combustion regions [Khan et al, 1972; Shimada et al, 1986; Van Gerpen et al, 1985]. Khan et al (1972) postulated that for a given overall equivalence ratio, there will be an optimum swirl value corresponding to the maximum entrainment of air. Increasing the swirl level above this will cause bending of the fuel jets, and increasing time for jet impingement on the piston bowl walls. However, in real engines an optimum swirl ratio is likely to be due to a trade-off with reducing volumetric efficiency rather than jet bending, which occurs at very high swirl levels of around 20 to 1 [Khan et al, 1972]. An exception to this might be the use of very small jet hole diameters which are prone to jet bending.

Effect of swirl on NOx emission

All the main variables (fueling rate, injection timing, engine speed, air-swirl and flow structure) affect NOx formation by changing the equivalence ratio, and temperature in NOx formation zones. It is the spatial history of equivalence ratio and temperature which determines NOx formation. The first portion of charge to burn creates very high local temperatures, and NOx values quickly approach equilibrium. Equilibrium values are sensitive to local air/fuel ratio, and hence depend on the swirl ratio which affects mixing rates [Van Gerpen et al, 1985].

NOx emissions increase with increasing swirl, if the start of injection is maintained constant. This is because of more rapid diffusion burning, and according to some researchers, a more advanced start of combustion caused by a shorter delay period [Khan et al, 1972; Hiroyasu et al, 1986]. The increase in heat release rate and rate of pressure rise during the initial stages of combustion, raise combustion temperatures and promote NOx generation [Shimada et al, 1986]. Increasing in swirl makes it possible to retard injection timing for optimum engine efficiency, which can be used to offset the increase in NOx [Khan et al, 1972].

Figure 2.21 below shows that although the effect of swirl on emissions of NOx is considerable, the effect of injection timing is a greater factor for NOx control.

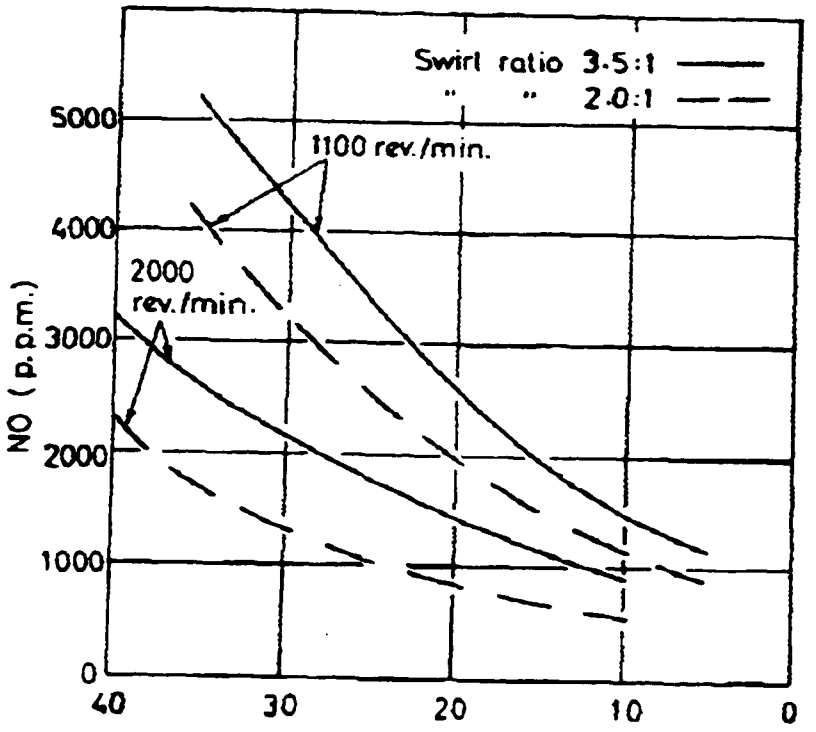

Figure 2.21 Effect of swirl (and injection timing) on NOx formation. The horizontal axis shows injection timing in degrees crank angle BTDC [Khan et al 1972].

The effect of swirl ratio on NOx formation is more significant at higher engine loads, as shown in 3D engine map of figure 2.22.

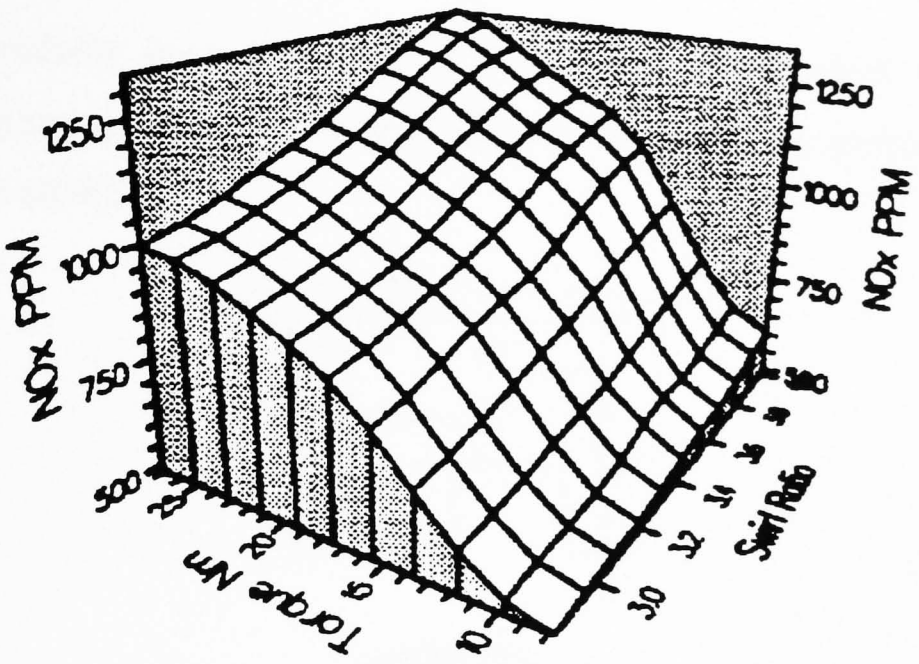

Figure 2.22 Variation of emission of NOx with swirl ratio, for different DI diesel engine loads [Rao et al, 1992(a)].

Effect of swirl on HC emission

HC emissions are reduced if swirl is increased. This is because of improved fuel/air mixing, as discussed for the formation of particulates. However, excessive swirl causes an increase in HC emission due to an increase in very lean regions, and the centrifuging of cool, un-burnt mixture towards the cylinder walls (also increases particulate emission) [Van Gerpen et al, 1985].

Matsui and Sugihara (1986) reported that at light loads an increase in swirl ratio caused an increase in HC emission, due to excessive air cooling (quenching) of unburned fuel or chemical species undergoing a combustion reaction. However, at higher loads they report a decrease in HC emission with increasing swirl, because the increased gas temperature maintained combustion.

2.4 Piston bowl shape and airflow: effect of squish

2.4.1 Definition and description of squish

Squish is the radially inward motion of compressed air, expelled from the gap between the piston top, and cylinder head face, as the piston approaches TDC during the compression stroke.

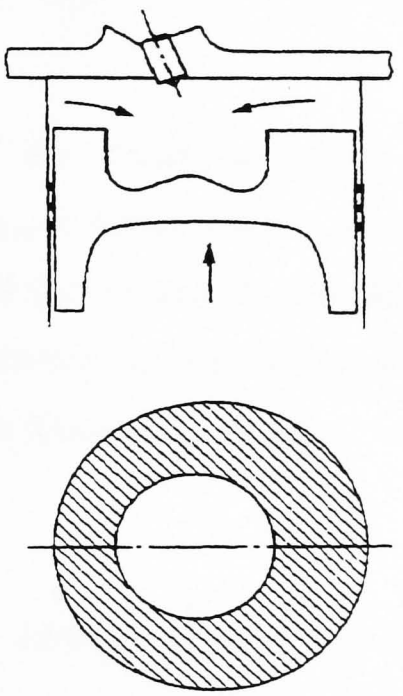

Figure 2.23 Bowl-in-piston DI diesel combustion chamber, showing squish flow above the piston face. The relative squish area is indicated by the shaded area in the plan view of the piston face and bowl-in-piston [Heywood, 1988].

Squish occurs in DI diesel engines because of the need to move air into the compact, bowl-in-piston, thereby increasing swirl. Squish is also used to modify airflow in the piston bowl at the end of compression, and during combustion [Ferguson, 1986].

Squish is defined by the instantaneous squish velocity, and for different combustion chamber shapes by the percentage squish area. The amount of squish is given by equation 2.4:

% Squish area = area of piston top which nearly meets cylinder head /
cylinder head area

Equation 2.4 Definition of squish area of bowl-in-piston engines

Air velocity and airflow Reynolds number in the combustion chamber are such that flow may be considered incompressible, and air density considered uniform within the combustion chamber. Assuming one-dimensional flow across the squish volume, squish velocity is given by equation 2.5:

$$\frac{v_{sq}}{S_p} = \frac{D}{4z}\left[\left(\frac{B}{D}\right)^2 - 1\right]\frac{V_B}{A_c z + V_B}$$

Equation 2.5 Calculation of the theoretical squish velocity for bowl-in-piston combustion chambers, where v_{sq} = squish velocity, V_B = volume of the piston bowl, A_C = the cross-sectional area of the cylinder, S_p = is the instantaneous piston speed, z = distance between the piston crown top and the cylinder head, D = bowl diameter at the throat and B = cylinder bore [Heywood, 1988].

If all other bowl parameters remain constant, the theoretical squish velocity is proportional to $(B^2 - D^2)/D$ [Fitzgeorge and Allison, 1962-63].

2.4.2 Measurement of squish

Visualisation and measurement of squish is possible using many of the same techniques as for swirl. Of particular use is LDV/LDA. Computational fluid dynamics (CFD), has proved very useful for prediction of flow fields. Visual indicators such as cotton tuffs, oil films and paint streaks may only represent the intake flow and not air motion induced during compression and squish flows [Alcock and Scott, 1962-63]. However, Shimoda et al (1985) have produced useful analysis based on motored engine results using the oil film method, and have obtained knowledge of both squish and swirl flows, by reducing the oil streaks to their component velocities.

2.4.3 Effect of piston bowl shape on squish

Re-entrant bowl designs increase squish velocity, turbulence and fuel/air mixing, by increasing the area of the piston top which nearly touches the cylinder head, whilst maintaining bowl volume (and thus compression ratio). A smooth cylinder head without recesses or valve cut-outs is required to maximise squish velocity. However, this may possibly compromise the engine valve timing [Bertodo et al, 1974].

The diagram below (see figure 2.24) shows the variation of theoretical squish velocity for different bowl diameters, in a cylinder of 63.5mm (2.5 inches) radius.

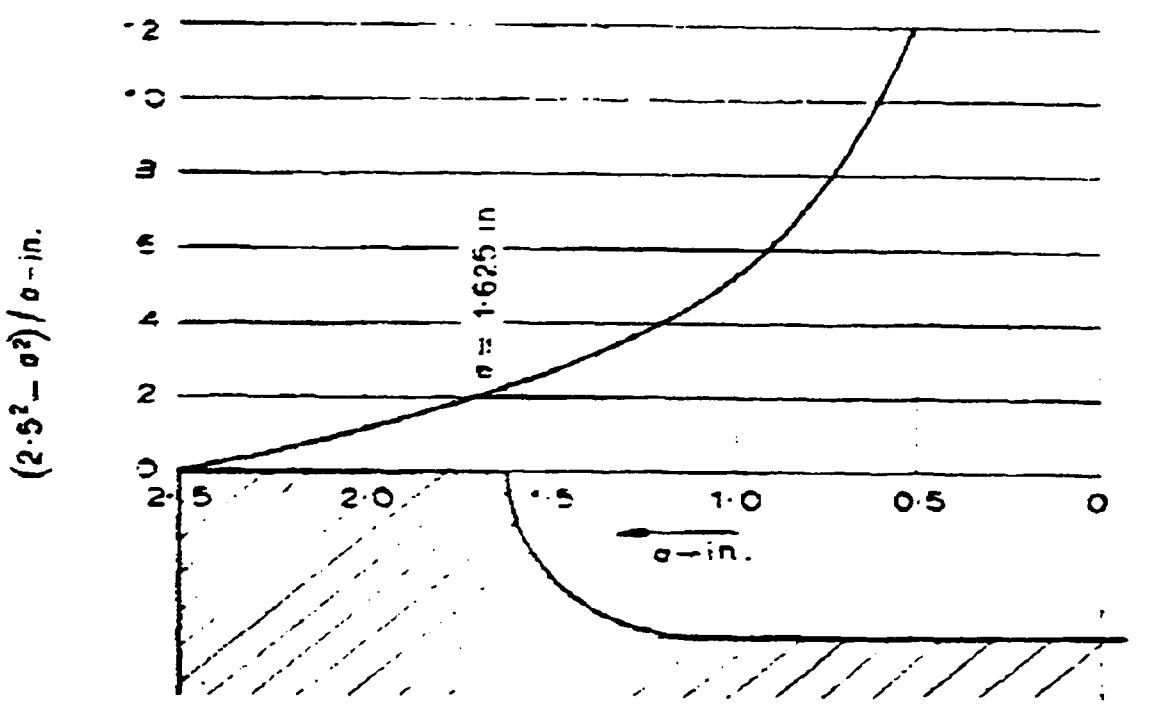

Figure 2.24 Variation of theoretical squish velocity, with the proportion of the piston which closely approaches the cylinder head. Squish velocity rises quickly as the piston bowl diameter is reduced [Fitzgeorge and Allison, 1962-63].

2.4.4 Variation of squish velocity during compression and combustion strokes

Squish velocity increases as the piston moves up the cylinder bore, towards TDC. The maximum squish velocity occurs at about 10 degrees BTDC [Heywood, 1988; Zolver,

1997], and after TDC becomes negative (reverse squish), as compressed charge flows from the piston bowl back to the squish region.

Reverse squish creates extensive turbulence in the re-entrant piston bowl, and above the bowl throat, aiding mixing and combustion. Reverse squish velocity decays rapidly as the piston moves down the bore and cylinder volume increases [Winterbone et al, 1993]. Squish velocity before TDC is significantly less than swirl velocity, and is roughly the same as piston speed (Arcoumanis, 1994, and Schapertons, 1986, report a factor of 3 and 4 respectively, between squish and swirl velocity). Therefore swirl, and not squish, forms the dominate flow structure for combustion.

However, squish velocity is very sensitive to the piston-to-head clearance. Figure 2.25 shows the theoretical squish velocity for different bump heights, calculated assuming the cylinder pressure is uniformly distributed.

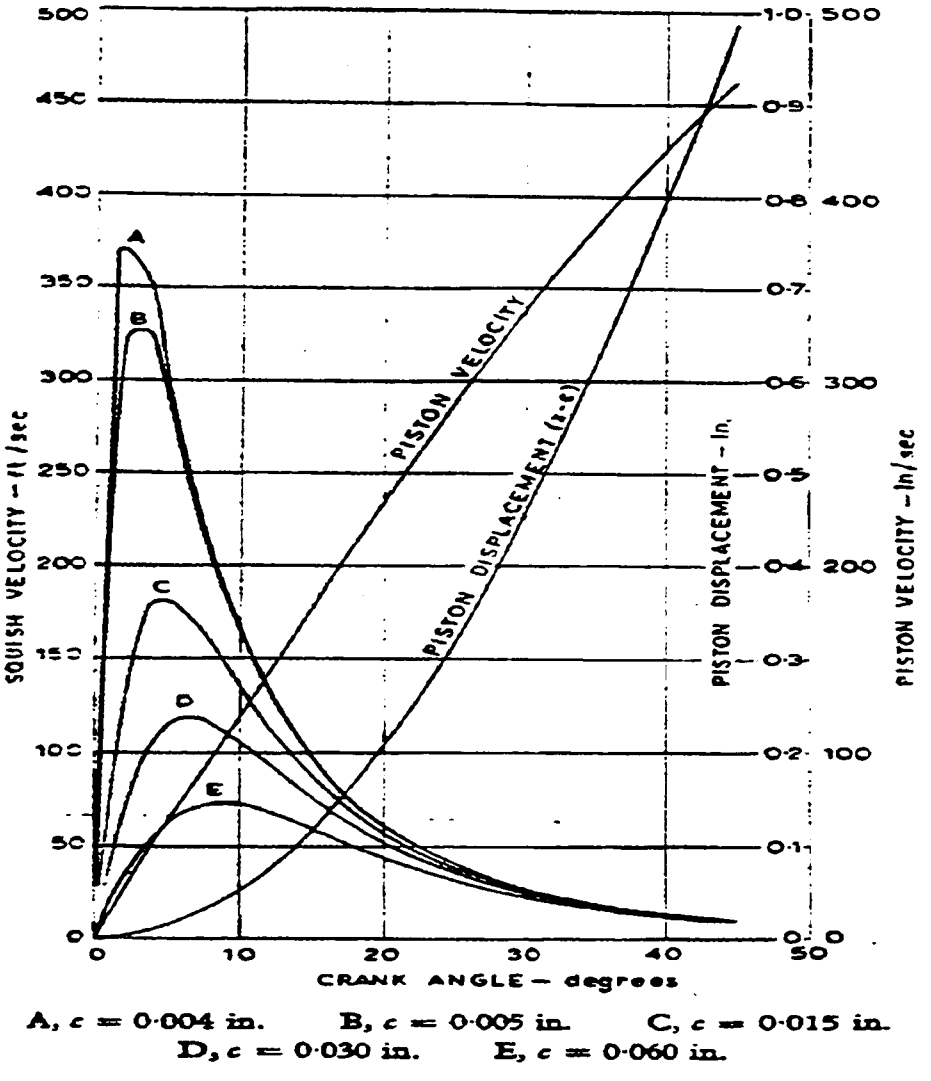

A, c = 0·004 in. B, c = 0·005 in. C, c = 0·015 in.
D, c = 0·030 in. E, c = 0·060 in.

Figure 2.25 The theoretical squish velocity for various bump heights, showing the importance of maintaining the optimum piston-to-head clearance (c), and consistency

between cylinder clearances for balanced combustion and cylinder pressures [Fitzgeorge and Allison, 1962-63].

The effect of bump height on the angular velocity of torodial air motion inside the bowl, whilst significant, is much less than that for squish velocity. This is because the energy of rotation imparted to the torodial air motion varies with the square of piston speed, whilst squish velocity is approximately proportional to piston speed. The effect of bump height is compounded at large bump heights, by a reduction of air mass in the bowl to which energy is transferred.

2.4.5 Effect of squish on in-cylinder bulk airflow

Structure of squish flow

Distortion of the classic, solid-body swirling air motion occurs near TDC, when the squish velocity reaches it peak [Arcoumanis, 1994]. Squish velocity profiles across the combustion chamber, indicate increasing velocity towards the bowl lip edge, and then reduced velocity as the air expands into the bowl volume. The highest air velocity, and thus heat transfer to the piston, occurs at the bowl lip edge, often combined with a vortex under the lip which may help or hinder fuel/air mixing and combustion [Schapertons, 1986].

Squish flow predicted by the KIVA computational fluid dynamics (CFD) simulation code, for a central bowl and an offset bowl-in-piston design, at 20 degrees BTDC is shown in figure 2.26 below.

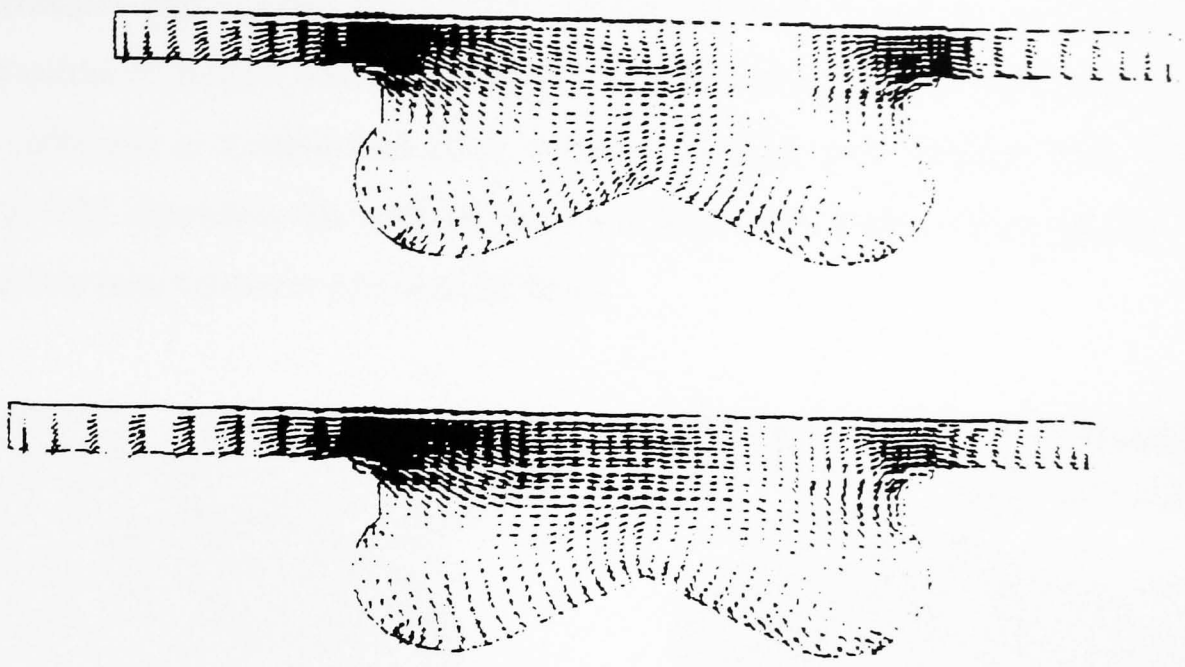

Figure 2.26 CFD simulation of airflow in a central (top picture) and an offset (bottom picture) bowl-in-piston DI diesel engine, at 20 degrees BTDC of the compression stroke. The length of vectors is proportional to the magnitude of squish velocity. Peak squish velocity occurs at the bowl lip edge [Schapertons, 1986].

Squish induces angular torodial motion in bowl-in-piston combustion chambers, which when combined with swirl induces particle motion similar to a 'winding on a ring-wound dynamo' [Fitzgeorge and Allison, 1962-63]. The effect of squish on torodial motion in different bowl shapes is indicated in figures 2.27 a, b, c below.

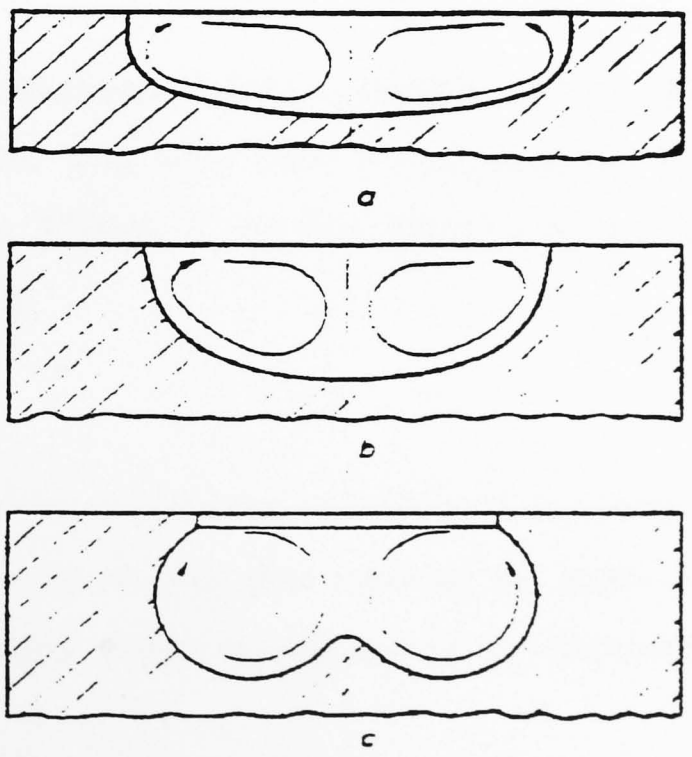

Figure 2.27 Torodial flow structure, typical of bowl-in-piston designs with low to medium swirl intensities [Fitzgeorge and Allison, 1962-63].

Traditionally, piston bowl and injector design has been based on the presumption of the structure of airflow shown in figure 2.27. However, airflow visualisation methods have indicated a complicated flow structure, which may deviate from this ideal. Figure 2.28 illustrates the airflow structure from two piston bowl shapes, and the interaction between swirl and squish flows.

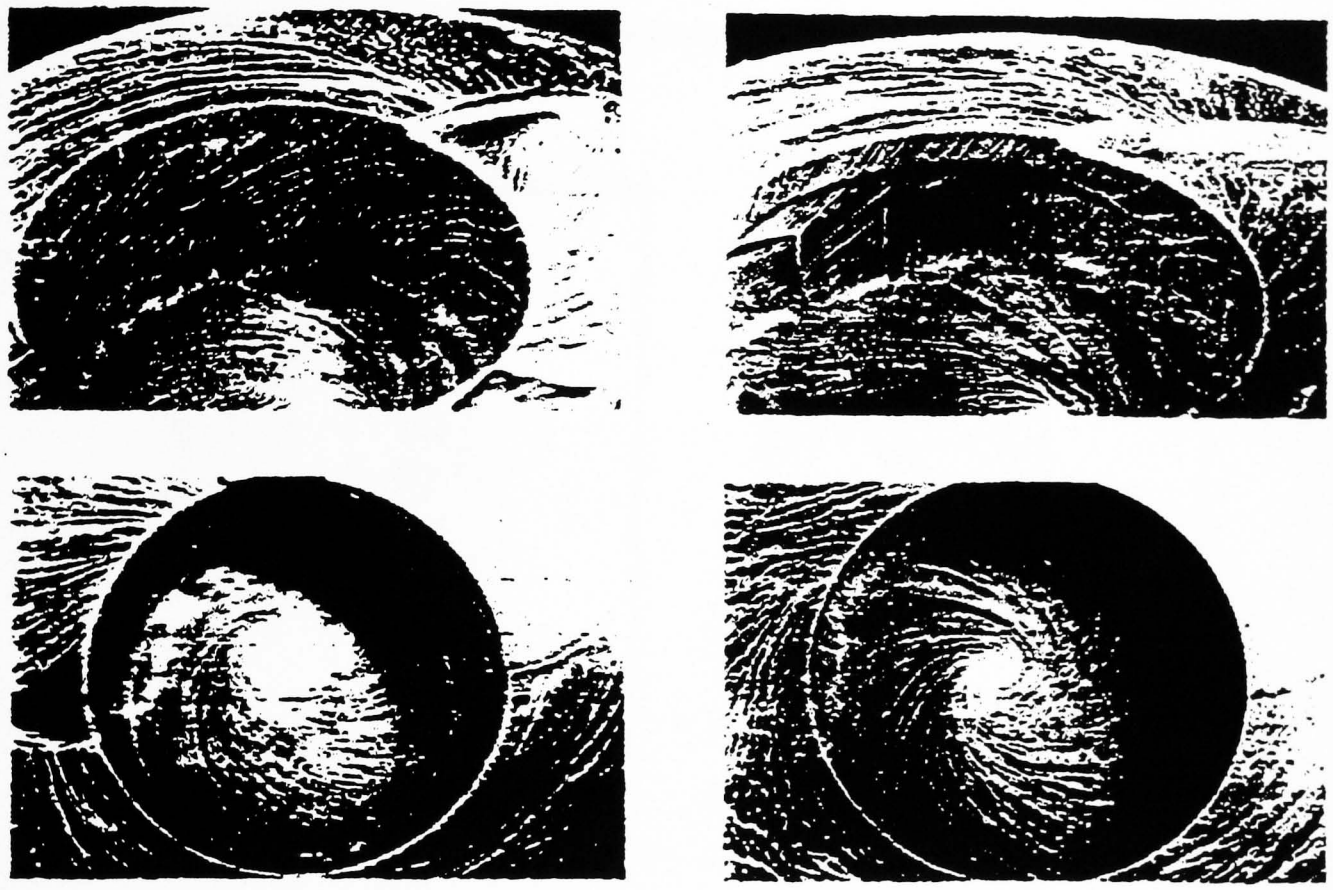

Figure 2.28 Airflow visualisation of the interaction of swirl and squish flows, using the oil film method. The 'Flat Dish' bowl is a conventional open chamber bowl-in-piston design, whereas 'HMMS 3' has four concaves in the side-wall of the piston bowl [Shigemori, 1983].

A striking indication of the complicated in-cylinder flow is shown (in figure 2.28) by the witness marks left in an oil film, after motoring the engine. Additional turbulence generated by the HMMS 3 design is indicated by the disorganised streak lines near sharp piston edges.

Effect of squish on torodial airflow and vortex rotation

As the piston approaches TDC, the strong squish flow induces a re-circulating vortex at the lip of the bowl, and modifies the cylinder angular momentum distribution [Borgnakke et al, 1981]. The interaction between squish and swirl is very complicated and difficult to define (more so with off-centre bowl-in-piston combustion chamber designs) [Heywood, 1988]. Figures 2.29 a, b, show the modification of torodial flow in open and re-entrant type bowl-in-piston combustion chambers.

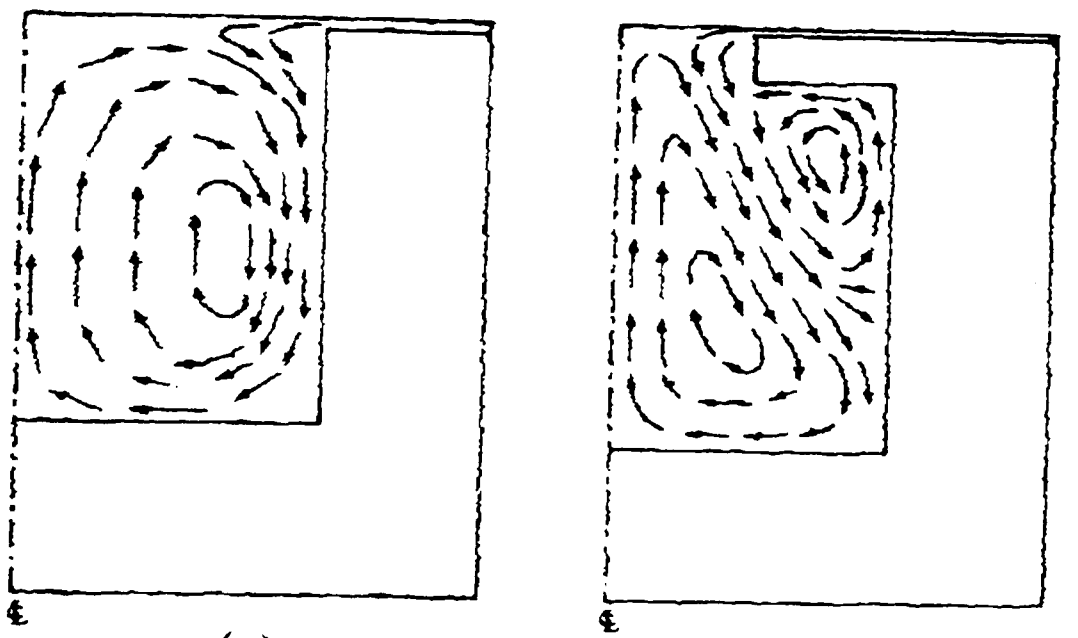

Figure 2.29 Bulk air motion viewed in a diametral plane, of two bowl in piston combustion chambers. Bowl (a) is an open bowl design, whilst bowl (b) is re-entrant [Kawamura et al, 1982].

The interaction of squish and swirl, in the piston bowl may change the direction of vortex rotation. Torodial airflow can be reversed in high swirl cases (as it was in figure 2.29), due to the centrifugal forces induced by the swirling air. Engine modelling by Naber and Reitz (1988), using the KIVA CFD code, shows (see figures 2.30 a, b,) how the direction of rotation of the torodial flow can change for similar engine conditions but different swirl levels. This has significant implications for fuel-air mixing and the effect of squish on combustion.

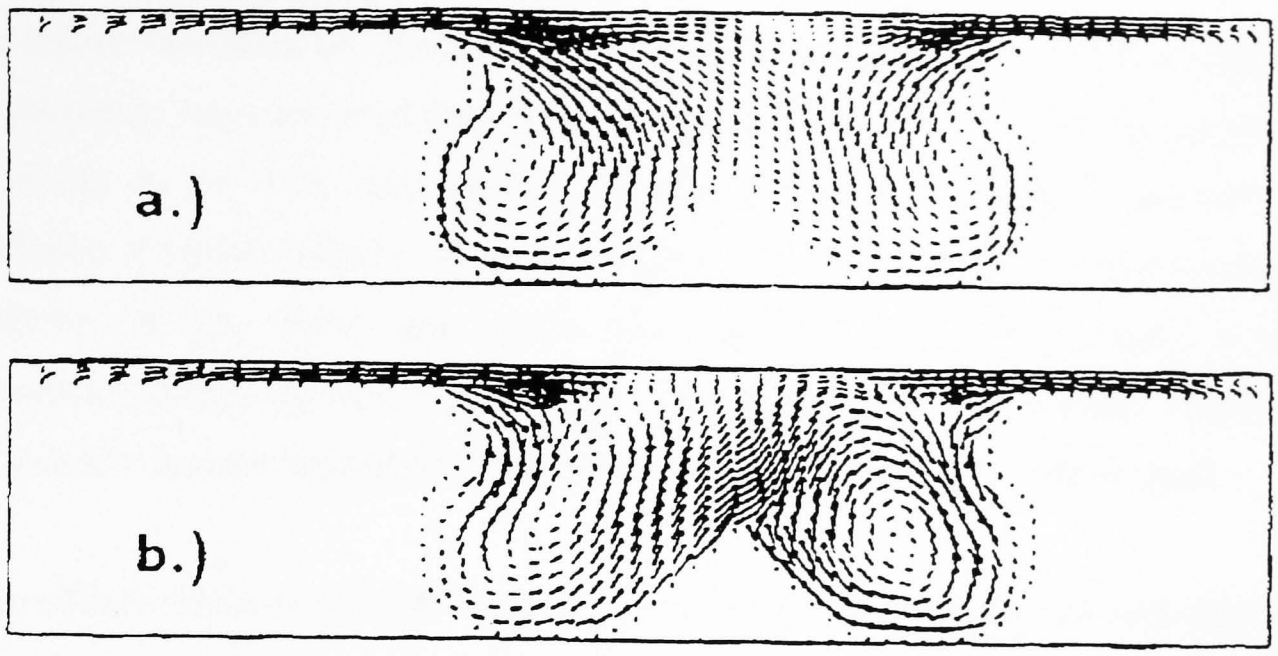

Figure 2.30 CFD simulation of DI diesel bowl-in-piston combustion chambers, at two different swirl ratio's near TDC at the end of the compression stroke. Diagram (a) shows a low swirl case (swirl ratio 0.5) in which the direction of rotation is of the traditional assumption. Diagram (b) shows a high swirl case (swirl ratio 2.9) in which the direction of rotation of torodial flow has been reversed [Naber and Reitz, 1988].

Similar results have been obtained by Wojik (1990) and Bertodo et al (1975). The return to solid-body type rotation of high swirl cases may explain the reduction of fuel/air mixing rates sometimes seen at very high swirl levels [Gosman, 1985].

Effect of squish on turbulence

Squish is generally accepted to increase air turbulence, resulting in faster mixing and combustion – essential for high speed DI diesel engine operation. Squish induced turbulence is more significant than induction generated turbulence, which decays considerably during induction and compression [Tindal et al, 1982].

Turbulence is at its highest around the lip of the bowl during compression, due to high shear levels created by the squish jet flow [Monaghan and Pettifer, 1981]. Turbulence intensity peaks near TDC, because of high squish velocity [Fansler, 1993], and later because of fuel injection and combustion [Morel and Keribar, 1985].

Factors which reduce squish velocity

High squish velocities are reduced by the effect of gas inertia, wall friction, leakage past the piston rings and heat transfer to the squish area surfaces. This causes pressure differences in the flow, and reduces the accuracy of the theoretical approach to calculation of squish velocity. Friction and gas viscosity effects always tend to oppose movement of air, whilst gas inertia may reduce squish velocity early in the compression stroke but assist squish near TDC [Fitzgeorge and Allison, 1962-63]. Heat transfer is more significant as squish velocity decreases away from its peak.

These effects, whilst small (although very sensitive to bump height), are such that in a motored engine, the reverse squish velocity is nearly equal to the forward squish velocity, and negligible energy is consumed from the engine overcoming the pressure differences. This is not true for a firing engine, where combustion generated gas expansion substantially increases the squish velocity early in the power stroke [Asanuma and Obokata, 1979].

2.4.6 Effect of squish on combustion and emissions

The faster fuel/air mixing caused by squish, increases NOx production, but reduces the emission of smoke. However, excessive squish, generated with very re-entrant bowl lips, can worsen BSFC by increased fluid transfer loses and, more importantly, by increased heat transfer from the working fluid to the combustion chamber surfaces [Middlemiss, 1978].

Combustion photography [Stone, 1992] suggests that turbulence generated by squish flow does not influence the initial stages of combustion, but increases the speed of diffusion burning later in the cycle. However, research by Spicher et al (1987), indicates that an increase in squish velocity reduced ignition delay, and resulted in faster burning (although the experimental method used also resulted in an increase in compression ratio, beacuse bump height was reduced). A reduction of flame penetration into the squish region at higher squish levels was also observed. Kuo et al (1988) have predicted increased deflection of the fuel jet during the early part of injection with high-squish re-entrant bowl shapes.

2.5 Piston bowl shape and airflow: effect of turbulence

2.5.1 Description of turbulence

Turbulent flow is random three-dimensional fluid flow, comprising of eddies and vorticies of varying sizes and lifetimes. Turbulent airflow is always present in the complex, unsteady charge air motion in an engine cylinder, superimposed on bulk airflow patterns such as swirl.

The character of turbulent flow in an engine cylinder is a complicated combination of turbulent shear layers, re-circulating flow, and boundary layers. Turbulent airflow plays an important role in the high speed DI diesel engine, by increasing the rate of momentum, heat, and mass transfer during fuel/air mixing and combustion. Turbulent fuel/air mixing rate is many times greater than the laminar rate, which relies on molecular diffusion. Turbulence requires energy to exist, and so without an energy supply all turbulent flow will decay due to viscous dissipation.

Viscous shear stresses within the turbulent flow cause continual break-up of vorticies. Smaller and smaller eddies are created, until finally the kinetic energy contained is dissipated as heat, increasing the internal energy of the fluid. The smallest eddies follow changes in flow direction most closely, and are more likely to be isotropic [Heywood, 1987].

Most of the initial turbulence is generated by the jet-like intake flow, which flows past the intake valve during induction, even though the level of turbulence decays during compression. The width of the jet-like intake flow approximates to the intake valve lift.

The radial and axial components of the intake jet flow are an order of magnitude greater than the piston speed, causing large shear stresses between the intake jet flow and cylinder charge-air, creating eddies and turbulence. The difference between the velocity of the intake jet and piston, causes the jet to impinge on the piston face and break up, creating further turbulence.

2.5.2 Characterisation and sizes of turbulence

Characterisation of turbulence

Turbulence is characterised by mean flow velocity, velocity fluctuation about the mean velocity, and length and time scales of the decaying vorticies/eddies. Characterisation is difficult because there are both cycle-to-cycle variations in the mean flow velocity and structure, as well as turbulent fluctuations about the mean flow velocity [Heywood, 1987].

Figure 2.31 below, illustrates the difference between measurement of actual velocity for a single engine cycle, the individual cycle mean, and the ensemble averaged velocity (over many engine cycles) [Reynolds, 1980].

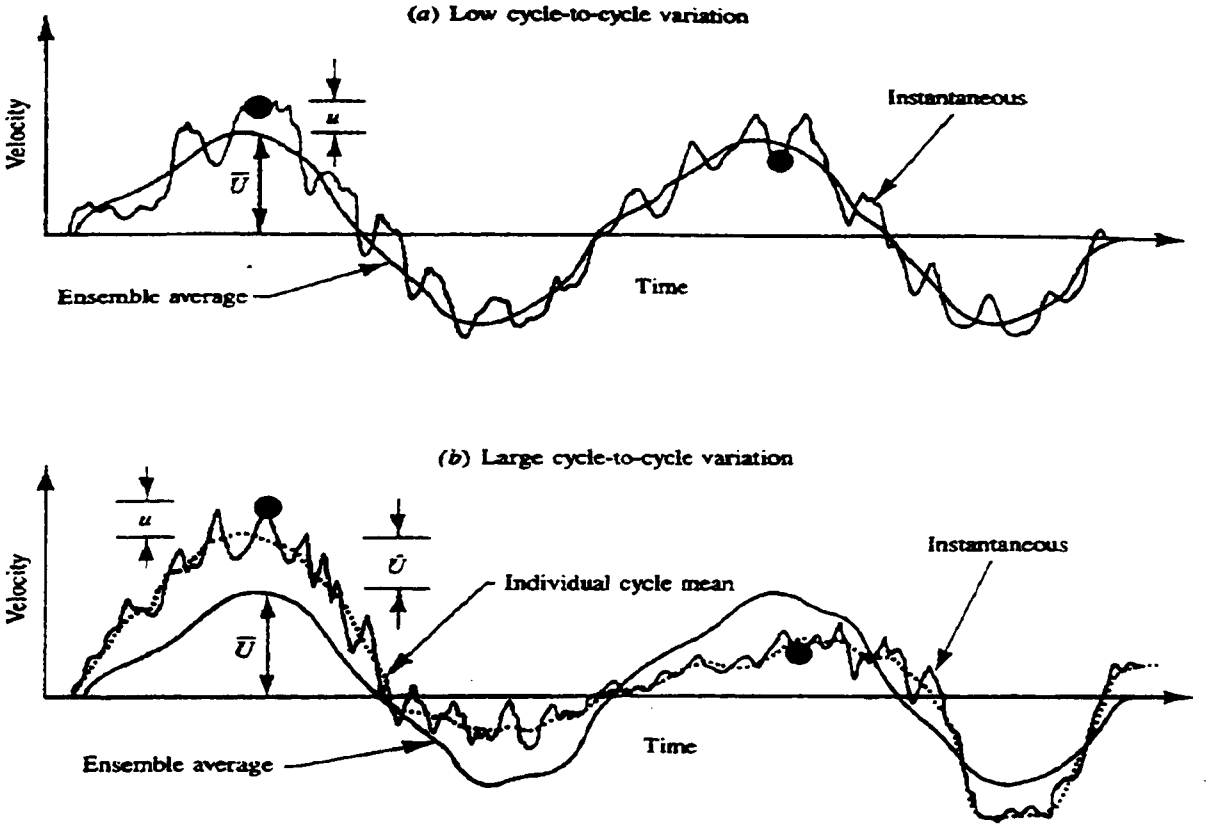

Figure 2.31 LDV measurements of instantaneous velocity, at a fixed position in an engine cylinder, during two complete cycles. Dots on the instantaneous velocity trace indicate actual measurements during the engine cycle. The dotted line is the mean of the instantaneous results from the two complete cycles. Ensemble averaged results over a large number of cycles is shown by the smooth solid line [Reynolds, 1980].

Turbulent fluctuation is the difference between the instantaneous velocity at a particular crank angle, and the individual cycle mean at that crank angle position. It is the high frequency velocity fluctuations that are termed turbulence, whereas the low velocity fluctuations, between the individual cycle mean and ensemble averaged velocity, correspond to variations in the mean flow. Turbulence intensity is defined as the ensemble averaged rms of the turbulence, at a particular time in the engine operating cycle.

Turbulent length scales

Only limited results are available describing turbulent length and time scales in real engines (typical values are detailed in a future section). The largest eddies are limited by the system boundaries, ie. the cylinder wall, cylinder head and piston face, whilst the smallest eddies occur at a molecular diffusion level [Heywood, 1987].

The three main length scales used to describe turbulence are summarised below:

(1) The integral scale (Li), is a measure of the largest scale structure (if velocity measurements in the flow are made at a distance less than the integral scale, the velocities recorded will be the same). These low frequency fluctuations in the velocity of flow are formed by distortion of the fluid.

(2) The second scale for characterising turbulence is the Taylor microscale (Lm). The Taylor microscale can be interpreted as the spacing between the smallest eddies. This is often called the sub-inertial range. Eddies in this range provide the medium for transfer of energy from large scale eddies, to small scale eddies, and as such exist only as long as there are large scale eddies to decay. The inertial sub-range is approximately proportional to $-5/3^{th}$ power of the wave number (defined by equation 2.6) [Saito et al, 1986].

(3) The smallest length scale is the Kolmogorov scale (L_k). It is at this level that viscous forces caused by shear in the fluid, dissipate fluid turbulent kinetic energy as heat. Turbulence on this scale is commonly referred to as small eddies.

An example of the turbulent length scales that exist during the induction stroke, are indicated in figure 2.32 below [Stone, 1992]. The intake jet-like flow generated during induction has a velocity many times greater than the piston speed, causing high fluid shear and turbulence generation.

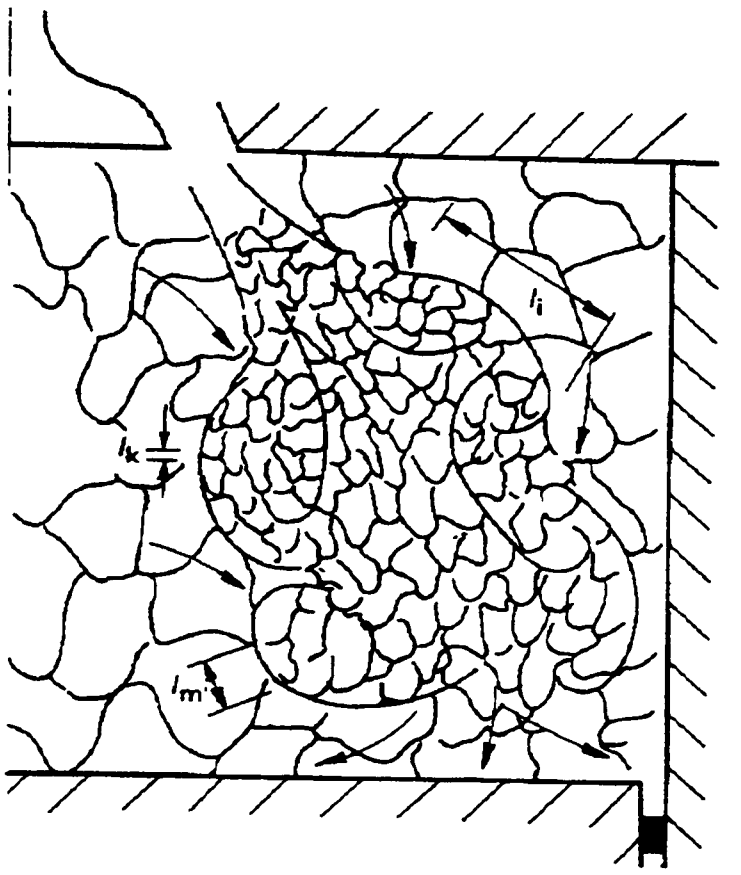

Figure 2.32 Turbulence generation during the induction stroke, showing the three turbulence length scales which characterise turbulent flow [Stone, 1992].

Turbulent time scales

Whilst turbulent length scales are well defined mathematically, they are difficult to measure in motored and firing engines. For this reason, the integral time scale of turbulence (defined as a correlation between two velocities at a fixed point in space, but separated in time) is measured and related to the integral length scale [Heywood, 1988].

However, the wave number can be used to indicate the length scale of turbulent energy. Graphs of turbulence intensity versus wave number, show the distribution of

turbulence within the cylinder. Wave number, k, is defined in equation 2.6 [Suzuki, 1997]:

$$k = {2\pi n_t}/{\overline{U}}$$

Equation 2.6 Calculation of turbulent wave number, k. Where n_t = frequency of turbulent fluctuation in the airflow, and $\overline{U}$ = mean velocity of the air in the cylinder (m/s) [Suzuki, 1997].

2.5.3 Measurement of turbulence

The measurement of turbulence is subject to different definitions and techniques, and it is also subject to cycle-to-cycle repeatability and randomness. For these reasons, statistical methods are used to analyse data collected from a large number of engine cycles, at a particular engine operating condition and position in the 4-sroke cycle (for example at a fixed crank angle, every firing stroke).

In-cylinder turbulence has been measured using HWA, but the most popular method is currently to ensemble average (or sometimes called phase average) data from LDA experiments of in-cylinder flow. In this process, the flow velocity is recorded from many cycles, and then averaged to give an 'ensemble averaged' velocity as a function of crank angle, at the measurement position in the cylinder. Ensemble averaged velocity data is often formed from results of velocity measurements at just one point in the cylinder (especially true for LDA/LDV measurement techniques), and is unlikely to be representative of the complete flow field considering the bulk flow distribution.

Pulsed laser sheet optics such as particle tracking can be used to obtain a true picture of flow at a given time, using a laser sheet through the area of interest. Particle Image Velocimetry (PIV) is currently the most powerful technique for flow visualisation, enabling analysis of 2D and 3D flow fields from a single engine cycle using high-speed copper vapour lasers [Maly, 1988].

2.5.4 Turbulence in DI diesel engines

Turbulence generation during the intake stroke

It is generally thought [Arcoumanis et al, 1982] that intake generated flow controls initial turbulence generation, but in low swirl engines this has all but decayed by the end of induction. Many researchers have reported decaying swirl after inlet valve closure and during compression [Arcoumanis et al, 1994]. However, careful design of the intake port can enhance intake-generated turbulence, some of which may persist to affect fuel/air mixing and combustion.

A sophisticated intake port shape, was developed by Hino Motors (named HMMS, see figure 2.33), in which the main airflow and sub-stream airflow are combined to increase small scale turbulence, due to the velocity difference between the two air-streams.

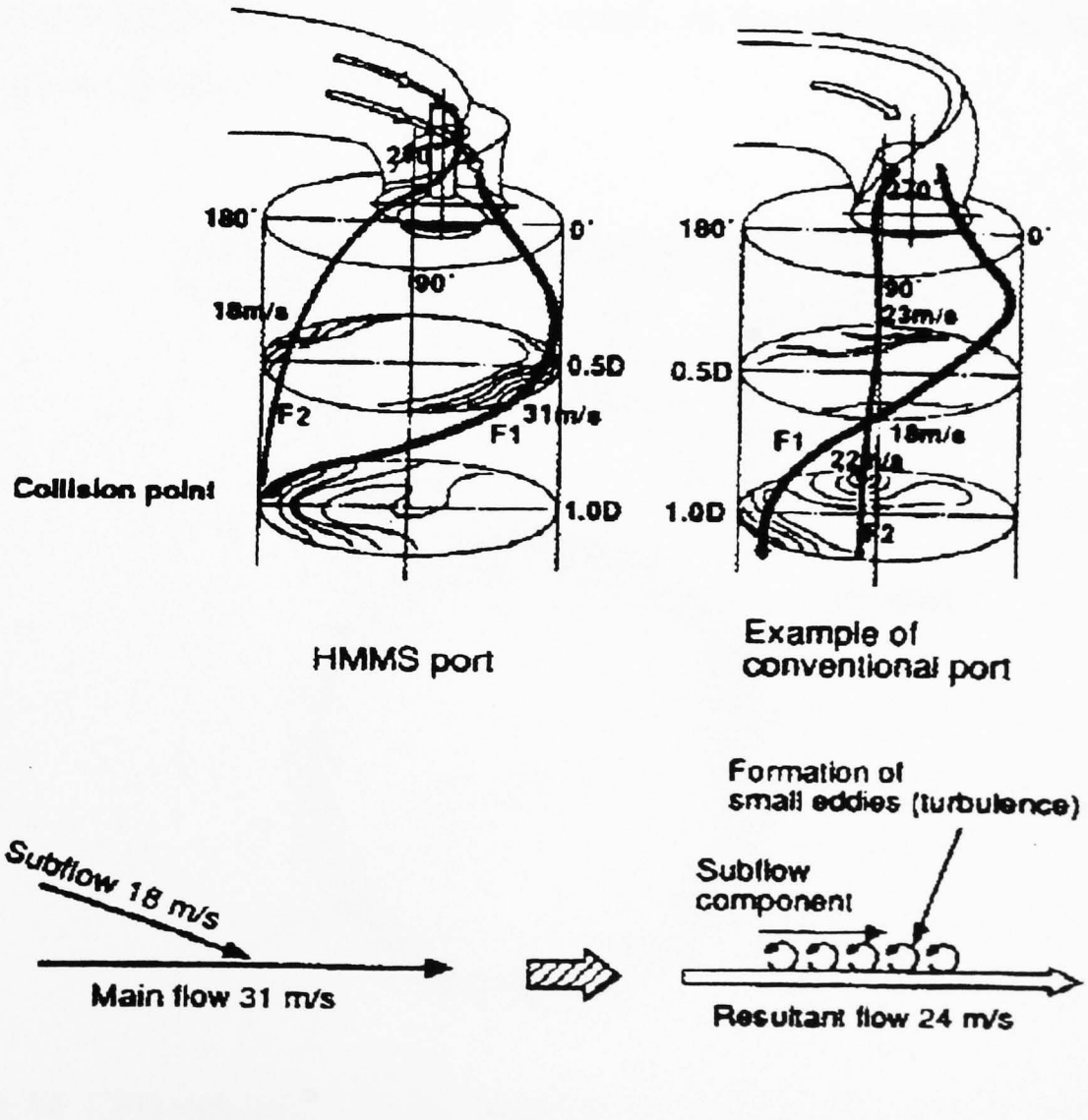

Figure 2.33 Comparison of an HMMS port (designed to promote intake-generated turbulence) and a conventional port design. The main and sub-stream flows, which are

combined to generate turbulence in the HMMS design are clearly shown [Suzuki, 1997].

Turbulence near TDC of the compression stroke

Many authors' opinions do not converge on the form of turbulence near the end of compression, and in particular whether the flow is homogeneous (ie, uniform) and isotropic (ie, independent of direction) is not well defined. This is unfortunate because it is the character and magnitude of turbulence close to TDC, and in particular during fuel injection and combustion, that is most important as it influences fuel/air mixing.

However, LDV measurements by Arcoumanis et al (1994), Ikegami et al (1987) and McKinley et al (1988), do indicate almost isotropic and homogeneous turbulence near TDC before injection, with the exception of the bowl centre where some fluctuation occurs [Arcoumanis et al, 1994]. One example of the turbulence distribution near TDC is shown in figure 2.34 below.

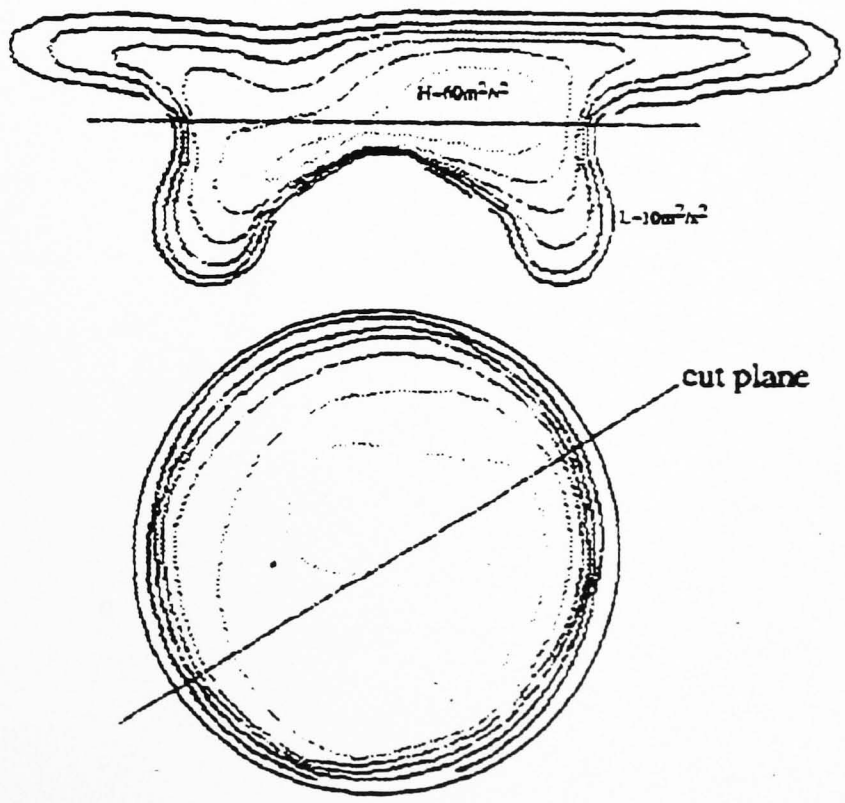

Figure 2.34 CFD simulation results using the KIVA code, from a re-entrant, torodial, bowl-in-piston combustion chamber. Contours of constant turbulent kinetic energy, indicate a concentration of turbulence towards the bowl centre, and asymmetry of turbulence field within the bowl [Zolver et al, 1997].

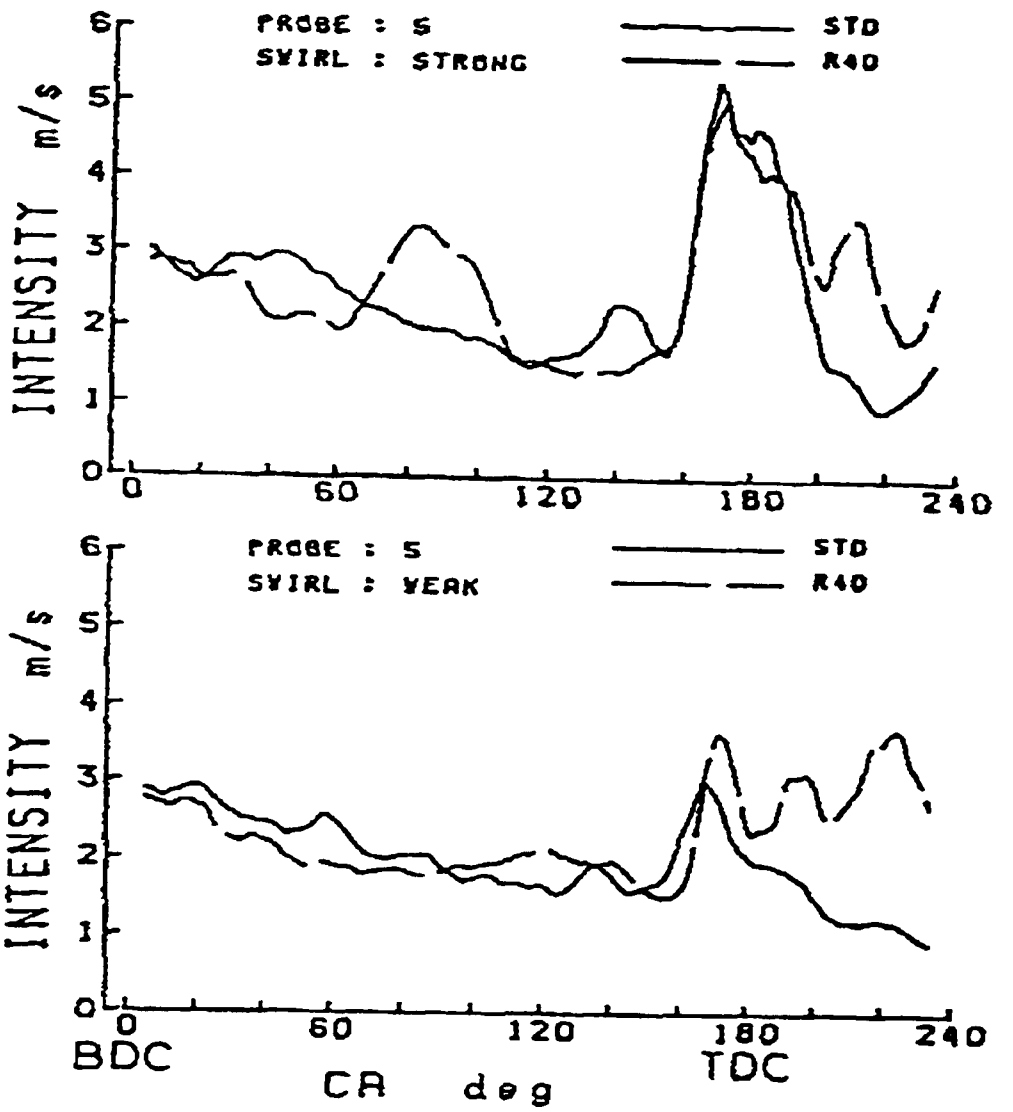

Figure 2.35 Comparison of an open bowl-in-piston (STD), with re-entrant bowl (R40) turbulence intensity during compression. Two different swirl cases are presented. Higher squish promoted by the re-entrant bowl design increases turbulence intensity [Saito et al, 1986].

The corresponding turbulence energy spectra, for the three piston bowl shapes tested (bowl STD, R40 and an additional bowl, DEEP) are shown in figure 2.36 below [Saito et al, 1986]:

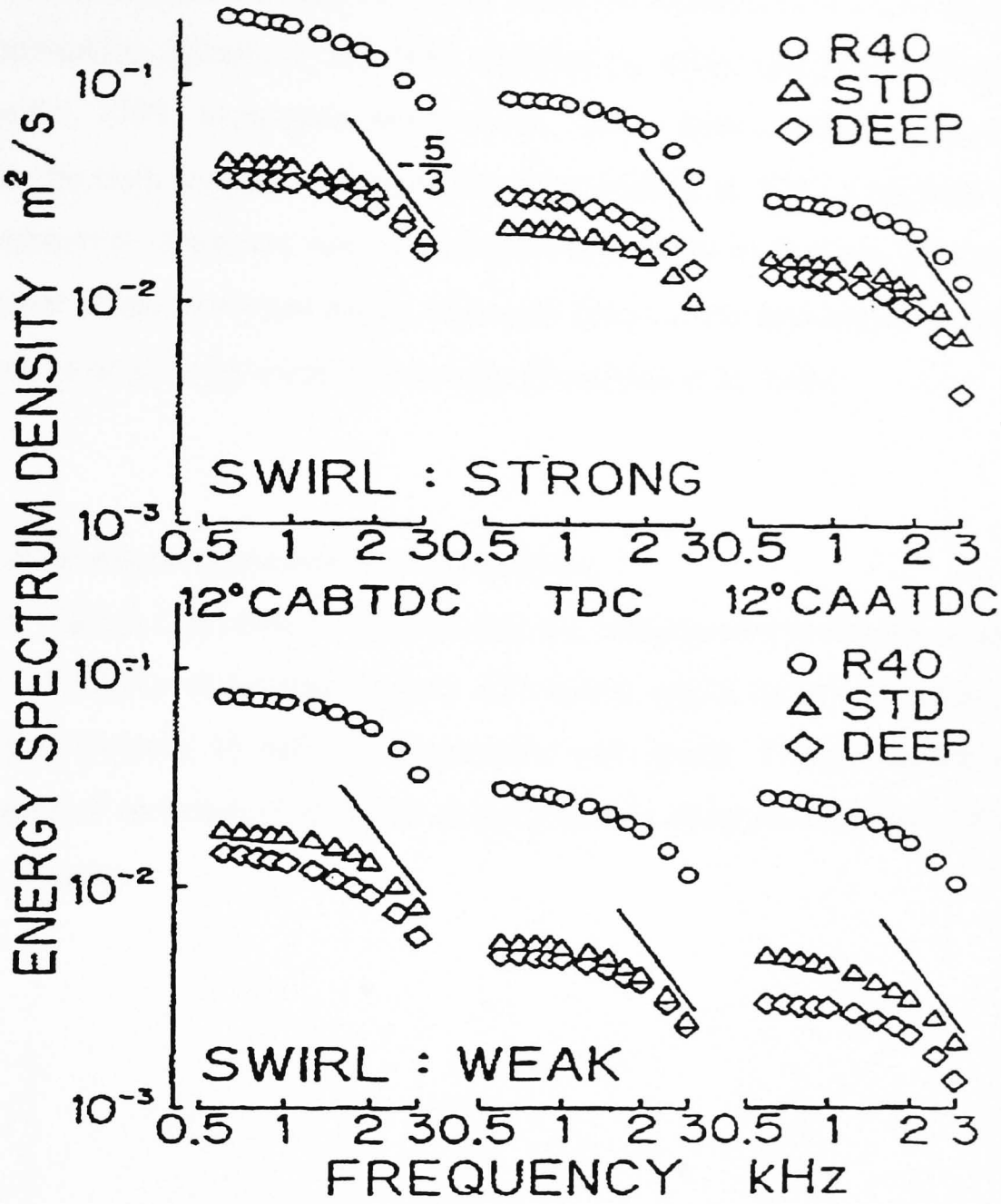

Figure 2.36 Comparison of turbulence scale distribution for three different bowl shapes. Bowl 'DEEP' is an open bowl design with small aspect ratio and large squish area (squish area is between the STD and re-entrant bowl types) [Saito et al, 1986].

The re-entrant design has significantly higher turbulence than the other bowl shapes tested. This increase occurs throughout the crucial range of engine crank angles, from fuel injection to early combustion. The turbulence energy spectra decays approximately according to the Kolmogrov –5/3 power law, indicating locally isotropic flow in the bowl-in-piston combustion chambers.

The increase in turbulence near TDC as a result of squish flow with re-entrant bowl design combustion chambers, has been reported by many researchers [Tindal et al, 1982; Fansler, 1993; Monaghan and Pettifer, 1981]. Fansler (1993) also reports an increase in the high frequency component of turbulence at TDC. Four-lobe bowl-in-piston combustion chambers have been shown to increase turbulence. This is because their irregular shape generates eddies, although this is at the expense of the bulk swirl ratio, which must give up some of its energy [Belardini et al, 1989].

Effect of other engine parameters on turbulence

Turbulence intensity at close to TDC during the compression stroke has been shown by Liou et al (1984), to increase linearly with speed, whilst Bopp et al (1986) reports only a slight increase in turbulence intensity with speed. The turbulence intensity (from a range of sources) of different engine types is show as a function of speed in figure 2.37 below.

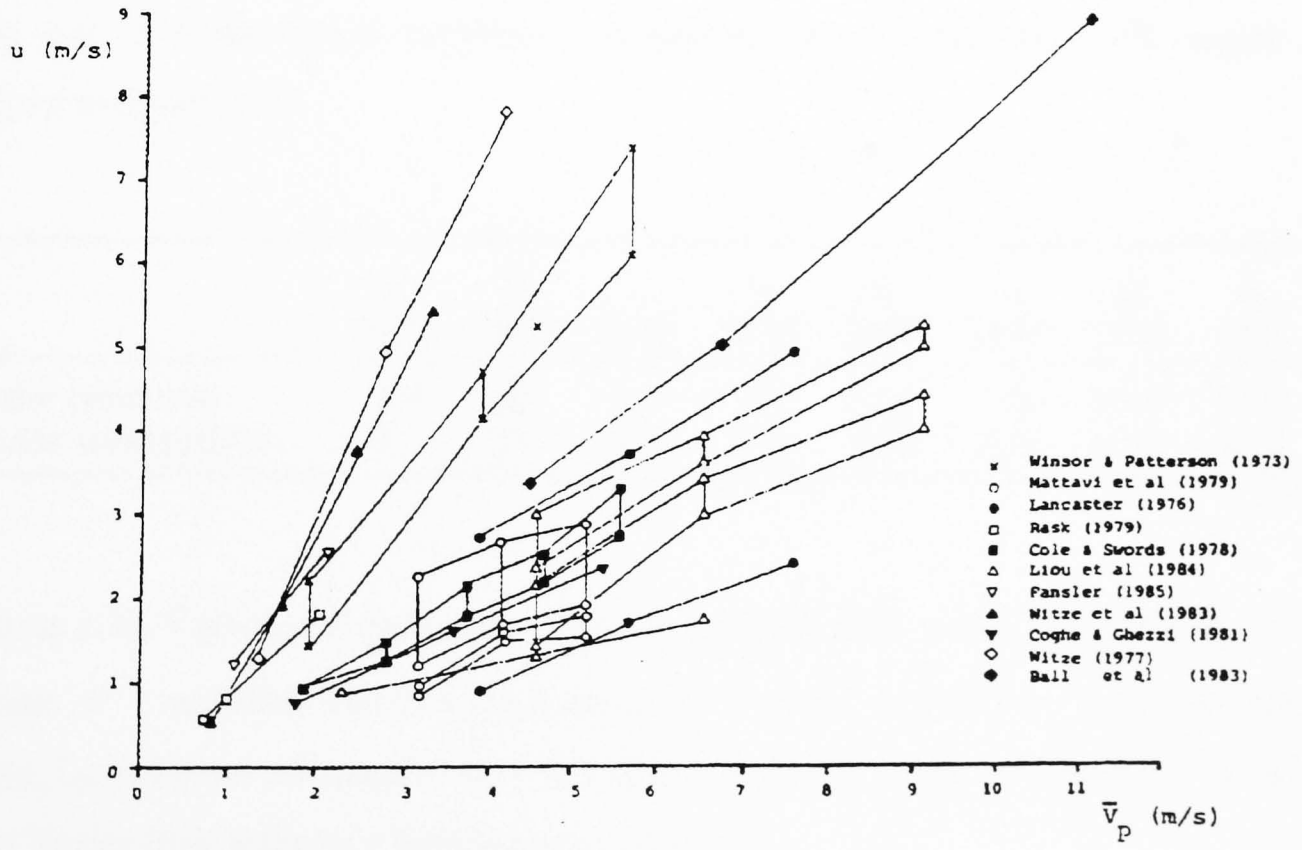

Figure 2.37 Results of turbulence intensity from many researchers, showing the relationship between turbulence intensity near TDC and mean piston speed. Where u = turbulent velocity fluctuation, $\overline{V}_p$ = mean piston speed [Bopp et al, 1986].

The graph (in figure 2.37) shows an approximately linear relationship between engine speed and turbulence intensity. This result is supported by many other researchers, and widely acknowledged [Zolver et al, 1997; Ikegami et al, 1987]. There are significant differences between the constant of proportionality for different engine configurations. This is mainly due to the measurement of ensemble average rms velocity, which in some cases includes the cycle-by-cycle variation in mean velocity, as well as turbulence intensity.

Turbulence is further enhanced by fuel injection, producing large-scale velocity fluctuations in the region of the fuel spray [Zhang et al, 1993]. It is the interaction between airflow, and the high velocity fuel jets that causes turbulence intensity to increase [Zolver et al, 1997]. Later combustion is thought to enhance turbulence significantly [Spicher, 1987].

Typical turbulent length and time scales

The size of some typical turbulence parameters from a motored CFR engine are shown in figure 2.38:

	u' (m/s)	$\bar{U}$ (m/s)	l_i (mm)	l_m (mm)	l_k (mm)	t_i (ms)	t_m (ms)	t_k (ms)
Mid induction	5.0	20	4.0	1.0	0.02	0.4	0.07	0.04
Late compression	15	10	4.0	1.0	0.03	0.8	0.20	0.12

Figure 2.38 Turbulence parameters from a motored CFR engine [Lancaster, 1976]. Where u' = turbulent velocity fluctuation, $\bar{U}$ = mean velocity, L_i = Integral length scale, L_m = Taylor microscale, L_k = Kolmogorov length scale, t_i = integral time scale, t_m = Taylor time scale, t_k = Kolmogorov time scale.

2.6 Piston bowl shape and airflow: effect of fuel spray impingement

2.6.1 Description of fuel impingement

Fuel impingement on the piston bowl sides occurs shortly after fuel injection. The mechanism, and effect of fuel impingement on the piston wall, is not well understood. Fuel impingement is often blamed for poor emissions of smoke and HC in many bowl designs [Kuo et al, 1988; Yu et al, 1980; Matsui and Sugaihara, 1986]. However, some combustion chambers such as the MAN bowl-in-piston design [Neitz and D'Alfonso, 1981], positively exploit fuel impingement to control the rate of combustion.

An indication of the complexity of fuel impingement, and the interaction of fuel jet and piston bowl walls in the swirling airflow, is shown in figure 2.39. Only one spray of the central mounted multi-hole injector is shown for clarity.

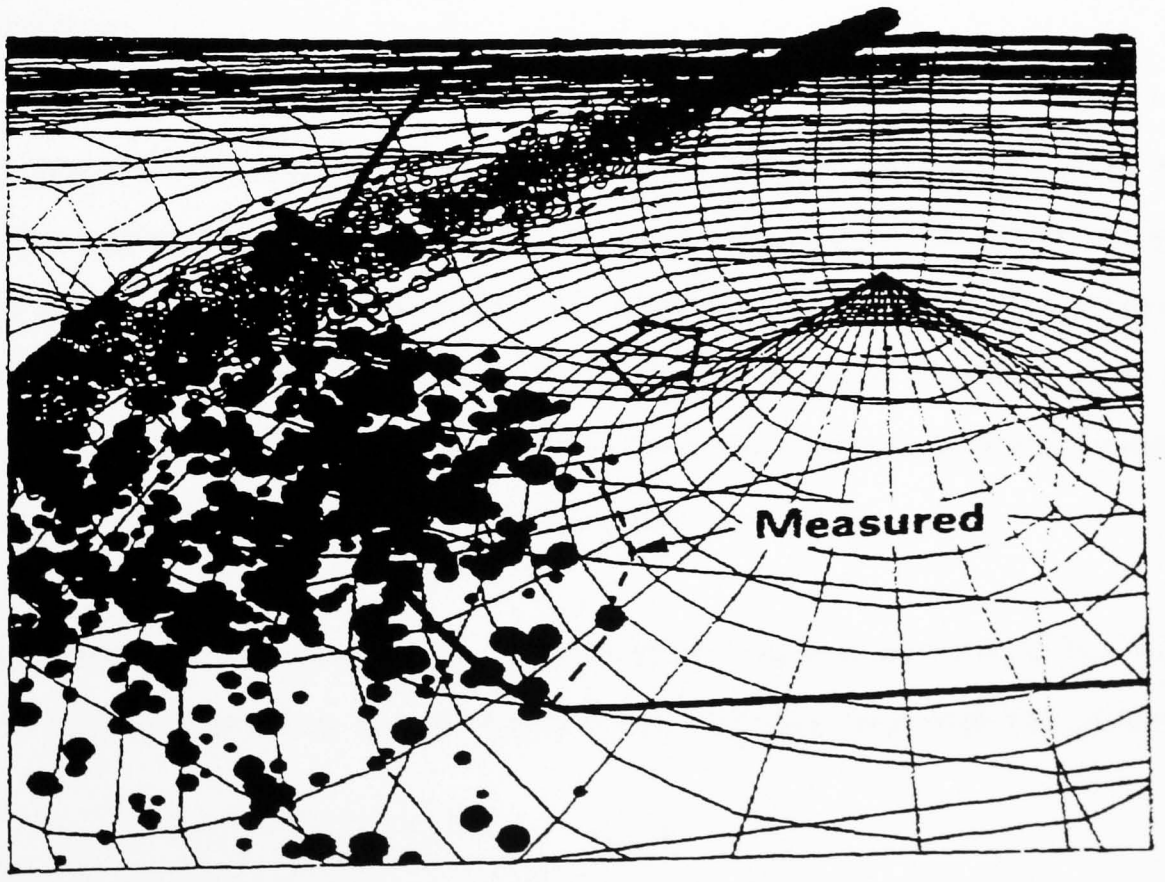

Figure 2.39 Perspective view inside a re-entrant type piston bowl, showing results of KIVA CFD simulation of fuel impingement on the bowl walls. Solid circles indicate

fuel droplets that have already impinged on the piston wall. Circle size is proportional to droplet size. Additional results from engine tests by Werlberger and Cartellieri (1987), are indicated by the dotted line [Naber and Reitz, 1988].

2.6.2 Fuel spray development

Modern high-speed DI diesel engines having four valves per cylinder, inject fuel from a multi-hole fuel injector, positioned at the top-centre of the combustion chamber. Diesel sprays consist of two-phase flow of a gas exterior and a liquid core. The liquid core travels many times faster than the gas exterior, which entrains air and loses momentum.

High-pressure fuel injection creates a high velocity jet, leaving the nozzle with a velocity greater than 100 m/s [Heywood, 1988]. As the jet leaves the nozzle, it becomes turbulent and mixes with surrounding air. The initial fuel that is injected loses momentum rapidly, as air is entrained and accelerated. Injected fuel that follows encounters less resistance to flow, because it passes through already accelerated rich fuel/air mixture.

The fuel penetrates further into the combustion chamber until it too slows, and is replaced by higher momentum injected fuel. As jet penetration proceeds, more air is entrained and the jet diameter increases accordingly. Jet penetration continues until sufficient time is available for fuel/air mixing, atomisation, and evaporation, or the jet encounters a boundary. In modern high-speed DI diesel engines, fuel will impinge on the piston bowl walls before complete evaporation.

It is worth noting that at idle or at very light loads, the tiny amount of fuel injected may have been dispersed or evaporated, prior to impingement with the piston bowl wall.

The schematic diagram in figure 2.40 below, shows the stages in fuel jet growth and penetration.

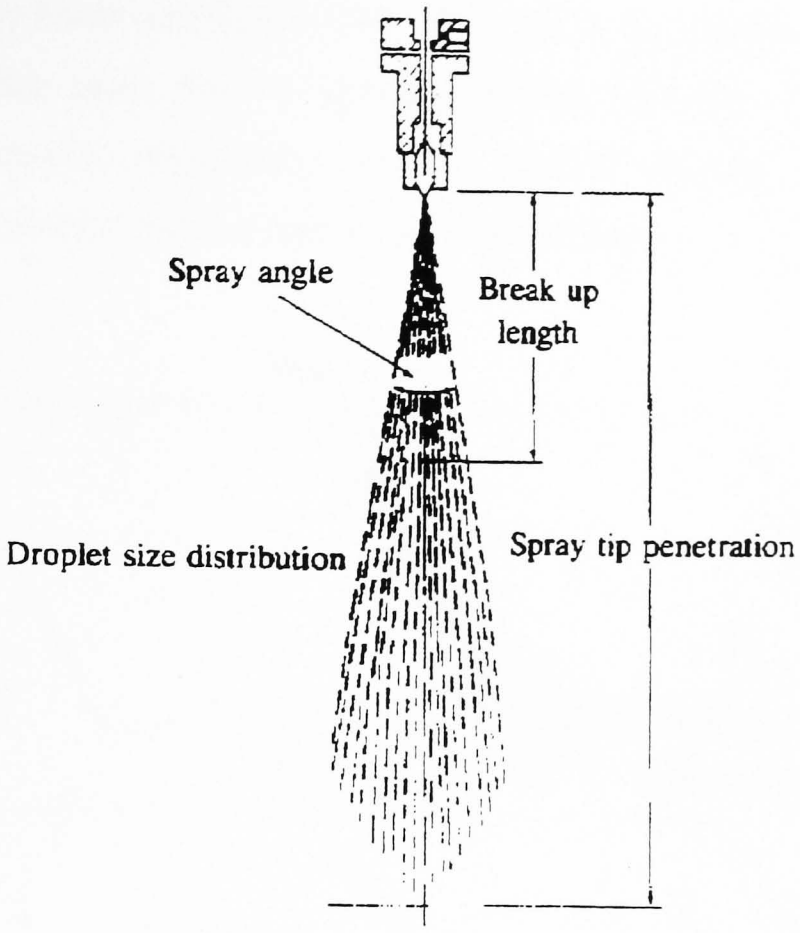

Figure 2.40 Schematic diagram of fuel spray growth and structure [Heywood, 1988].

The maximum spray tip penetration length will not be achieved in modern high-speed DI diesel engines, because of the interaction of the spray with the piston bowl walls. Breakup length is the length at which the liquid spray core is considered to have broken up into droplets of various sizes.

2.6.3 Fuel impingement

Deflection of fuel spray upon impingement

Detailed experimental analysis of droplet impingement is difficult. This has led to the increasing use of computer modelling techniques, and in particular CFD to gain a greater understanding than would otherwise be possible. However, many experimental studies are performed by impinging fuel sprays onto flat plates.

CFD modelling by Naber and Reitz (1988), focused on the spray/wall interaction. The results showed that small droplets approaching the wall (at a small angle) were deflected away from the impingement zone by the wall jet flow, as shown in figures 2.41 a, b, of gas velocity and fuel droplet size respectively

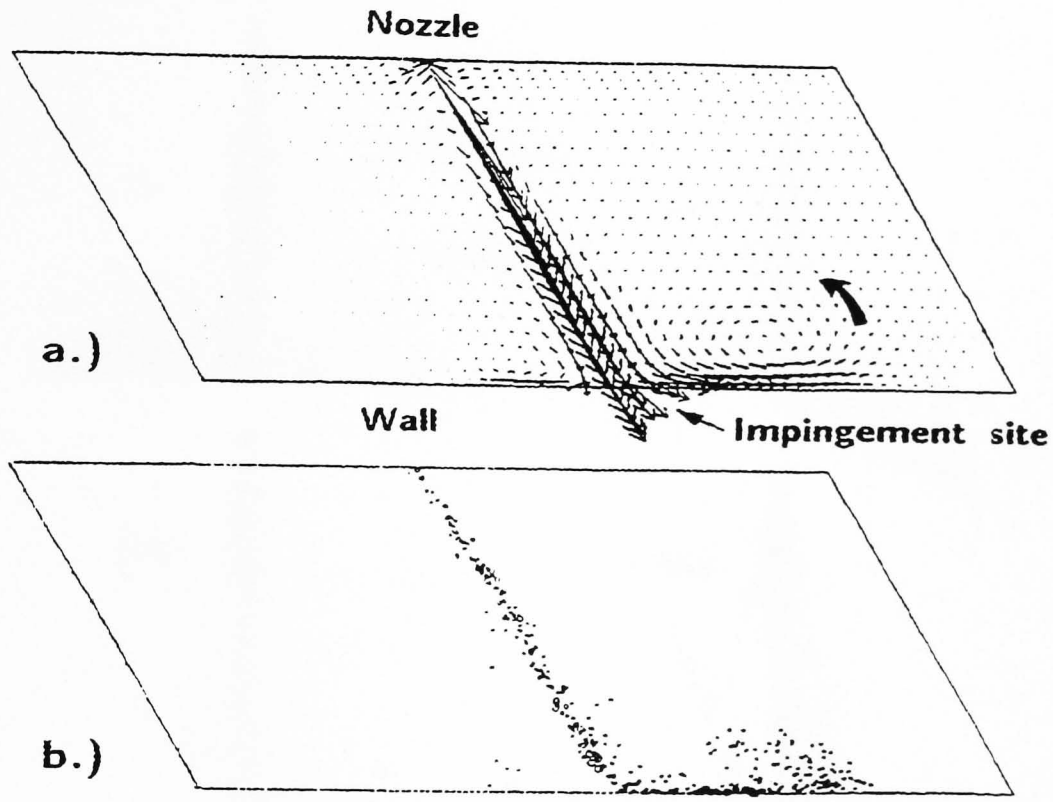

Figure 2.41 (a) Gas velocity vectors viewed in a plane through the fuel injection centre-line. Vectors indicate the magnitude of gas velocity. (b) Droplet size and location, some time after impingement. Circle size is proportional to droplet size. Droplets indicated by solid circles have already impacted upon the piston wall [Naber and Reitz, 1988].

The wall jet flow and re-circulating vortex are clearly apparent in Figure 2.41. Higher momentum droplets are not deflected by the wall jet flow, and impact on the 'piston' wall, moving along to form a liquid wall jet. Smaller droplets are deflected away, and entrained in the re-circulating vortex. Impingement generates considerable turbulence, which would enhance mixing and the rate of combustion.

Effect of the angle of fuel impingement on spray deflection

The angle of fuel impingement significantly modifies the spray envelope upon impingement. Figure 2.42 shows how the interaction between the piston wall, and impinging spray, reduces as the angle of impingement becomes more oblique.

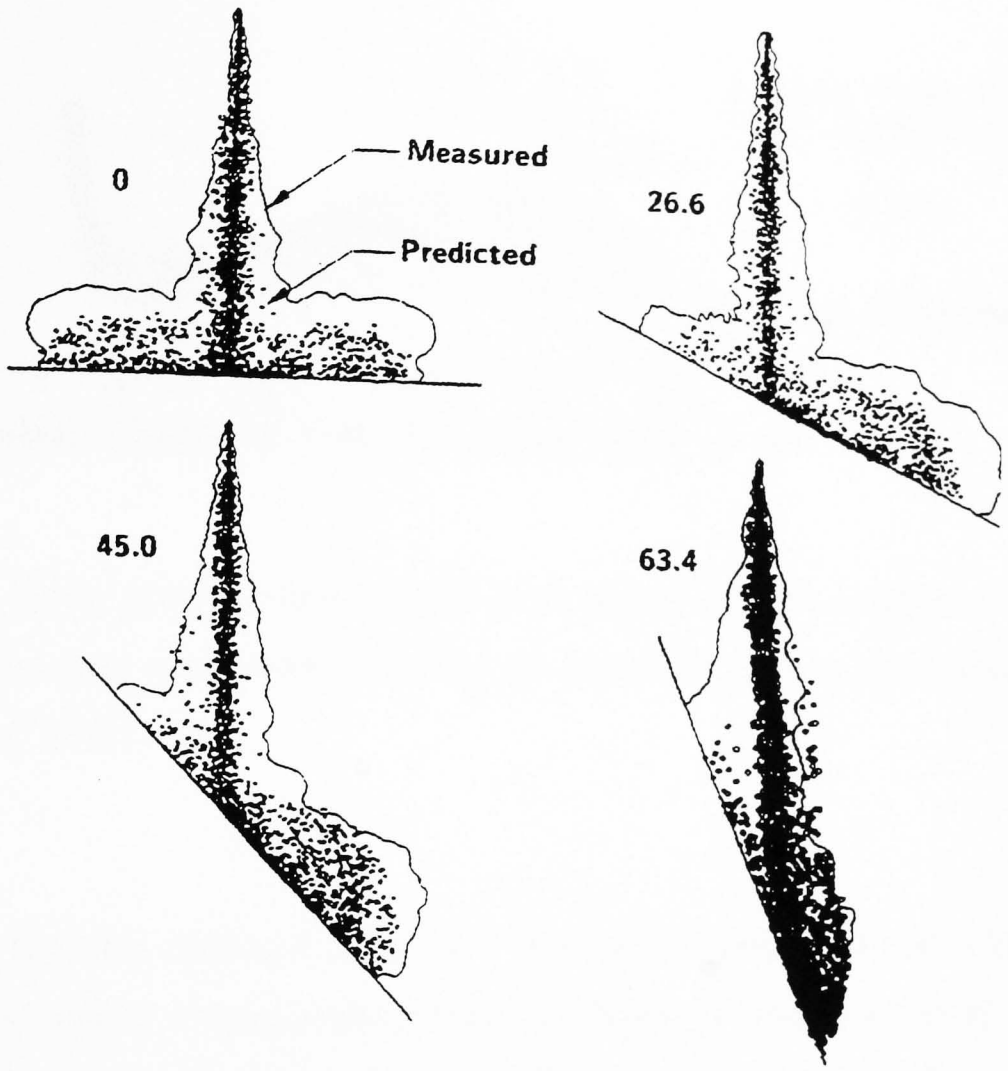

Figure 2.42 Effect of the angle of fuel impingement, on spray and wall jet development. Solid circles indicate droplets which have already impinged on the flat wall [Naber and Reitz, 1988].

The proportion of fuel remaining on the wall, forming a liquid fuel jet, increases as the angle of impingement becomes more oblique. This has significant implications for the design of the impingement area in the bowl-in-piston.

2.6.4 Wall jet flow development

A flat wall impingement study by Naohito et al (1989), shown in figure 2.43, indicates how the growth of the spray on the wall changes with time.

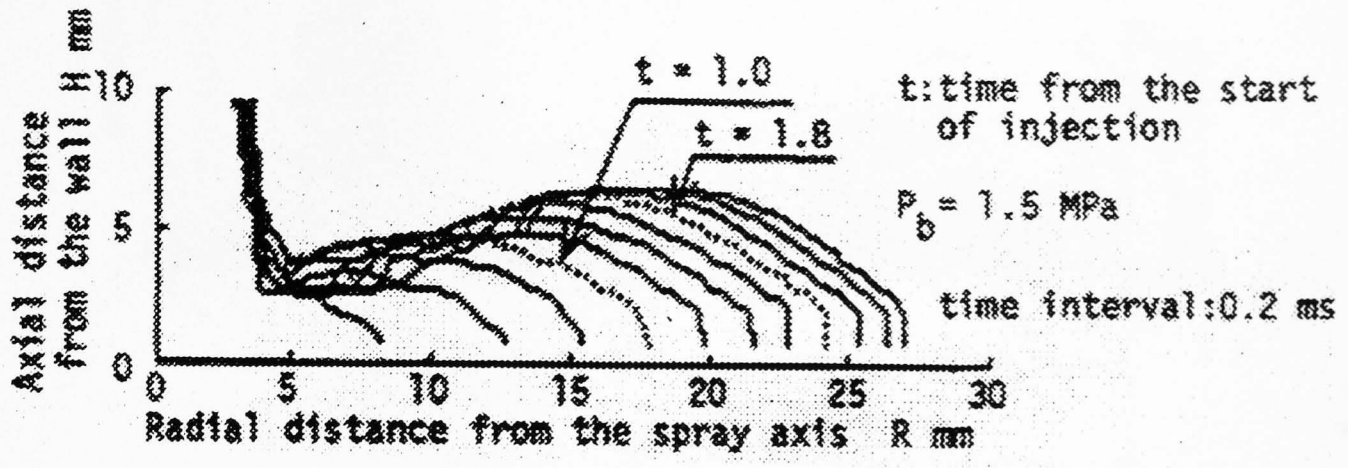

Figure 2.43 Spray growth reconstructed from scattered light images of impinging spray on a flat plate. Successive contours are spaced equally in time steps of 0.2ms [Naohito et al, 1989].

Initially, the normally impinged spray (see figure 2.43) takes on a disk like shape (or an ellipse for oblique impingement angles, according to Fujimoto et al, 1990), but then fuel impinged at the edges moves away from the wall. The rate of propagation of the outer edges of the impinged spray also reduces, indicating the spray slows as more air is entrained. The liquid fuel wall jet has greater momentum and continues to propagate along the wall, displacing lower momentum spray.

The distance from the injector to the wall, has little effect on the shape and structure of the impinged spray, as the central liquid spray core from fuel injection maintains its momentum regardless of spray length [Katsura et al, 1989]. Similarly, if injection pressure is increased, spray momentum increases, and the impinged spray and wall jet grow faster.

A schematic diagram of an impinging diesel fuel jet, normal to a flat wall in figure 2.44 below, shows the main features and structure of the impinged spray.

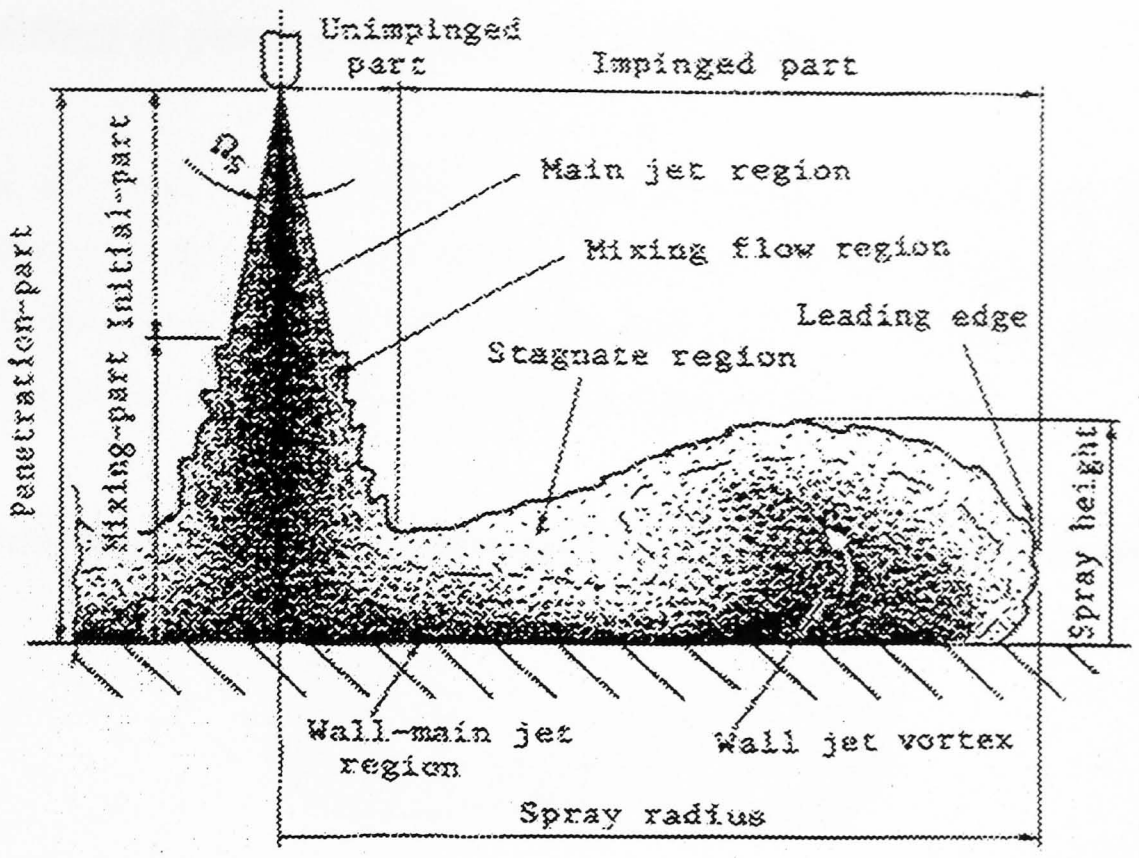

Figure 2.44 Schematic diagram of fuel impingement, normal to a flat plate, based on results of spray visualisation studies [Katsura et al, 1989].

The majority of the spray impinges before atomisation, but after jet break-up. Some mixing occurs at the edges of the spray. Upon fuel impingement, the wall jet is formed, and moves outwards from the point of impingement. The droplet density and momentum in the wall jet is large. Droplet density is highest at the periphery and stagnation regions of the spray [Katsura et al, 1989; Suzuki et al, 1993], as well as near the wall and impingement point [Fujimoto et al, 1990]. However, the momentum of droplets in the vortex and stagnation region is reduced.

Zone distribution of equivalence ratio exists in the impinged spray, and mirrors droplet density as expected. High concentrations occur at the point of impingement and stagnation areas either side of the spray. Equivalence ratio distribution is substantially modified for oblique angles of spray impingement, with a large re-circulating and stagnation region downstream of the impingement point [Hiroyasu et al, 1990].

2.6.5 Effect of piston bowl shape on wall jet flow

Modern DI diesel engines having re-entrant bowl-in-piston combustion chambers, cause the impinged wall jet to be swept down the torodial radius, and eventually towards the central bowl pip. This is indicated in figure 2.45 below, showing fuel impingement and wall jet flow in a section through the piston bowl.

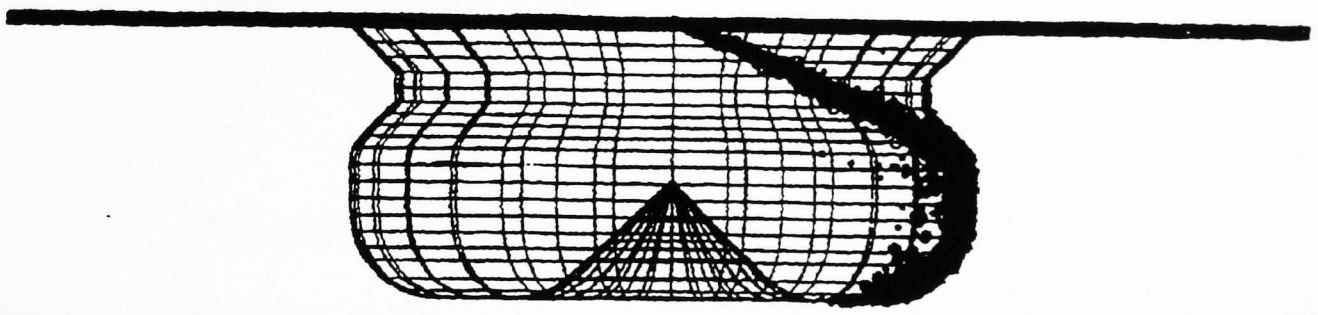

Figure 2.45 CFD simulation (using the KIVA code) of fuel impingement in a section through the piston bowl. Solid circles in the diagram indicate fuel droplets which have already impinged on the piston wall. Circle size is proportional to fuel droplet size [Naber and Reitz, 1988].

Wall jet flow down the side of the bowl, in this low swirl case, is evident. The wall jet flow consists primarily of heavy fuel droplets that have already impinged on the piston wall. Smaller droplets are deflected away from the wall, and will quickly vaporise to within combustible limits and be consumed.

2.6.6 Effect of swirl on wall jet flow

Upon fuel impingement, the wall jet film and vapour are dispersed away from the point of impingement, in a direction depending on the angle of impingement, geometric profile of the piston bowl, and bulk air motion. Hydraulic analogue experimentation of injection and impingement of 'fuel', in swirling and quiescent conditions, is shown in figure 2.46 and 2.47 below [Packer et al, 1985].

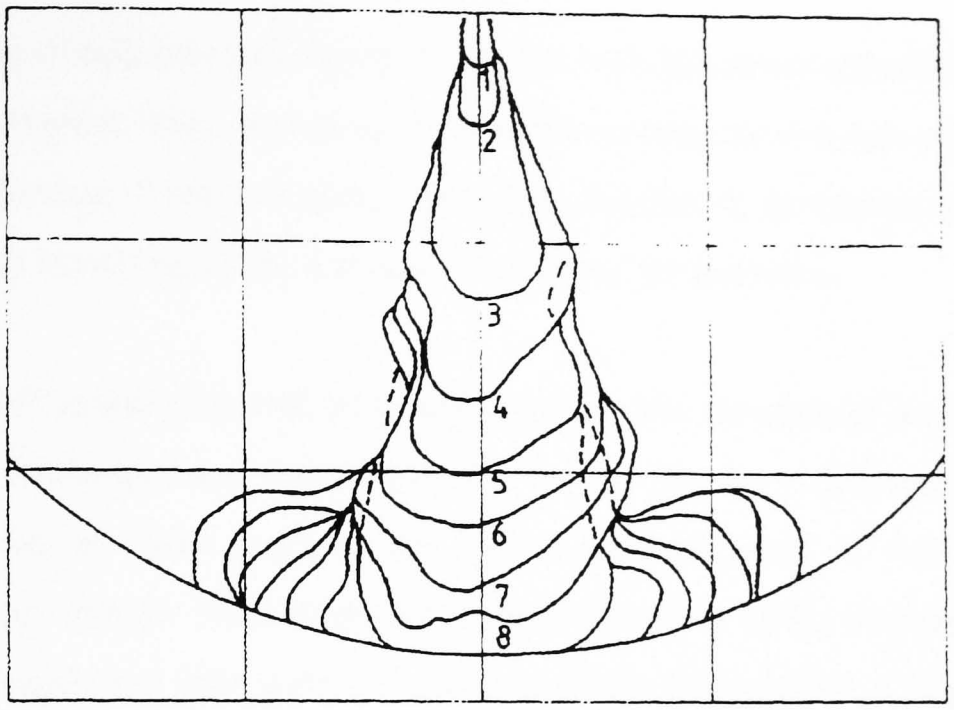

Figure 2.46 Hydraulic analogue experimentation of fuel injection and impingement, in quiescent conditions. Contours indicate the periphery of the spray (constant equivalence ratio of 25:1) at successive time frames [Packer et al, 1985].

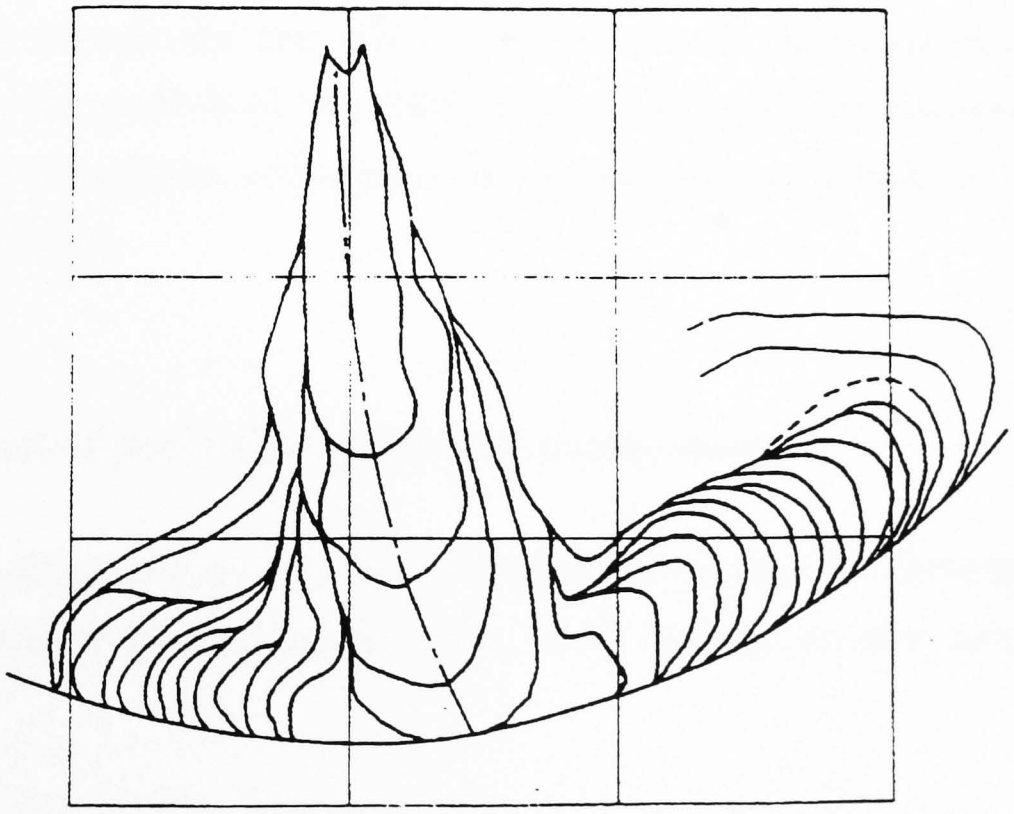

Figure 2.47 Hydraulic analogue experimentation of fuel injection and impingement in swirling conditions. Contours indicate the periphery of the spray (constant equivalence ratio of 25:1) at successive time frames [Packer et al, 1985].

Under swirling conditions (see figure 2.47), the wall jet moves around the simulated combustion chamber wall, increasing the fuel/air mixing rate and rate of evaporation. Progressive slowing of the fuel spray, from fuel injection to movement of the wall jet is evident from bunching of the contours of constant air/fuel ratio.

Increasing swirl spreads the wall jet over the wall in the direction of swirl [Naber and Reitz, 1988; Welberger and Cartellieri, 1987]. Wall jets from different nozzles will eventually meet at some point in the combustion chamber, if fuel injection is maintained long enough. Wall jet growth is predominantly on the downstream side of impingement, and very little growth occurs upstream of the point of impingement in the swirling air stream. This increases the area of wall jet exposed to the swirling airflow, and the surface area in contact with the hot bowl walls. This results in a reduction in the ignition delay period, but the rate of evaporation of fuel from the wall jet and rate of combustion increases [Acroumains and Chang, 1992].

Swirling air changes the distribution of droplet size and momentum of droplets that impinge on the piston bowl wall. Only larger droplets that have not evaporated, and have higher momentum, will impinge on the wall to form the wall jet [Arcoumains and Cutter, 1995].

2.6.7 Effect of fuel impingement on combustion

Initial sites of ignition are most common in the vapour cloud just down-stream of the point of impingement [Arcoumanis et al, 1994]. Ignition can also occur under the bowl lip.

Swirl increases the amount of vapour down stream of the point of impingement, because of increased evaporation from the wall jet. This can reduce the ignition delay period, and will increase the rate of subsequent combustion. The wall jet concentrates combustion near the piston wall. This is further enhanced by the centrifuging effect of

swirl, although less fuel will impinge on the bowl wall in high-swirl conditions because of reduced jet penetration and increased rate of evaporation, especially of small droplets.

In-cylinder photographic analysis by Rao et al (1992b), showed that at engine speeds above 2000rpm, the momentum of the swirling air was so high (especially once combustion had started) that the wall jet was completely entrained in the gas flow. Wall wetting only appeared when very high injection pressures were used.

Although much of the previous work of researchers on this topic has been performed at conditions chosen to enhance wall jet flow (for example low engine speed, cool combustion chamber surfaces, short spray path lengths and low swirl ratio's), current work on high speed DI diesel engine fuel injection confirms fuel impingement at almost all operating conditions.

The temperature of combustion surfaces upon which fuel sprays impinge can also affect mixing, combustion and emissions. In general, cool combustion chamber surfaces will reduce the rate of evaporation, and thus fuel/air mixing, whereas hot surfaces may promote combustion and reduce ignition delay. However, some studies have shown that excessively hot combustion chamber surfaces may actually reduce the rate of evaporation [Ueda et al, 1979]. This occurs because a film of fuel vapour or vapour pocket forms between the impinged fuel, and the hot combustion chamber surface, reducing the heat transfer coefficient.

Fuel that has impinged on the bowl wall, burns in a burning diffusion mode. The rate of burning is controlled by the rate of evaporation of fuel from the wall, into the air-stream. Flame temperature increases away from the stagnation point as a higher proportion of vapour is prepared to within combustible limits. The outer regions burn with the most luminous flames. However, the heat flux of impinging sprays is approximately constant across the wall jet, as the increase in temperature radially, is balanced by a reduced heat transfer coefficient [Kamimoto et al, 1982].

2.6.8 Effect of fuel impingement on emissions

Experiments performed in a combustion bomb, to compare impinging and non-impinging fuel sprays by Okajima and Kumagai (1990), showed that very strong turbulence and internal EGR effects were achievable by impinging the injected fuel spray on a flat plate. This increased significantly the rate of combustion, resulting in a reduction of the emission of smoke.

Emission of NOx was also reduced, because of the effect of localised internal EGR. However, Yoshikawa et al (1989) reported an increase in NOx from a series of parametric experiments using different impingement distances (although this resulted in changing other bowl parameters, which may have also affect emissions). Increased NOx could have been due to the increased rate of mixing, caused by impinging the spray on the bowl wall.

HC emissions of impinging sprays depend on the amount of wall quenching. Yu et al (1980), report a marked increase in the emission of unburned HC if the piston wall temperature is reduced by reducing the coolant temperature.

2.7 DI diesel engine emissions

2.7.1 Overview of emissions

Description of the main emissions affecting DI diesel engines

Diesel engines suffer from the emission of harmful products contained in the exhaust gas. The most significant of these are oxides of nitrogen (NO and NO_2, which are collectively termed NOx), particulate matter (of which smoke is a constituent), and to a lesser extent un-burnt hydrocarbons (UHC or HC). Compounds containing sulphur (oxides of sulphur, SO_2, SO_3 and sulphuric acid, SO_4), and the emission of large quantities of carbon dioxide (CO_2), also cause concern. Production of carbon monoxide (CO) is small in diesel engines because of the inherently lean mode of operation.

The pollution caused by each species of emission, varies in severity and quantity of production. The main effects attributed to the emission of CO_2, NOx and UHC are the 'greenhouse effect'. Oxides of sulphur and particulate matter are considered responsible for local urban pollution, and can be carcinogenic.

Reduction of harmful emissions from the exhaust of diesel engines, has become necessary because of the introduction of legislation, following concern of the effect of urban pollution on human health, and global pollution on global warming and the environment. Legislative limits apply to each species of emission depending on the perceived harmfulness. Limits are regularly tightened in line with the anticipated growth of the usage of vehicles, and the need for reducing the overall output of harmful emissions.

Formation of DI diesel engine emissions

Harmful emissions in the exhaust of diesel engines, are greater than that predicted by equilibrium values for the overall constituents obtained from chemical experimentation. This occurs because the rate of combustion in the engine cylinder is too rapid for equilibrium values to be established. During combustion the

concentration of emissions quickly increase, but are then 'frozen' at higher than equilibrium concentrations, as the combustion gases quickly cool during rapid expansion in the power stroke.

Reduction of harmful emissions from diesel exhaust is difficult because of the inherent dependence on the in-cylinder combustion process. Further complications arise because of the conflicts of reducing one emission at the detriment of another, or reducing engine efficiency.

Particulates versus NOx trade-off

The most significant trade-off in diesel engine emissions is that of NOx verses particulates. NOx is predominately formed during pre-mixed combustion, whilst particulates are predominately formed during diffusion burning. Actions which reduce the relative amount of pre-mixed burning (and NOx formation) will increase the importance of diffusion burning (and particulate emissions) and vice-versa. The main aim of modern successful diesel engine design is to improve the overall NOx/particualtes trade-off, whilst maintaining or improving fuel economy.

The development and introduction of catalysts capable of reducing emissions of NOx or particulates, or both, will change the emphasis and operating region of the NOx/particulates trade-off. It is likely that some form of catalyst, suitable for lean operation of diesel engines, will be necessary to meet long term emission legislation. Catalysts of a suitable conversion efficiency, cost and durability for production vehicles are not yet commercially available. For this reason, current DI diesel engine design must focus on reducing the overall NOx/particulates trade-off, and not on one particular emission.

2.7.2 Emissions of oxides of nitrogen (NOx)

Formation of NOx

NOx is formed when nitrogen and oxygen mix at a high temperature, and for sufficient time for reaction. The conditions present during combustion provide such an environment for NOx production. Nitrogen is present in the intake air, and oxygen remains during combustion, because of the inherently overall lean air/fuel ratio, and due to dissociation of CO_2 and H_2O.

NO and NO_2 are collectively called NOx. However, NO is by far the most abundant chemical species of the two, accounting for typically 90% of the total concentration of NOx. Chemical equilibrium at in-cylinder combustion temperatures, suggests that the concentration of NO_2 should be negligible. The existence of measurable quantities of NO_2 in the exhaust (especially when operating at light loads), is thought to be due to quenching of the NO_2 to NO conversion reaction by the cooler intake air [Hilliard and Wheeler, 1979; Merryman and Levy, 1975], or insufficient time for reaction [Hawley et al, 1998].

Effect of temperature on NOx formation

The main factor affecting the amount of NOx produced, is the local temperature at the point of NOx formation. NOx formation is most favourable in the high temperature regions of the burning, and burnt gases, at close to stoichiometric air/fuel ratio's. However, it is the NOx that is formed in the early burned gas which dominates engine-out NOx emissions.

The flame front of combustion is thin (approximate 0.1mm [Heywood, 1988]) due to the high cylinder pressure, and therefore the residence time for NOx formation in the flame itself is small. Subsequent burned gas is compressed by combustion, raising its temperature and pressure up to peak cylinder conditions, and promoting NOx formation. Early burned gases also have the longest residence time in which to approach equilibrium NOx values, before being quenched upon expansion. Slower

engine speeds allow a longer time for NOx formation, and hence produce higher NOx concentrations.

Oxygen for NOx formation is supplied by the intake air. The majority of nitrogen which forms NOx also comes from the intake air, although some fuel compounds containing nitrogen can participate in NOx formation.

The dependence of NO formation on gas temperature and air/fuel ratio is shown in figure 2.48 below [Heywood et al, 1971]. Increasing temperature and lean mixture air/fuel ratio's (high oxygen concentration), significantly increases NOx formation rates.

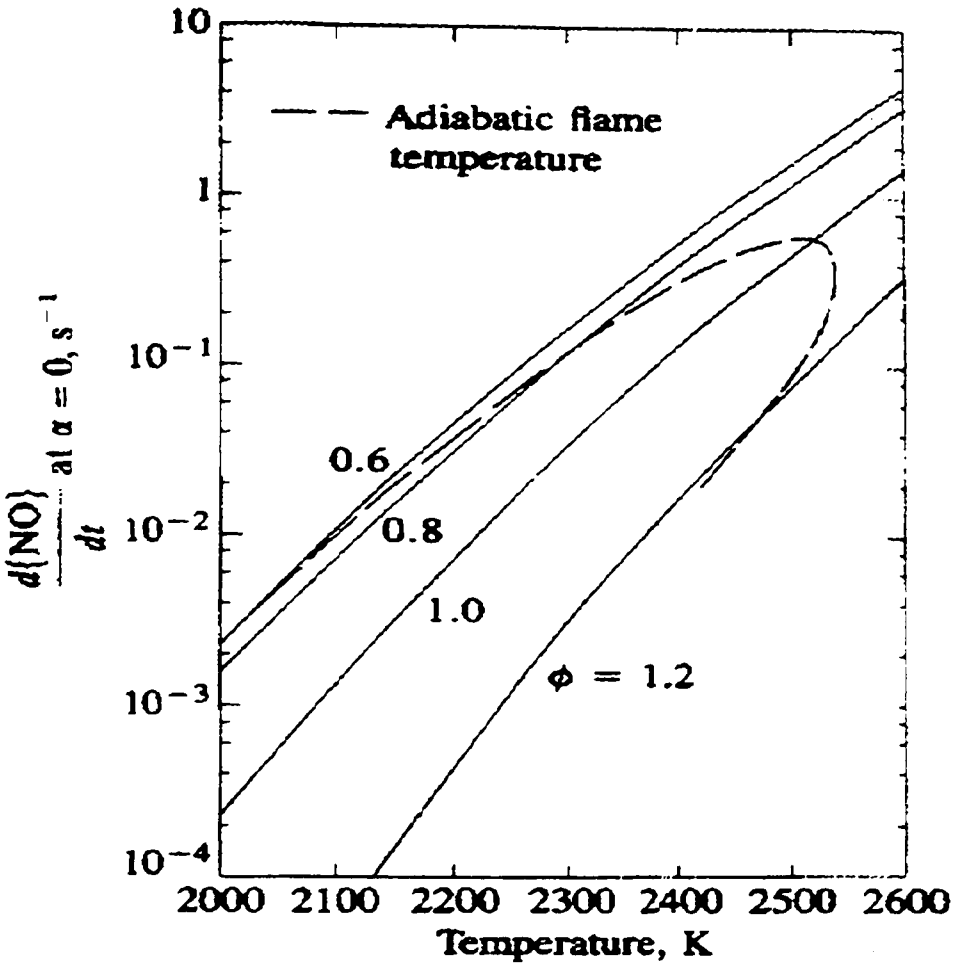

Figure 2.48 Effect of gas temperature on the rate of formation of NO, for a range of equivalence ratio mixtures, at 15 atm pressure. The dotted line indicates the adiabatic flame temperature for a typical hydrocarbon fuel (kerosene) under similar conditions [Heywood et al, 1971].

Mechanisms of NOx formation

The mechanisms of NOx formation are well understood. The Zeldovich mechanism details the three main chemical reactions involved in the formation of NO. The first step is the slowest, and therefore the rate-determining step.

$$O + N_2 = NO + N \quad (1)$$
$$N + O_2 = NO + O \quad (2)$$
$$N + OH = NO + H \quad (3)$$

The rate of formation of NO is the most significant parameter affecting NOx formation, as equilibrium values will not be attained in practice. This is because the reactions are quenched when the combustion gases expand on piston decent, and mixing with cooler gases and surfaces occurs. The rate of formation of NO must be limited to reduced NOx concentration in the exhaust.

The total formation of NO is also strongly temperature dependant. Figure 2.49 shows the calculated total formation of NO, at various temperatures.

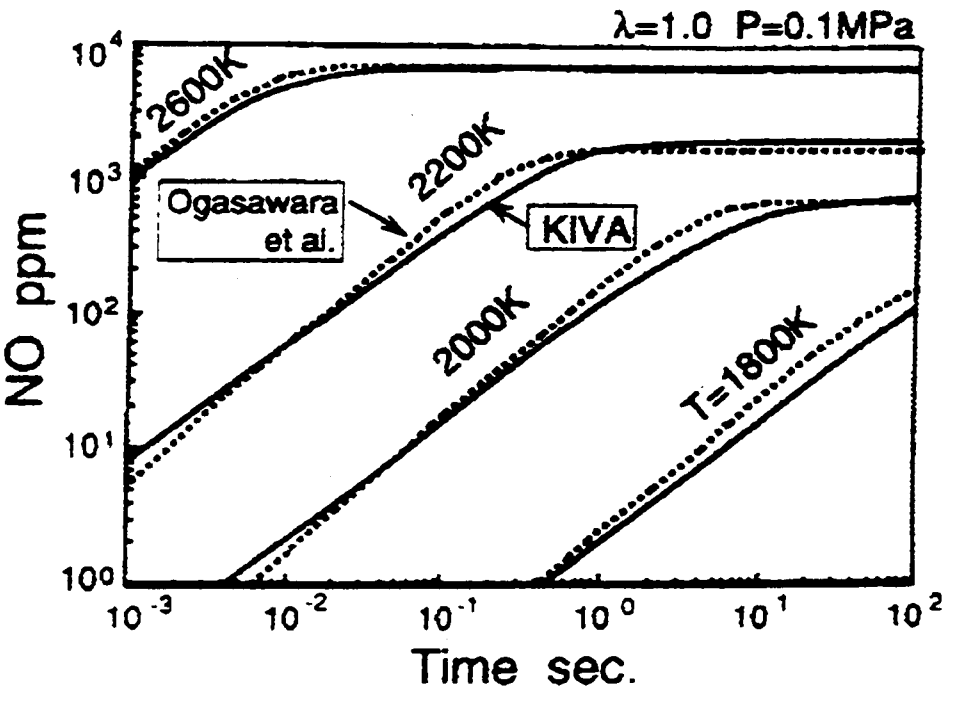

Figure 2.49 Effect of gas temperature on the total formation of NO. CFD combustion simulated results (using the KIVA code) are indicated by solid lines, and compared with experimental results of Ogasawara et al, (1973). Experiment performed at stoichiometric air/fuel ratio, and atmospheric pressure [Chikahisa, 1994].

In practice, in-cylinder conditions do not allow enough time for equilibrium concentrations of NO to be achieved. The NOx concentration within the engine cylinder, as a function of engine crank angle, is shown in figure 2.50 below.

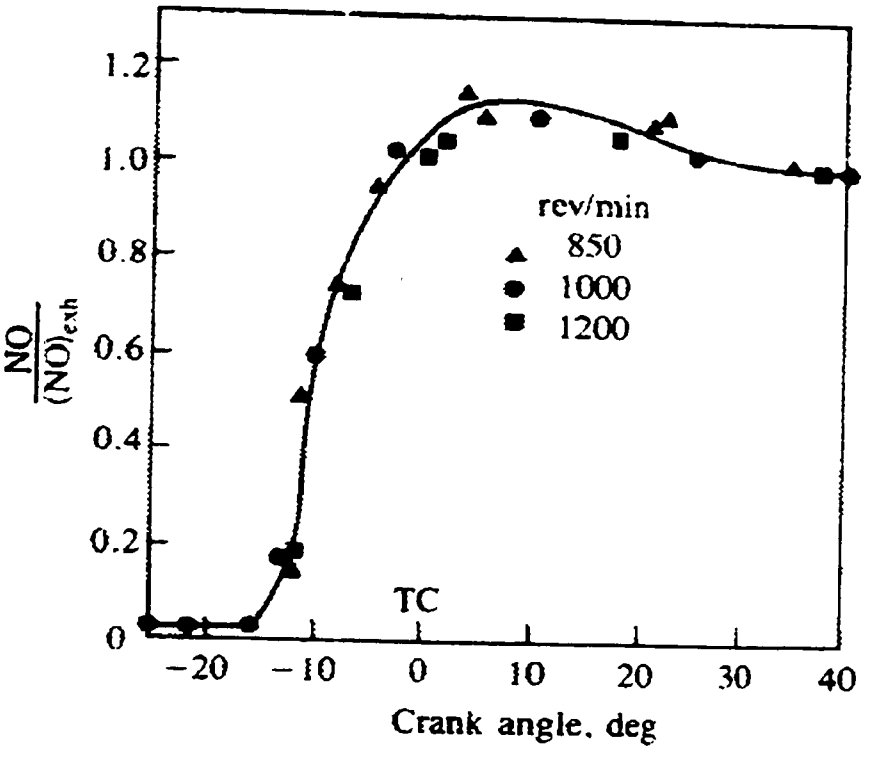

Figure 2.50 Ratio of in-cylinder NOx concentration to exhaust concentration, as a function of engine crank angle for a DI diesel engine [Vioculescu and Borman, 1978].

Upon combustion (see figure 2.50), NOx concentration increases rapidly, but only decays slightly during expansion, as the reactions are quickly frozen. It is important to limit the rate of NOx formation to reduce engine-out NOx emissions.

Effect of ignition timing on NOx formation

Injection timing is critical to the formation of NOx, because it directly affects the peak cylinder temperature and pressure. Retarding of injection timing is used to limit NOx formation, especially for light and medium load operating conditions. However, retarding the injection timing results in an increase in the emission of smoke, and a reduction of fuel economy.

The introduction of common rail fuel injection systems may allow the use of pilot injection for NOx, peak temperature and pressure, and noise control. An investigation into the use of pilot injection showed that NOx could be reduced by up to 25% at light loads, due to a reduction of the ignition delay period [Minami et al, 1995].

Effect of exhaust gas re-circulation (EGR) on NOx formation

The use of exhaust gas re-circulation (EGR) is very effective at reducing the emission of NOx. It causes a considerable reduction of flame temperature and comparable reduction of NOx. EGR increases the heat capacity of the intake charge, and reduces the availability of oxygen for combustion, oxidation of nitrogen, and compounds containing nitrogen to NOx.

The effect of the concentration of oxygen in the intake-air, on NOx concentration is illustrated in figure 2.51 below.

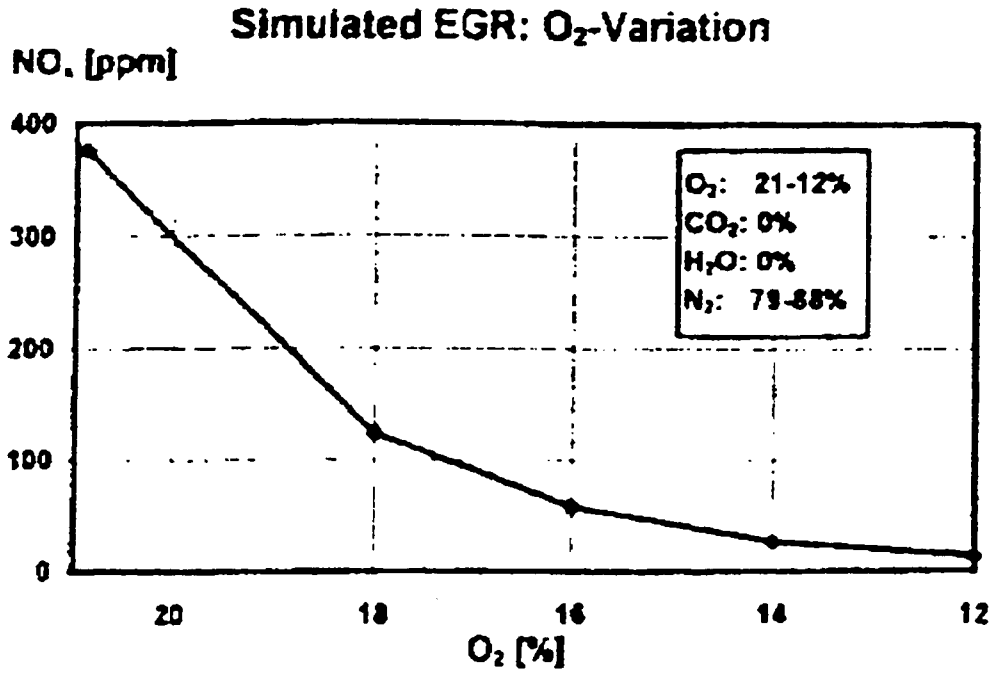

Figure 2.51 Simulated effect of intake oxygen concentration, on the exhaust concentration of NOx [Hentschel, 1996].

Figure 2.51 shows that reducing oxygen concentration substantially reduces NOx formation, primarily through a reduction in flame temperature. The effectiveness of adding various diluents to the intake-air of a DI diesel engine, on NOx formation in the exhaust is shown in figure 2.52.

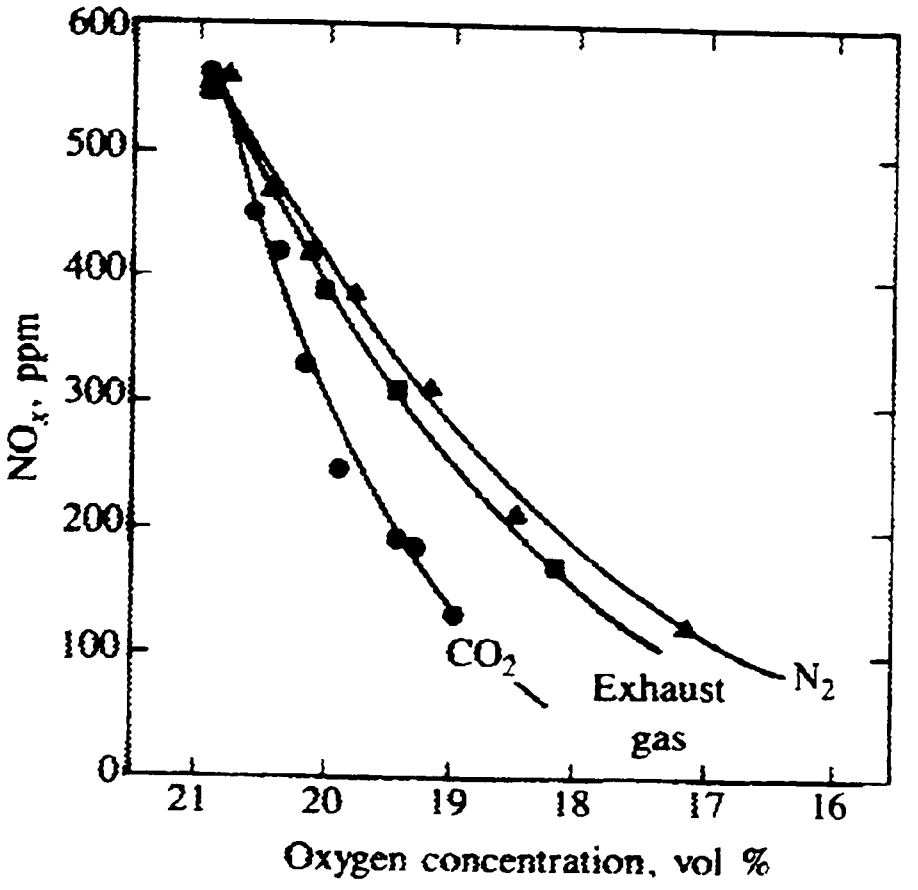

Figure 2.52 Effectiveness of N_2, CO_2 and exhaust gas as dilutents in the intake air, on DI diesel exhaust NOx emissions [Yu and Shahed, 1981].

The difference between the effectiveness of each dilutent is caused by different heat capacities. CO_2 has the highest heat capacity of the dilutents shown here, and is therefore the most effective at reducing the temperature of combustion. Exhaust gas is also suitable for use as a dilutent. Its effectiveness at reducing flame temperature can be increased by cooling the exhaust gas prior to entry into the engine cylinder [Ladommatos et al, 1996(a)], and can also help to control particulates by an associated increase in air mass entering the cylinder [Ladommatos et al, 1996(b)].

The composition of exhaust gas also changes according to the engine overall equivalence ratio. EGR is most effective at a high equivalence ratio, because of the high concentration of CO_2 (high heat capacity), and low concentration of O_2. However, exhaust gas temperature at a high equivalence ratio will be high, creating a balance between a shorter ignition delay and higher flame temperature.

2.7.3 Smoke and particulate emissions

Formation of soot

Soot forms from carbon in the fuel, around the very rich regions of the injected fuel spray, when heating of the fuel by combustion gases occurs. Results from photographic analysis of bomb experiments by Kamimoto and Won (1992), indicate that soot formation is most prominent at the spray tip, in free-forming sprays. Figure 2.53 illustrates regions of soot formation in the free spray.

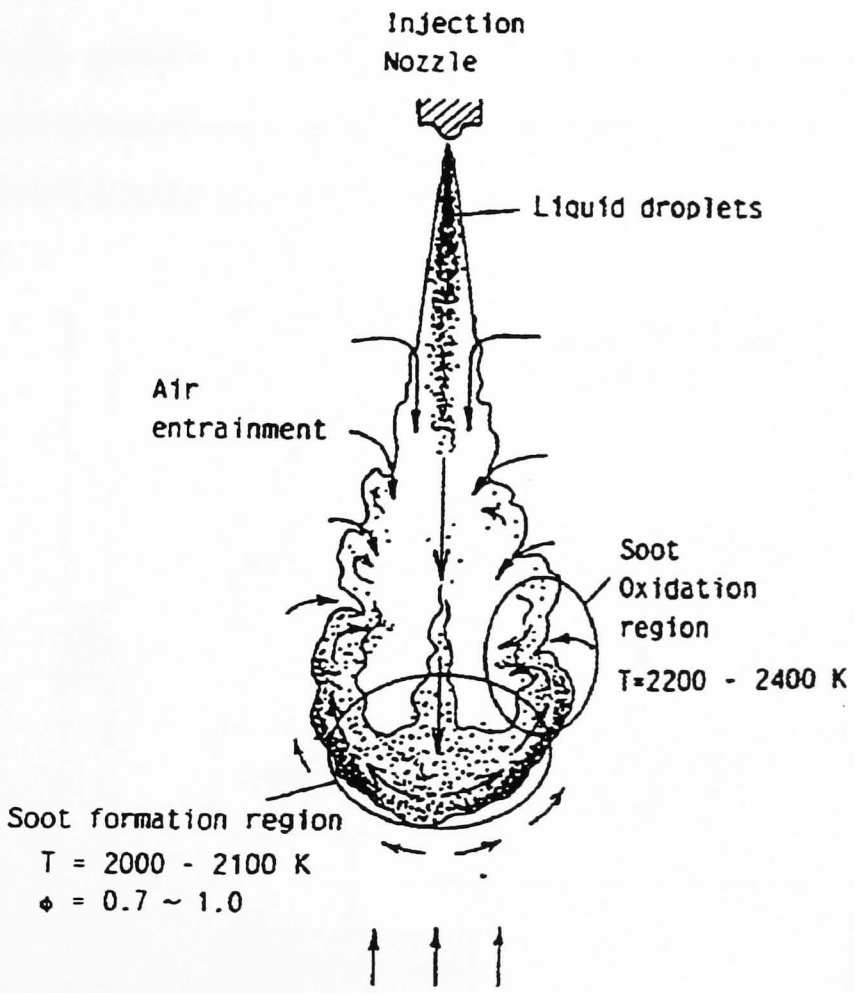

Figure 2.53 Schematic diagram of soot formation, based on results from free spray penetration in a rapid compression machine [Kamimoto and Won, 1992].

Soot formation is high at the spray tip, because of the low equivalence ratio and high temperature. Soot oxidation is most prominent at the spray edges, due to entrainment of fresh charge air.

The particulates formed are predominately composed of carbon, but contain a significant proportion of heavy HC molecules, which have condensed on soot particles at the exhaust sampling temperature. Hydrocarbons typically account for 15-45% of the total particulate mass [Heywood, 1988]. The structure of particulates consists of small carbon spherules which have conglomerated, and been coated with hydrocarbons and other heavy emissions as the exhaust gas cools. Soot is visible in the engine exhaust as smoke.

Soot particle growth

The formation and growth of particulates from within the engine cylinder, to exhausting into the atmosphere, consists of several main stages. These are displayed in figure 2.54 below [Amann and Siegla, 1982].

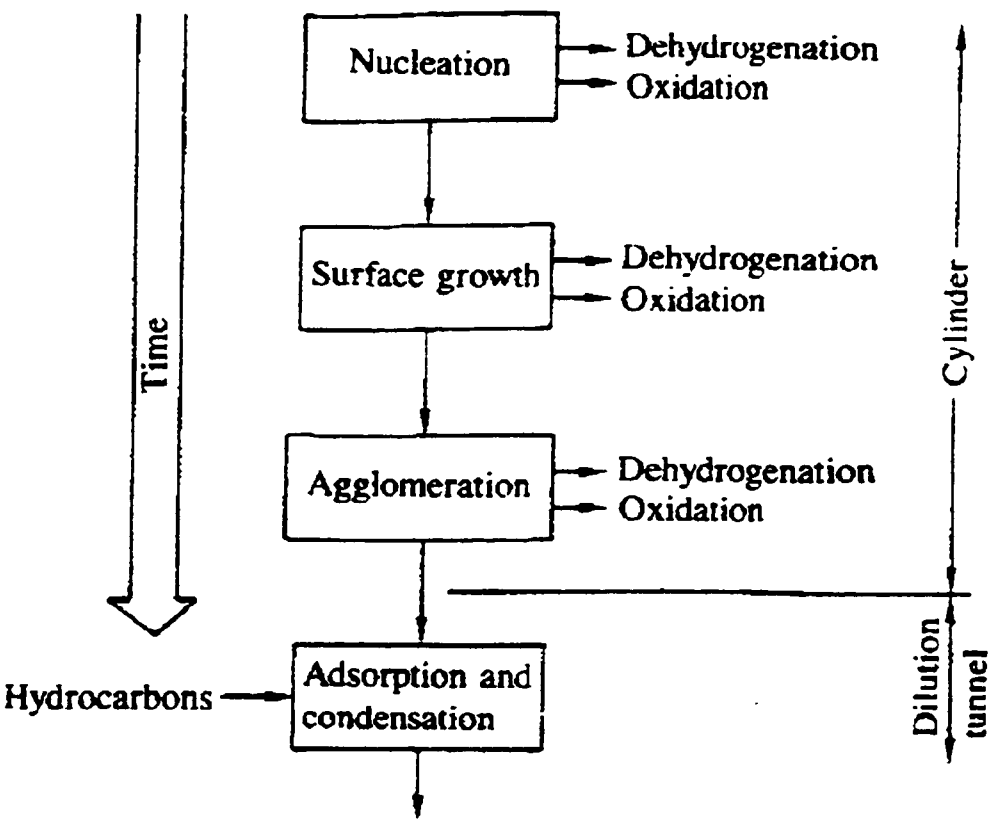

Figure 2.54 Schematic diagram of particulate formation, from initiation to exhaust-out emission in diesel engines [Amann and Siegla, 1982].

Nucleation includes fast and slow routes to forming nuclei for particulate growth. Fast routes involve aromatic fuel compounds (based on benzene), which condense to form a graphite like structure. Slow routes to nucleation include pyrolysis (reactions not

involving oxygen, but brought about by high temperature) of aromatics, and open chain molecules which then polymerise to form large molecules and nuclei.

Particle/surface growth is the stage during which most of the solid phase material is produced. Nuclei grow by deposition of pyrolysis products onto their surface, to form small spherules of 10-50 nm diameter.

Agglomeration occurs when particles collide and stick together to form larger, more irregular particles, of typically 50-220 nm diameter. No mass is added during this stage, but the number density reduces as particles combine.

Adsorption and condensation occurs as the exhaust cools. Heavy hydrocarbon fractions from fuel and oil condense on to the soot particles, increasing particulate mass typically by 15-30%. This extra mass is termed the extractable fraction, because it can be removed from the soot by dissolving in suitable organic solvents.

In practice there may be overlap between the different stages of formation. The measured distribution of particulate size and chemical content will depend on these stages of formation, and thus on in-cylinder physical conditions and mixture distribution. Increased soot formation occurs if the load is increased (increasing the overall equivalence ratio), temperature increases or the diffusion burning process lengthens, thereby giving less time for oxidation at a reduced temperature, late in the expansion stroke.

Variation of soot concentration during combustion

Soot concentration increases rapidly soon after combustion starts. Very high local particulate concentrations are present in the fuel spray, due to pyrolysis of the fuel. Approximately 50% of the local fuel carbon content, can be sampled as particulate in the fuel spray [Heywood, 1988]. Almost all of the early-formed soot is oxidised in a diffusion burning flame, as the soot mixes with fresh air, and leaner air/fuel mixtures. Burning of soot produces the characteristic bright luminous flames associated with diffusion burning in diesel engines. Soot concentration can be reduced if the duration of diffusion burning is reduced by better mixing.

Figure 2.55 shows the increase in soot concentration, sampled from a DI diesel engine during one combustion cycle.

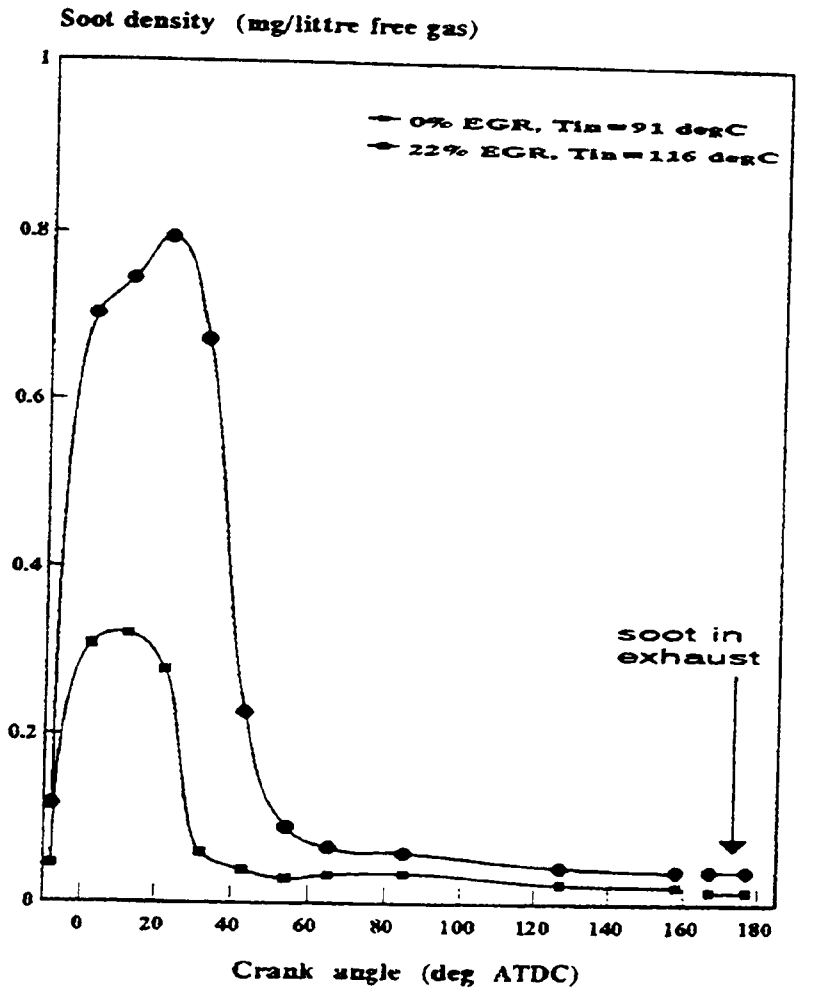

Figure 2.55 Variation of soot concentration during the expansion stroke of a DI diesel engine, obtained using a fast acting in-cylinder sampling valve. The two curves represent different levels of EGR [Zhao et al, 1996].

Soot concentration quickly increases upon combustion, and during diffusion burning, but most of the early-formed soot is rapidly oxidised as it mixes with lean mixture or fresh air. Soot concentration has stabilised at close to the exhaust-out concentration by about 60 degrees after TDC.

Increased temperature promotes soot oxidation late in the expansion stroke. Increased oxygen concentration (occurring at lighter loads or increased boost pressure) also increases soot oxidation, although to a lesser extent than an increase in gas temperature [Lida, 1993; Ladommatos et al, 1996(c)].

Effect of piston bowl shape on soot formation

Soot concentration in HSDI engines can be reduced by impingement of injected fuel on the bowl walls. Piston bowl shapes with small bowl-in-piston diameters, and thus high levels of fuel impingement, have been shown to reduce smoke emissions [Yoshikawa et al, 1989]. It is likely that this is due to improved fuel/air mixing, because of fuel impingement, or an increase in the ignition delay period, allowing a greater proportion of the injected fuel to be burned in a pre-mixed mode (NOx is increased) and not a soot producing diffusion burning mode.

Partial oxidation of engine oil from the cylinder walls, and oil vapour entrainment in the intake air (from crankcase re-circulation of blow-by gases and turbocharger bearing leakage) can also contribute to particulate mass.

2.7.4 Hydrocarbon (HC) emissions

Origin of HC emissions

HC emissions consist of a range of hydrocarbon species that have not been oxidised during the in-cylinder combustion process. HC species differ in their reactiveness and harmfulness to the environment and human health.

Un-burned HC emissions originate from mixture strengths outside combustible limits (overly rich mixture near the spray core, and lean regions), by quenching of flames on cool surfaces prior to complete combustion, and by absorption and subsequent desorption of fuel in the cylinder wall oil film.

Good correlation between the fraction of mixture too lean for combustion, and the over penetrated fuel fraction, with increased HC emissions has been shown [Kuo et al, 1988]. Crevices around the top land region, injector sac volumes, valve seat cut-outs, injector recesses and head gasket gaps are also sources of HC emission due to flame quenching. However, the most significant source of HC emissions in DI diesel engines is considered to be incomplete combustion of weak mixtures.

Mechanisms of HC formation

A summary of the mechanisms of HC emission formation is given in figure 2.56 [Yu et al, 1980].

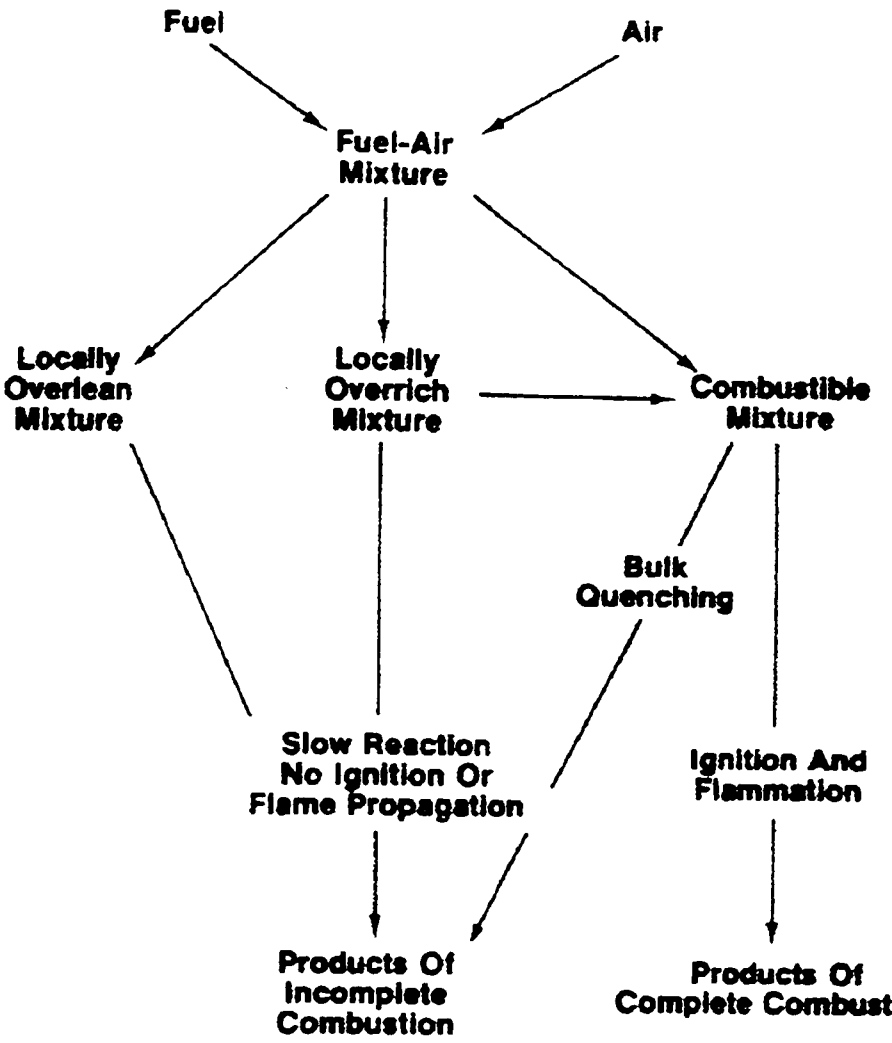

Figure 2.56 Summary of HC formation mechanisms in DI diesel combustion. Products of incomplete combustion produce HC emissions in the exhaust [Yu et al, 1980].

Upon fuel injection, and during the ignition delay period, fuel mixes with air into a wide range of equivalence ratio's. Fuel/air mixture prepared close to the stoichiometric ratio will combust, producing little HC emission, if bulk quenching does not affect flame propagation. Lean mixtures may not combust completely, unless the mixing process subsequently involves fuel-rich mixture. Similarly, rich mixtures must mix with air or lean mixtures to avoid producing HC emissions.

Effect of piston bowl design on HC emissions

Piston bowl design can directly affect HC emissions by wall wetting [Matsui and Sugihara, 1986], and in-directly by affecting airflow, mixing rates and ignition delay. The temperature of the piston bowl wall can also be an important factor in HC emission. However, much of the HC emission produced by wall quenching is rapidly oxidised during subsequent combustion of the bulk mixture [Heywood, 1988]. Figure 2.57 shows the effect of reducing fuel jet path length, thereby increasing the proportion of fuel that impinges on the bowl walls.

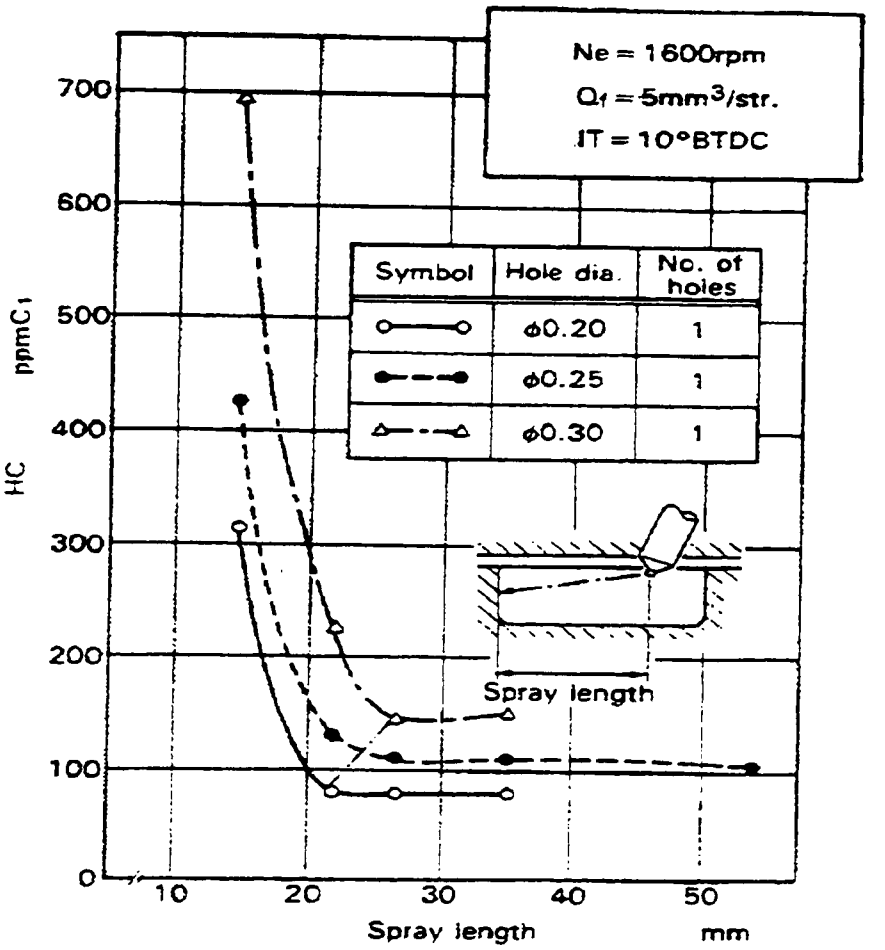

Figure 2.57 Effect of increased fuel impingement on HC emissions of a small HSDI diesel engine, for three different injector hole diameters [Matsui and Sugihara, 1986].

HC emissions rise considerably, as the proportion of fuel impinging on the bowl wall increases (see figure 2.57). The steep rise in HC emissions below a fuel spray length of about 25 mm, corresponds to the theoretical induction length for fuel break-up. Any distance below this induction length significantly increases wall wetting and HC emission.

The depth of fuel jet impingement down the piston bowl sides is thought to affect the amount of, and timing of, flame propagation into the clearance volume. Flame propagation into the clearance volume maybe quenched at certain operating conditions, increasing HC emissions. Low loads are particularly venerable to flame quenching in this way [Matsui and Sugihara, 1986].

Effect of engine operating conditions on HC emissions

Ignition delay is a significant factor in the formation of HC emissions. It directly effects the amount of fuel which is likely to be mixed too lean for combustion, and the amount of fuel which wets the piston bowl walls [Hawley et al, 1998]. EGR exaggerates the effect of mixing outside combustible equivalence ratio limits.

Late fuel injection or poor nozzle seating can be another source of HC emission, although in modern injector design this is considered to be negligible [Hawley et al, 1998].

HC emissions are also sensitive to engine load. At light loads, the ignition delay period is long, and very weak mixtures are formed around the periphery of the spray, causing incomplete combustion and high HC emissions. This can be more of a problem in high-speed DI diesel engines, because of the rapid mixing effects of swirl and squish, and increased rate of cooling during the expansion stroke, quenching the reaction early. As load increases, the ignition delay shortens and HC emissions reduce accordingly. The effect of engine load on HC emissions is shown in figure 2.58 below.

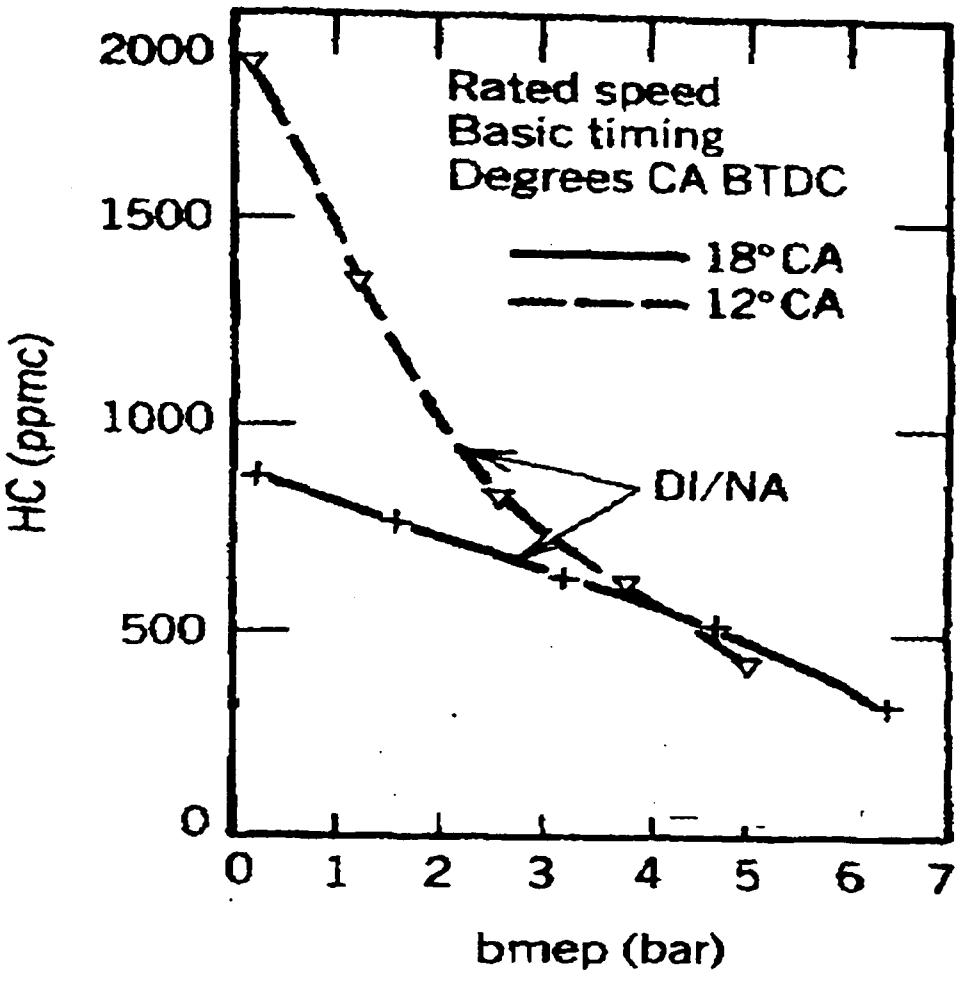

Figure 2.58 Effect of engine load (and therefore overall equivalence ratio) on exhaust HC emissions at two different injection timings [Ferguson, 1986].

HC emissions are higher for the retarded injection timing case, because of a longer ignition delay, and cooler combustion temperature later in the expansion stroke. Over-fuelling at very high loads (not present in figure 2.58), can cause very high HC emissions, along with increased smoke and particulates.

The effect of over-fuelling is shown in figure 2.59, of HC emission from a DI diesel engine, as the engine load is increased at constant speed.

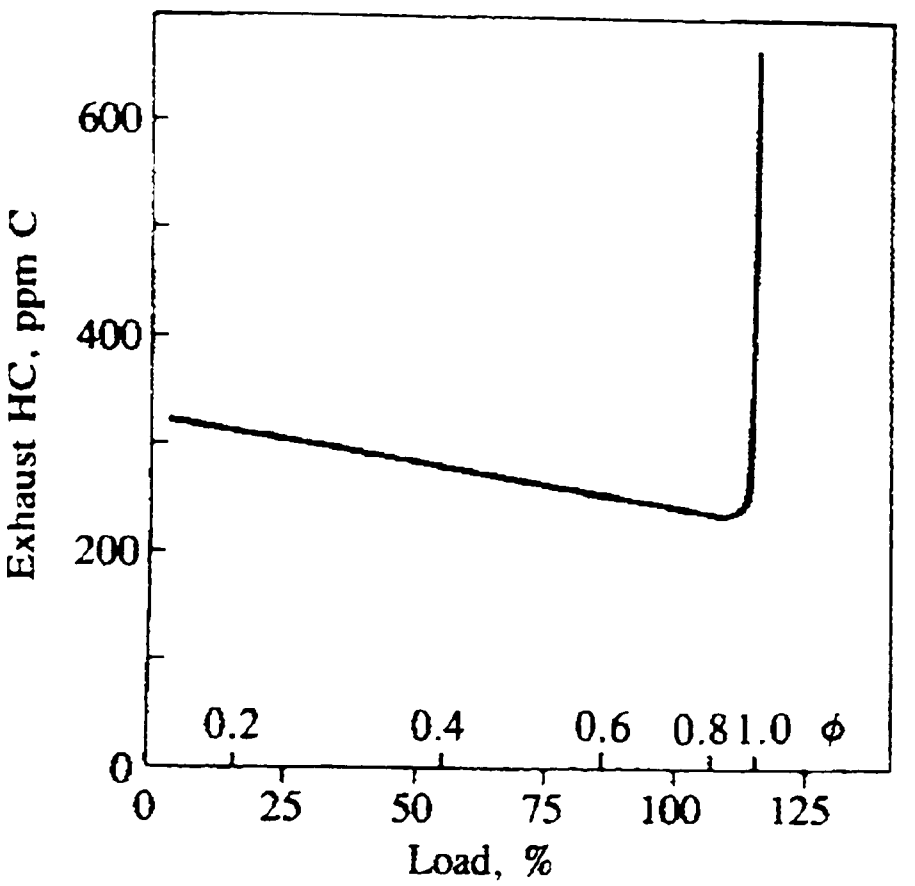

Figure 2.59 Effect of over-fuelling on HC emission of a DI diesel engine. Engine speed has been kept constant, and injection timing adjusted to give minimum ignition delay period [Greeves et al, 1977].

The steep rise of HC emissions observed in figure 2.59, is caused by the inability to mix all the injected fuel and air in sufficient time for combustion. Modern HSDI diesel engines can achieve an equivalence ratio of up to 0.9, before over-fuelling occurs. The effect of over fuelling is not so common during steady state operation of well maintained diesel engines, but can occur during transient operation. Careful mapping of the fuelling requirement of turbo-charged engines, and accurate measurement of intake-air mass-flow rate, can eliminate this problem, without a reduction in transient performance.

2.7.5 Emissions legislation

Evolution of emissions standards

The emission of gaseous pollutants from passenger car diesel engines is controlled by testing of sample vehicles or engines (or production-line equipment, more representative of the whole vehicle fleet), over a simulated drive cycle. Different

standards exist for Europe and the USA. Current European testing procedure consists of a simulated urban driving cycle (ECE-15), followed by high-speed operation (EUDC).

A summary of the past, present, and future emissions limits, imposed by the European standards is given by Hawley et al (1998), as shown in figure 2.60 below.

European Diesel Passenger-Car Emission Standards

	CO (g/km)	NO_x (g/km)	HC + NO_x (g/km)	PM (g/km)	Comments
Stage 1 (DI)	3.81		1.36	0.20	In force (1)
(IDI)	2.72		0.97	0.14	
Stage 2 (DI)	1.0		0.90	0.10	In force (2)
(IDI)	1.0		0.70	0.08	
Stage 3	0.64	0.5	0.56	0.05	(3)
Stage 4	0.5	0.25	0.30	0.025	(4)

Figure 2.60 Table of European emission legislative limits for passenger car diesel engines [Hawley et al, 1998].

Stages 1 and 2 (implemented in 1994 and 1996 respectively), have differing limits for DI and IDI diesel engines, reflecting the relative merits and difficulty of each design. Diesel engine emissions limits are standardised for stages 3 and 4 (to be implemented in 2000 and 2005 respectively).

Changes to the way in which testing is conducted for stages 3 and 4 (due to be introduced in the year 2000 and 2005 respectively), will cause the reduction of emissions demanded to be greater than the numerical values infer. Sampling of emissions will in future commence upon engine cranking, whereas in the past, a 40 second warm-up period was allowed. Limits for stage 4 are at the moment provisional, with some plans to introduce CO_2 limits by imposing fuel economy requirements of 5 litres/100km in 2005, and 3 litres/100km in 2010 [Hawley et al, 1998].

Reduction of the particulates versus NOx trade-off

Of particular importance and major challenge to diesel engineers, is the reduction of the NOx/particulates trade-off which is necessary to meet future legislation. The reduction in the trade-off, determined by the European emission stage limits tabulated above, is shown in figure 2.61 below.

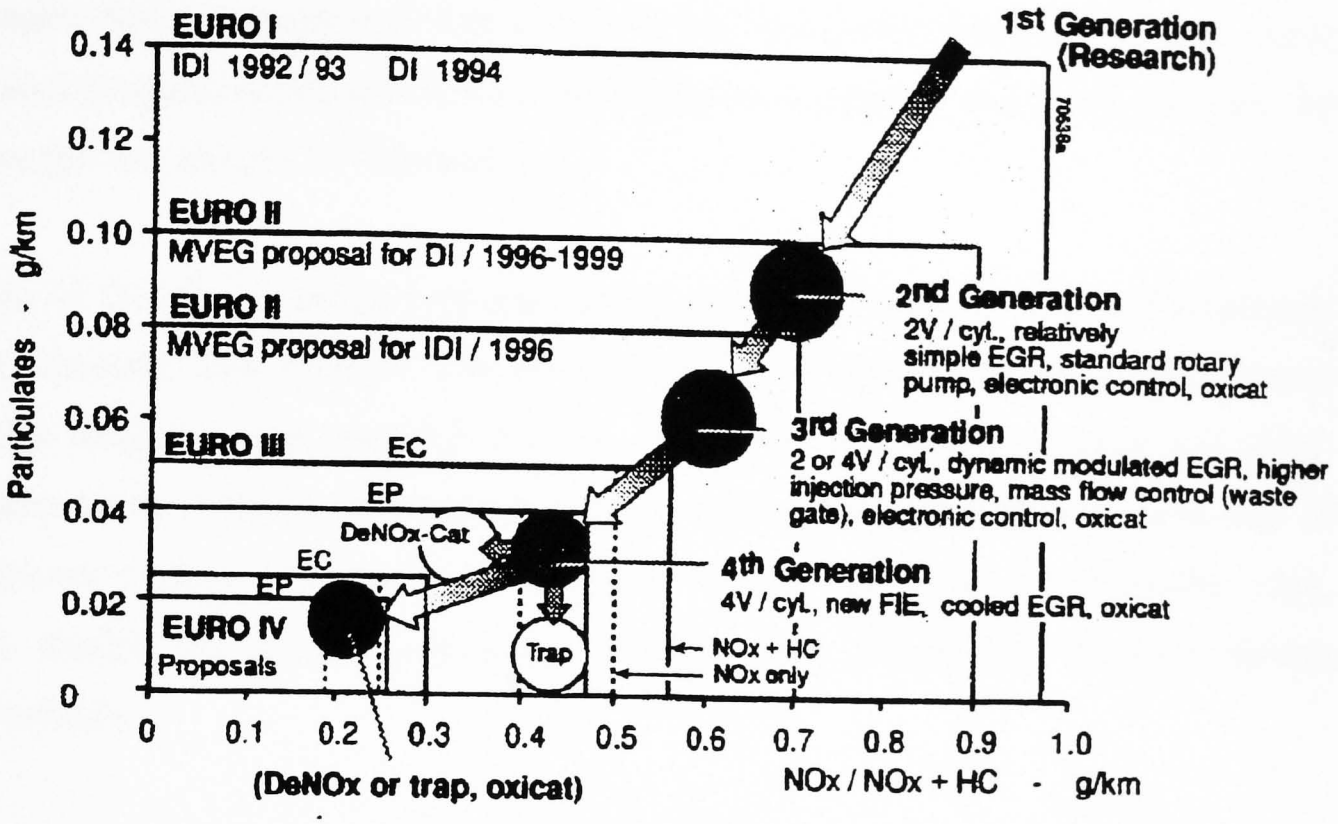

Figure 2.61 Previous, current, and future requirements of European emission legislation, applied to the NOx versus particulates trade-off (note that stages 1 and 2 specify HC and NOx limits combined, whereas future limits specify NOx emissions seperately) [Herzog, 1998].

General observation of the trend in reduction of the NOx versus particulates trade-off achieved in the past (see figure 2.61), indicates that either a NOx cataylst, or particulate trap, will be necessary to meet Euro 4 limits. This will enable diesel engineers to focus on either NOx or particulates reduction, as the classic trade-off in emissions will be modified by exhaust after-treatment.

2.8 Conclusions

Research into diesel combustion and emissions has enabled engineers to develop the diesel engine into the high-speed, efficient and clean engine that it is today. Fundamental understanding has increased through the use of optical access engines and combustion bombs. More recently, CFD has enabled greater understanding of the complex mixing processes of fuel and air in the combustion chamber. However, there is much progress to be made if the diesel engine is to prosper as a power plant for the passenger car into the 21st century.

Many of the crucial design problems facing diesel engineers are trade-off's between one parameter and another. The most important of these for modern HSDI diesel engine design, is the trade-off between the production of particulates and NOx, present in the exhaust. Piston bowl shape is critical for the successful reduction of emissions trade-offs. Future introduction of de-NOx catalysts, or particulate traps, will change the desired operating condition and philosophy of bowl design accordingly.

Successful piston bowl design can be judged primarily on its ability to reduce the NOx versus particulates trade-off. Control of other key emissions to within legislative limits, and good fuel economy are also essential. Other important attributes of bowl design are insensitivity to small geometric changes such as injector position, and EGR level.

Current fundamental understanding of the effect of piston bowl shape on fuel/air mixing and subsequent performance and emissions is limited. Most studies relating to piston bowl shape have been parametric studies were little understanding is gained, apart from what works well on a particular engine type. Studies of this type cannot be universally applied to a wide range of engines, because combustion and emissions are very system specific. This work aims to increase the fundamental understanding of the effect of piston bowl shape on the processes governing performance and emissions in HSDI diesel engines.

Chapter 3:

Experimental facility and test engine

Chapter 3: Experimental facility and test engine

3.1 Introduction

The installation, commissioning and development of the project engine and instrumentation into the modern, computer-controlled dynamometer, used for experimentation, is described in this chapter. Considerable development of the engine test facility was necessary before full testing could begin.

The project engine supplied by Ford was a development, pre-production, four-cylinder, HSDI diesel engine. The project engine is known commercially as the 'Lynx Upgrade', and will be referred to as this or the 'project engine' in future discussion.

The project engine required a dynamometer capable of maintaining high engine speed and torque during the duration of testing. Ease of changing operating condition (dynamometer torque and speed) was essential for rapid testing, when small changes were required. For these reasons, a modern eddy-current dynamometer was chosen for the experimental test facility.

The dynamometer was already installed in a dedicated test cell at Brunel University, having a control room adjacent to the test bed with a viewing window and cable access to the engine. The project engine was installed by designing and manufacturing mounts for the engine and bell-housing/gearbox. Ancillary engine components were sized and installed, such as the charge-air inter-cooler, and EGR control system.

Considerable time was spent planning, installing, and testing the extensive engine instrumentation, vital to subsequent testing programs. A good understanding, and some modification of engine and dynamometer fluid control systems, was also required to ensure successful and safe engine commissioning.

The project engine had an electronically controlled fuel injection pump, requiring considerable electronic hardware and a comprehensive software control program,

which also allowed engine monitoring and control. This system was commissioned with some difficulty, owing to its complexity, and universal application to an engine installation in a vehicle, rather than an engine test facility. The electronic hardware was modified to ensure fail-safe control.

A considerable range of instrumentation was installed on the engine to allow detailed analysis of combustion, performance, and emissions. Initially, the cylinder head was machined to provide access for a cylinder-pressure transducer through the glow-plug hole. Later, on a similar cylinder head, a new slimmer pressure transducer became available from Kistler, and was mounted in the original glow plug hole using a special glow-plug adapter.

The instrumentation was installed to provide data to calculate overall engine parameters such as BSFC, volumetric efficiency, and emissions, and also specific information about combustion (focussing on an individual cylinder), such as fuel injection line pressure and injector needle lift.

Subsequent sections in this chapter describe in more detail the dynamometer test cell, engine hardware and software, including the variable intake swirl system, engine fluid and auxiliary control systems, and, finally, the engine instrumentation and emissions measurement equipment.

3.2 Dynamometer and control system

3.2.1 Description of dynamometer and control system

A Schenck eddy current dynamometer type W130 was used for testing throughout the project duration. The eddy current dynamometer consisted of a thin disk mounted on a shaft, connected to the engine through a rubber coupling to isolate the dynamometer from high frequency engine vibration. The disk rotated inside a stationary casing, in which a magnetic field with its flux field normal to the rotor was generated. This created an opposing torque to shaft rotation.

The strength of the magnetic field determined the torque applied to the shaft (and thus engine torque if there was no acceleration, as in steady-state testing), and was controlled externally from the Schenck dynamometer control panel. Eddy currents generated within the rotor were short-circuited, generating considerable heat. The dynamometer was cooled by water in what was effectively a total loss system. Figure 3.1 shows a simplified diagram of the Schenck eddy current dynamometer and control panel.

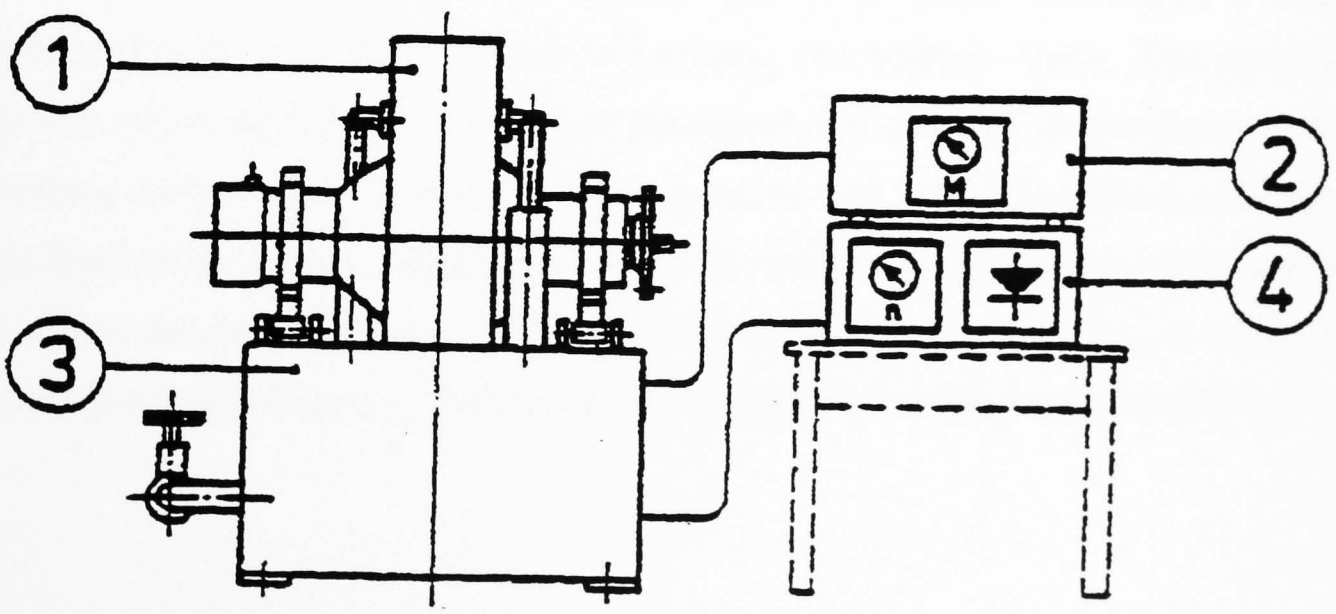

Figure 3.1 Eddy-current dynamometer, used for absorbing power developed by the engine, together with a simplified control system [Schenck, 1983].

Key to figure 3.1:

(1) dynamometer containing magnetic-field-producing-stators and eddy current rotating disk

(2) torque measuring unit, connected to the load-cell which was mounted between (1) and (3) (load cell not shown)

(3) dynamometer base made from a large concrete block surrounded by a metal frame

(4) simplified control unit for control of engine speed and torque

Engine torque was equal to the torque reaction on the dynamometer casing if there was no acceleration. This was measured by a load cell mounted on the side of the case, and together with a speed sensor, formed the inputs for a closed loop control system for control of dynamometer torque and speed. The signal from the load sensor was automatically low-pass-filtered to eliminate high frequency engine vibrations.

3.2.2 Dynamometer and engine installation

The engine is connected to the Scheck dynamometer rubber coupling by a shaft, running through a modified engine bell-housing and gearbox casing. This provided suitable mounting points for the rear of the engine, and provided greater clearance for ancillary components. The engine was mounted on four individual rubbers, onto rigid legs fixed to the dynamometer/engine base. The height of each base leg was adjusted, to ensure accurate alignment of the dynamometer-to-engine coupling, to minimise coupling stresses. Figure 3.2 below, shows a photograph of the engine installation.

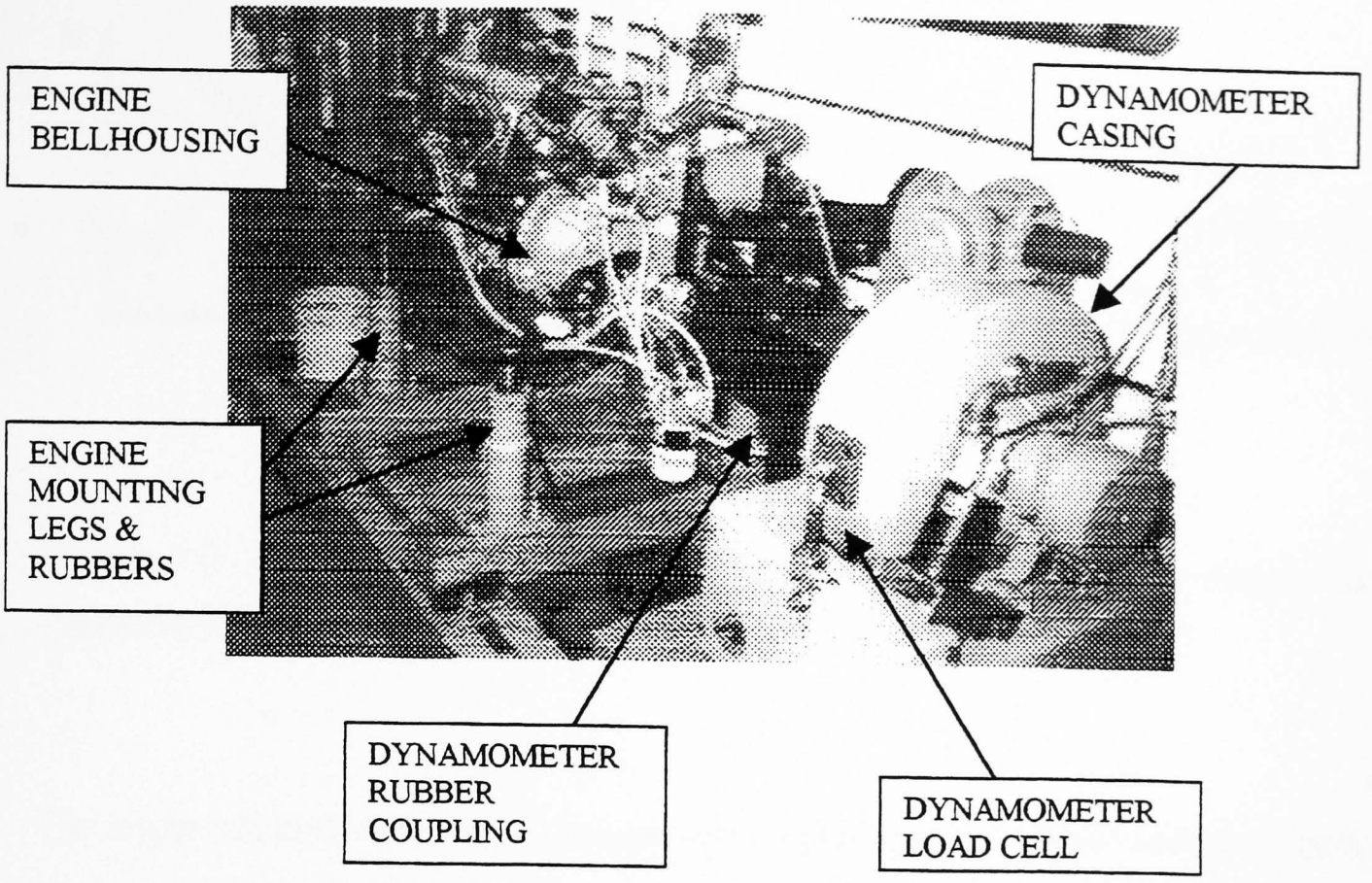

Figure 3.2 Photograph of the engine installed on test bed, attached to the Schenck eddy-current dynamometer.

Clearly visible in figure 3.2 are the test bed, mounting legs, engine rubbers, engine bell-housing and modified gearbox, dynamometer, and load cell. The dynamometer-to-engine coupling is partly concealed by a safety cover.

3.2.3 Dynamometer operating characteristics

Care was taken to ensure the engine and dynamometer would function under stable operating conditions. Diesel engine torque generally decreases with speed, for a given fuelling demand. To ensure stable operation, dynamometer torque must increase with speed. Examples of stable and unstable operating conditions of typical engine and dynamometer installations are shown in figure 3.3.

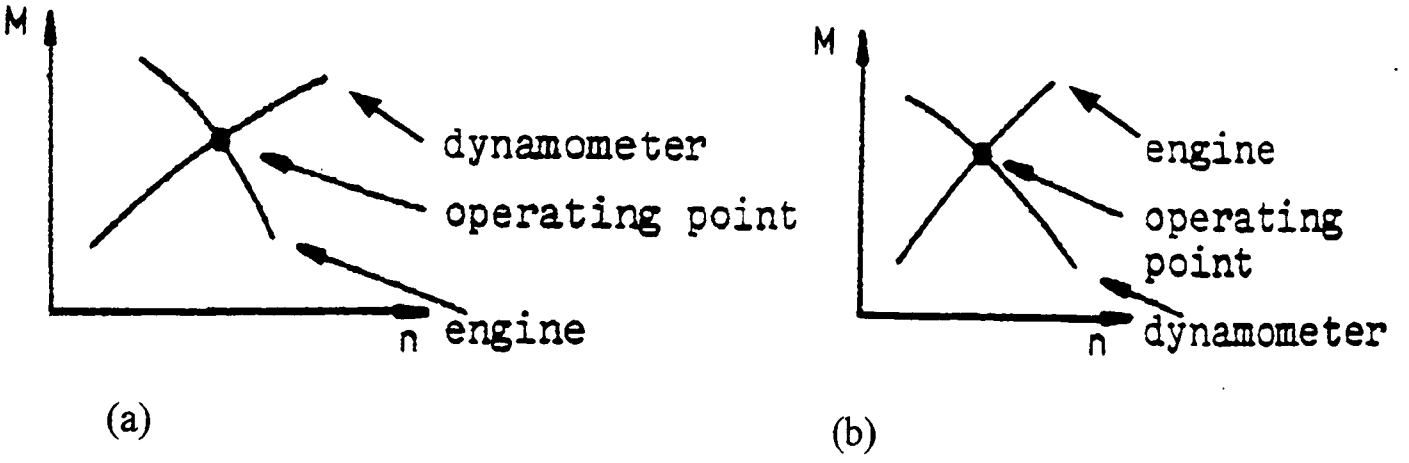

Figure 3.3 Stable (a), and unstable (b), operating points of an engine and dynamometer [Schenck, 1983].

The engine characteristic curve changes with engine fuelling, whilst the dynamometer characteristic curve for an eddy current dynamometer can be changed, within a limiting envelope of performance, by the operator.

If a small change or disturbance of engine condition, such as an increase in speed, occurs in the stable operating regime, the desired operating point will be recovered, as dynamometer torque automatically increases to compensate (see figure 3.3a). However, if engine speed was to increase in an unstable operating condition, dynamometer torque reduces, further increasing engine speed (see figure 3.3b). The system would then be unstable. In practice, an extremely unstable operating condition is not common, but similar effects can occur near the operating envelope of the dynamometer.

The Schenck dynamometer used allowed control of the testing regime by the operator. Four modes of control were available. These were constant speed control, constant torque control, torque control proportional to the square of engine speed, and steep characteristic control. Of these, only constant speed and constant torque control modes were used during testing. Details of these modes of operation are shown in figures 3.4 and 3.5 below.

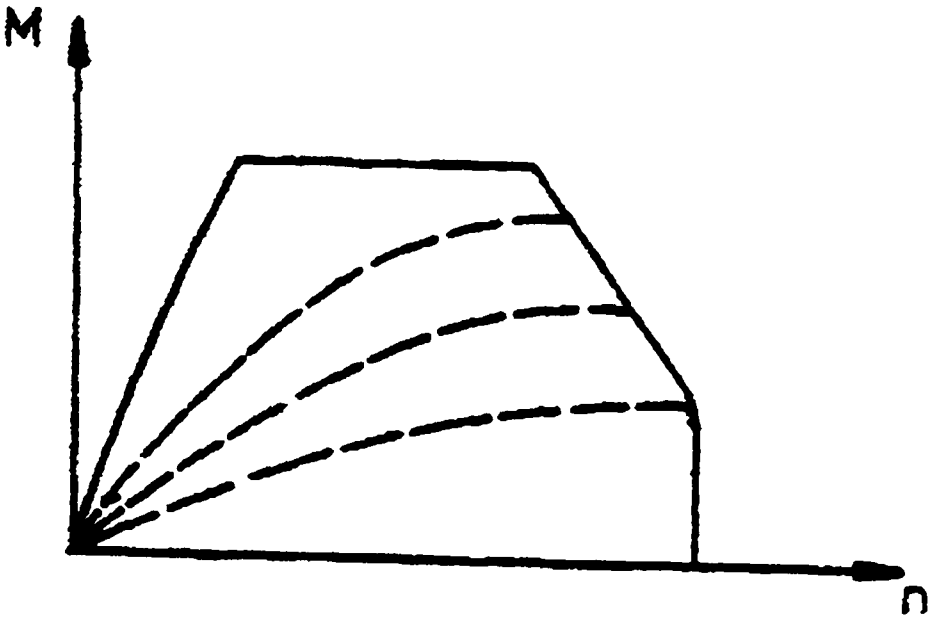

Figure 3.4 Constant current intensity (torque) control. 'M' is dynamometer torque, 'n' is engine speed [Schenck, 1983].

The operating envelope of the dynamometer in figure 3.4, is indicated by the exterior solid line shown. Constant dynamometer current intensity lines are shown broken. These do not correspond directly to constant dynamometer torque. In practice, some adjustment of the current intensity is necessary to maintain constant torque as speed is changed.

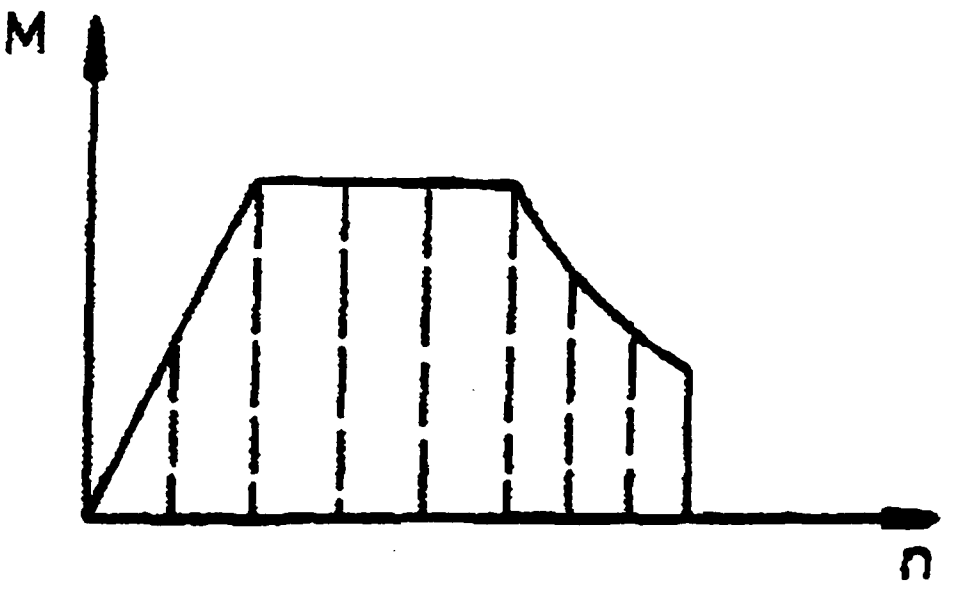

Figure 3.5 Constant speed control. 'M' is dynamometer torque, 'n' is engine speed [Schenck, 1983].

Within the operating envelope shown in figure 3.5, the dynamometer (and therefore engine) speed is maintained constant by automatically changing dynamometer current intensity (and therefore torque) to match changes in engine torque.

Constant speed control was used most often (except at very light or idle loads) during engine testing. Engine torque can change due to changes in fuelling, airflow, EGR etc.

3.2.4 Dynamometer speed control theory

The Schenck control system maintained constant speed by comparing the actual speed value, with the demanded value input by the operator. The difference was applied to a PID controller, and depending on the PID pre-set values, a correction to dynamometer current intensity and, hence, torque was made. It was necessary to change the PID pre-set values during commissioning of the test cell, to ensure stable operation in the constant speed mode (stable operation in this context meaning the response of the system to a step input).

A step input can be approximately generated by swiftly turning the speed control potentiometer to a higher value during engine operation, and observing the engine speed response. Engine speed will always lag the desired input, set by the speed potentiometer, but tuning the values of PID will optimise the transition and minimise any over-shoot or oscillation. Figure 3.6 a, b, c, d, illustrate common faults in the response to a step input, and the likely cause.

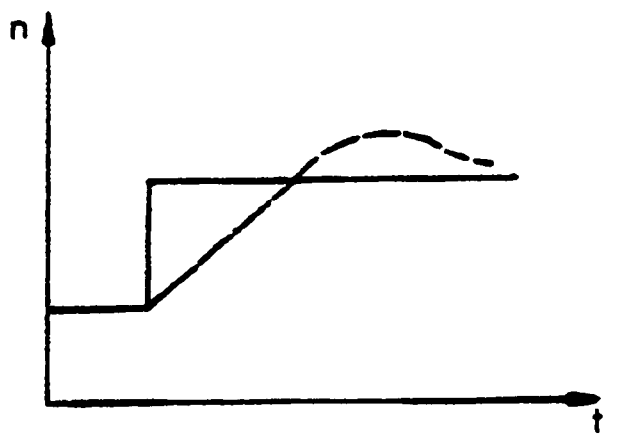

(a)

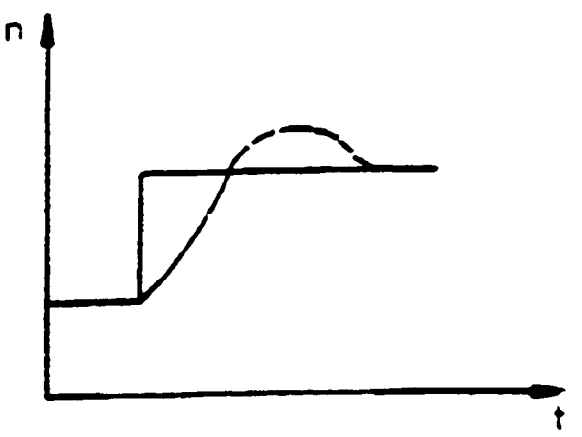

(b)

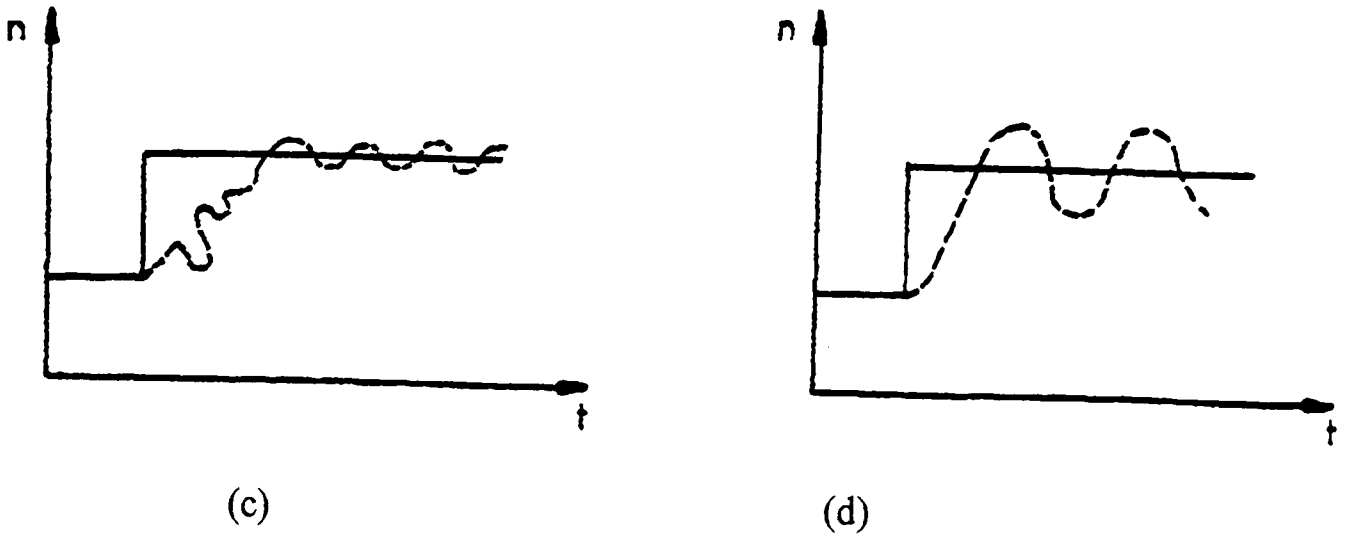

(c) (d)

Figure 3.6 Problems associated with dynamometer response to a step increase in the desired value of rotational speed.

In figure 3.6 (a), the response to the step input (shown by the solid line) was too slow, although stable. The P (gain) component of the PID controller may be too small or the I (integrating) component too large.

In figure 3.6 (b), significant overshoot may cause problems if the engine was already at a high speed. Overshoot can be reduced by increasing the D (differentiating) component.

In figure 3.6 (c), excessive high frequency oscillation and noise indicated that the D (differentiating) component was too large.

In figure 3.6 (d), repeated large-scale oscillation may cause damage to the coupling or engine. The P (gain) component was too large.

In general, if the gain (P) was increased, then it reduced the offset, but also reduced stability. Integrating action (I) removed offset, but also reduced stability. Differentiating action (D) increased the effective damping, had no effect on offset, but amplified noise.

3.2.5 Description of dynamometer control panel

The main control panel contained potentiometers for PID control behind a cover, as well as the potentiometers for mode selection and control of dynamometer speed and torque. The control panel had analogue displays for engine speed and torque (used for quick reference), as well as a digital display for torque.

The control panel also served to monitor a range of selected engine pressures and temperatures, engine ignition, starting and cut-off, and trip switches for water temperature, engine over-speed, low oil pressure, and low dynamometer coolant fluid flow. Power electronics for dynamometer control were contained in a free-standing instrument tower, placed along-side the control panel. A picture of the control panel is shown in figure 3.7 below.

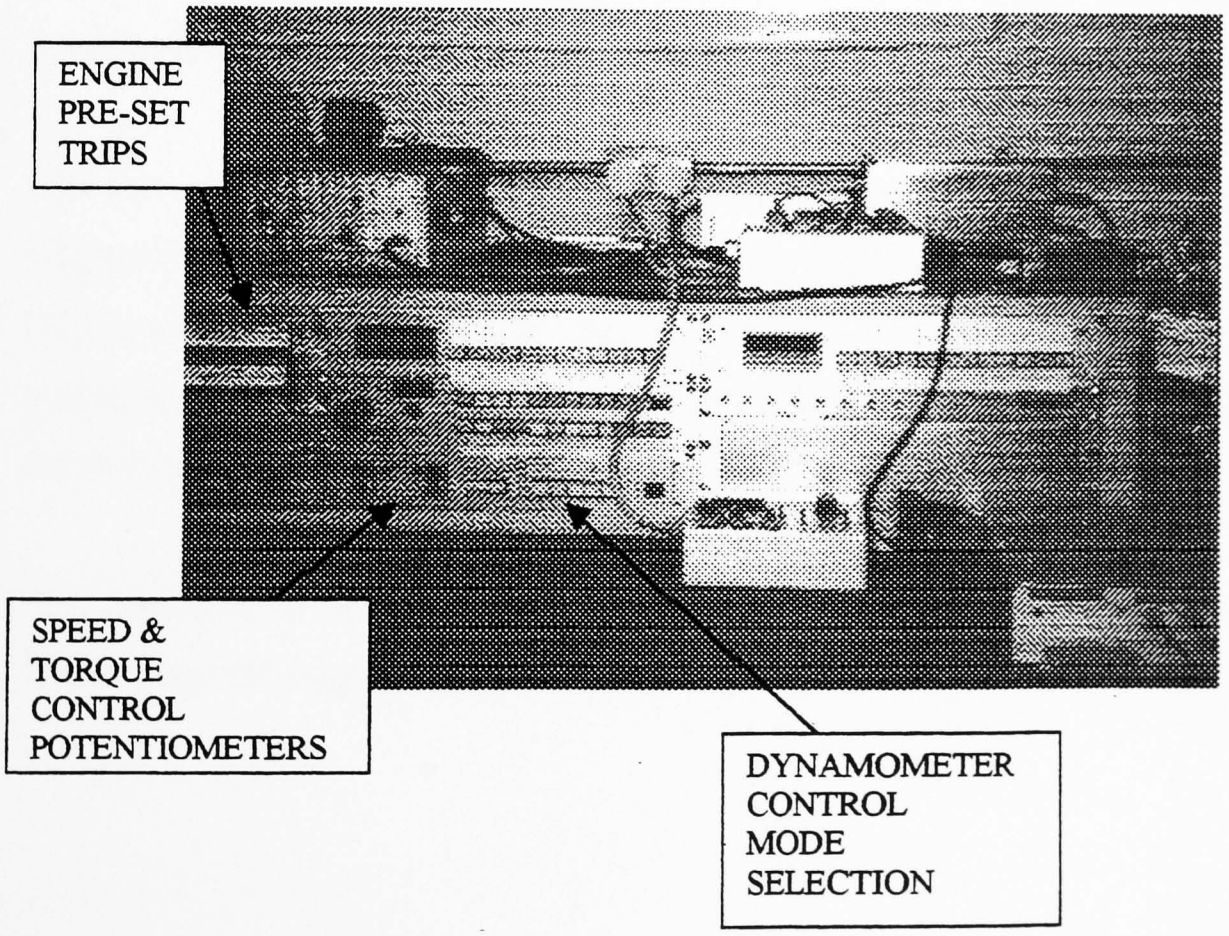

Figure 3.7 Photograph of the control panel containing the PID control, dynamometer operating characteristic controls (engine speed and torque), and engine monitoring display.

3.3 Engine description

3.3.1 Engine chosen for testing

A four-cylinder HSDI diesel engine (named the Lynx Upgrade engine), supplied by the Ford motor company, was used for all engine tests. It was a prototype, pre-production engine, having four-valves per cylinder, and a central, vertical injector.

A multi-cylinder engine was chosen, in preference to a single-cylinder engine, despite the complications of cylinder-to-cylinder variations, because of the need to accurately replicate modern HSDI combustion chamber geometry, characteristics, and performance.

The desire to implement an improvement in combustion and emissions on an engine intended for mass production, as a direct result of this work, was also a primary consideration in choosing the Lynx Upgrade engine.

The use, or simulated use, of a turbo-charger would have also been difficult on a single-cylinder engine. Furthermore, a readily available supply of blank pistons for the Lynx Upgrade engine for manufacture of different piston bowl shapes, and technical support from Ford, were important factors in the decision to use this pre-production engine.

The diagrams in figure 3.8 below, show two side views of the Ford Lynx Upgrade engine used for engine testing.

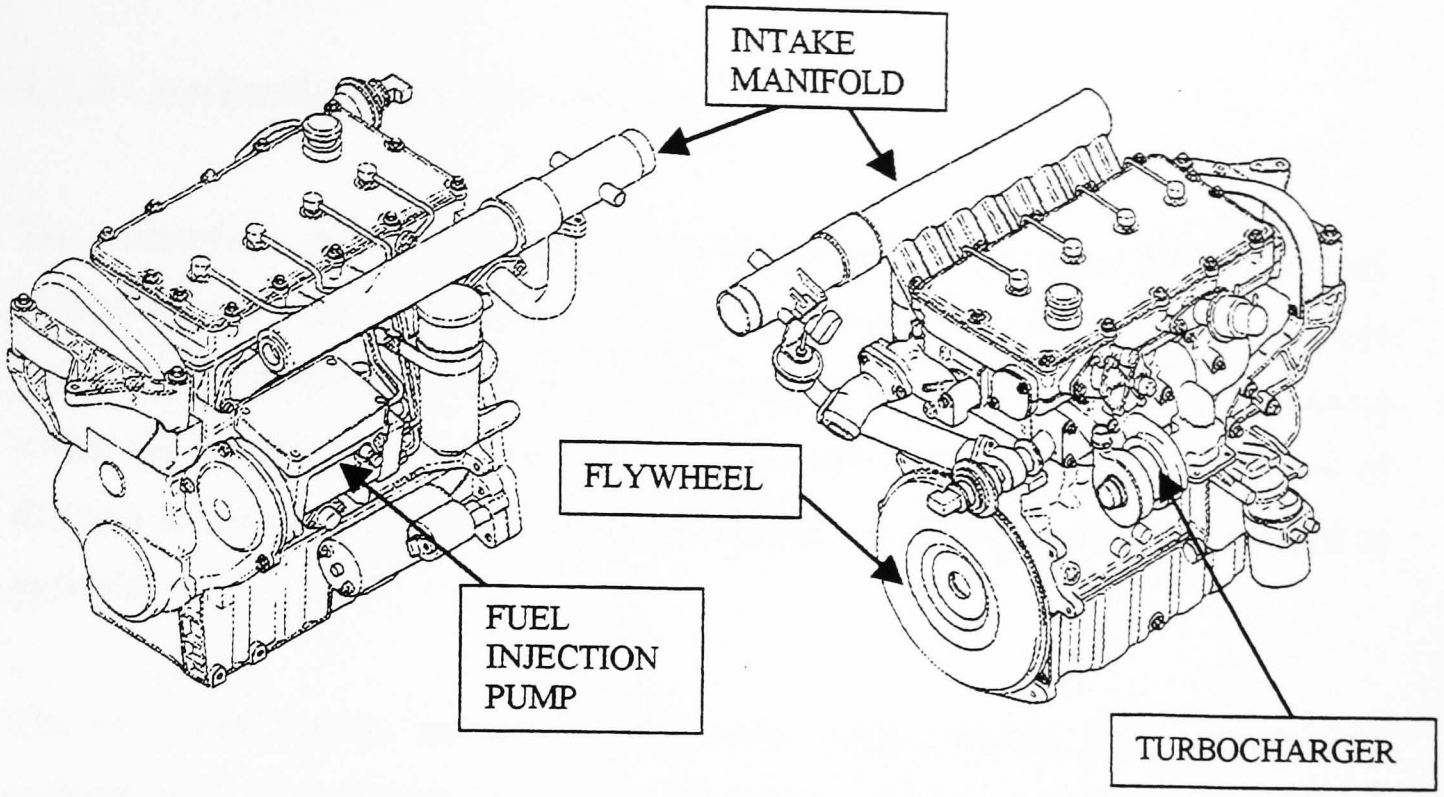

Figure 3.8 Two perspective drawings of the Lynx Upgrade project engine [Ford internal publication, 1997].

The actual project engine, installed on the test bed at Brunel University, is shown in figure 3.9.

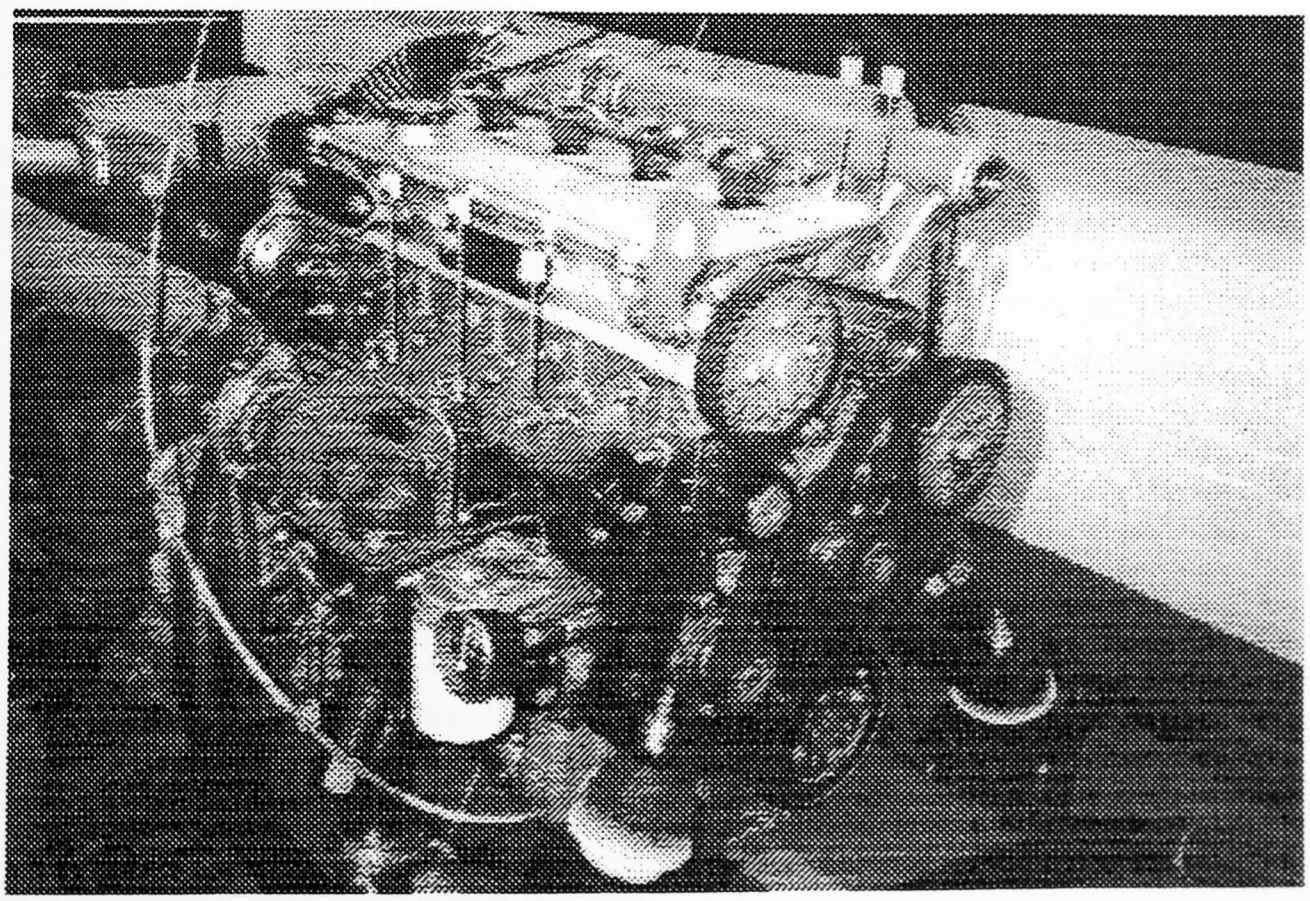

Figure 3.9 Photograph of Lynx Upgrade project engine installation on the test bed at Brunel university.

3.3.2 Combustion chamber design

The combustion chamber had four-valves per cylinder, allowing the use of a central, vertical injector. Central injector systems promote better combustion, and allow more precise optimisation of the combustion chamber, owing to more even fuel distribution within the combustion chamber. The cylinder was almost 'square', with a bore of 82.5mm and a stroke of 82mm. A more detailed list of engine data is presented in appendix A.

The two intake-valves and two exhaust-valves were mounted flush with the flat cylinder head. The exhaust-valves were of simple directed-port design and exited into a siamesed exhaust port, cast into the cylinder head. The two intake-valves had different designs to create the desired intake-air swirl and turbulence flow structure. One intake-valve generated high swirl by its tight helical port design, whilst the other had a weaker helical design and some directed-port properties. Each intake-valve had a separate intake port, and this feature was utilised in the variable swirl system (described in section 3.3.3).

A compact bowl-in-piston combustion chamber generated high swirl and squish velocities, to aid fuel/air mixing and promote rapid combustion. The turbo-charged engine had a compression ratio of 19.6:1, necessary for good starting and low load performance. The bowl design was of the torodial, re-entrant type, with a central pip to optimise the air velocity distribution. The piston had a large squish area, made possible by the re-entrant bowl design, and operated with minimal bump clearance to maximise squish velocity.

A drawing of a section through the combustion chamber and cylinder head of the Lynx Upgrade project engine is show in figure 3.10.

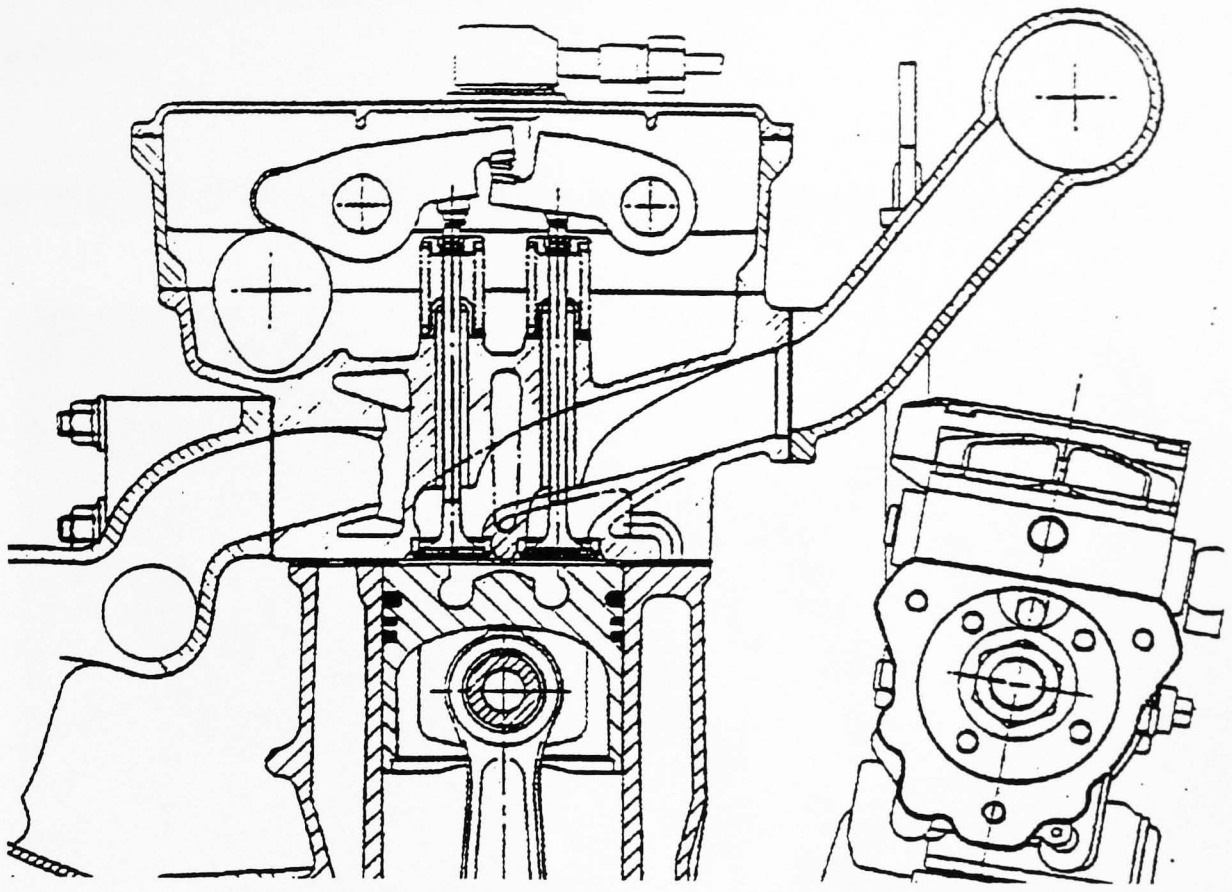

Figure 3.10 Section of the combustion chamber of the Ford Lynx Upgrade engine (viewed from the front) used for testing [Ford internal publication, 1997].

The intake-valves only are shown in figure 3.10, illustrating the different intake port designs. The two exhaust-valves for this engine cylinder are positioned behind the section shown. The left-hand port was the predominant swirl-producing port. The piston in figure 3.10 is shown positioned at TDC.

3.3.3 Variable intake swirl system

The dual intake ports of the Lynx Upgrade engine were suitable for port deactivation, to achieve different in-cylinder swirl levels by external control. Airflow through the ports, in normal operation (when both ports are fully open), was roughly equal between each port. Only small differences in the flow rate existed, depending on the flow coefficient of each port. However, the variable swirl (port deactivation) system progressively closed the more 'directed-type' of the two ports, forcing all the air to flow through the high-swirl helical port. This allowed a moderate increase in swirl,

over the standard combined port design, although at the expense of a small reduction in airflow.

A photograph of the port deactivation system is shown in figure 3.11 below.

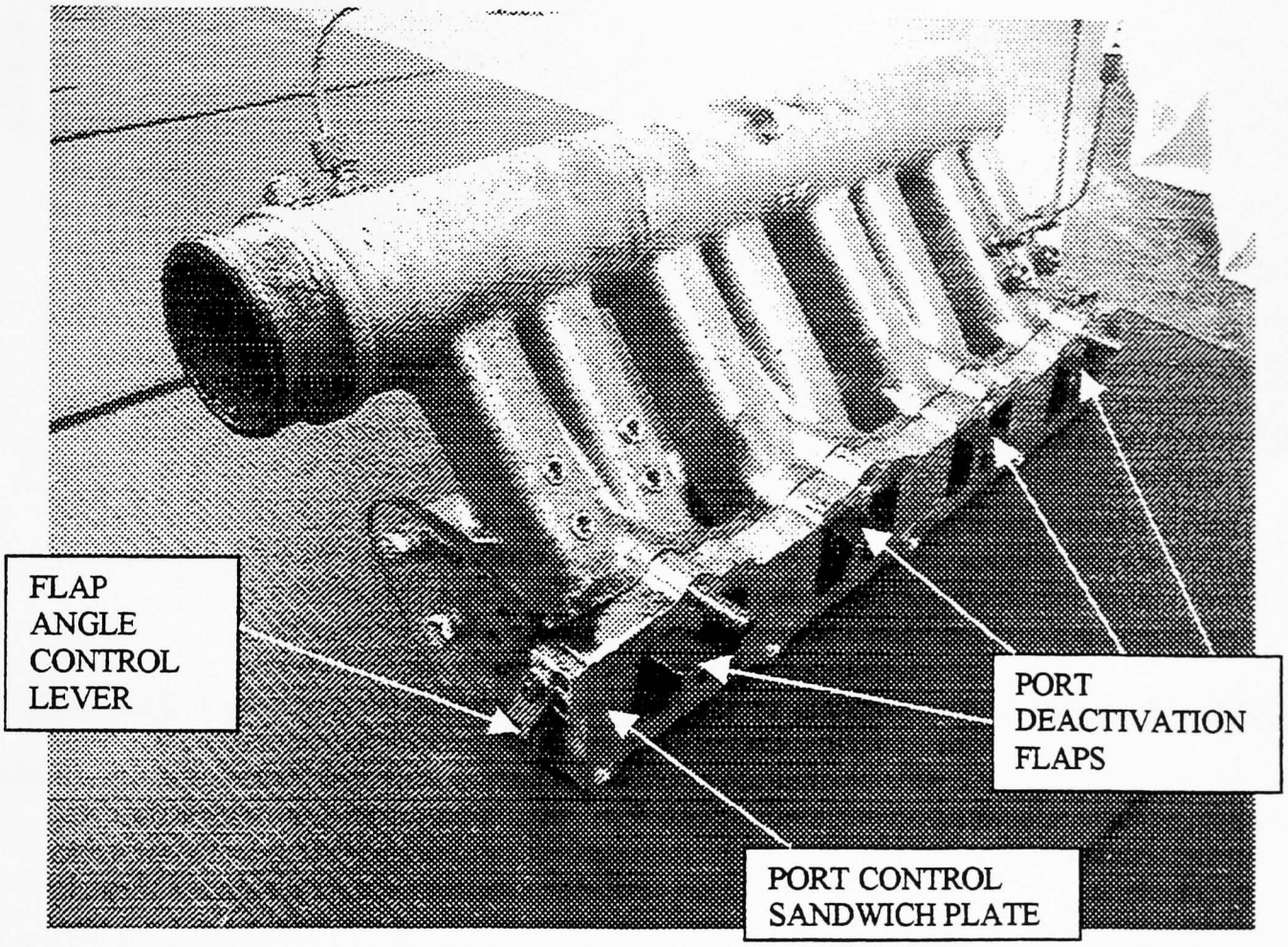

Figure 3.11 Photograph of the port deactivation sandwich plate and port deactivation flaps, fitted to the intake manifold. Flap angle was controlled by a sliding lever mounted on the end of the manifold.

In testing, the angle of the port deactivation flaps was varied between fully open (0 degrees) and fully closed (90degrees) in steps of 30 degrees, giving four settings. Figure 3.12 below, shows the variation of in-cylinder swirl with port flap deactivation angle (calibration curve from a similar cylinder head supplied by Ford).

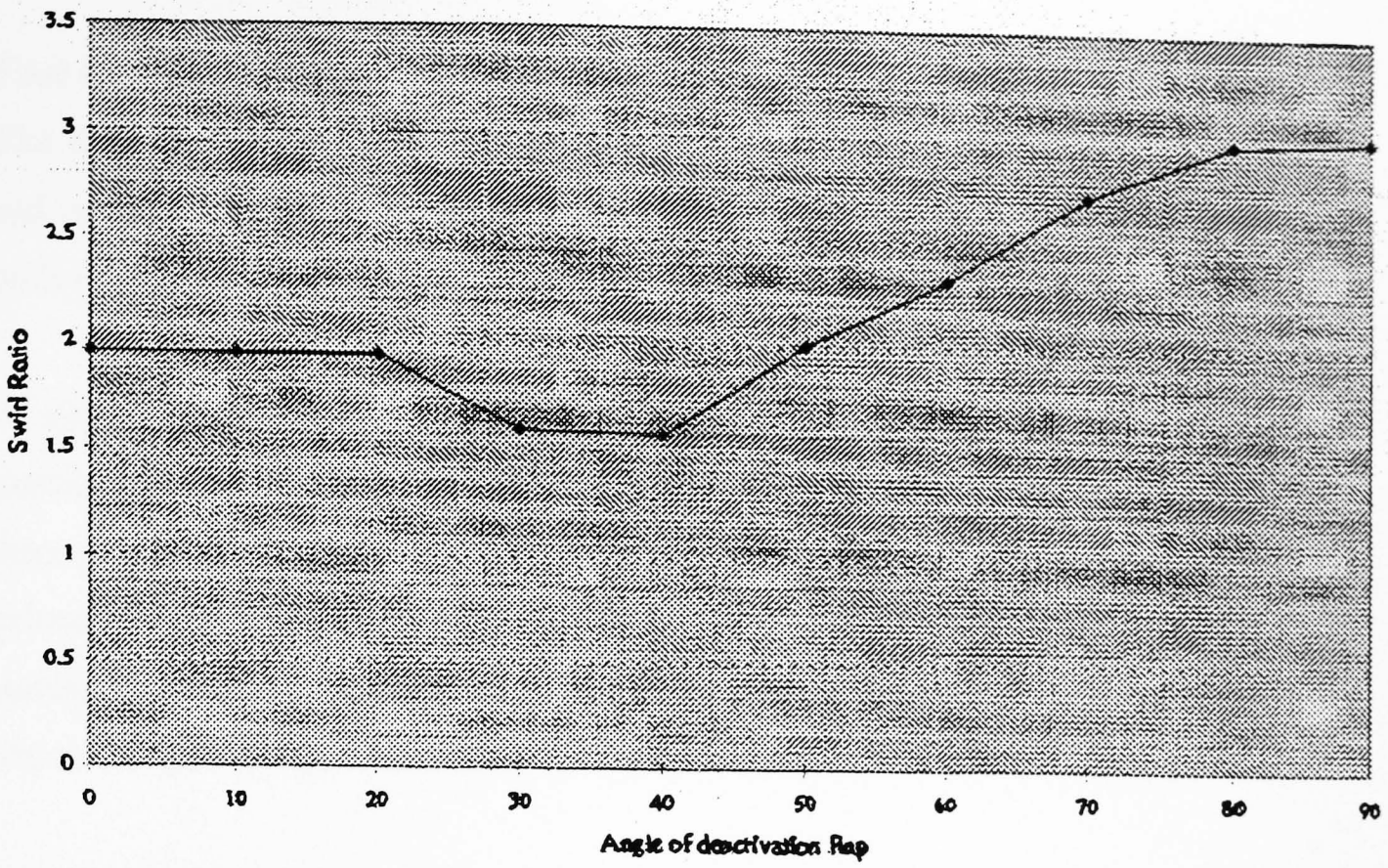

Figure 3.12 Variation of in-cylinder swirl ratio with port deactivation angle [Ford, internal publication].

It is worth noting in figure 3.12, that little variation of swirl occurs before 40 degrees port deactivation angle.

3.3.4 Fuel injection system

The Lynx Upgrade test engine was fitted with an electronically controlled distributor-type fuel injection pump, and dual-spring, two-stage, hole-type injection nozzles with 6 orifices. High injection pressure, and a multi-hole nozzle, combined to maximise fuel/air mixing, and the rate of diffusion burning.

Fuel injection pump (Bosch type VP30)

The fuel injection pump was of the distributor type, featuring an electronic actuator and integral timing device. Drive for the pump was taken from a toothed crankshaft pulley, which was driven at half of crankshaft speed.

A single, cam-plate-driven plunger-and-barrel assembly generated pressure and distributed fuel to each of the four cylinder injectors. As the pump plunger turned through one revolution, it completed a number of strokes, equal to the number of cylinders in the engine. The stroke of the plunger was the same under all operating conditions. Fuel demand was controlled by an electronic spill-valve and control collar, which dumped fuel pressure when the desired fuel quantity had been injected.

Injection timing was controlled by an internal electronic timing device, which mechanically changed the phase angle between the input drive and the cam plate. A limited mechanical range of injection timings was possible. Typically, this was between –15 degrees and +15 degrees of TDC, providing all necessary values for full engine testing and mapping.

Fuel was supplied to the pump under low pressure, in a re-circulating flow circuit to ensure a supply of cool fuel at all times.

Fuel injectors (Bosch 17mm, minisac, 2-spring)

The fuel injectors were mounted centrally in the cylinder, in-between the intake and exhaust valves. They were constrained in size to fit within this space, having a small diameter of 17mm and long overall height.

The nozzles were of the hole type, having 6 orifices of 0.152mm nominal diameter, from which fuel was injected. The 6 holes were spaced equally around the circumference of the nozzle, and had a nominal cone angle of 145 degrees between opposite holes. A diagram of a section through the injector tip in figure 3.13, illustrates the cone angle of the injector holes, and the injector needle design.

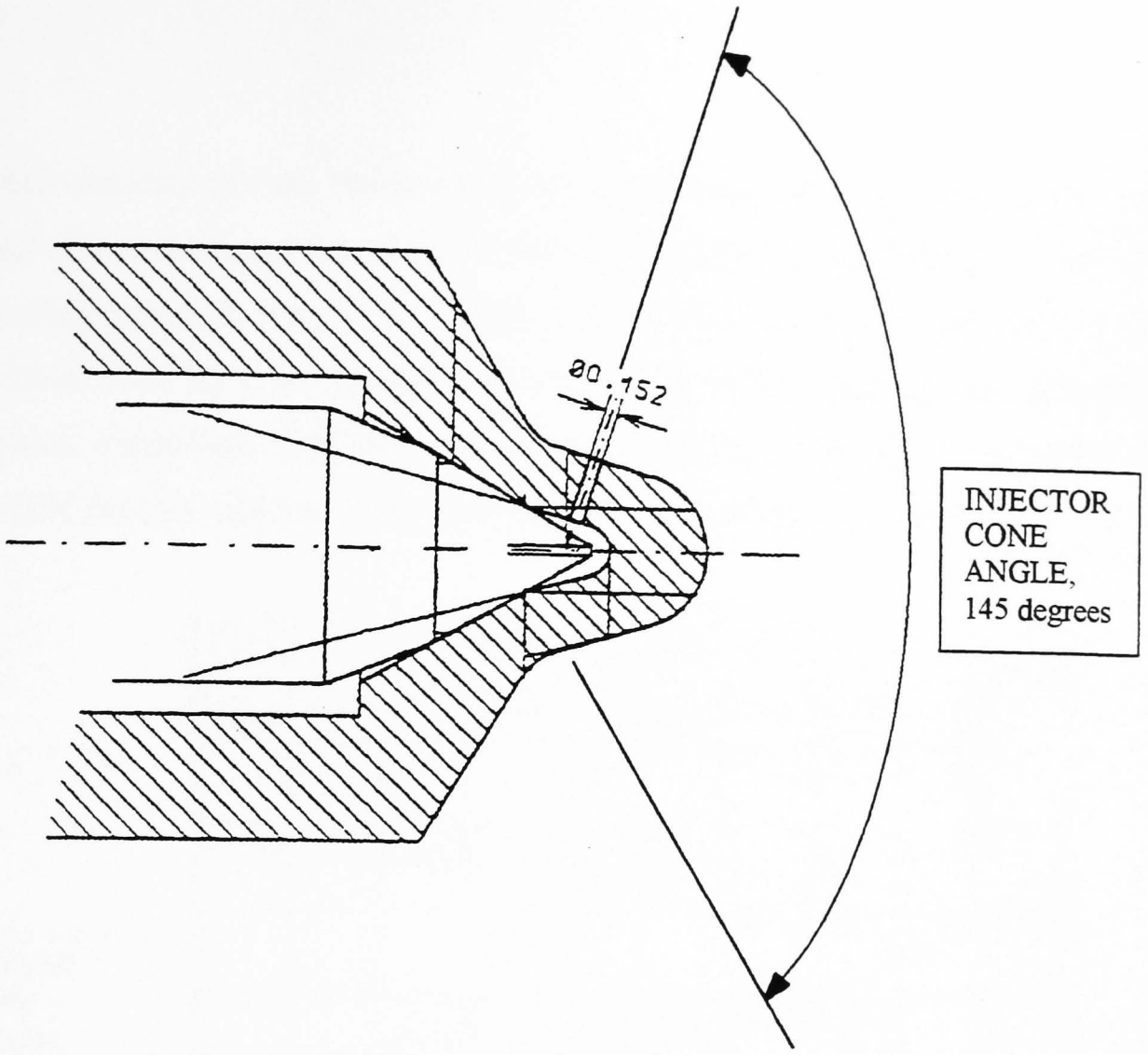

Figure 3.13 Section of the Bosch 17mm minisac injector tip used in the Lynx Upgrade engine [Bosch internal publication, 1996].

Only one injector nozzle hole is shown in figure 3.13 for clarity. Note the small injector sac volume to minimise HC emissions from late evaporation of fuel from the injector nozzle sac.

The design of hole-type injector nozzles is, generally, focused on rapid opening and closing rates to optimise spray structure, by rapidly establishing the desired spray pattern. Spring pressure keeps the needle seated until such time as the fuel pressure (acting on the difference of area of the needle and seat) creates a force greater than the spring force, when the needle will start to lift. Once needle lift has started, the area of the needle exposed to fuel injection pressure increases dramatically, ensuring rapid nozzle opening. The needle does not seat again, until the fuel line pressure has dropped to well below the opening pressure.

Fuel injectors used in the Lynx Upgrade engine were of 2-spring design. With this design, the injector opens in two stages. It opens slightly in the first stage, releasing a

small quantity of fuel, followed by its normal opening. This was used to modify the rate of fuel discharge into the cylinder to control noise and emissions. The first nozzle opening pressure was set at 200bar, whilst the main nozzle lift pressure was set at 360bar. Fuel injection pressure, subsequent to nozzle opening, was well above these values, exceeding 1000 Bar at high engine speeds. A typical fuel injector needle lift profile for this injector, at medium load demand, is shown in figure 3.14.

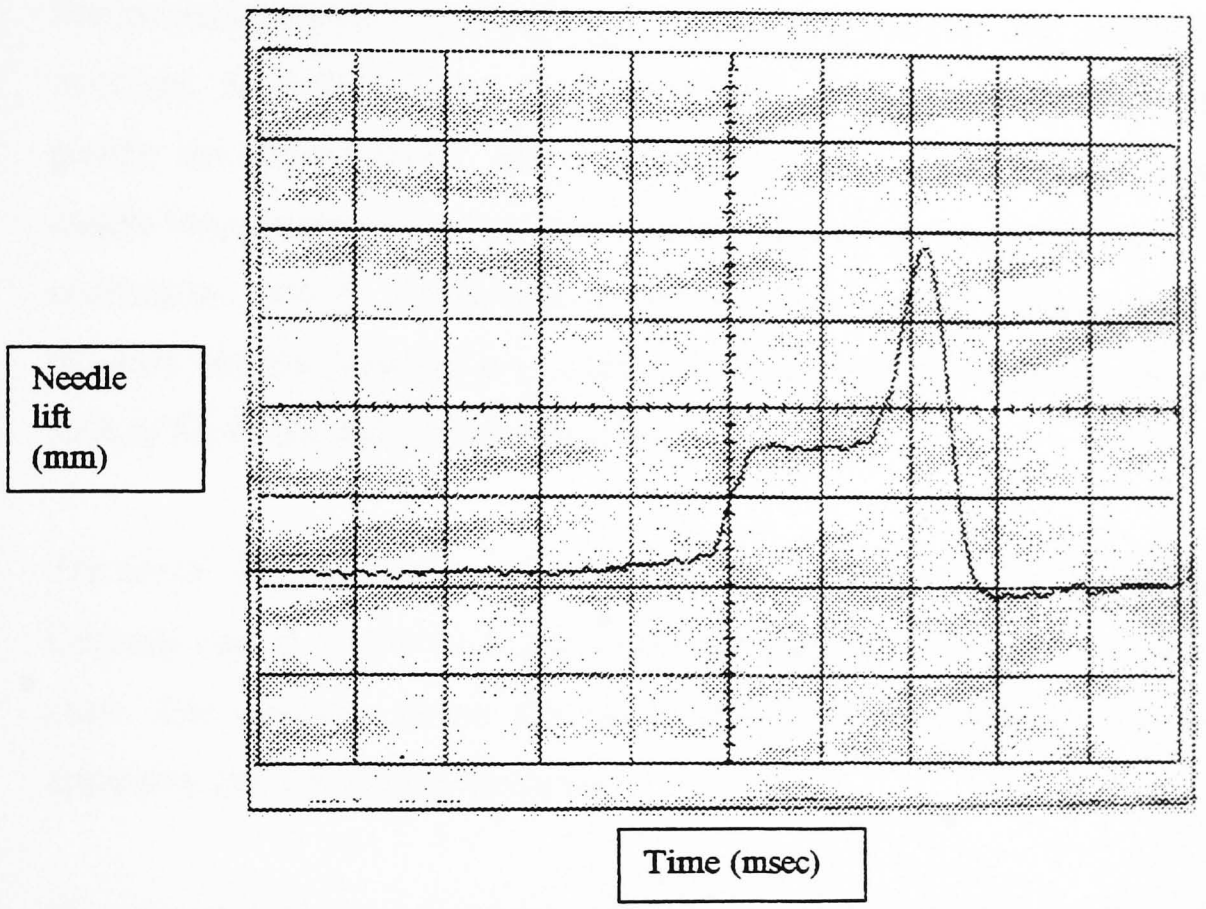

Figure 3.14 Oscilloscope trace/diagram of injector needle lift for the Bosch 17mm minisac injector (not to scale).

A distinct step exists between the first and second needle lift stages (shown in figure 3.14), corresponding to the different rate springs. The needle lift of the first stage was just 0.02 mm, whilst the maximum needle lift in figure 3.14 did not reach the injector limiting value of 0.35 mm (only achieved when operating at high engine load).

3.3.5 Engine management system

Engine management was by Bosch electronic control hardware, and Bosch VS100 engine management software. The system was suitable for application to a complete vehicle testing installation, and was very comprehensive. The vast majority of functions were not used during engine testing.

Engine management systems primarily change the injected fuel quantity and timing of injection, according to the torque demand of the driver (through the accelerator pedal), the engine speed, and secondary inputs such as coolant temperature. The engine torque response to driver demand is limited at any particular speed by several constraints, such as production of visible smoke in the exhaust, and peak cylinder pressure. Engine management systems are also used to change many other functions such as EGR rate and port deactivation.

The overall layout of the engine management system used during testing of the Lynx Upgrade engine is shown in the schematic diagram of figure 3.15, on the following page. The diagram shows the interaction between different electronic hardware apparatus, and the engine hardware.

The operating strategy and calibration maps were contained within the Bosch VS100 software. At the start of each testing run, the calibration strategy was loaded onto the PC work-base and downloaded into the EPROM of the electronic control unit (ECU), via the INCA (integrated calibration and application tools) box. The calibration strategy loaded as a duplicate copy. One copy contained a reference calibration strategy, and the other contained the working calibration strategy. The working calibration strategy could incorporate the users own calibration modifications. During testing, the reference and working copies of the calibration strategy were maintained the same. When the system went on-line, the calibration strategy stored in the working side of the ECU was used to communicate with the pump control unit (PCU), and ultimately control the engine operating condition.

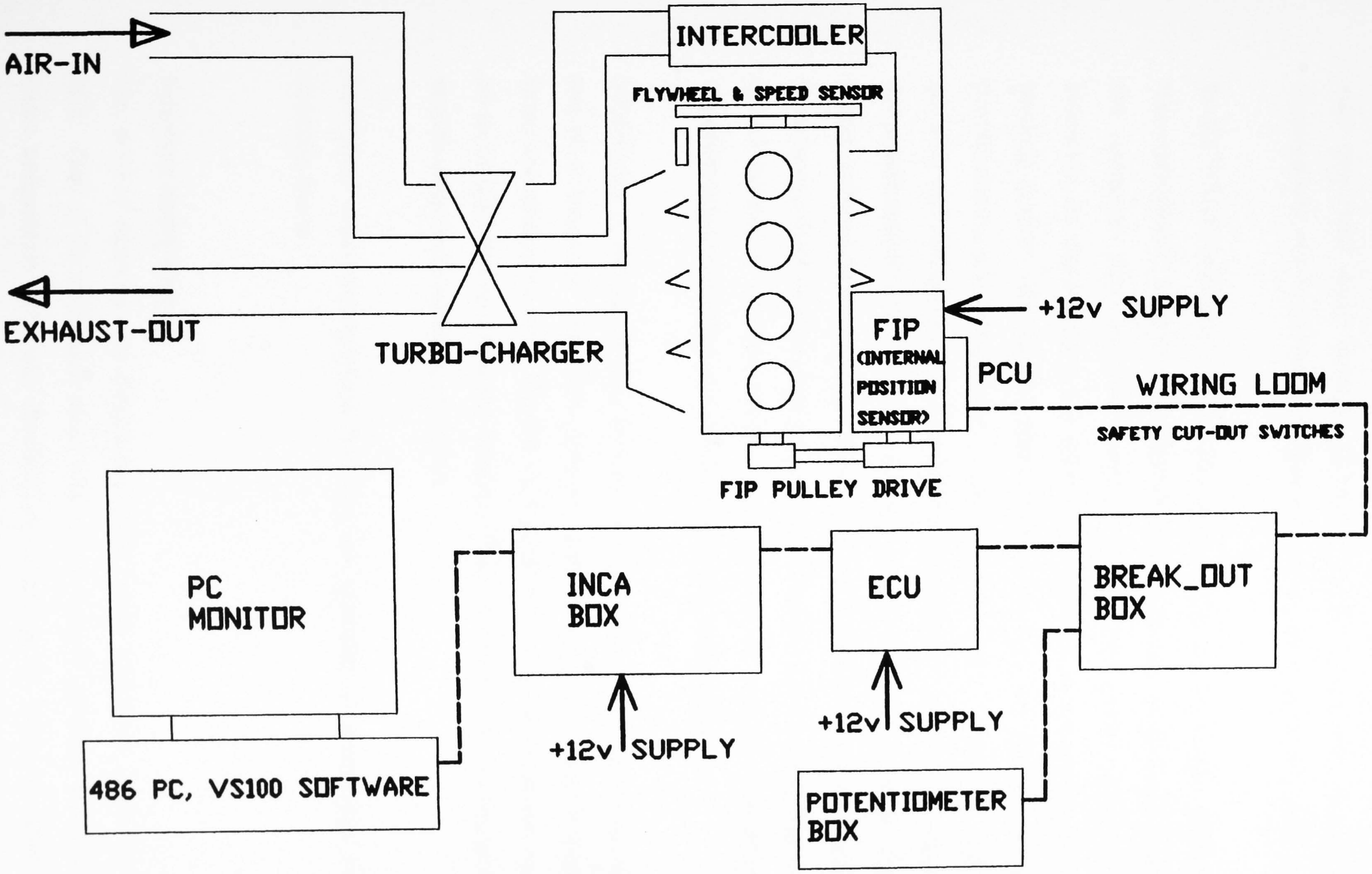

Figure 3.15 Schematic diagram of engine management system and engine hardware

The PCU had the job of converting the set-point demand signal from the ECU into fuel quantity and timing drive signals for the fuel injection pump hardware. The pump also processed other internal functions, such as camshaft speed and pump temperature, which enabled it to maintain its own performance and consistency.

In the VS100 software designed for application to vehicle testing, fuelling quantity was controlled by a throttle potentiometer, and injection timing changed according to the numerous other calibration maps to obtain the desired operating condition. However, for engine testing, the system was converted so that independent control of fuelling quantity (for engine torque control) and injection timing was possible. A potentiometer box, containing 10-turn potentiometers, controlled fuel injection quantity and injection timing. The fuelling potentiometer was a direct replacement of the potentiometer which would have been a function of throttle position. The injection timing potentiometer replaced a thermistor, the resistance of which would normally have been a function of coolant temperature. The calibration strategy was exploited to obtain control of injection timing, by modifying an existing calibration map for injection timing correction as a function of coolant temperature.

Monitoring of the signals sent from the ECU to the PCU was made possible by the use of a 'break-out' box. This contained pull-out connecting plugs between wiring loom communication lines. Signals such as the flywheel position sensor were viewed on an osscilloscope to determine dynamic TDC. The brake-out box also enabled easy modification to the wiring loom layout.

Individual engine management functions are explained in more detail in the sub-sections, below.

Injection timing control

The start of injection was determined from several calibration maps stored in the ECU. One of the calibration maps was a correction of injection timing for coolant water temperature. This was modified by extending the range of injection timing variation, and using an external potentiometer in the 'pot box' for its control.

Only a limited range of injection timing change was available, typically corresponding to 15 crankshaft degrees either side of TDC. The fuel injection pump was positioned such that its mechanical 'window' of injection timing range corresponded with the desired intelligent software 'window' timing range.

Fuel injection quantity

Fuel injection quantity was calculated in the ECU and metered in the PCU. The quantity of fuel to be injected was normally determined using time-synchronous calibration maps stored in the ECU, although some functions were calculated as speed-synchronous calculations, to cope with the fast response necessary during transient operation.

The only inputs that were given for calculation of the fuel injection quantity during testing, were the accelerator position and engine speed. This allowed completely independent control of fuelling, and allowed over-fuelling if required. If the engine was installed in a vehicle, many other inputs would have been used, such as intake-air mass flow rate, manifold pressure and coolant temperature. A series of calibration maps stored in the ECU were used to determine the required fuel injection quantity for the demanded operating condition. Calibration maps were determined such that the desired operating condition was achieved in the minimum time, consistent with emission and fuel economy limits, and limiting torque (and hence cylinder pressure).

The engine starting fuel quantity initially ramped up to a limiting value during cranking, until the engine started. If the engine would not start, the fuelling reduced. It was necessary to reset the ignition switch on occasions to re-initiate the starting fuel map.

Engine speed and position sensors

An electromagnetic sensor was positioned close to the flywheel edge. The flywheel had trigger holes which enabled the calculation of engine speed, and also the position of TDC. The position in the four-stroke cycle was determined by the injection pump,

as it rotated at half crankshaft speed and, therefore, once every four-stroke cycle. The TDC identification was used to set the engine crankshaft encoder position for data acquisition.

Turbocharger boost pressure

Whilst the engine management software did have provision for turbocharger boost control, this was not used for the engine installation at Brunel University. The turbocharger used was of conventional waste-gated type, responding to intake manifold pressure. Intake manifold pressure was restricted by the waste-gate to approximately 2 bar absolute pressure. The turbocharger was sized such that full boost was achieved at approximately 2000 rpm and full-load, thereafter being waste-gated to control the turbine speed and boost.

EGR control

Control of EGR was by an external system commissioned at Brunel, using the existing vacuum actuator and new pressure-to-vacuum actuators, which converted a high velocity air stream into a vacuum via a venturi. EGR quantity was measured indirectly by recording the reduction in engine airflow as a result of the EGR, at any particular engine speed and load. This gave a repeatable measure of EGR on a volumetric basis, but this was not proportional to the mass of EGR trapped in the engine cylinder, because the EGR temperature was not considered.

3.4 Engine fluid systems

The complete dynamometer installation in the test cell included several important engine fluid systems. These were essential to supply fuel and air for combustion, but also to maintain the engine at the desired operating condition (ie. maintain temperatures within a desired range).

3.4.1 Engine cooling fluid and engine oil

The engine cooling fluid (a mixture of water and anti-freeze solution) and engine oil were maintained at a temperature pre-set by the operator, by means of a closed-loop control system. Typically, during testing, the coolant temperature was maintained at 90 degrees C, whilst the engine oil temperature was kept at 120 degrees C. A schematic diagram of the combined engine coolant and oil coolant systems is shown in fig 3.16, on the following page.

The cold reservoir used as the cooling sink for the heat exchangers was a large water storage tank, installed on the roof of the laboratory tower, of large heat capacity. Temperature sensors were installed at the exit of the engine cooing water and engine oil cooling circuits. These were used as inputs for the Schenck closed-loop control circuit. Three-way fluid control valves controlled the fluid-flow distribution to maintain the pre-set temperatures.

3.4.2 Fuel supply

The fuel supply circuit comprised the supply and return lines to the high-pressure fuel injection pump and injectors, and also the fuel supply measuring apparatus. A schematic diagram of the fuel supply circuit is shown in figure 3.17, in the following pages.

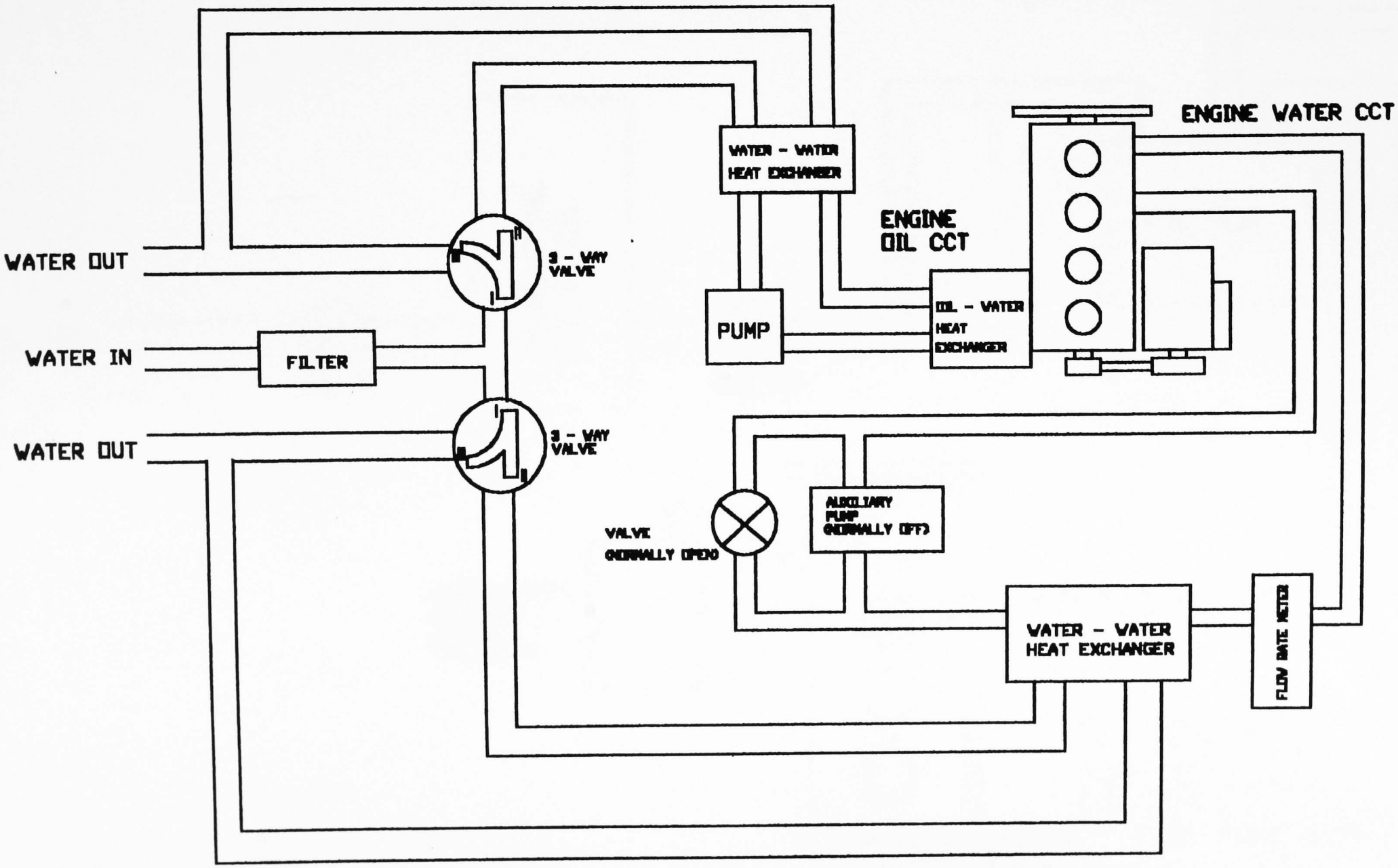

Figure 3.16 Schematic diagram of engine coolant and oil coolant systems.

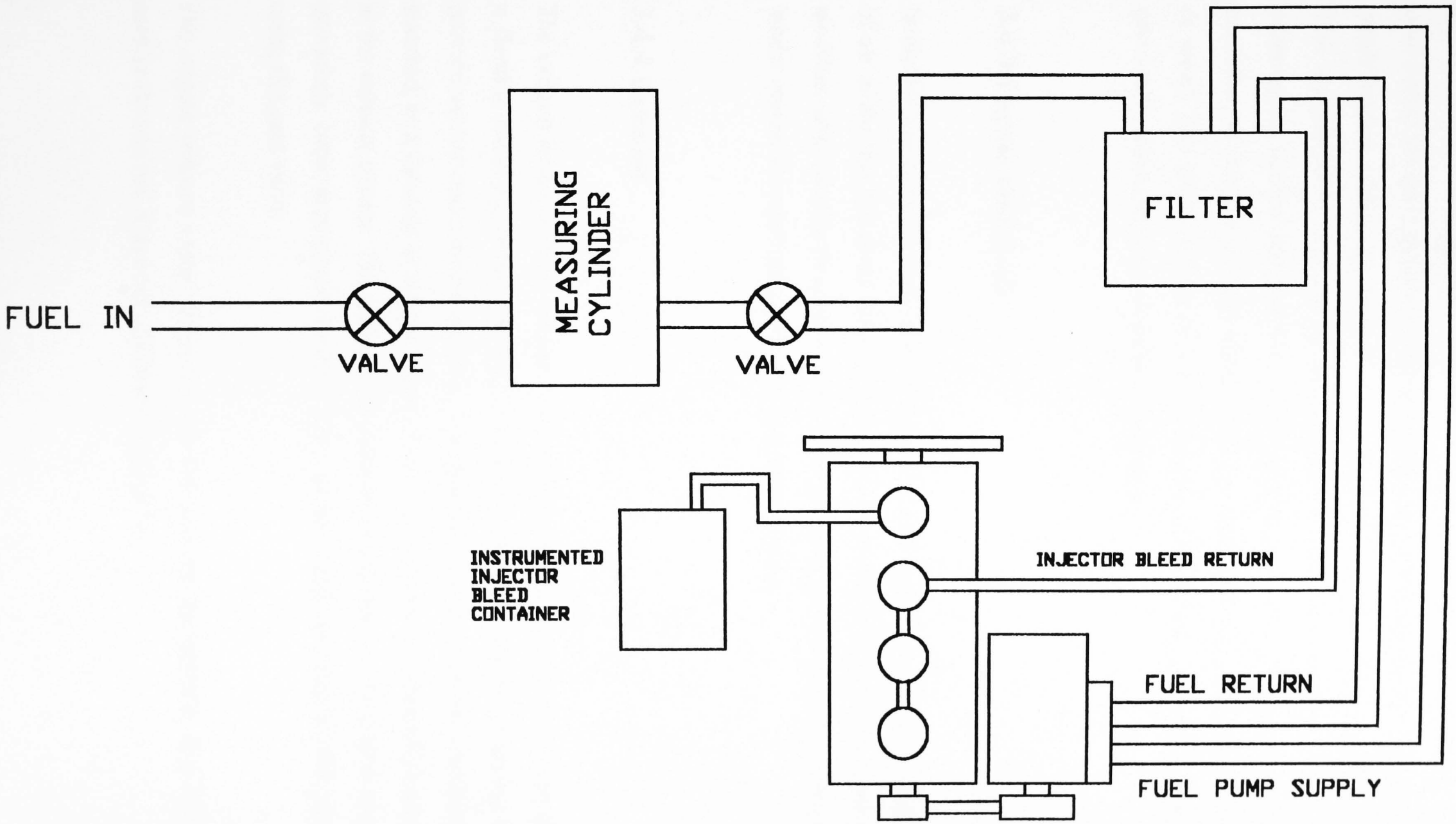

Figure 3.17 Schematic diagram of fuel supply circuit.

Excess fuel was re-circulated from the fuel injection pump to the fuel filter, to ensure cool fuel at the fuel injection pump inlet at all times. Internal injector leakage caused a small fraction of the high-pressure fuel supplied by the fuel injection pump to be lost. This was normally returned to the fuel filter to be consumed by the fuel injection pump again, but fuel leakage from the instrumented injector was piped to a collection container, to monitor injector leakage (and therefore for early indications of problems or wear). The small amount of fuel not consumed by the engine, but which had been previously measured, was considered negligible.

3.4.3 Engine intake air

Intake air was drawn from within the test cell (a ventilation fan ensured a clean supply of air to the test cell at all times from outside the cell), through the standard vehicle air-filter, after passing through a positive displacement airflow-rate meter. The vehicle intake system was replicated until the compressor intake.

3.4.4 Exhaust

The exhaust from the turbo-charger turbine exited into the exhaust down-pipe through a flexible coupling, before passing through an oversized exhaust silencing box to provide unrestricted exhaust gas flow. The exhaust back-pressure characteristics were matched, as a function of engine speed (at full load), by adjusting an in-line gate valve in the exhaust system. The variation of exhaust back-pressure with engine speed had previously been determined by Ford from an in-vehicle installation, and replicated using this gate valve.

The engine exhaust exited from the test cell into the atmosphere, at a high level outside the test cell to provide adequate dispersion.

3.5 Engine instrumentation and data acquisition

3.5.1 Overview of instrumentation and data acquisition

The engine was equipped with extensive instrumentation to enable detailed analysis of combustion, performance, and emissions, all being vital to understanding the effect of piston bowl shape on combustion and emissions. Cylinder number four was chosen for instrumentation for combustion analysis, and fitted with a cylinder pressure transducer, a pressure transducer for measurement of fuel injection line pressure, and an instrumented injector for accurate injector needle-lift history.

High-speed data acquisition of crank angle dependant functions was performed using the 'Computerscope ISC-16' data acquisition system. It consisted of a 16-channel, 12-bit, A/D converter installed in a 386 PC, an external interface, and scope driver software. It was used to sample cylinder pressure, fuel injection line pressure, injector needle lift and TDC at each clock signal of one-degree crank-angle. Maximum sampling rate capability was 1MHz for a single channel, but the actual sampling rate was determined during testing by engine speed, as the sample was triggered by the crank-angle clock signal. A 128 K byte buffer was used to store data, before saving onto a diskette for post analysis.

Post-processing of data was performed using proprietary combustion analysis software. The software was divided into three main sections. The first was used to condition the data into standard format for heat release analysis, by setting the crank angle position of TDC, and correcting any offset of cylinder pressure data to the measured intake manifold pressure at the test condition (which changed significantly in the turbo-charged engine). The second stage of the combustion analysis software was then used to calculate heat release rate parameters, and plot graphs of interest for presentation. Single cycle analysis only was possible, although comparison of many different cycles showed there was little cycle-by-cycle variation. The combustion analysis was performed according to the first law of thermodynamics, with heat loss from the engine combustion chamber surfaces estimated using the Woschni heat transfer correlation [Heywood, 1988].

3.5.2 Cylinder pressure

Cylinder pressure was measured using the Kistler type 6055B80 minature piezoelectric pressure transducer. The charge signal was then amplified to produce a voltage proportional to cylinder pressure (the pressure transducer was calibrated previously at Kistler), and then logged as a function of crank-angle by the Computerscope data acquisition system.

The pressure transducer was mounted in a special glow plug adapter, designed to fit in the original cylinder head glow plug hole without any modification. A diagram of the pressure transducer mounted in the glow plug adapter is shown in figure 3.18 below.

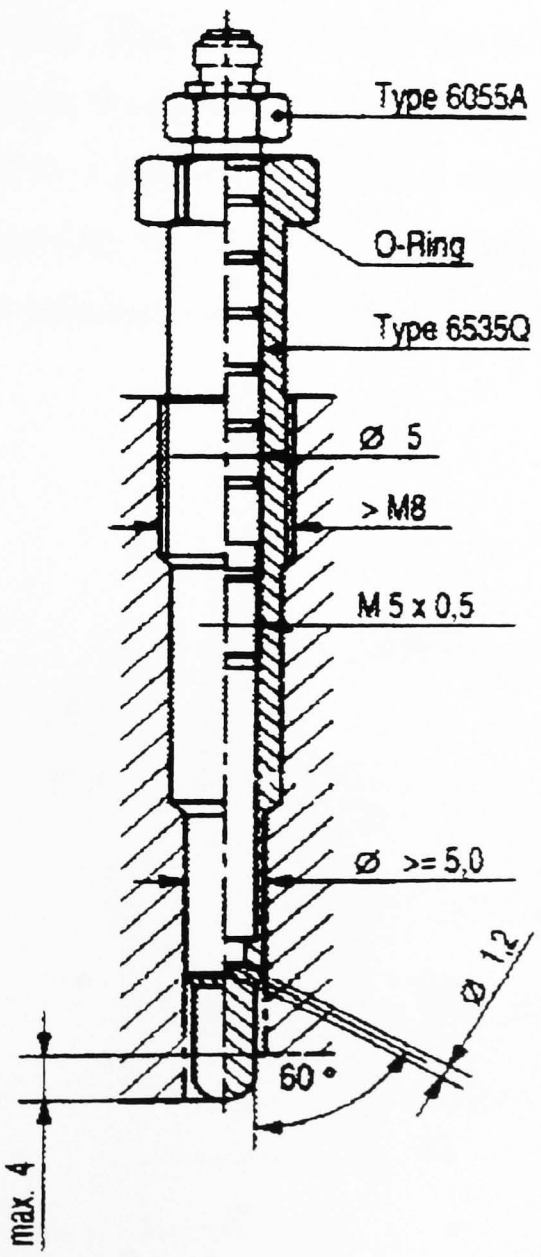

Figure 3.18 Kistler type 6055B80 cylinder pressure transducer, installed in a glow-plug adapter similar to the one used for the Lynx Upgrade engine [Kistler, 1997].

The pressure transducer diaphragm (see figure 3.18) was exposed to cylinder pressure through small holes in the glow plug adapter tip. Testing showed that the relatively small and long cavity between the main cylinder volume, and the measurement diaphragm, did not cause excessive ringing of the pressure trace at most operating conditions.

3.5.3 Fuel line injection pressure

Fuel injection line pressure was measured using a Kistler type 4067 A2000 high-pressure sensor, capable of measuring the dynamic fluid line pressure of up to 2000 Bar during fuel injection. This was critical for use in CFD calculations, where the rate of fuel injection had to be known for accurate combustion modelling. The charge signal was amplified by a Kistler type 4618A2 charge amplifier. Data was logged at each engine crank angle by the Computerscope data acquisition system. A diagram of the fuel line pressure transducer and mounting clamp is shown in figure 3.19.

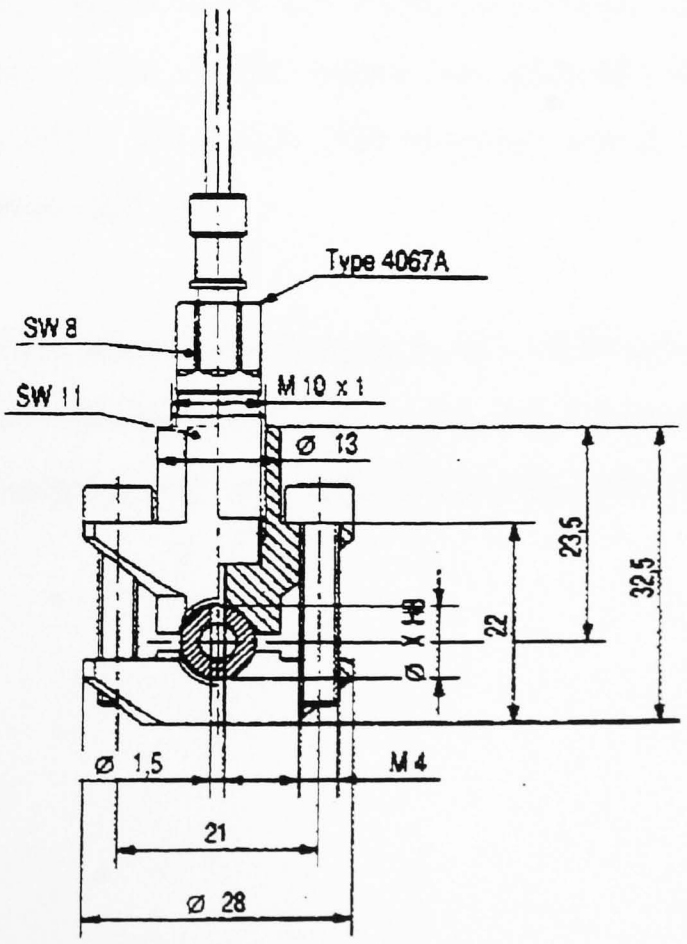

Figure 3.19 Kistler type 4067 A2000 high-pressure transducer used to measure dynamic fuel line injection pressure [Kistler, 1995].

The fuel line pressure transducer was mounted as close to the injector as possible, to reduce the effect of wave propagation on the timing of results. The pressure transducer was clamped onto the high-pressure fuel injection line, and subjected to fuel pressure through a small drilling made in the fuel line.

3.5.4 Injector needle lift

Injector needle lift was measured to determine the actual start-of-injection, and for use in calculation of the rate of fuel injection (when combined with fuel line pressure and nozzle dimensions). A special Bosch 17mm injector supplied by Ford was used during engine tests. This featured a ferrous core which followed injector needle lift, situated inside a coil of wire. Needle lift changed the inductance of the coil of wire.

A Lucas CAV, frequency-modulated (FM) type amplifier and remote oscillator box were connected to the needle lift coil, forming a tuned circuit. The motion of the injector needle caused changes in the coil inductance which, in turn, caused shifts in the oscillator frequency. Thus, an FM signal was generated by the needle motion, which was demodulated by the Lucas FM amplifier into an amplitude-modulated (AM) voltage output from this unit.

The AM signal for needle lift was also output to an oscilloscope, and used for setting injection timing at each test condition. The signal was displayed on screen, together with the TDC, crank-angle clock, and cylinder pressure channels. This is shown in figure 3.20 below.

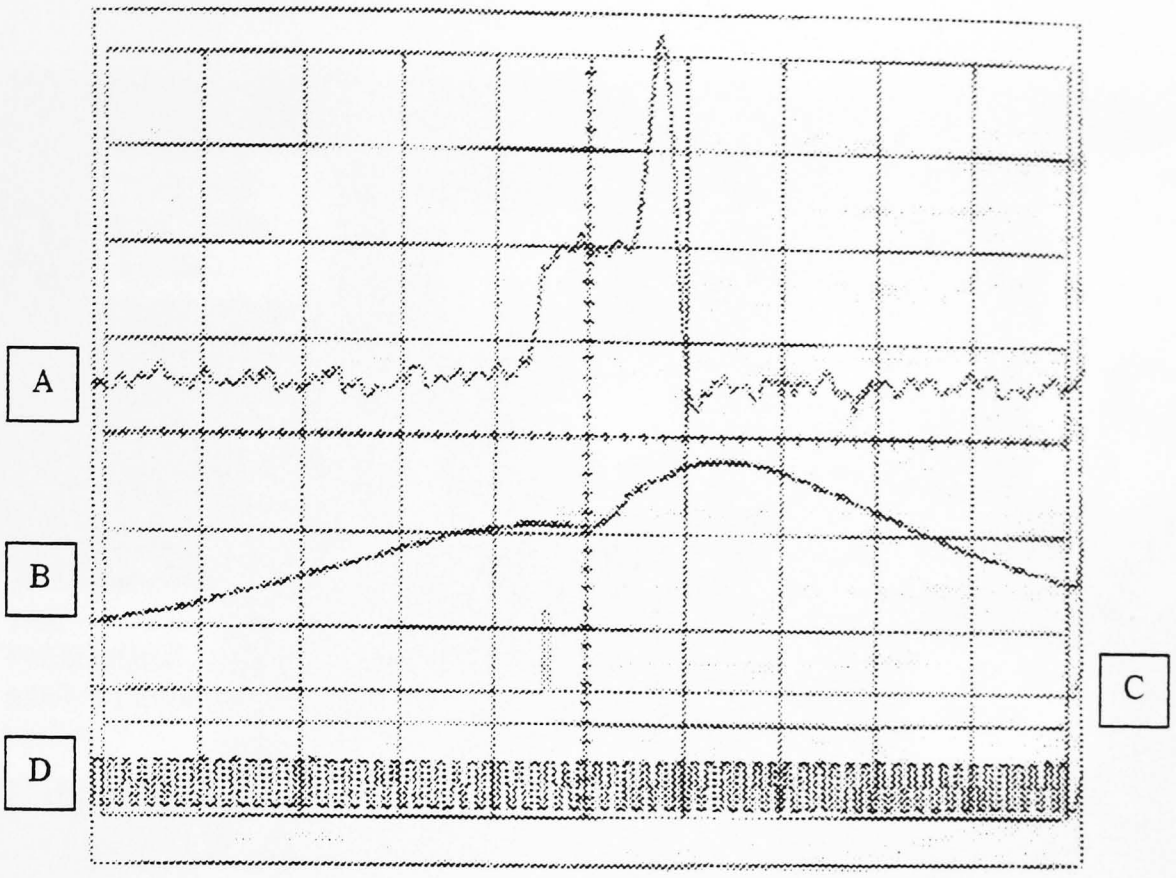

Figure 3.20 Oscilloscope trace showing from the top: (a) injector needle lift, (b) cylinder pressure, (c) TDC flag and (d) crank angle clock signal (1 pulse per degree).

The start of injector needle lift was compared with the TDC flag and crank-angle clock signal to determine the start of injection.

3.5.5 Crank angle position

After much modification a reliable shaft encoder system was developed at Brunel, using the 'Mini-coder' type GEL 244 pick-up head and 360-tooth gear wheel with separate TDC flag. This was used to accurately measure engine TDC position and crank-angle position in increments of one crank-angle division. A picture of the shaft encoder installation on the engine is shown in figure 3.21.

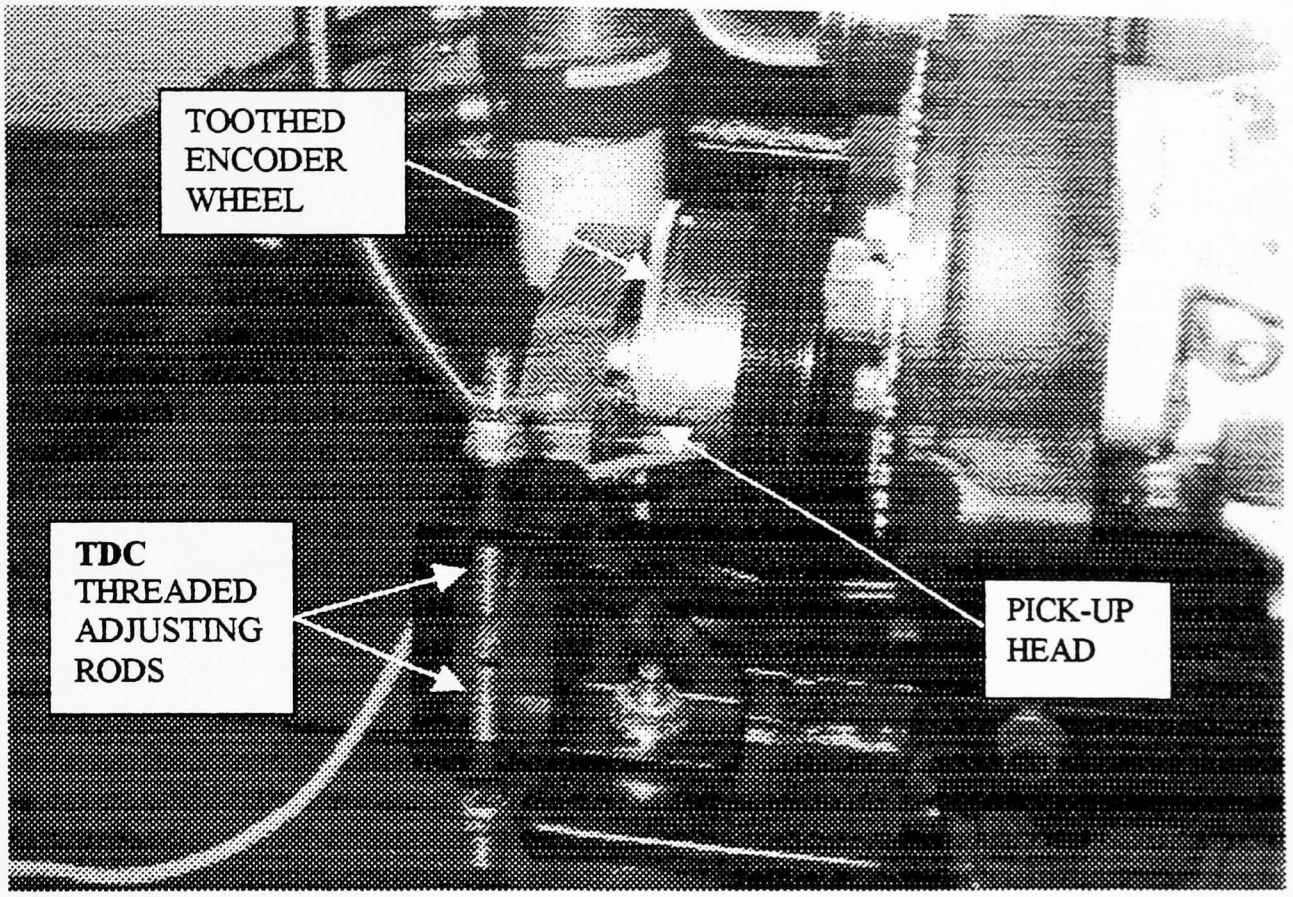

Figure 3.21 Photograph of the shaft encoder installed on the engine. The 360-tooth encoder wheel, pick-up head, and adjustment treaded rods are clearly visible.

Accurate alignment of the TDC flag on the toothed gear-wheel, with the actual engine TDC was made possible using treaded adjustment rods, which positioned the pick-up head relative to the toothed wheel. Actual engine TDC was measured from a signal sent to the ECU from the flywheel pickup when the engine was running. This corresponded to ten-degrees after TDC.

The signal was displayed on an oscilloscope with shaft encoder TDC and crank angle clock signal as shown in figure 3.22. The pick-up head position was adjusted to synchronise shaft encoder and engine TDC.

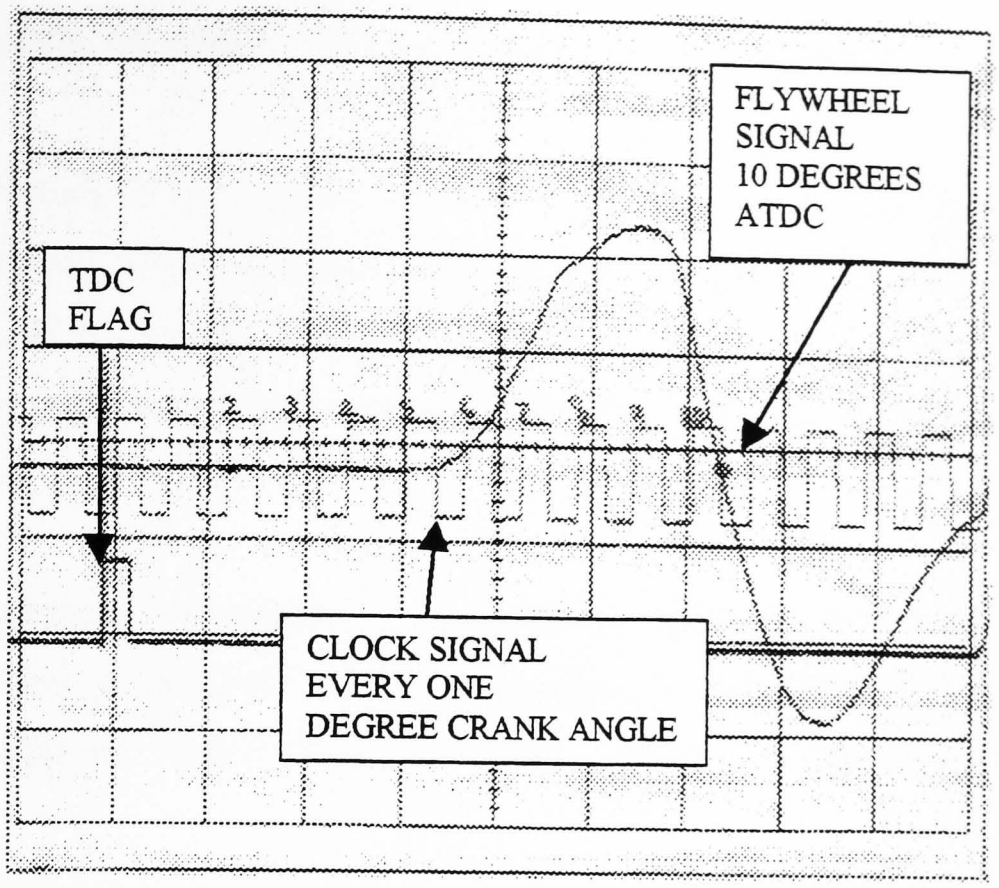

Figure 3.22 Oscilloscope trace showing the method of determining shaft encoder TDC. Flywheel signal was used as a reference at 10 degrees ATDC.

Prior to the shaft encoding system described above, optical shaft encoders purchased off-the-shelf were used. These could not withstand the harsh vibration environment, and failed frequently, resulting in considerable loss of test time.

3.5.6 Quasi-steady data acquisition

In addition to the high-speed data acquisition of crank-angle dependent parameters (such as cylinder pressure), low-speed quasi-steady pressures and temperatures were recorded at key points on the engine.

Many K-type thermocouples were positioned to measure the temperature at various points in the intake manifold system, exhaust manifold, turbine intake, the exhaust down-pipe, engine coolant and engine oil etc. Similarly, many steady-state pressure measurements at points of interest enabled calculation of pressure ratios and efficiencies. A selection system of valves made it possible to sample a large range of pressure points, using only a small number pressure transducers of the appropriate range.

3.6 Overview of emissions measuring equipment

The primary focus of this project was the trade-off between particulate mass and oxides of nitrogen, when the piston bowl shape was modified. For this reason, the measurement of the emission of smoke, HC and NOx was essential. CO and CO2 were also measured, as they were useful indicators of combustion efficiency and EGR level.

Emissions equipment was regularly maintained and calibrated before each reading, or each set of tests, as required. Where on occasion it was necessary to change the emission equipment, back-to-back comparison tests were performed to confirm repeatability.

3.6.1 NOx measurement

A chemiluminescent analyser, AAL model 443, was used to measure NOx during all engine tests. The unit proved very reliable and repeatable. The meter was able to measure both NO and NO_2 concentrations separately if required, but was always used to measure total NOx during engine tests.

The unit contained a heated sample module, allowing it to directly sample exhaust gas in the 'wet' condition. NO_2 was first catalytically converted into NO, and then the exhaust sample was passed into a low-pressure heated vacuum chamber. Here, ozone (O_3, created by a high-voltage electrical discharge through oxygen gas) was mixed with the exhaust sample, some of which reacts with the NO to form NO_2, emitting a photon of light in the process, which was recorded by a photomultiplier tube. The intensity of light was proportional to the concentration of NOx. Calibration using a span gas of known NOx concentration gives the absolute NOx concentration.

3.6.2 Smoke measurement

Smoke was measured by an AVL type 415, automatic-variable-volume sampling smoke meter. A short length of tube connected the smoke meter sampling port to the engine exhaust.

When a measurement was required, a remote switch caused a sample volume of exhaust to be drawn into the meter, where it was sucked through a clean piece of filter paper tape (supplied in the form of a roll). The blackness of the filter paper was measured automatically by a calibrated reflectometer head. Using the reflectometer value, and the known volume of exhaust sample, the smoke meter ECU calculated the soot concentration in units of Bosch Smoke Number (BSN).

The system was automatic, with fresh filter paper being supplied from an internal roll. The unit proved very reliable and repeatable.

3.6.3 HC measurement

Reliability problems with an AAL model 523 FID hydrocarbon analyser, meant that measurements were also taken from a Signal 3000HM hydrocarbon analyser. Repeated back-to-back tests confirmed similar results for the two different analysers, and no differentiation was made between the two in the presentation of results.

The method of operation of both analysers was similar, operating on the flame ionisation detection (FID) method. A continuous sample of exhaust gas entered the analyser, after being transported from the engine through a heated sample line to prevent condensation of the heavier hydrocarbon fractions. A small amount of the sample was burnt in a hydrogen flame. Compounds in the sample which contained the H-C bond were ionised and caused a current to flow between collector plates. This current flow was amplified and related to the concentration of hydrocarbon molecules, through calibration.

As engine the exhaust consisted of a range of hydrocarbon species, the analyser was calibrated using propane (having a carbon number of three, C_3). A nominal propane concentration of 500ppm corresponded to a hydrocarbon reading of 1500ppm for C_1 molecules. The hydrocarbon meter, thus, acted effectively as a carbon counting meter, or equivalent concentration of methane.

3.6.4 CO and CO2 measurement

A multi-gas Richard Oliver K650, non-dispersive infra-red emission analyser was used to measure CO and CO_2 emissions, although its function extended to HC and O_2 measurements as well (O_2 by means of a garvanic cell). The concentration of each gas was measured by the infra-red energy absorbed by the exhaust sample at various wavelengths (corresponding to CO or CO_2). Each species (eg. CO or CO_2) absorbs energy at a different infra-red wavelength, which is known, and the extent of absorption can be related through calibration to the concentration of the species (eg. CO or CO_2) in the exhaust sample. The measurement of CO_2 was particularly useful for checking the concentration of EGR between similar testing conditions.

3.7 Conclusions

The experimental test facility, including the dynamometer, engine installation, instrumentation, and data acquisition, was commissioned and developed to enable the testing program to begin. Many teething and reliability problems were initially encountered, but solutions were found which were reliable and accurate.

A standard test and recording procedure was developed, and all measured parameters were logged for future reference if needed. Immediately after the experimental test facility was commissioned, base-line tests were performed to validate engine performance and emissions against the previous engine installation at Ford. Comparison of results proved satisfactory, allowing the experimental testing program to proceed.

Chapter 4:

Bowl design changes and philosophy

Chapter 4: Bowl design changes and philosophy

4.1 Introduction

A complete parametric study of the large number of piston bowl shape factors was not possible within the time constraints of this project. In addition, performing a parametric study whilst maintaining constant compression ratio, would have made it difficult to isolate one piston bowl shape factor for analysis without affecting many others.

The method of testing adopted for this project was one of learning from the results of each bowl shape tested, and implementing appropriate changes in the subsequent bowl design to test the understanding gained.

A short description of the critical parameters which affect piston bowl shape are included in this chapter. The four piston bowl shapes tested in this project are presented and discussed briefly here. A more detailed rationale of the reasons for the piston bowl shapes tested will become apparent in subsequent chapters, dealing with the analysis of results.

Generation of manufacturing drawings using solid revolution models within AutoCAD, the manufacturing process, subsequent inspection, checking and installation of piston bowl shapes is also described in this chapter.

4.2 Critical parameters of bowl design

The compression ratio (and thus piston bowl volume) was maintained constant at 19.6:1 throughout all engine tests. Compression ratio has a large effect on performance and emissions, so it was essential to eliminate this variable from piston bowl shape testing. For this reason, changes to one shape parameter of the piston bowl inevitably had a knock-on effect on other shape parameters, due to the desire to maintain the piston bowl volume and compression ratio constant.

A short description of the main features of HSDI piston bowl design, thought to affect engine performance and emissions, is given in the subsections below. All piston bowl shapes tested were symmetrical about their centre-line axis of rotation.

4.2.1 Throat diameter

The diameter of the throat was defined as the minimum diameter between the piston bowl edges, near the piston top face. The ratio of the throat diameter to the maximum bowl diameter defined the amount of re-entrancy of piston bowl design. The throat diameter is shown in the section through a typical HSDI piston bowl in figure 4.1.

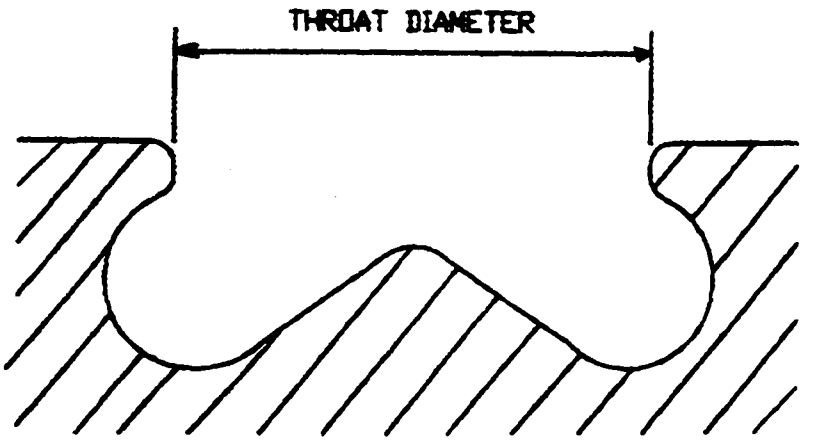

Figure 4.1 Section through a typical HSDI piston bowl showing the throat diameter.

The ratio of the throat diameter to the cylinder bore size also defined the percentage squish area. A small throat diameter caused a larger fraction of the piston face to closely approach the cylinder head, and therefore produced a higher squish velocity.

High velocity airflow into the bowl, and combustion gas out of the bowl, creates large temperature gradients and high heat transfer rates to the piston bowl top surfaces. The piston bowl lip is often the hottest part of the piston bowl internal surface. During the early combustion phase, the close proximity of the piston face to the cylinder head means that early burning flames are quenched on the relatively cool upper surface, and unburned fuel will not initially oxidise.

4.2.2 Maximum bowl diameter

The maximum bowl diameter was defined as the largest diameter parallel with the piston face at any position through a section of the piston bowl. The ratio of the maximum bowl diameter to the bowl depth defined the piston bowl aspect ratio. Figure 4.2 shows the maximum bowl diameter on a section through a piston bowl.

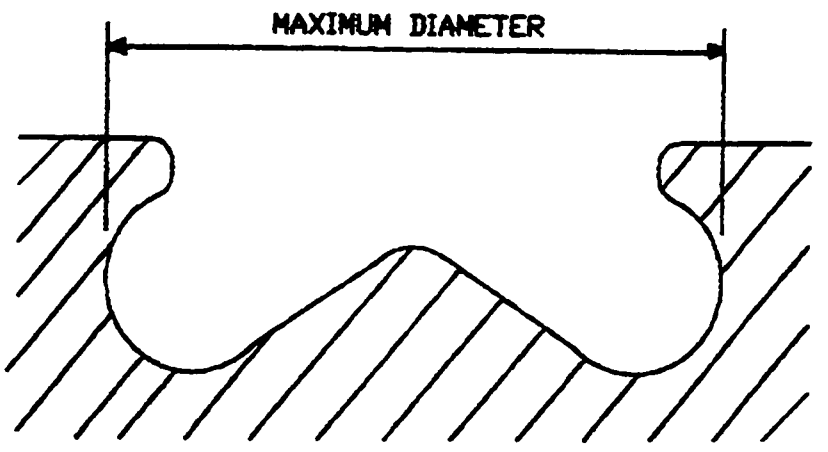

Figure 4.2 Section through a typical HSDI piston bowl showing the maximum bowl diameter.

The maximum bowl diameter is important because it affects the bulk swirl velocity at the end of compression. Increasing bowl diameter will reduce the swirl velocity in the bowl. This reduces the rate of air/fuel mixing, but can reduce heat transfer and other energy losses.

The maximum bowl diameter also affects wall wetting after injection, as fuel can be swept down the bowl into the main torodial radius. Bowl diameter may therefore be a significant factor in the production of smoke.

The piston bowl total volume, and thus compression ratio, is largely controlled by the maximum bowl diameter. This was one of the first parameters to be set when designing a new piston bowl shape.

4.2.3 Central pip

The central pip was used to occupy a volume in the centre of the piston bowl, where the air velocity is low. Low air velocity in the centre of the swirling flow-field results in poor air/fuel mixing rates. The central pip allowed this volume to be redistributed further from the centre of rotation, resulting in a higher mean airflow velocity and better air/fuel mixing. Figure 4.3 shows a typical central pip design, although pip shapes can change significantly between different piston bowls.

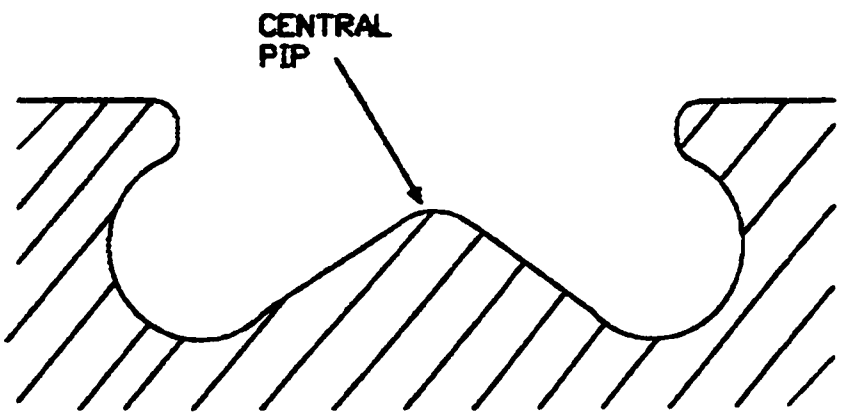

Figure 4.3 Section through a typical HSDI piston bowl showing the central pip.

Piston pip design is constrained by the need to prevent injector tip-to-piston contact when the engine is running (thermal expansion and inertial forces must be considered), and to prevent wall wetting of the piston pip by closely approaching fuel sprays.

The central pip shape occupies a relatively small proportion of the total bowl volume. Changes in the shape of the pip can be readily accommodated by small changes in other key dimensions further from the piston centre-line.

4.2.4 Bowl depth

Piston bowl depth was defined as the maximum depth from the face of the piston, to the bottom of the main torodial radius (in conventional bowl designs). Maximum bowl depth is indicated in figure 4.4.

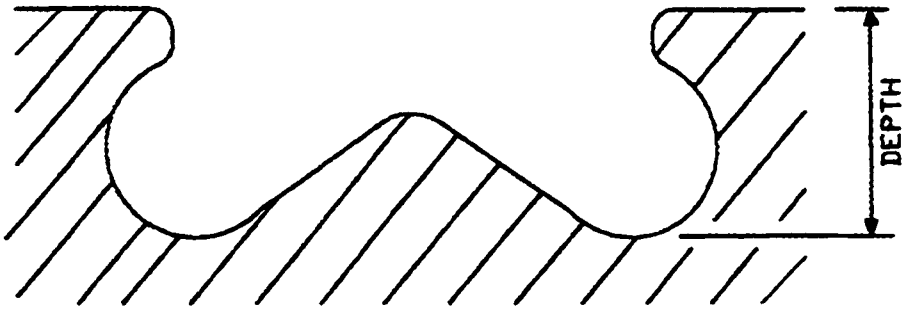

Figure 4.4 Section through a typical HSDI piston bowl showing the maximum bowl depth.

Bowl depth can affect the proportion of fuel that resides on the bowl floor until late in the combustion process, and thus affect the emission of smoke. Deep piston bowl depths tend to increase wall-wetting of the lower bowl surface, by preventing re-entrainment of fuel into the air-stream.

The bowl depth is closely linked with the need to provide a certain depth of fuel spray impingement area, and was often balanced with the volume occupied by the piston pip.

4.2.5 Main torodial radius

A diagram of the main torodial radius is shown in figure 4.5. The majority of combustion occurs in the main torodial radius volume. The main torodial radius was

one of the initial parameters defining a new bowl design, because it occupied such a large percentage of the total bowl volume.

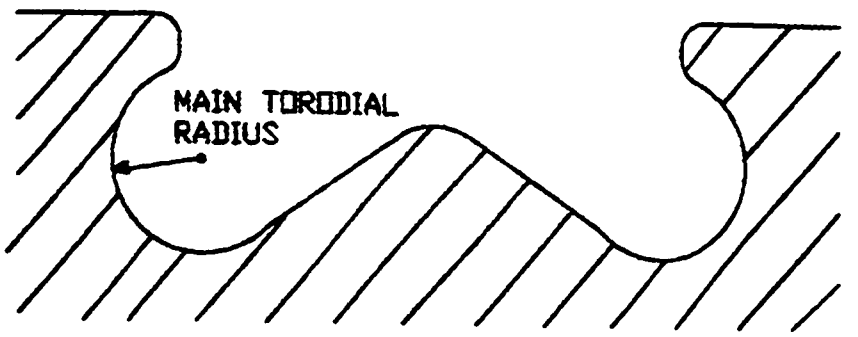

Figure 4.5 Section through a typical HSDI piston bowl showing the main torodial radius.

The volume contained within the main torodial radius affects modification of the airflow induced by squish action, and flame propagation and development towards the piston bowl pip. The main torodal radius often constrained the design of the piston pip (if the pip was designed to meet the main torodial radius at a tangent), to avoid discontinuities in the bowl section profile.

4.2.6 Impingement area

The area at the side of the piston bowl where high velocity fuel impinges during fuel injection is known as the impingement area. Figure 4.6 shows one such impingement point.

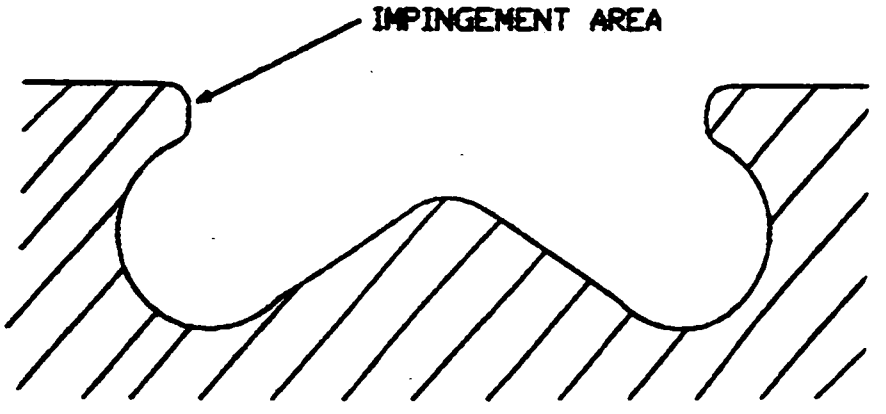

Figure 4.6 Section through a typical HSDI piston bowl showing the fuel impingement area.

Fuel impingement can be seen by inspecting the piston of an operating engine. Dark brown soot marks appear where the liquid fuel jet impinges on the piston side. Figure 4.7 indicates the points of fuel impingement on a Ford 2.5 litre, HSDI diesel engine piston. Five impingement points corresponding to the five injector nozzle holes can be seen.

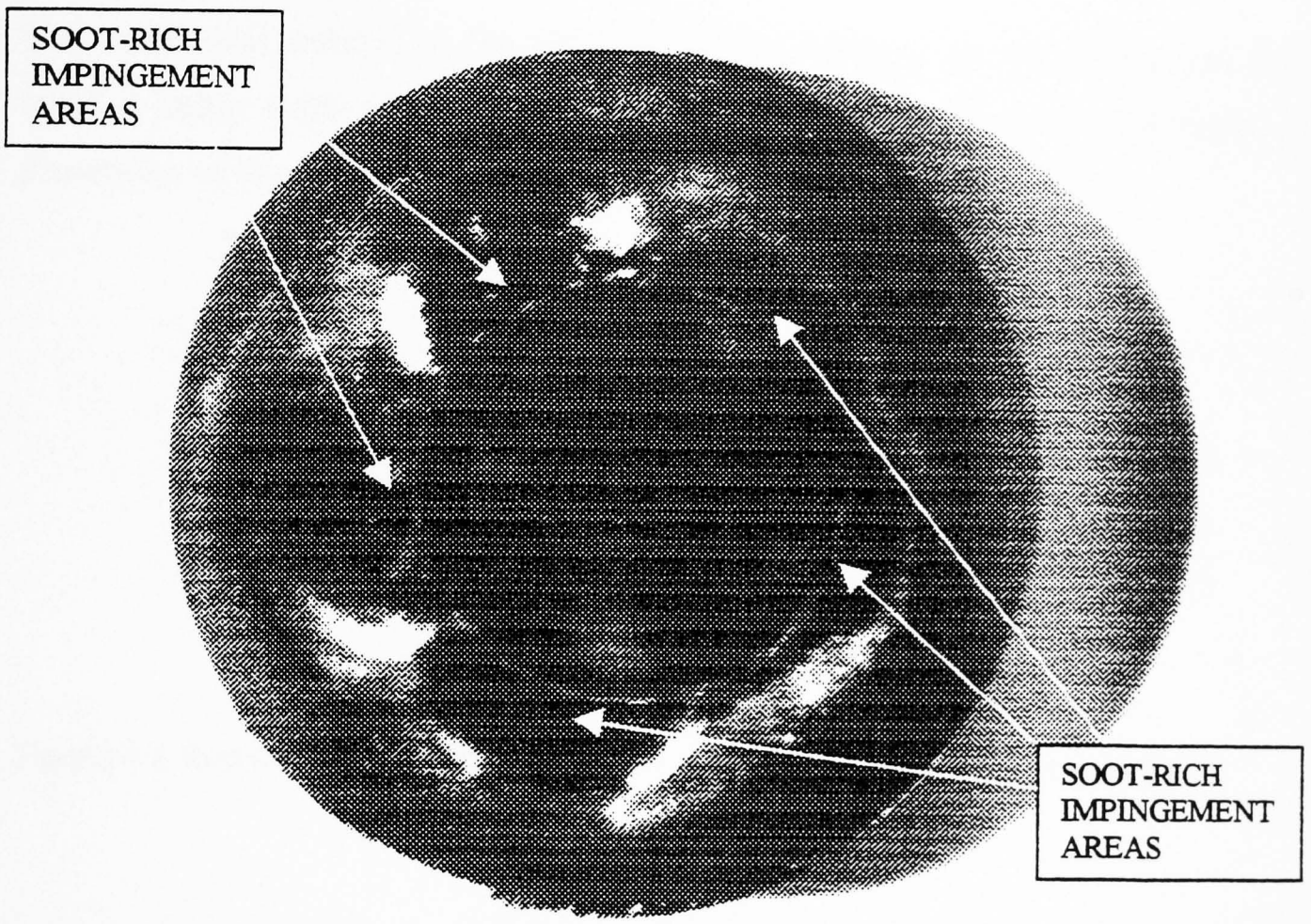

Figure 4.7 Photograph of a Ford 2.5 litre, HSDI diesel engine piston top-face, illustrating the points of impingement of the five fuel sprays. Note the bowl is offset to compensate for the off-centre injector position, necessary with two-valve per cylinder engines.

The impingement area is most significant in the early stages of fuel injection and combustion. It can affect the ignition delay and initial rate of pressure rise, by controlling the amount and composition of fuel/air mixture prepared for initial combustion.

The impingement area will change with engine speed, load (which affects SOI and EOI), and injection timing (SOI), because the piston position relative to the fuel injection spray changes.

4.2.7 Minor radii

The minor radii refered to the two radii which blended the piston face and main torodial radius with the impingement area. The diagram in figure 4.8 shows an illustration of the minor radii.

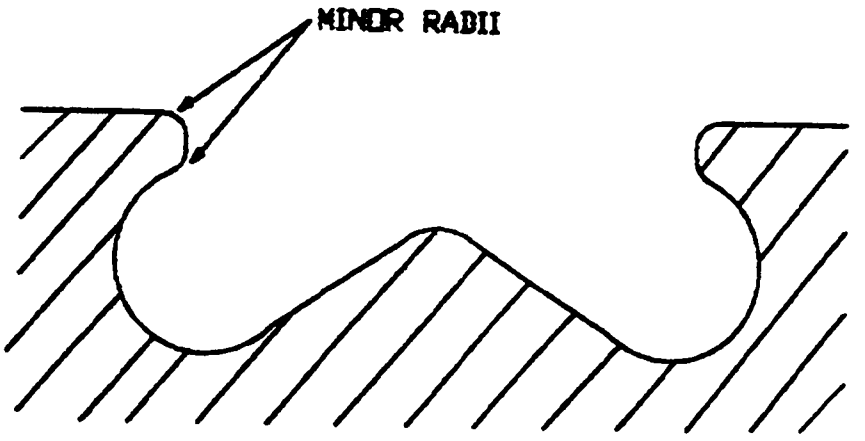

Figure 4.8 Section through a typical HSDI piston bowl showing the minor radii.

Although the minor radii only occupied a small fraction of the piston bowl volume, they can affect airflow resulting from squish during compression, and change the out-flow of hot combustion gases during combustion. Consideration of flow through orifices, nozzles, and diffusers, suggests that the gas flow will be modified by the value of these radii, and they may well affect the turbulence levels.

The size of the minor radii were limited by the need to prevent excessive thermal stresses and hot-spots in the piston bowl.

4.3 Piston bowl designs chosen

Four piston bowl designs were tested during this project. The first piston bowl shape tested was the standard Lynx Upgrade engine piston bowl. Pre-production testing at the Ford motor company indicated that this bowl achieved good performance and emissions results, consistent with the next generation of emissions legislation.

Comprehensive testing of the standard bowl shape was performed at Brunel University, to act as the baseline against which all other new piston bowl shapes would be compared.

Diagrams showing a dimensioned section through each piston bowl shape tested is given in figure 4.9, on the next page, and a tabulated summary of the main bowl dimensions, compared with other HSDI bowl designs is given in table 4.1. An introduction to the philosophy behind the design of each piston bowl shape, and a description of the main features of each piston bowl is now presented.

Full manufacturing drawings of each piston bowl shape (ONE, TWO and THREE), are included in appendix B.

4.3.1 Standard bowl shape (STD)

The standard piston bowl shape (see figure 4.9) was of conventional design, but was notable for its truncated low pip height. This potentially created a large region of low velocity or stagnant air just above the pip, which may have reduced the rate of fuel/air mixing and air utilisation. The piston had a relatively large area of impingement, which swept gradually into the main torodial radius, via the R5.0 minor radius.

The standard piston bowl volume was nominally 17.18cc, giving a compression ratio of 19.60:1. This was maintained constant throughout all engine tests.

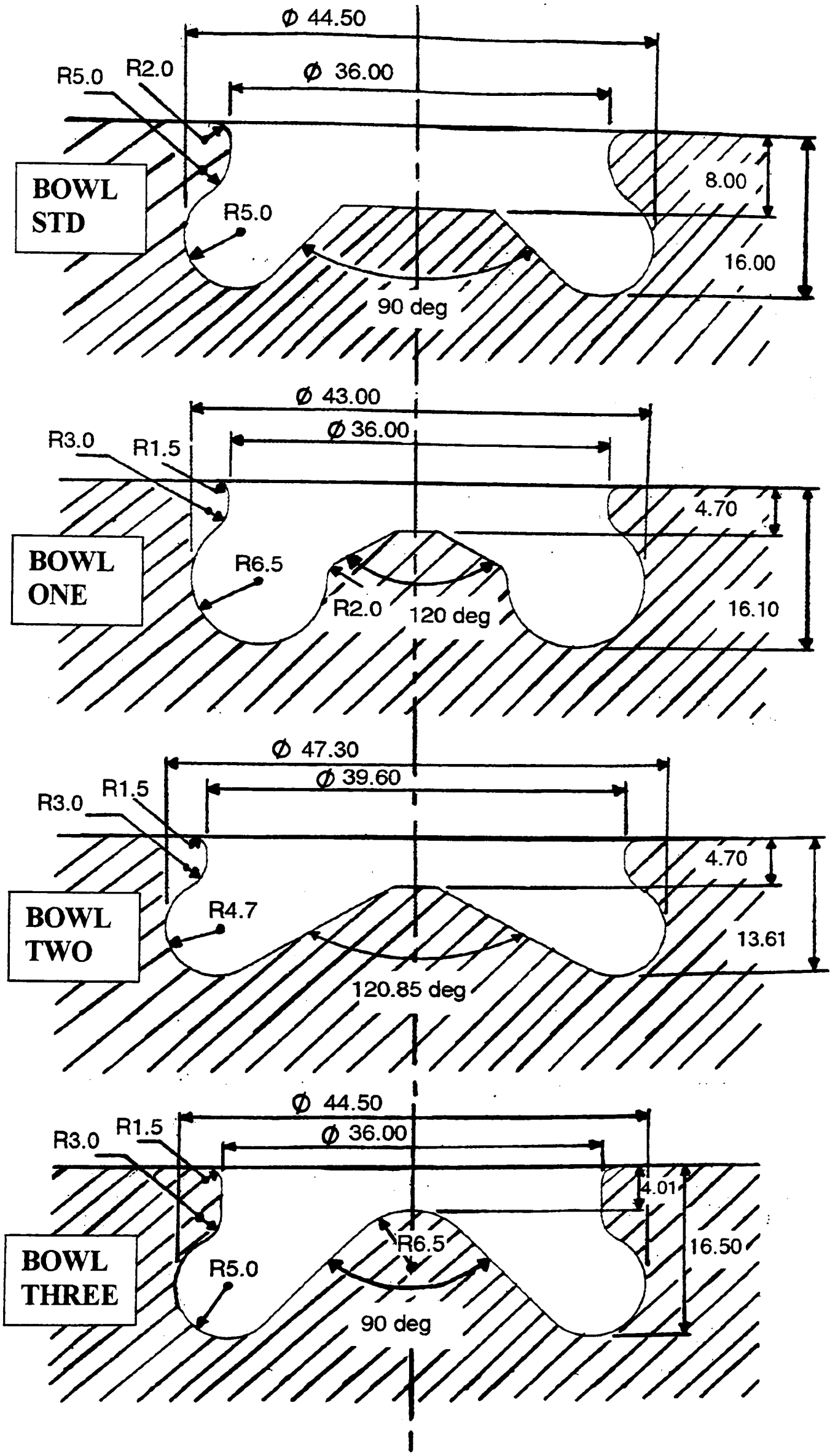

Figure 4.9 Sectional drawing of each of the four piston bowl shapes tested.

Engine	Bowl Type	Application	Bore (mm)	Stroke (mm)	Capacity (cc)	Power (PS)	Bowl Vol. (cc)	C.R.	Bowl Lip Dia. (mm)	Min Bowl Dia./Bore (throat/bore)	Max Bowl Dia. (mm)	Max Bowl Dia./Bore	Bowl Depth (mm)
2.5 NA	FORD	2.5	93.67	90.54	2496	70	22.37	20.7:1	40.0	0.43	45.8	0.49	18.0
2.5 TC	FORD	2.5	93.67	90.54	2496	85	25.62	19.3:1	44.0	0.47	48.8	0.52	17.8
2.5 TCI	FORD	2.5	93.67	90.54	2496	100	27.05	19.3:1	44.0	0.47	48.8	0.52	18.4
1.8 TCI	FORD	Lynx Upgrade	82.50	82.00	1753	Proto	17.18	19.68:1	36.0	0.44	44.5	0.54	16.0
1.8 TCI	AVL	Lynx	82.50	82.00	1753	Proto	16.17	-	36.0	0.44	43.0	0.52	16.0
1.8 NA	FORD	Lynx Upgrade	82.50	82.00	1753	Proto	15.49	21.0:1	35.0	0.42	41.0	0.50	16.0
1.8 TCI	RICARDO (early)	Lynx Upgrade	82.50	82.00	1753	Proto	18.13	18.85:1	37.5	0.45	44.0	0.53	15.0
1.8 TCI	RICARDO (latest)	Lynx Upgrade	82.50	82.00	1753	Proto	17.15	19.59:1	33.6	0.41	40.8	0.49	16.9
2.0	AVL (Bowl1)	Puma	86.00	86.10	2000	Proto	19.97	-	38.5	0.45	45.5	0.53	17.5
2.0	AVL (Bowl2)	Puma	86.00	86.10	2000	Proto	21.02	-	39.5	0.46	46.5	0.54	18.0
2.4 TCI	FORD 41C	Puma	94.60	89.90	2400	Proto	25.41	-	40.4	0.43	48.5	0.51	17.2
2.4 TCI	FORD 42D	Puma	94.60	89.90	2400	Proto	25.21	-	41.5	0.44	48.6	0.52	17.0
1.8 TCI	FORD (std)	Lynx Upgrade	82.50	82.00	1753	Proto	17.18	19.6	36.0	0.44	44.5	0.54	16.0
1.8 TCI	BRUNEL (One)	Lynx Upgrade	82.50	82.00	1753	Proto	17.12	19.6	36.0	0.44	43.0	0.52	16.1
1.8 TCI	BRUNEL (Two)	Lynx Upgrade	82.50	82.00	1753	Proto	17.15	19.6	39.6	0.48	47.3	0.57	13.6
1.8 TCI	BRUNEL (Three)	Lynx Upgrade	82.50	82.00	1753	Proto	17.15	19.6	36.0	0.44	44.5	0.54	16.5

Table 4.1 Comparison of major bowl dimensions and parameters, including the four Lynx Upgrade piston bowl shapes tested.

4.3.2 Bowl shape one (ONE)

Following completion of comprehensive testing on the standard piston bowl shape, piston bowl shape ONE was designed. The shape was based on a piston used successfully on an earlier version of the engine, but was modified to achieve the standard piston bowl volume of 17.18cc, from an original volume of 16.17cc. The volume was raised by increasing the main torodial radius.

The main differences between bowl STD and bowl ONE, were the reduction of maximum bowl diameter to 43 mm from 44.50 mm, the increase in the main torodial radius, and perhaps most notably the change in the pip shape. It was likely that these changes combined to move the centre of rotation of torodial-swirling air, slightly inwards towards the piston pip. More importantly, the distribution of airflow across the combustion chamber was expected to have been more uniform (ie. the majority of air would closely approximate the mean airflow, because most of the volume of air was contained within the main torodial radius). The area of stagnant air above the piston pip was much reduced.

Also of note, was the reduction in size of the minor radii around the piston bowl lip. These served to increase the sharpness of the piston lip, which it was though might aggravate the airflow flowing to and from the piston bowl, and generate increased turbulence.

4.3.3 Bowl shape two (TWO)

Bowl shape two was a significant departure from previous piston bowl designs. Following analysis of results from piston bowl shape STD and ONE, it was decided to increase the aspect ratio of the bowl by increasing the maximum bowl diameter, and throat width, by 10% over bowl shape ONE. The piston bowl volume was recovered by decreasing the main torodial radius. To maintain a similar piston pip shape as in bowl ONE, the bowl depth was reduced until the torodial radius was at a tangent to the pip sides.

The changes to the bowl shape had the effect of significantly reducing the in-bowl swirl level, and increasing the injector spray path length. A full set of injector optimisation tests were performed on this bowl shape, by varying the injector protrusion into the combustion chamber, and by changing the injector cone angle. Results from these tests proved critical to the understanding of the effect of bowl-wall fuel impingement on performance and emissions.

4.3.4 Bowl shape three (THREE)

Bowl shape THREE was designed to exploit what had been learnt from testing of all previous bowls shapes. The design used the basic dimensions of bowl STD, which had proved successful for low emission production.

The area of impingement was increased, following the discovery of a clear link between the point of fuel impingement on the bowl walls, and performance and emissions. This was achieved by moving the centre of the main torodial radius down, and reducing the size of the minor radii, relative to bowl shape STD. The area of fuel impingement was increased to contain the majority of fuel impingement within the impingement area.

Figure 4.10 shows the range points of fuel impingement, which could be achieved during injector optimisation. The piston in figure 4.10 is shown positioned at TDC. The two extremes of fuel impingement were determined by the depth of the injector tip in the combustion chamber, and the fuel spray angle.

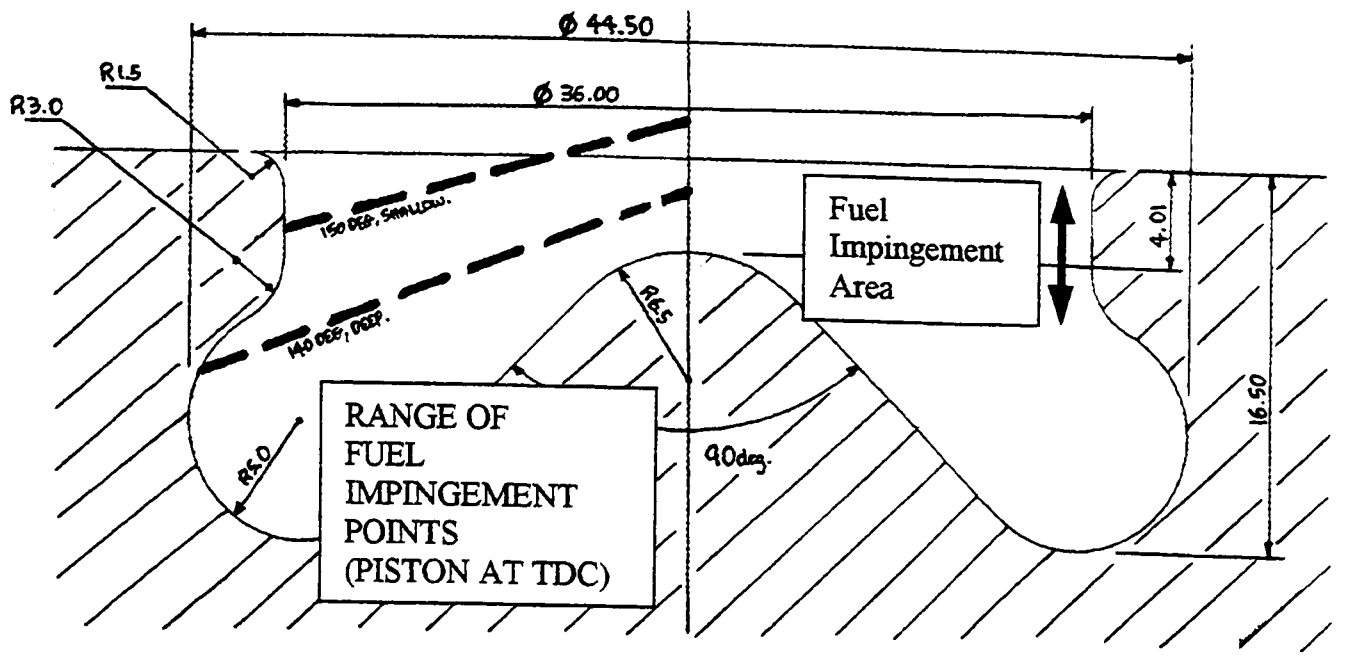

Figure 4.10 Range of fuel impingement points possible, with the piston positioned at TDC, during injector optimisation.

The actual instantaneous point of fuel impingement depended on the piston position in the cylinder (piston is show here at TDC), injection timing, and duration of injection (depending on engine load). The pip volume was increased to capitalise on the benefits observed with piston bowl shape ONE, and to increase the mean swirling air velocity.

4.4 Calculation of piston bowl volume and cylinder compression ratio

Piston bowl design and calculation of piston bowl volume were performed simultaneously, to ensure the correct cylinder compression ratio was maintained. Calculation of piston bowl volume was achieved using solid of revolution models, within the AutoCAD software drawing package. Cylinder compression ratio was not checked on the test engine, because the piston bowl volume was closely controlled by the manufacturing process. However, an understanding of the factors affecting cylinder compression ratio was useful during engine rebuilding and piston matching (discussed later in this chapter).

4.4.1 Piston bowl volume

It was possible to calculate the volume of the piston bowl shape analytically, but this required knowledge of the equation of the line describing the perimeter of the piston bowl. This would have involved several discontinuous functions, which mapped the different profiles defining the bowl perimeter. Instead, the AutoCAD (version 12 and 13) computer-aided software design package was chosen to calculate the piston bowl volume.

The basis of the calculation was the creation of a solid 3D model within AutoCAD. This was achieved by drawing the bowl perimeter from a series of discontinuous curves and lines in a conventional manner, then creating a continuous polyline from its components. The polyline was then revolved to create a solid model (the bowl perimeter was always revolved by 180 degrees to avoid computational problems, and the resultant volume doubled). Properties of the solid model were available within AutoCAD, one of these being the bowl volume.

Initially, the process of bowl volume calculation was tested by calculating the volume of revolution of simple shapes, and comparing the result with the analytical calculations. Adjustment of the number of calculation-iterations performed by AutoCAD, was done to produce accurate results in a reasonable computational time. The final bowl volume calculation was repeated using the maximum number of iterations to confirm the piston bowl volume. Typically, thirty design changes were required to achieve the desired piston bowl shape, with a nominal bowl volume of 17.18cc. The extremes of dimensional tolerances were checked to ensure that the piston bowl volume, under all manufacturing tolerances, would remain within the volume tolerance of 0.5cc.

AutoCAD was also used to obtain the centres of blending radii necessary for bowl manufacture on a CAD/CAM CNC lathe, and discrete points describing the periphery of the bowl profile for CFD simulation (see chapter 6).

4.4.2 Cylinder compression ratio

Cylinder compression was maintained constant at 19.6:1 for all engine tests. This was important to ensure variation in performance and emissions was attributable to piston bowl shape changes only. Cylinder compression ratio was maintained constant by ensuring all the pistons fitted had the same bowl volume, and all other clearance volumes were maintained the same.

Cylinder compression ratio is given by equation 4.1:

Compression ratio (C.R.) = maximum cylinder volume / minimum cylinder volume

Equation 4.1 Calculation of cylinder compression ratio [Heywood, 1988].

Factors which contributed to the clearance volume (the volume remaining in the combustion chamber when the piston was the end of the compression stroke) are listed below:

(1) Piston bowl volume
(2) Piston-to-head clearance (or gasket space) volume
(3) Valve recess/protrusion volume
(4) Injector recess/protrusion volume
(5) Glowplug recess/protrusion volume
(6) Piston ring top-land volume

When changing pistons, the bowl volume and piston bump height (affecting the piston-to-head clearance) were always measured, and adjustment made possible using different height cylinder head gaskets. Piston installation is discussed in more detail in section 4.5. The effect of injector recess/protrusion during injector optimisation tests was negligible.

4.5 Piston machining and inspection

The complex piston shapes and tight dimensional tolerances meant piston machining could not be performed manually at Brunel University. The only machines capable of producing the piston bowl shape with the requested accuracy were computer-controlled lathes and milling machines. As all the piston bowl shapes were symmetrical about the piston centreline, computer controlled lathes offered the most accurate method, and best machined surface finish.

Piston machining was sub-contracted to a small precision engineering company (Eljays Group Limited, Middlesex). Manufacturing drawings and blank pistons were supplied to Eljays Group Limited, from which they produced a test sample in an aluminium rod bar, and following successful approval, machined a single set of four pistons for each bowl design. Figure 4.11 shows the spatial relationship between the piston bowl shape and the piston casting, for bowl shape ONE.

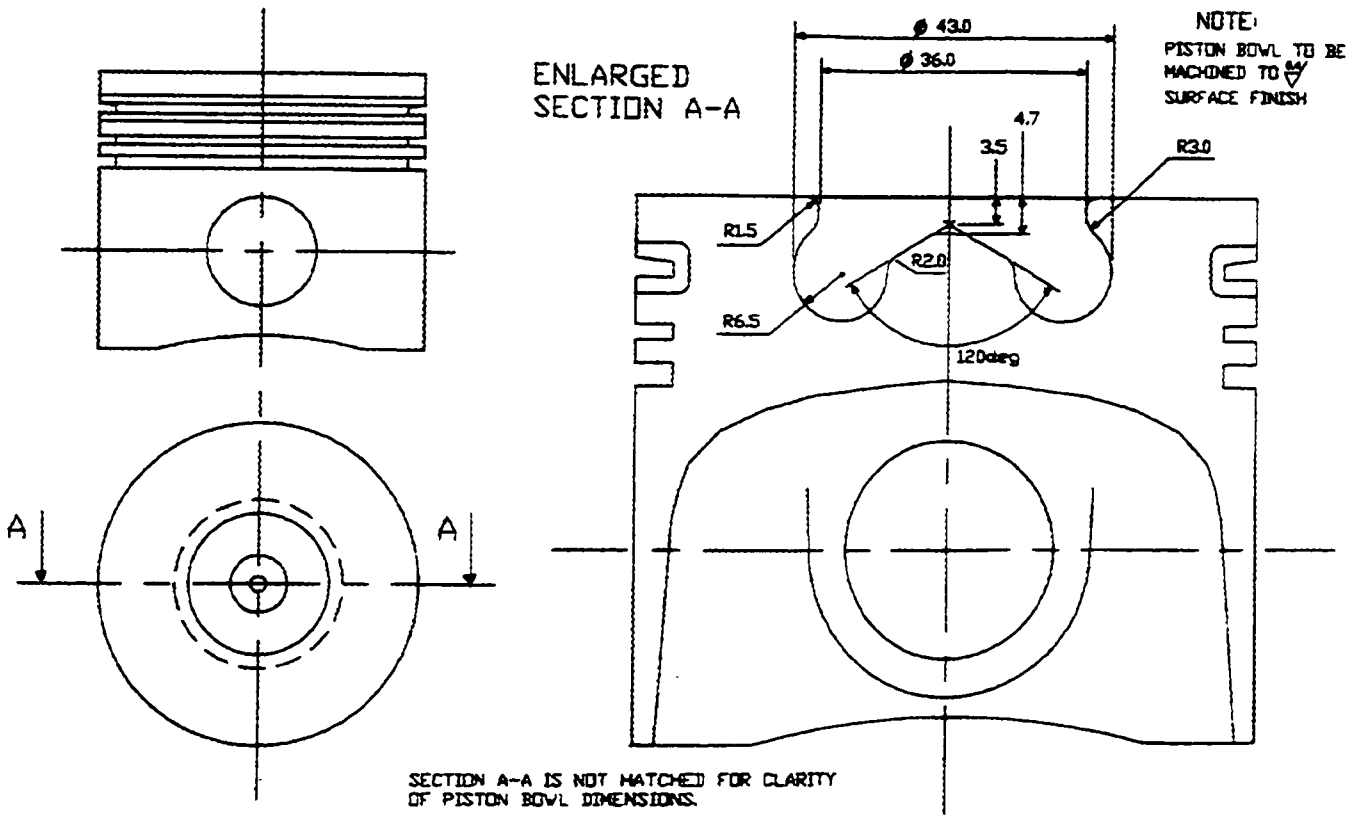

Figure 4.11 Illustration of the spatial relationship between the piston bowl volume and piston casting.

Special offset, spoon-shaped turning tools were used to machine the torodial radius and generate the re-entrant bowl shape. The radius of the spoon tool was made small enough to enter the narrowest gap between the piston pip and piston lip, but large enough to obtain a good surface finish on the main torodial radius.

Practical machining limits might have placed a constraint on the design of piston bowl shape possible, but the shapes designed in this project were machined without compromise. Several rough-cuts were performed before the final cut was taken at a reduced tool feed speed.

The manufacturing drawing was redrawn in the dedicated CAM computer, where it was sent directly to the CNC lathe. Care was taken during the preparation of manufacturing drawings, to ensure the radii centres specified formed a continuous bowl profile. The CAM system rejected any discontinuous profiles. The CNC lathe worked on a point-to-point basis, describing the bowl periphery. It was necessary to split the main torodial radius into two sections, to ensure the bowl depth was a specified point (crucial to bowl volume accuracy).

A test sample was first machined by the company, in the end of a round bar of aluminium and delivered to Brunel University for volume and major dimension checks. The bowl volume was tested at Brunel University by filling the bowl (covered with a piece of clear perspex) with a measured quantity of water.

Figure 4.12 shows a schematic diagram of the bowl volume testing apparatus.

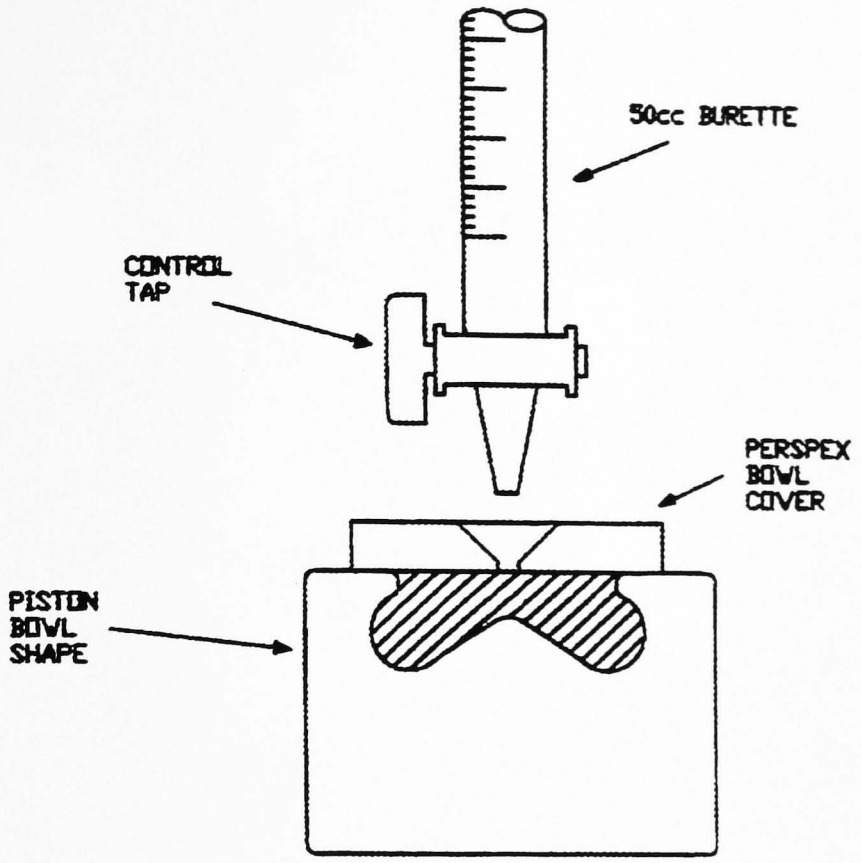

Figure 4.12 Piston bowl shape volume testing apparatus. A test sample, machined in the end of a billet bar of aluminium is shown in the diagram.

A good seal was obtained between the perspex top and piston test sample using a light smear of grease. Bowl volume measurement was accurate to 0.05cc. The round bar test sample was sectioned using an electrode wire eroding technique for presentation use.

After the piston bowl major dimensions had been checked, four pistons were machined using a special soft jaw chuck. The photograph in figure 4.13 shows the round bar, sectioned test sample of piston bowl shape ONE, placed on top of the final machined piston.

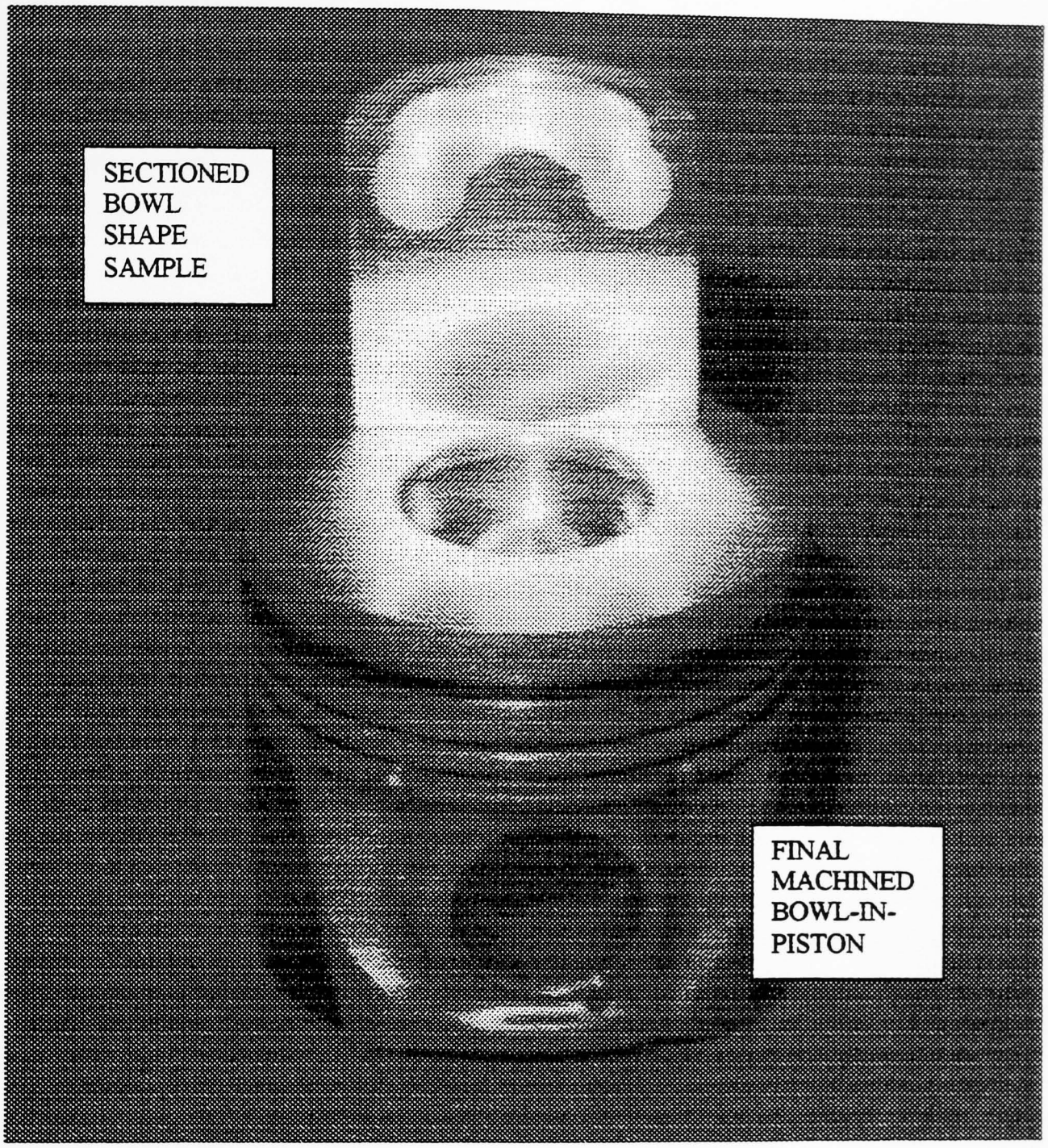

Figure 4.13 Photograph of a sectioned test sample of piston bowl shape ONE , placed on top of the final machined piston.

After final piston machining, all pistons were checked for correct bowl volume.

4.6 Piston installation and run-in schedule

Piston bowl shape STD provided a reference set-up against which all subsequent piston shapes were compared. The piston installation procedure is summarised in the stages below:

(1) The bump height (protrusion of the piston top face above the cylinder block) of piston bowl shape STD was measured on all four cylinders, and used as a reference during subsequent piston assembly. Piston bump height was measured using a 0-25mm depth micrometer, as indicated in figure 4.14.

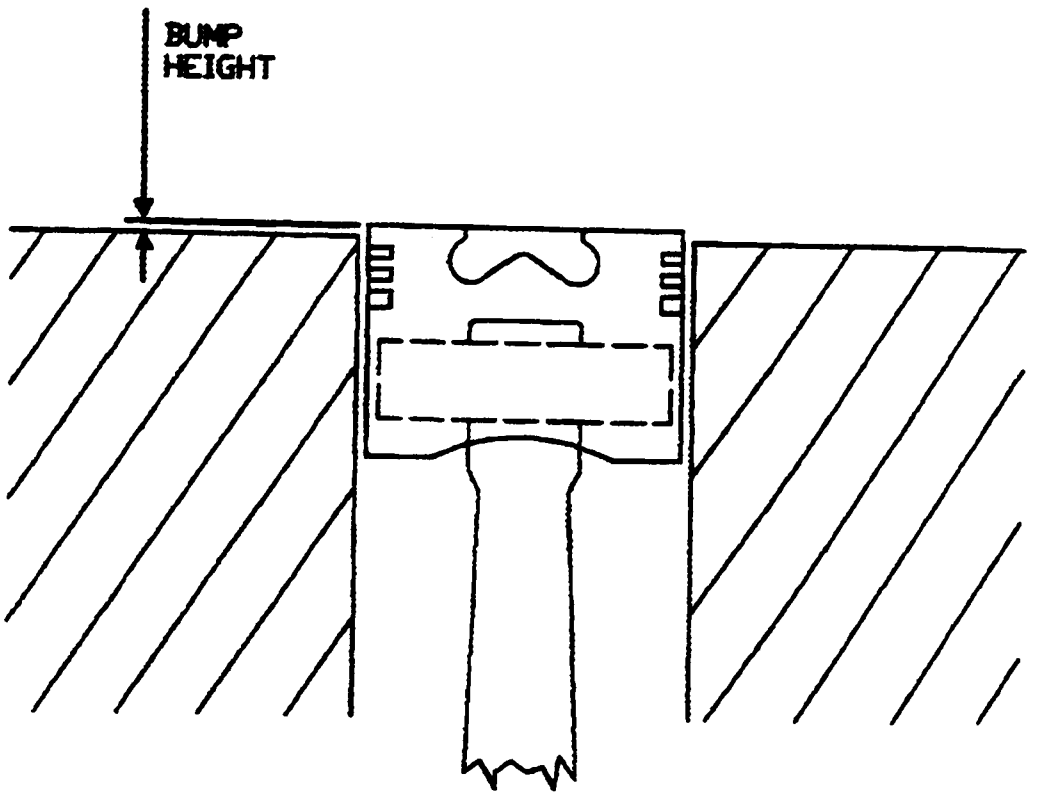

Figure 4.14 Measurement of piston bump height. The bump height was measured using a depth micrometer, either side of the gudgeon pin axis (most accurate position as the piston 'rocks' on this axis).

(2) The standard (STD) pistons were removed from the engine after cleaning carbon deposits from the top-land region, and their individual gudgeon-pin to piston top face heights were measured. Figure 4.15 shows this procedure. This was used as a reference for all future pistons, prior to installation into the engine.

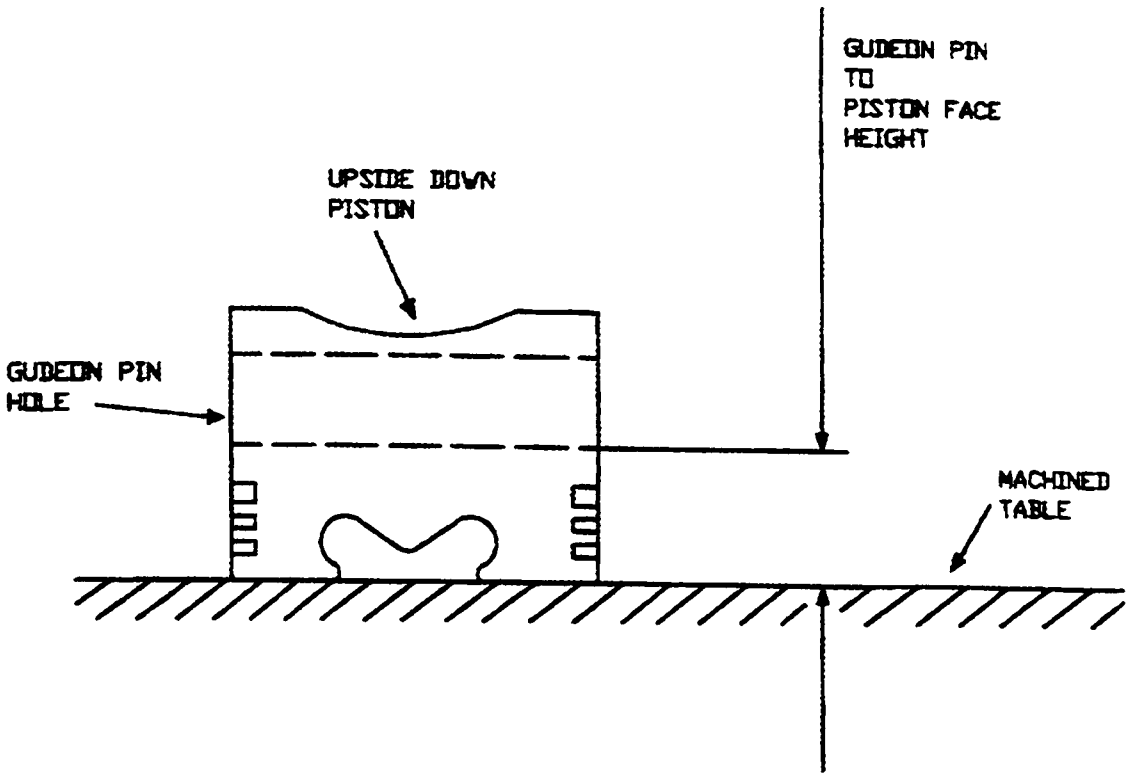

Figure 4.15 Measurement of the gudgeon-pin to piston top face. Measurement was performed using a dial gauge, mounted on a magnetic base.

(3) The gudgeon pin to piston face height of the new set of pistons was then measured, and compared to the STD piston measurements. If the results were the same as the standard (STD) bowl (most common situation), then the pistons were installed. Differences between individual pistons were matched using graded length connecting-rods (four grades available). Differences common to a set of pistons, were matched using cylinder head gaskets of different thickness' (three grades available).

(4) After any connecting-rod or cylinder head gasket changes had been made, the pistons were installed in the engine, and a final check made to ensure they had the same bump height as the standard pistons (within the range 0.521-0.620mm for the standard cylinder head gasket height). The original piston rings were fitted to each new set of pistons to reduce the piston running-in time.

To speed up the process of piston change-over, the engine sump was modified to eliminate the need for removal of the engine bell-housing, to access the connecting-rod, big-end retaining bolts.

Once installed, the pistons were bedded in on the cylinder bores using fresh engine oil for approximately twenty engine running hours. The engine was run at a relatively low speed to minimise inertial loading (with would have had limited effect on the piston skirt to cylinder bore pressure), but moderate to high loads (to increase the side loading on the piston and rings through the action of combustion pressure). Engine speed was for the first fifteen hours maintained at 1500 and 2000rpm, with loads between idle and 80% of maximum. The final five hours of engine run-in alternated between high speed (3000rpm) and low speed conditions.

4.7 Conclusions

Initially, the major factors affecting piston bowl design and possible implications of changes were identified. There was not sufficient experimental time to perform a full parametric study of these factors. Instead, a process of learning from the results, and implementing the understanding gained was adopted.

Four piston bowl shapes were designed and tested. Reasons postulated for the observed changes in performance and emissions were tested in each subsequent bowl design. The continual learning process is discussed in detail in the results and analysis chapters that follow.

The process of bowl design, calculation of bowl volume by creating a solid revolution model within AutoCAD, and production of manufacturing drawings proved successful. The close relationship afforded with the piston machining company, resulted in improvements in the presentation of drawing information, and faultless machining of blank pistons. Careful checking of bowl volume and engine re-assembly, allowed testing to proceed with the minimum delay, in the confidence that changes in performance and emissions would not be due to changes in the compression ratio.

Chapter 5:

Injector optimisation results and discussion

Chapter 5: Injector optimisation results and discussion

5.1 Introduction

The purpose of injector optimisation was to find the best vertical position of the injector nozzle, and the best injector cone angle for each new piston bowl design. The optimum configuration was then used during subsequent bowl comparison testing (discussed in chapter 7). Injector optimisation produced some of the most important findings of this project. One of the most important findings was a link between the spray impingement point on the bowl surface, and emissions.

With each new bowl design, the significance of injector optimisation became apparent. Therefore, as more experience was gained, the injector optimisation tests were refined with each new bowl shape tested. The optimum injector configuration was judged in terms of its emission of NOx and particulates, and its part-load EGR performance. Testing conditions were chosen to accentuate the effect injector position and spray cone angle.

The aim of the analysis of the injector optimisation results, was to identify reasons for the link between production of emissions and the fuel-spray impingement point observed. This was supported by CFD simulation of combustion in the piston bowl in chapter 6, and heat release analysis.

This chapter describes the testing conditions chosen, and presents results in the form of particulates versus NOx trade-offs, and other performance parameters. The effect of the point of fuel spray impingement is then analysed, and supported by heat release analysis and CFD work (see chapter 6). The optimum injector configuration from each piston bowl shape is considered, and reasons for differences discussed.

5.2 Matrix of injector optimisation

5.2.1 Details of injector optimisation matrix

Piston bowl shape STD was supplied by Ford with the Lynx Upgrade project engine, ready for testing. Injector optimisation had already been performed at Ford for this bowl shape. Injector optimisation on bowl shape ONE was performed by varying the injector nozzle depth only, as the optimum engine performance was achieved without varying injector cone angle. Piston bowl shapes TWO and THREE were subjected to a matrix of testing, changing both injector depth and cone angle.

The choice of injector depths and cone angles to be tested in the matrix was constrained by the availability of injector nozzles with different spray angles, and the range of injector depths which could be accommodated in the combustion chamber. Piston-pip to injector clearance provided an additional constraint for high-pip bowl designs.

The injector cone angle (see fig 3.13 in chapter 3, for a description of injector cone angle) was controlled by the angle of holes in the injector nozzle, set during manufacture. Three different cone angle injectors were available. These were 140, 145 and 150 degree spray-cone angles.

Injector nozzle depth or position in the combustion chamber was controlled by changing the depth of washers under the seat of the injector. Three different washer depths were tested, but intermediate depths were available if the resolution was too coarse. In practice, no finer resolution proved necessary to achieve the optimum injector configuration for each bowl shape. The washer depths available were 2.5, 4.0 and 5.5mm, with an accuracy of 0.1mm between washer sets.

A 4.0 mm washer corresponded to an injector nozzle hole protrusion of 0.7mm into the combustion chamber, as shown in figure 5.1 (note that the start of the spray was considered to originate from inside the nozzle hole, at its inner surface).

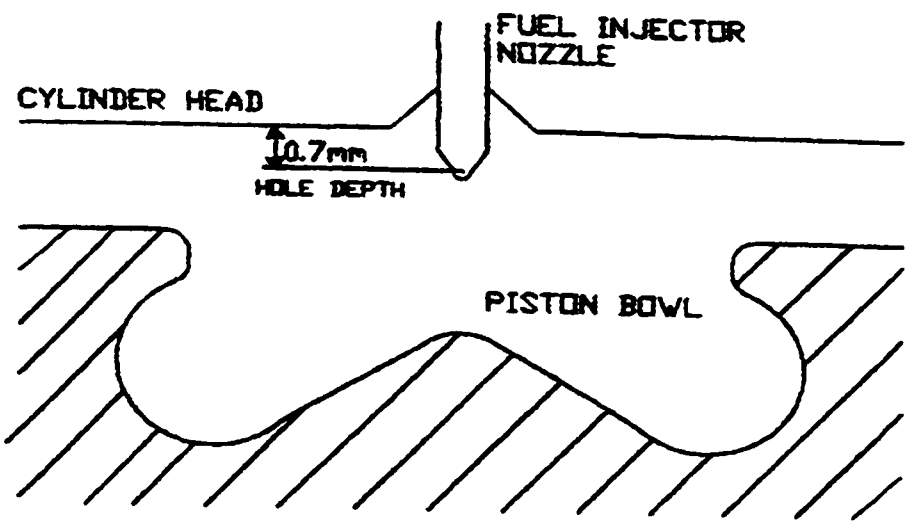

Figure 5.1 Illustration of injector nozzle hole protrusion into the combustion chamber, using the 4.0 mm depth washer.

The 2.5mm (Deep) washer resulted in the greatest protrusion into the combustion chamber and bowl, whilst the 5.5mm (Shallow) washer caused the point of injection to be behind the cylinder head face, inside the injector recess. The injector optimisation matrix, of different injector depth and injector cone angle combinations available, is shown in table 5.1.

	140 degrees	**145 degrees**	**150 degrees**
2.5mm, Deep	9	8	6
4.0mm, Medium	7	5	3
5.5mm, Shallow	4	2	1

Table 5.1 Injector optimisation matrix, indicating the range of injector cone angles available, and the range of washers used to vary the injector nozzle depth.

The number corresponding to each matrix condition represents the point of impingement from the top to the bottom of the bowl impingement area. The points of impingement are numbered in sequence from 1 to 9, from the highest point (point 1) down to the lowest point (point 9), as shown in figure 5.17 in a later section. This is referred to in detail during discussion of results.

Each matrix condition required removal of the complete injectors to change the washer depth or injector type. Injector nozzles could not be removed from the injector

body, because all injectors were checked after assembly at the factory for first-stage and second-stage opening pressure, and fuel flow rate.

5.2.2 Details of matrix testing conditions

Engine test conditions were chosen to highlight the effect of the fuel impingement point on the particulates versus NOx trade-off. Three full-load test points were used, because they were, by definition, at the limit of mixing for combustion, before the production of excessive smoke. Full-load conditions also produced high NOx because of the high peak temperature reached during combustion.

In addition to the full-load test points, two part-load conditions with EGR were selected for testing from the '14-mode test' (a full list and description of the 14-mode test is given in chapter seven, Table 7.1). These points were representative of 'drive-cycle' operation, upon which different bowl designs were ultimately to be compared.

The actual point of impingement for a given bowl design depended not only on the matrix condition tested, but also on the injection timing. The five test points chosen encompassed a wide range of injection timings for comparison. At each of the five test conditions, the injector depth and cone angle were altered systematically to obtain optimum combustion. Matrix test point conditions are listed in table 5.2.

TEST NO.	Speed (rpm)	Load (Nm)	SOI (degCA)	EGR (%)
1	1500	166.4 (100%)	-2	0
2	2000	214.2 (100%)	-3	0
3	4000	156.5 (100%)	-9	0
4	1800	27.9	+5	30
5	3200	69.8	-6	40

Table 5.2 Full-load and part-load engine operating conditions used for injector optimisation tests. Start of injection (SOI) is relative to TDC, positive values being after TDC.

5.3 Results of particulates versus NOx trade-offs and other performance parameters from injector optimisation

The results of each piston bowl shape are presented separately in this section. The optimum injector configuration was decided by considering the particulates verses NOx trade-offs, brake specific fuel consumption (BSFC) at full-load, the emission of carbon monoxide (CO) at part-load, EGR conditions and other performance parameters. The production of smoke at test condition 1 (1500rpm, full-load) was often the deciding factor in selection of the optimum injector configuration.

A more detailed analysis of the effect of fuel impingement is the subject of section 5.4, where the mechanisms and reasons for trends observed are discussed.

5.3.1 Calculation and post-processing of results

Correction to standard atmospheric conditions

Atmospheric pressure; temperature and humidity changed on different test days. This affected the atmospheric air density and air compression characteristics. A correction factor was applied to allow direct comparison between tests performed on different days under various atmospheric conditions.

Engine power (and other related parameters) were corrected according to the EEC directive 88/195. The relevant calculations and procedure for correction of engine power to standard atmospheric conditions are given in appendix C. Standard temperature is 298 K (25 degrees C) and standard total pressure is 100 kPa. All data presented in this thesis has been corrected to standard atmospheric conditions where applicable.

Calculation of specific emissions

The emission of NOx, HC and CO were recorded in parts-per-million by volume (ppm), or percentage volume. Data is sometimes presented in this thesis in terms of

emission in ppm, but was normally converted into units of grams of emission per kilogram of fuel burnt (g/kg fuel), or into grams of emission per unit energy produced (g/kWh). These units allowed direct comparison between different engine test conditions, and even between different engine designs. They essentially represented the effectiveness of the engine at avoiding production of a particular emission.

Conversion from ppm into g/kg fuel, and then g/kWh was performed using the equations below [Abdelhalim, 1998].

Equation 5.1: $NO(g/kg\ fuel) = 1.0359 \times 10^{-3} \times NO(ppm) \times (1 + AFR)$

where the air/fuel ratio (AFR) is a mass ratio.

$$NO(g/kWh) = NO(g/kg\ fuel) \times BSFC(g/kWh\ fuel) \times {}^{1}/_{1000}$$

Equation 5.2: $NO_2(g/kg\ fuel) = 1.5884 \times 10^{-3} \times NO_2(ppm) \times (1 + AFR)$

$$NO_2(g/kWh) = NO_2(g/kg\ fuel) \times BSFC(g/kWh\ fuel) \times {}^{1}/_{1000}$$

Equation 5.3: $HC(g/kg\ fuel) = 0.5525 \times 10^{-3} \times HC(ppm) \times (1 + AFR)$

$$HC(g/kWh) = HC(g/kg\ fuel) \times BSFC(g/kWh\ fuel) \times {}^{1}/_{1000}$$

Equation 5.4: $CO(g/kg\ fuel) = 0.9669 \times 10^{-3} \times CO(ppm) \times (1 + AFR)$

$$CO(g/kWh) = CO(g/kg\ fuel) \times BSFC(g/kWh\ fuel) \times {}^{1}/_{1000}$$

The multiplication constants in equations 5.1 to 5.4 were generated from the molecular mass of the emission. Total NOx emission was calculated assuming the molecular mass of NO only.

Calculation of particulates

Particulates are composed of a combination of soot particles and heavy HC molecules absorbed on the particulate. Particulates were not measured directly, but were estimated using a correlation by Greeves and Wang (1981), shown in equation 5.5 below. The correlation, based on experimental results, estimated the particulate mass from the emission of smoke and hydrocarbons.

$$Particulates(g/m^3) = 1.024 \times smoke(g/m^3) + 0.505 \times HC(g/m^3)$$

Equation 5.5 Estimation of particulate mass from the emission of smoke and hydrocarbons [Greeves and Wang, 1981].

Smoke was measured in units of Bosch smoke number. To convert to units of smoke in grams per meter cubed (g/m3), an experimental correlation developed by Fosbery and Gee (1961) was used. This is shown graphically in figure 5.2.

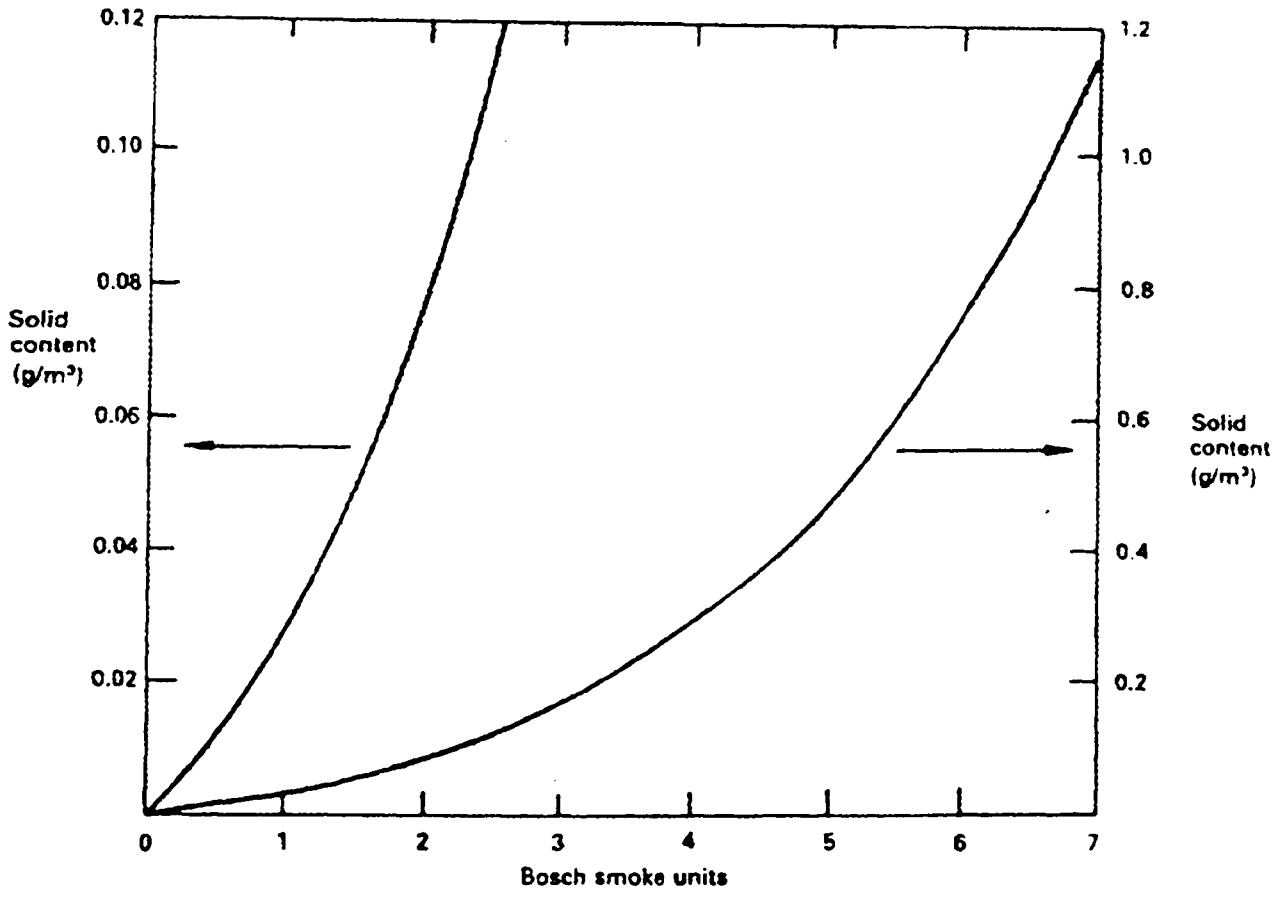

Figure 5.2 Experimental correlation between Bosch smoke number and the solid content in the exhaust gas, developed by Fosbery and Gee (1961).

To enable automatic conversion between the emission of smoke and estimation of solid content in the exhaust, a polynominal equation describing the complete range of smoke values possible was generated. This is shown in figure 5.3.

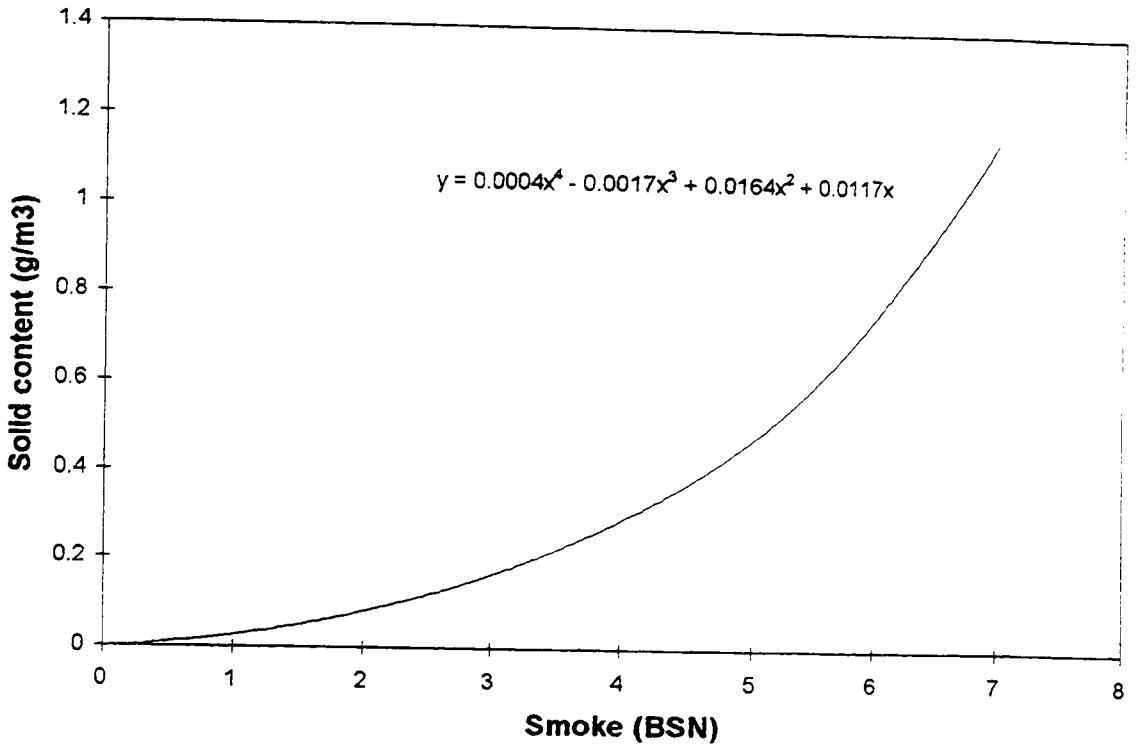

Figure 5.3 Equation used for automatic conversion from smoke measurement in units of BSN, to solid content in units of g/m3.

This equation formed the basis of a speadsheet for automatic conversion from the measurement of smoke and hydrocarbons, into an estimation of particulate mass in the exhaust.

To convert particulate mass into grams of emission per hour, the following equation was applied.

$$Particulates(g/hr) = Particulates(g/m^3) \times Airflow(kg/hr) \Big/ \rho_{air}(kg/m^3)$$

Equation 5.6 Calculation of particulate mass in g/hr.

Calculation of brake specific fuel consumption (BSFC)

Brake specific fuel consumption was an important parameter indicating the efficiency with which fuel was converted into mechanical power at the crankshaft. It is given by the fuel flow rate per unit power output, calculated using equation 5.7.

$$BSFC(g/kWh) = \dot{m}_{fuel} / P_{brake}$$

Equation 5.7 where $\dot{m}_{fuel}$ is the fuel flow rate in g/h, and P_{brake} is the engine brake power in kW.

5.3.2 Injector optimisation results from bowl shape STD

Injector optimisation was performed by Ford for the standard piston bowl shape. The optimised injector configuration for the STD bowl was a 145-degree cone angle injector, using a washer depth of 4.0 mm.

The fuel spray impingement points, NOx, and smoke emissions are shown in figures 5.4 to 5.6, at the start of injection (SOI) and end of injection (EOI) for this bowl, at the three full-load test conditions (test conditions 1, 2 and 3, table 5.2). Each figure represents a section through the bowl at a different test condition. The theoretical points of impingement at the start of injection, and end of injection are shown, together with the engine-out emissions measured from the engine exhaust (time averaged, not a function of crank-angle).

The theoretical point of impingement was calculated from the spray centre-line, assuming the spray was un-deflected by the action of air motion. This is true for modern high-pressure fuel injection systems, as shown by many researchers [Hiroyasu and Nishida, 1989; Naber and Reitz, 1988; Welberger and Cartellieri, 1987].

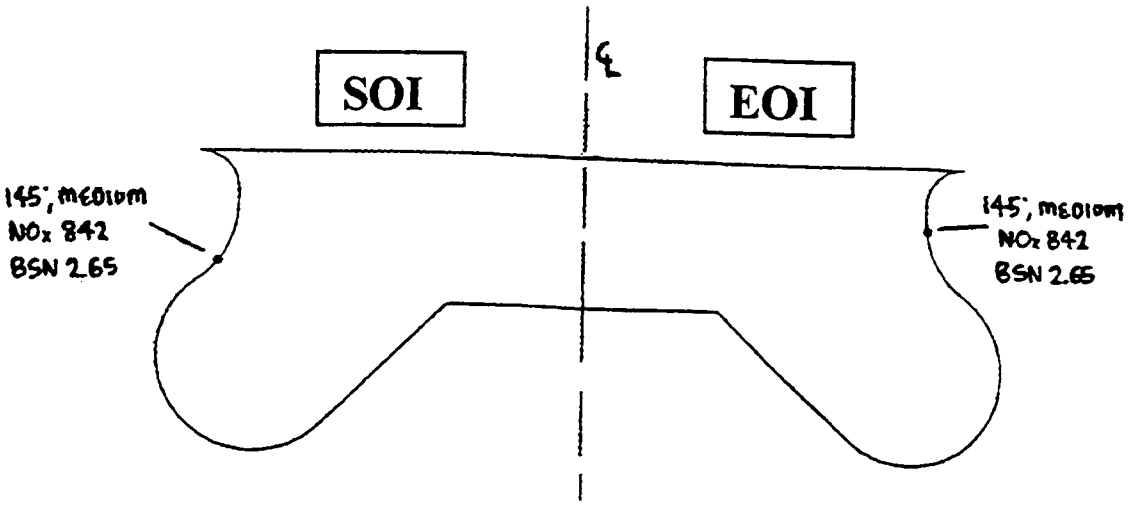

Figure 5.4 Test 1 (1500 rpm, 166.4 Nm – full-load), bowl shape STD showing the points of impingement at SOI (2 degrees BTDC) and EOI (16 degrees ATDC), with the engine-out emissions results.

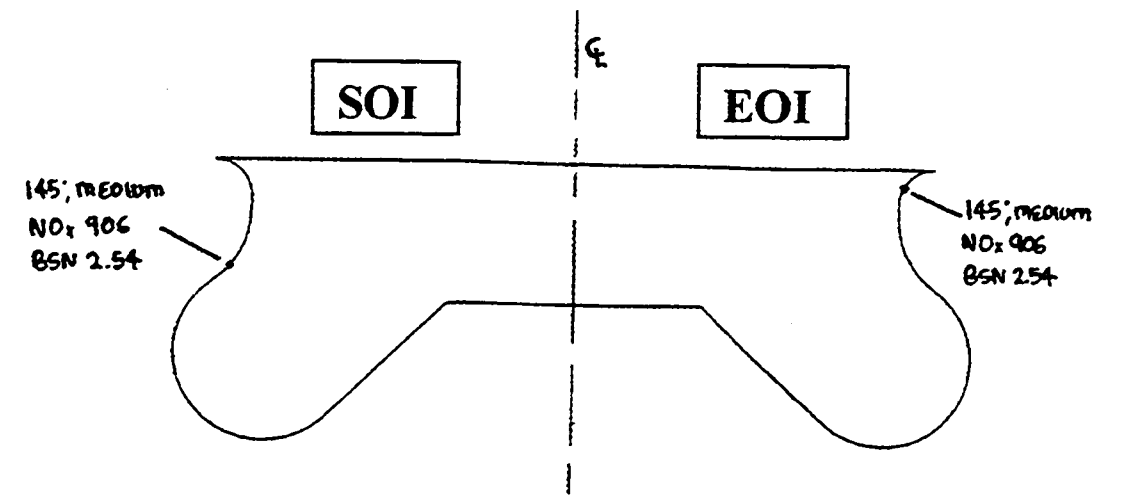

Figure 5.5 Test 2 (2000 rpm, 214.2 Nm – full-load), bowl shape STD showing the points of impingement at SOI (3 degrees BTDC) and EOI (24 degrees ATDC), with the engine-out emissions results.

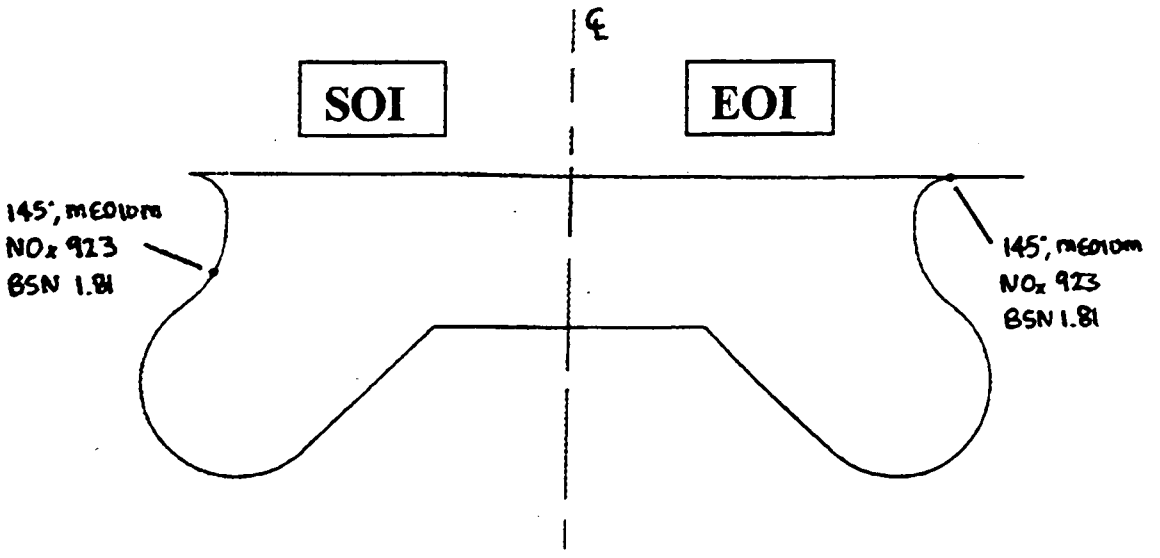

Figure 5.6 Test 3 (4000 rpm, 156.5 Nm – full-load), bowl shape STD showing the points of impingement at SOI (9 degrees BTDC) and EOI (28 degrees ATDC), with the engine-out emissions results.

The point of impingement sweeps between the SOI and EOI, as the piston moves up at the end of the compression stroke, and then downwards during the expansion stroke. Piston bowl shape STD produced quite low smoke emissions at all of the full-load test conditions. A significant observation from the impingement diagrams of optimised injector position, was the containment of fuel impingement within the 'impingement' lip area. Whilst the majority of fuel impingement in the 1500rpm, full-load case occurred low in the impingement area, there was no 'spill-over' of the fuel spray on the piston crown by the EOI in the 4000rpm, full-load case.

It was difficult to postulate about the effect of the point of impingement on emissions without a range of optimisation results for this bowl shape (STD), but it did add another dimension for comparison with subsequent bowl shapes tested.

5.3.3 Injector optimisation results from bowl shape ONE

Piston bowl shape one was subjected only to injector depth optimisation. NOx and smoke emissions from three full-load, and two part-load test points are presented in the bar charts in figures 5.7 and 5.8 below.

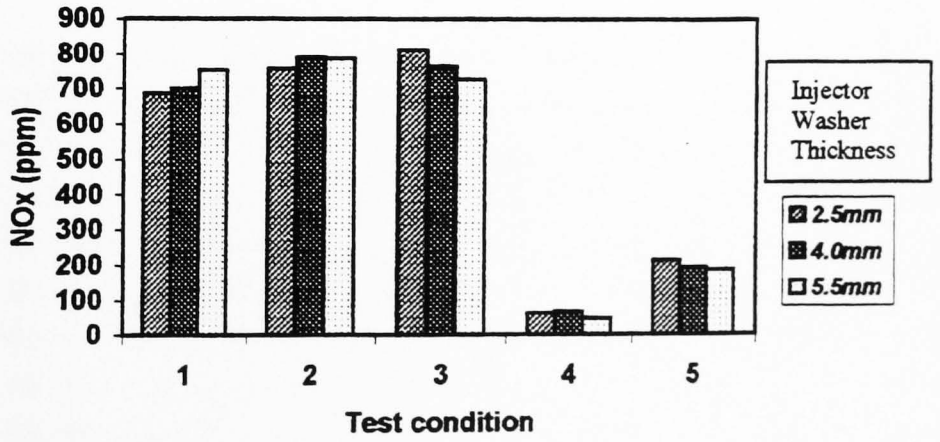

Figure 5.7 Comparison of NOx formation at different injector depths, for each of the test conditions shown in table 5.2.

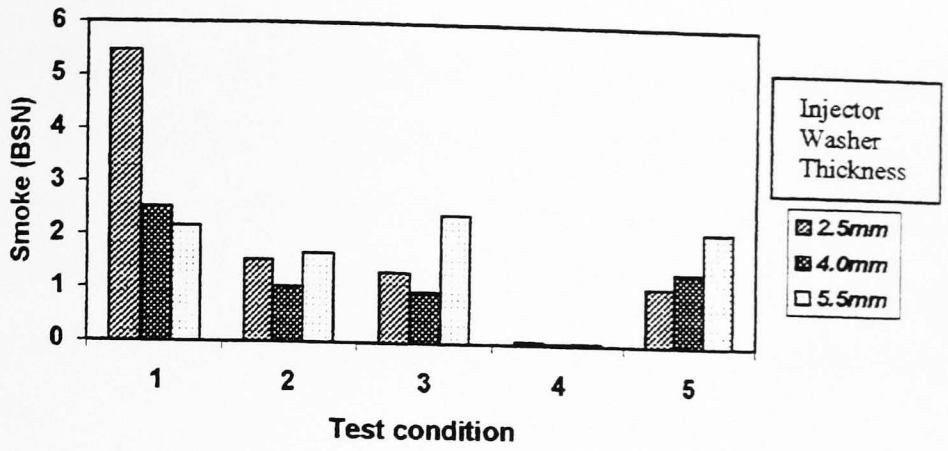

Figure 5.8 Comparison of smoke formation at different injector depths, for each of the test conditions shown in table 5.2.

NOx emissions

The NOx performance at each injector depth was similar, increasing slightly with engine speed. Although the time for reaction and NOx formation decreased with engine speed, the increase in peak cylinder temperature and pressure more than compensated, and this resulted in an *increase* in NOx formation.

Figure 5.9 demonstrates the maximum increase in cylinder pressure for the 145 degree, 4.0 mm injector combination case, during the three full-load test conditions.

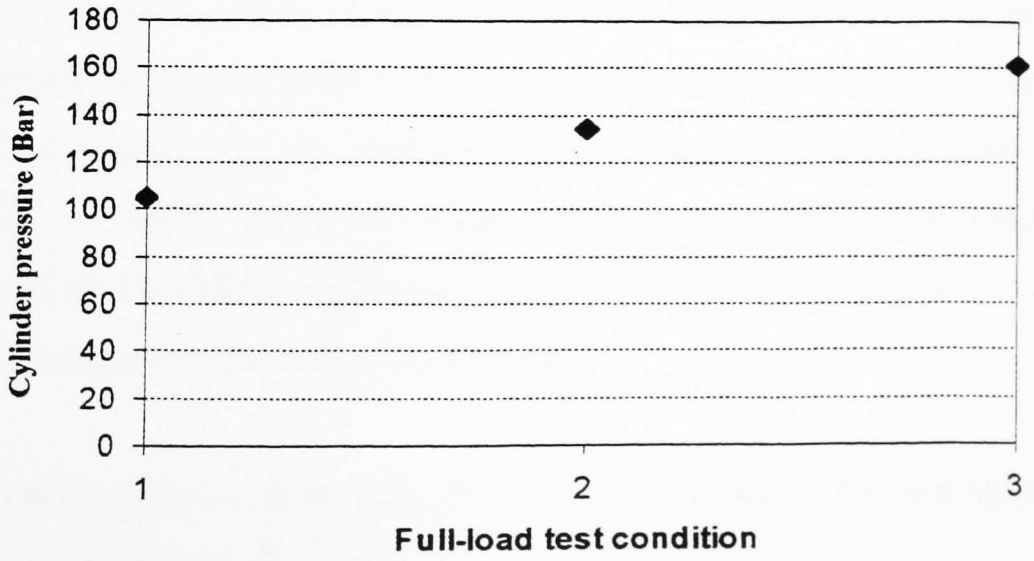

Figure 5.9 Cylinder pressure variation with the three full-load test conditions, shown in table 5.2 (Injector, 145 degree cone angle, 4.0 mm washer thickness).

Figure 5.7 shows the emission of NOx from the two light-load engine test conditions (4 and 5), to be considerably lower than the corresponding emissions for full-load engine test conditions (1, 2, and 3). The local peak cylinder temperature and pressure of the light-load conditions would have been drastically reduced compared to the full-load conditions, because of reduced fuel heat input and the addition of significant quantities of EGR.

Of the two light-load engine test conditions, test 4 produced only a tiny fraction of the emission of NOx compared to test 5. This was probably because of the lower engine load, and the difference in the injection timing between the two conditions. Test four required the engine to operate with a SOI of 5 degrees *after* TDC, whereas test five had advanced timing of 6 degrees *before* TDC. This significantly reduced the peak cylinder temperature, and hence NOx formation was also reduced.

Smoke emission

The emission of smoke was widely different between different engine test conditions and different injector depths. The full-load performance at test condition 1 was the most sensitive to injector depth.

Although the time spent at high-loads in a typical drive-cycle test is small, the emission of excessive smoke at any test condition is undesirable for a development engine intended for mass-production. Smoke was a found to be good indicator of combustion efficiency and air utilisation, and smoke values above 3 Bosch smoke units (BSU or BSN) were not acceptable on a modern production engine. Consideration of the smoke emissions with an injector washer thickness of 2.5 mm, indicated the emission of smoke to be too high.

Of the remaining injector depths, the 4 mm washer produced the minimum emission of smoke at the other test conditions.

Injector depth chosen for bowl ONE

The emission of NOx and smoke clearly indicated the 4 mm washer thickness offered the best compromise. It had good full-load performance (test conditions 1, 2, and 3), and little penalty at the light-load test conditions (4 and 5).

Interestingly, in the light-load engine tests, the 2.5 mm washer thickness had the lowest HC emissions, and good tolerance to EGR. But as figure 5.10 showing the variation in BSFC confirms, the 4 mm, medium protrusion injector, had the best overall performance.

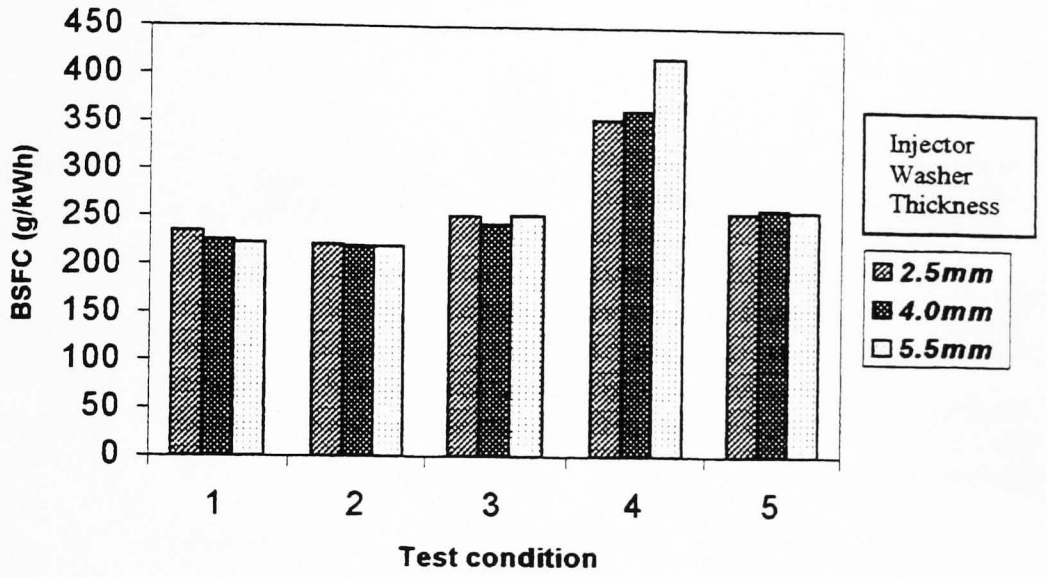

Figure 5.10 Variation of BSFC with injector depth for the five engine test conditions (see table 5.2).

Impingement diagrams for bowl shape ONE at the three full-load engine test conditions (table 5.2) are shown in figures 5.11 to 5.13, on the next page. As with the STD bowl shape, the point of fuel impingement of the chosen injector configuration did not occur over the top edge of the bowl lip. However, the impingement point at the SOI was much lower in the bowl than for bowl standard, and thus may be related to the high smoke values obtained using the deep protrusion, 2.5 mm injector washer thickness (discussion of fuel impingement is covered in more detail in section 5.4).

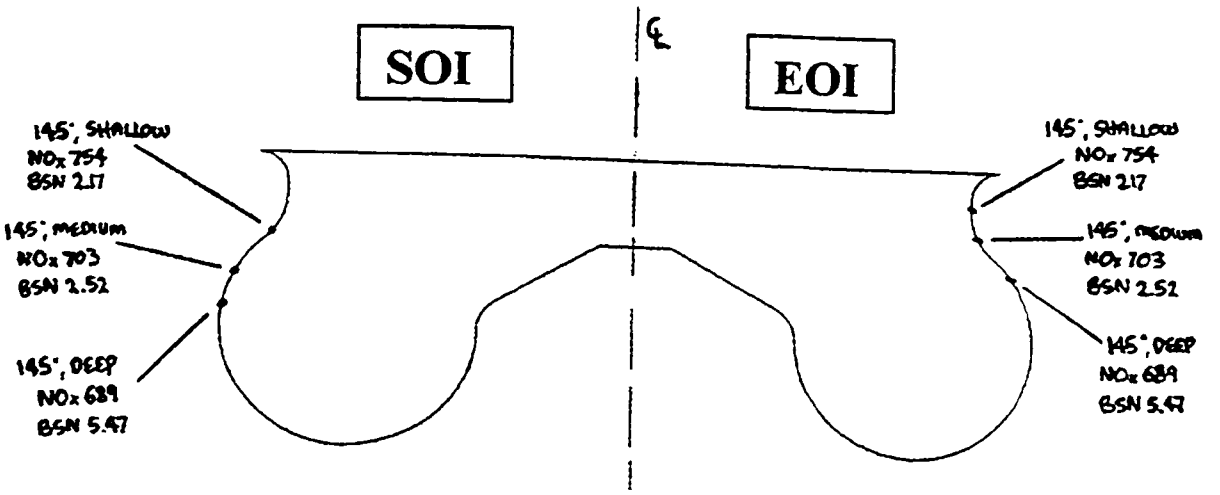

Figure 5.11 Test 1 (1500 rpm, 166.4 Nm – full-load), bowl shape ONE showing the points of impingement at SOI (2 degrees BTDC) and EOI (16 degrees ATDC), with the engine-out emissions results.

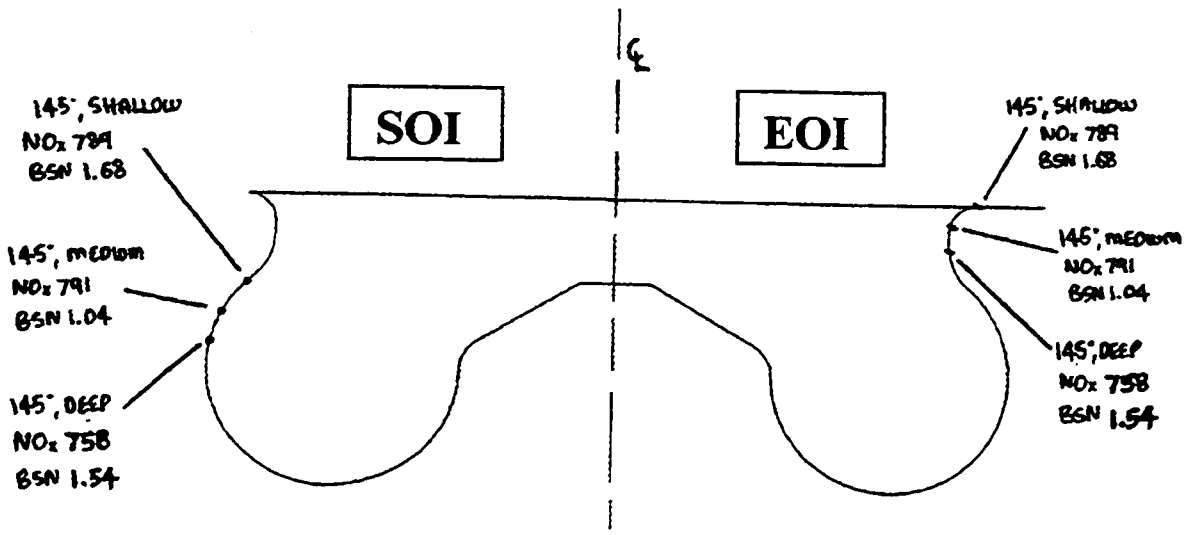

Figure 5.12 Test 2 (2000 rpm, 214.2 Nm – full-load), bowl shape ONE showing the points of impingement at SOI (3 degrees BTDC) and EOI (24 degrees ATDC), with the engine-out emissions results.

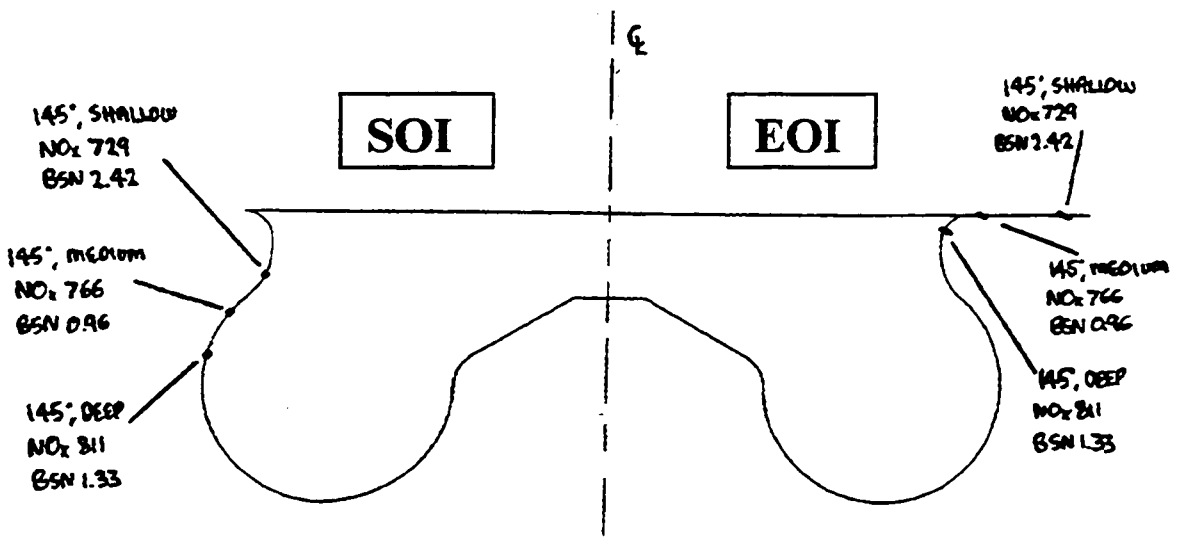

Figure 5.13 Test 3 (4000 rpm, 156.5 Nm – full-load), bowl shape ONE showing the points of impingement at SOI (9 degrees BTDC) and EOI (28 degrees ATDC), with the engine-out emissions results.

5.3.4 Injector optimisation results from bowl shape TWO

For each of the five engine test conditions, a matrix of NOx and smoke results was compiled. Tabulated results are presented in appendix D.

Particulates versus NOx trade-offs

The injector optimisation results were represented in terms of particulates versus NOx trade-offs. Figures 5.14 to 5.16 show the trade-offs for each of the three full-load test conditions (table 5.2), where differences in performance were most apparent.

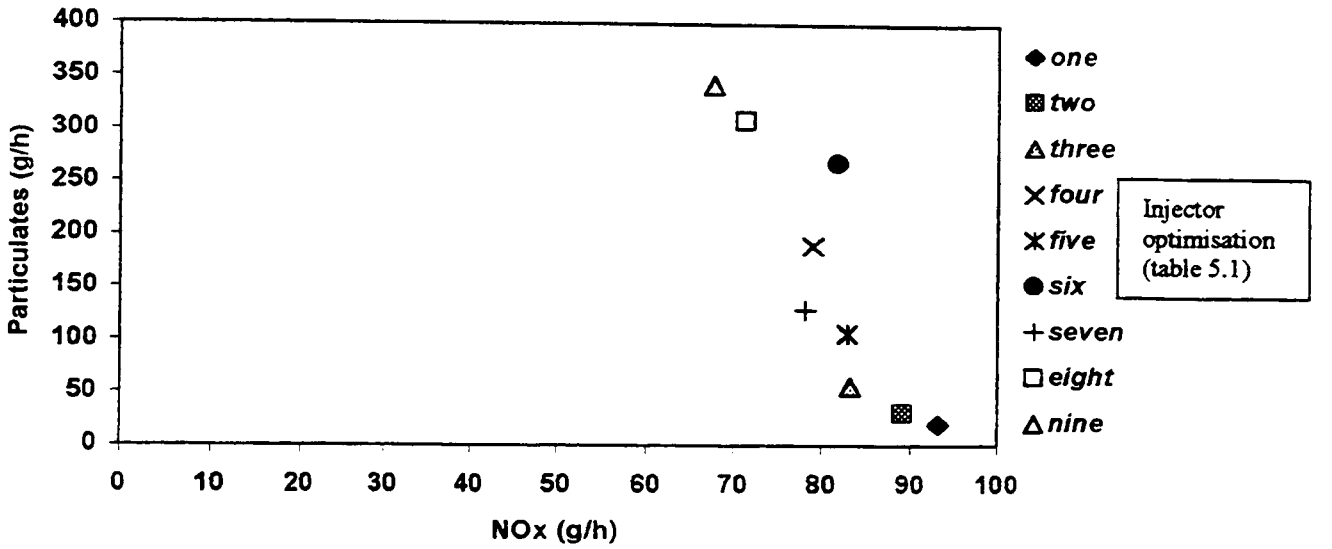

Figure 5.14 Particulates verses NOx trade-off for injector depth and cone angle optimisation at engine test condition 1 (1500rpm, full-load (166.4Nm), SOI 2 degrees BTDC, EGR 0%).

Engine test condition 1 favoured the three points of impingement occurring higher up the bowl, close top the lip (numbered from 1 to 3 in table 5.1). There was very little trade-off between particulates and NOx in this case, with large reduction in particulates possible with only a small increase in NOx.

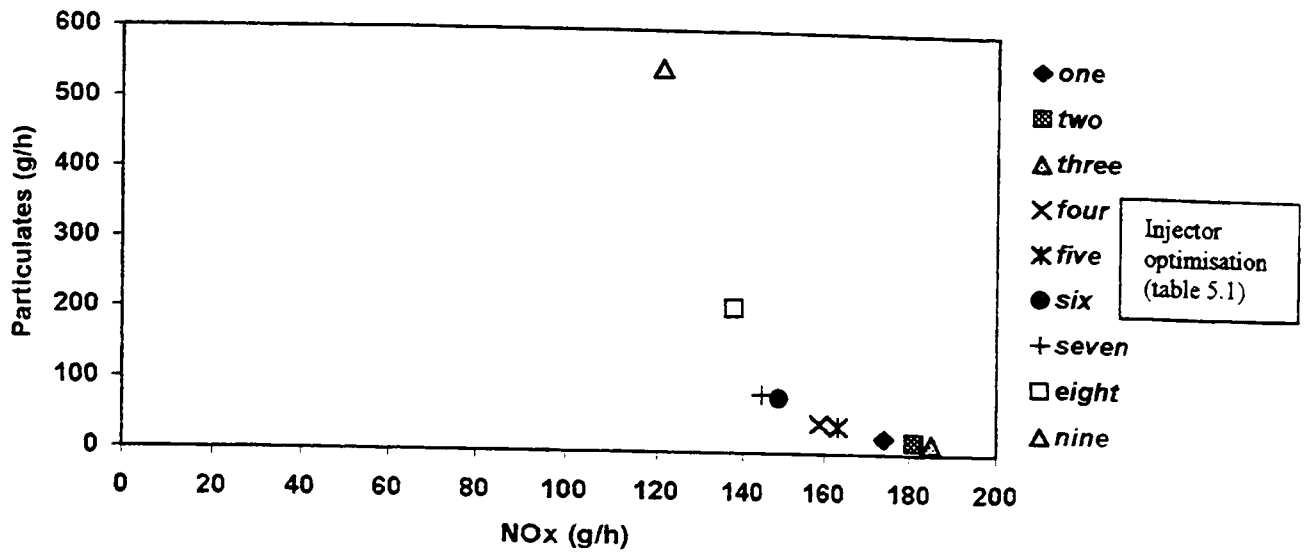

Figure 5.15 Particulates versus NOx trade-off for injector depth and cone angle optimisation at engine test condition 2 (2000rpm, full-load (214.2 Nm), SOI 3 degrees BTDC, EGR 0%).

Engine test condition 2 revealed a classic NOx-particulates trade-off shape. However, the increase in particulates as the point of impingement was lowered, was much greater than the reduction in NOx. The three points of impingement higher up the bowl side again performed best, even though the point of impingement at EOI now spilled over the bowl lip onto the piston crown, for the 150 degree, shallow injector combination (5.5 mm injector washer, see figure 5.18, discussed later).

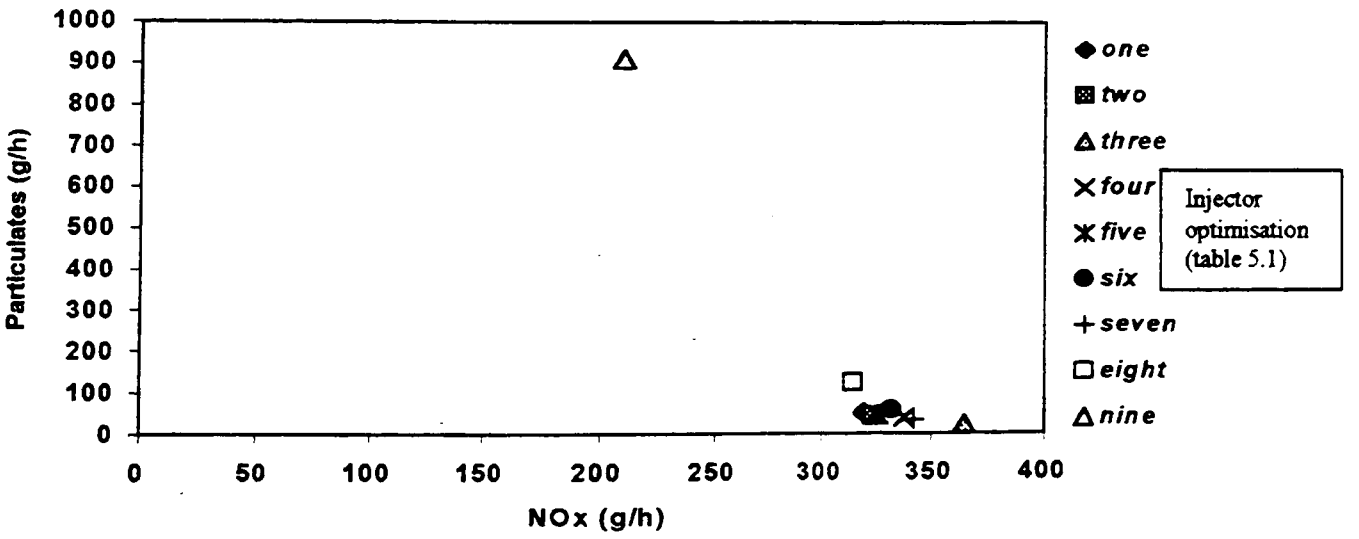

Figure 5.16 Particulates versus NOx trade-off for injector depth and cone angle optimisation at engine test condition 3 (4000rpm, full-load (156.5 Nm), SOI 9 degrees BTDC, EGR 0%).

The results from engine test condition 3 were masked by very poor particulates emissions of the deepest injector protrusion combination (140-degree spray cone angle, 2.5mm washer). However, again, injector combinations having high impingement points (closer to the bowl lip) performed well.

A general increase in the emission of NOx between engine test condition 1 to 3 was observed, similar to the results of bowl shape one.

Impingement diagrams of bowl shape TWO

The three full-load engine test results (conditions 1, 2, and 3) were plotted on a template of piston bowl shape TWO, as shown in figures 5.17 to 5.19, on the following pages. These were used as an aid for selection of the optimised injector configuration, and helped with understanding the effect of the point of fuel impingement on emissions.

Other performance parameters

A characteristic of bowl shape TWO was very high smoke emission during the full-load engine test conditions. This was most apparent at the lower speed, full-load test condition 1 (1500 rpm, 166.4 Nm, SOI 2 degrees BTDC). Figure 5.20 shows the variation in the emission of smoke with the point of fuel impingement, for engine test condition 1. Smoke emission proved to be the deciding factor in the choice of the optimum injector combination for this bowl. The only acceptable results were achieved using the 150-degree, 5.5 mm washer thickness which produced the highest point of impingement (ie. closest to the bowl lip).

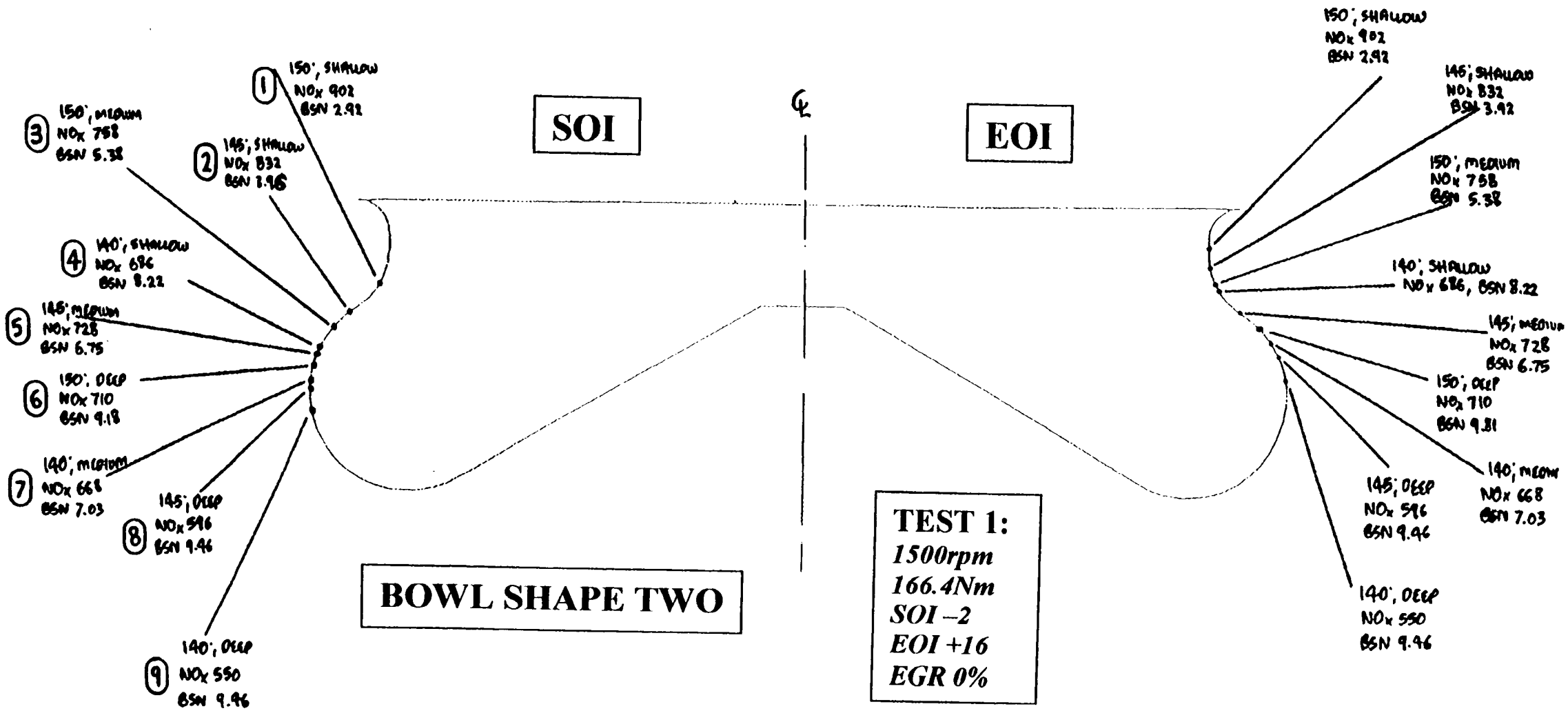

Figure 5.17 Test 1, bowl shape TWO showing the points of impingement at SOI and (2 degrees BTDC) and EOI (16 degrees ATDC), with the engine-out emissions.

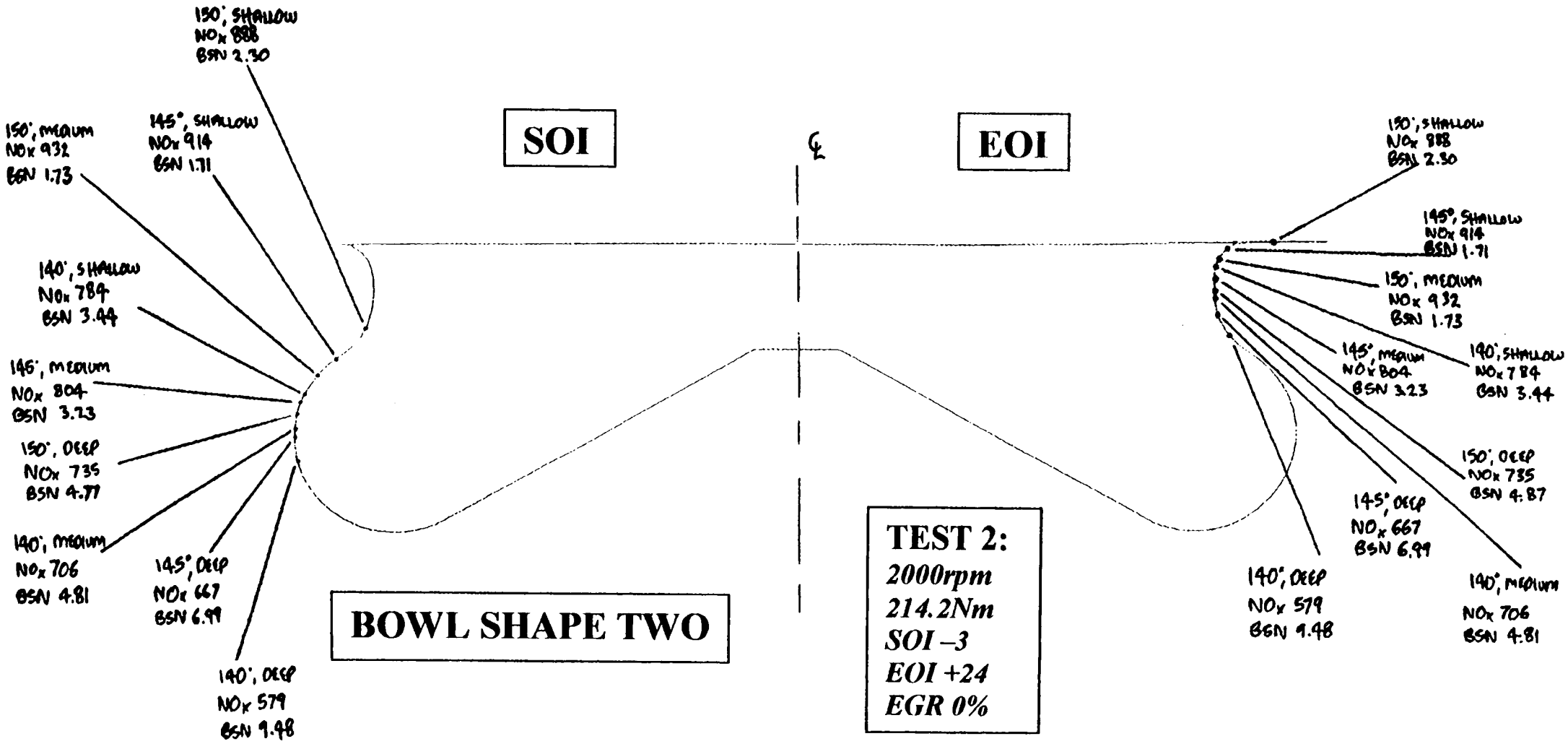

Figure 5.18 Test 2, bowl shape TWO showing the points of impingement at SOI and (3 degrees BTDC) and EOI (24 degrees ATDC), with the engine-out emissions.

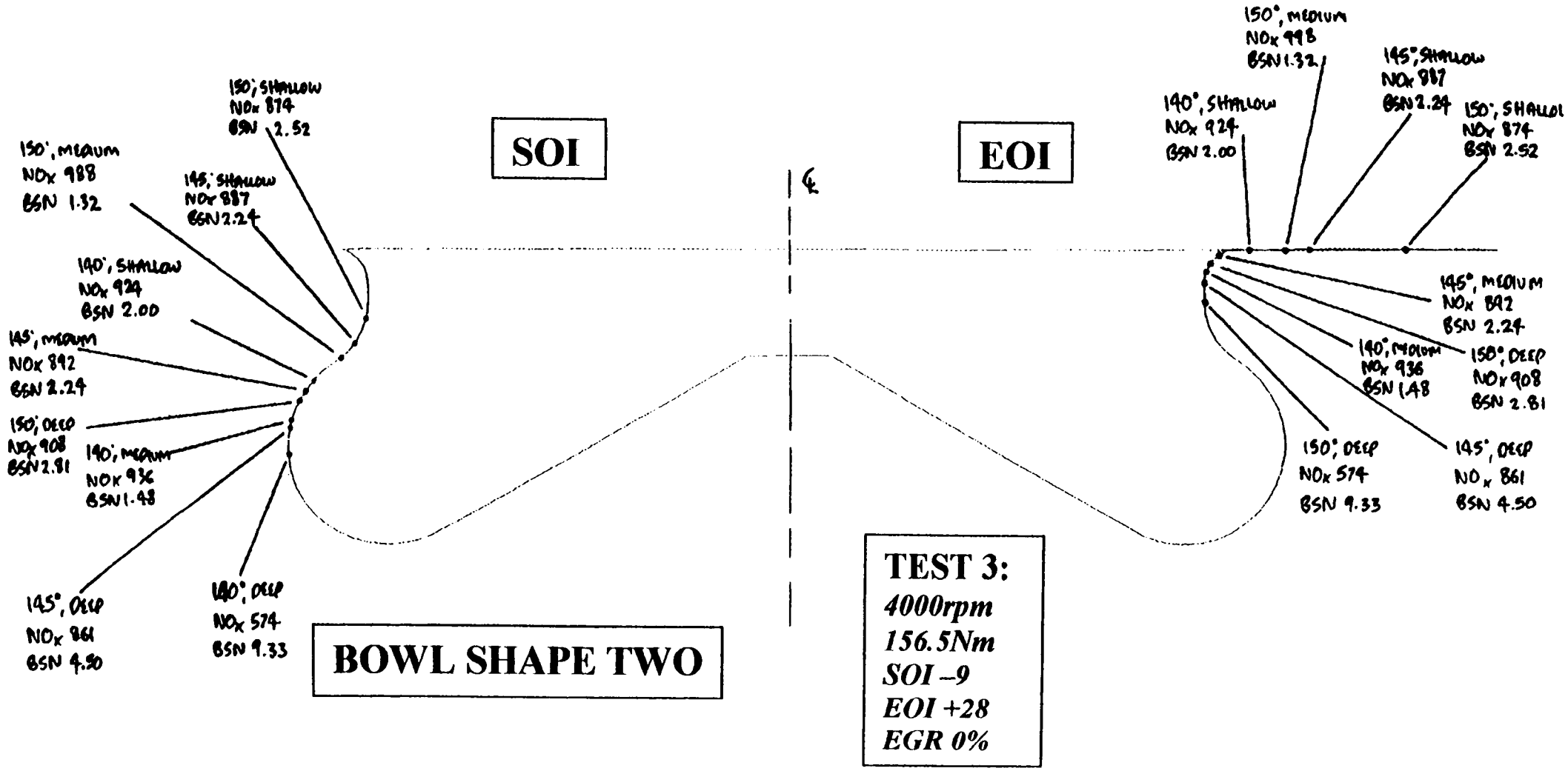

Figure 5.19 Test 3, bowl shape TWO showing the points of impingement at SOI and (9 degrees BTDC) and EOI (28 degrees ATDC), with the engine-out emissions.

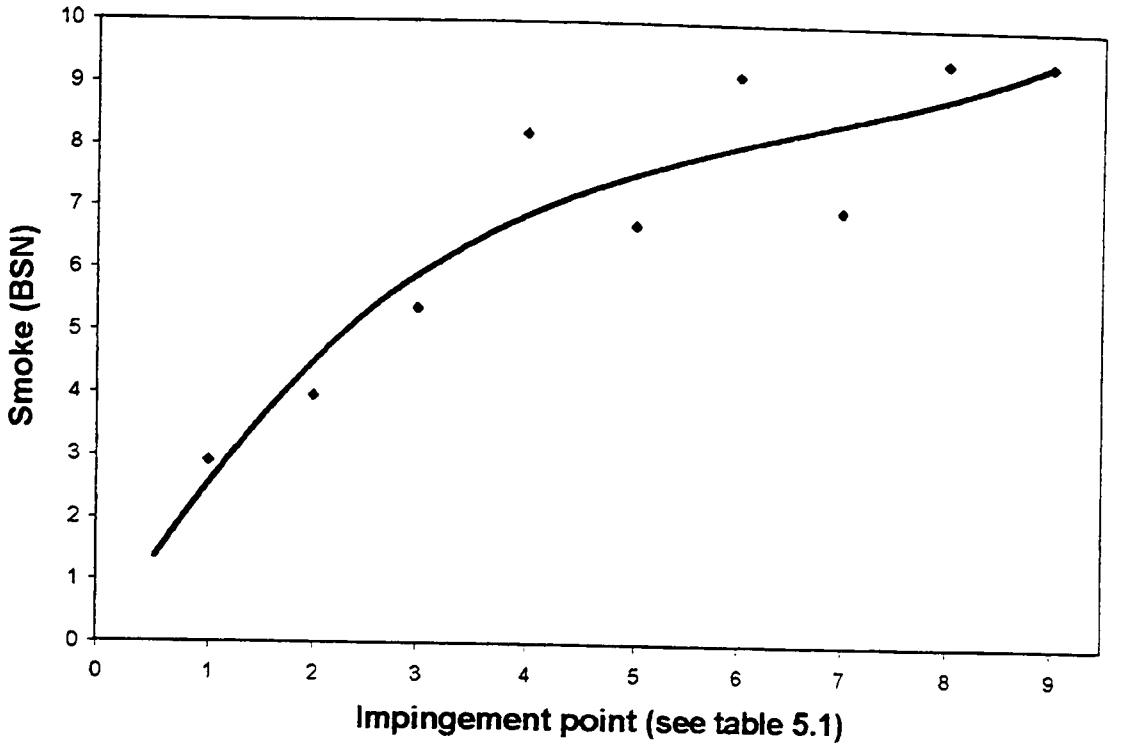

Figure 5.20 Effect of the point of fuel impingement on the emission of smoke at engine test condition 1 (1500 rpm, 166.4 Nm, SOI 2 degrees BTDC).

The variation of specific air consumption at test condition 1 (see figure 5.21), further highlighted the poor air utilisation for injector configurations giving impingement points lower down the bowl sides (ie. lower down from the bowl lip). Specific air consumption is defined as the engine intake air mass flow rate, per unit power produced.

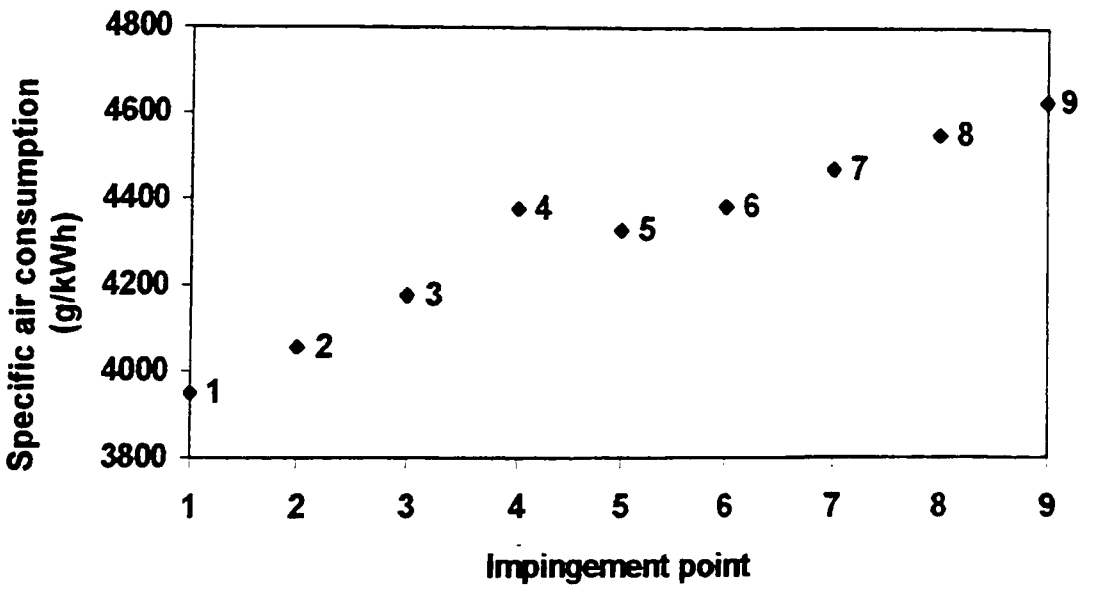

Figure 5.21 Variation of specific air consumption with impingement point (see table 5.1) at test condition 1 (1500rpm, full-load (166.4Nm), SOI 2 degrees BTDC, EGR 0%).

For a given power output (which was maintained constant for the nine injector configurations), the air consumption and emission of smoke gave an indication of the combustion efficiency. High impingement point conditions (impingement points 1, 2 and 3) showed low specific air consumption, and low emissions of smoke as well. However, specific air consumption was closely related to turbocharger performance (which was itself a function of many other engine operating conditions), and must be considered with together with smoke, intake airflow and other engine parameters to determine meaningful results.

Injector depth and cone angle chosen for bowl TWO

The injector configuration giving the highest impingement point was chosen, primarily because of its particulates versus NOx performance, and its relatively low emission of smoke at 1500rpm, full-load.

Part-load test conditions showed little variation between the highest impingement point combinations, and were not a significant factor in the selection of the optimum injector configuration (cone angle / washer thickness combination).

5.3.5 Injector optimisation results from bowl shape THREE

Again, the choice of the optimum injector configuration (cone angle and washer thickness combination) for bowl shape THREE was primarily determined by comparing NOx and smoke emissions at each particular injector configuration. For each of the five engine test conditions, a matrix of NOx and smoke results was compiled. Tabulated results are presented in appendix D.

Impingement diagrams of bowl shape THREE

Results were plotted graphically on a template of the piston bowl, relating the position of impingement to the emission of NOx and smoke. These are shown in figures 5.22 to 5.24, for the three different full-load test points (1, 2, and 3, see table 5.2). Full-load engine testing highlighted the greatest changes in emissions.

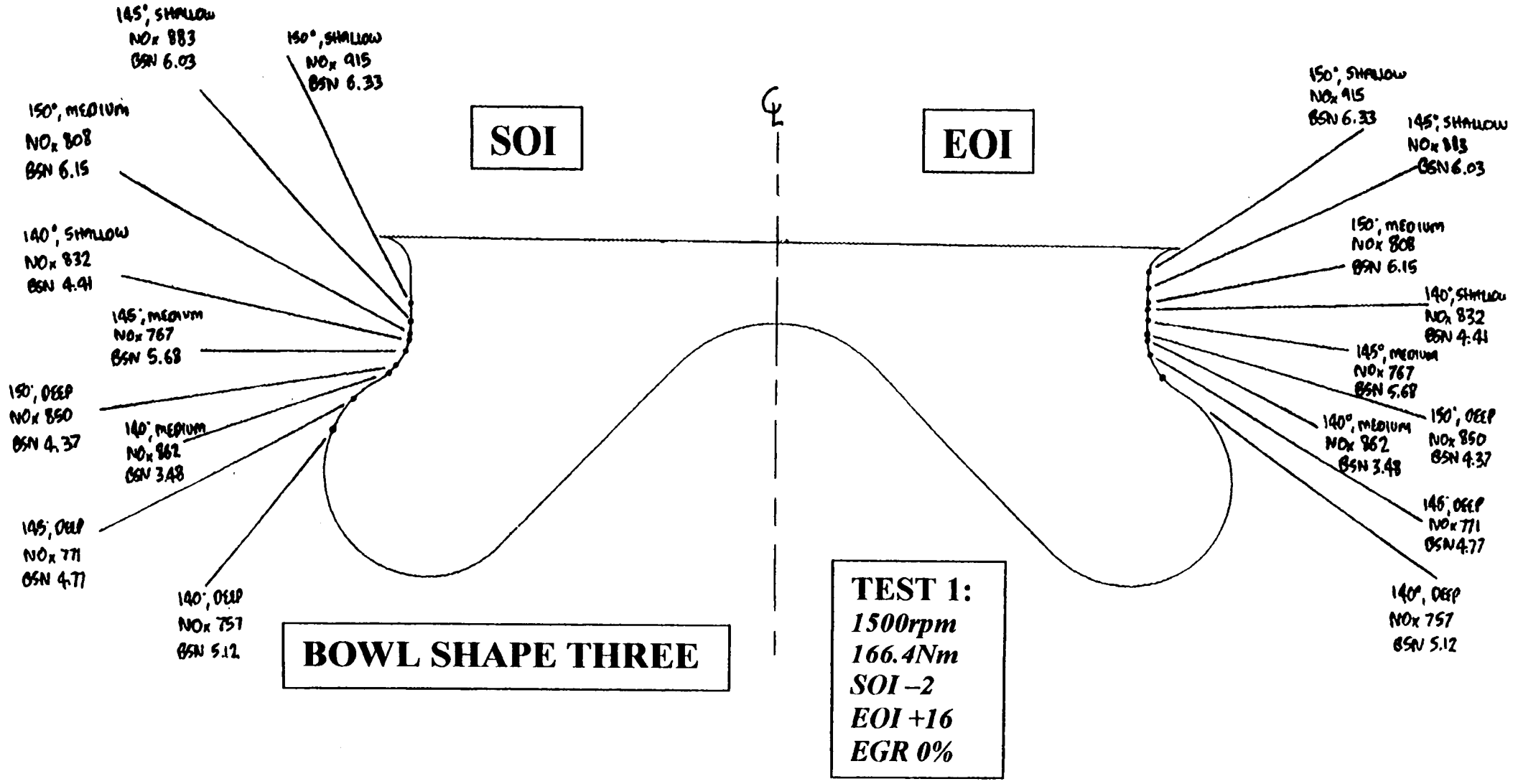

Figure 5.22 Test 1, bowl shape THREE showing the points of impingement at SOI and (2 degrees BTDC) and EOI (16 degrees ATDC), with the engine-out emissions.

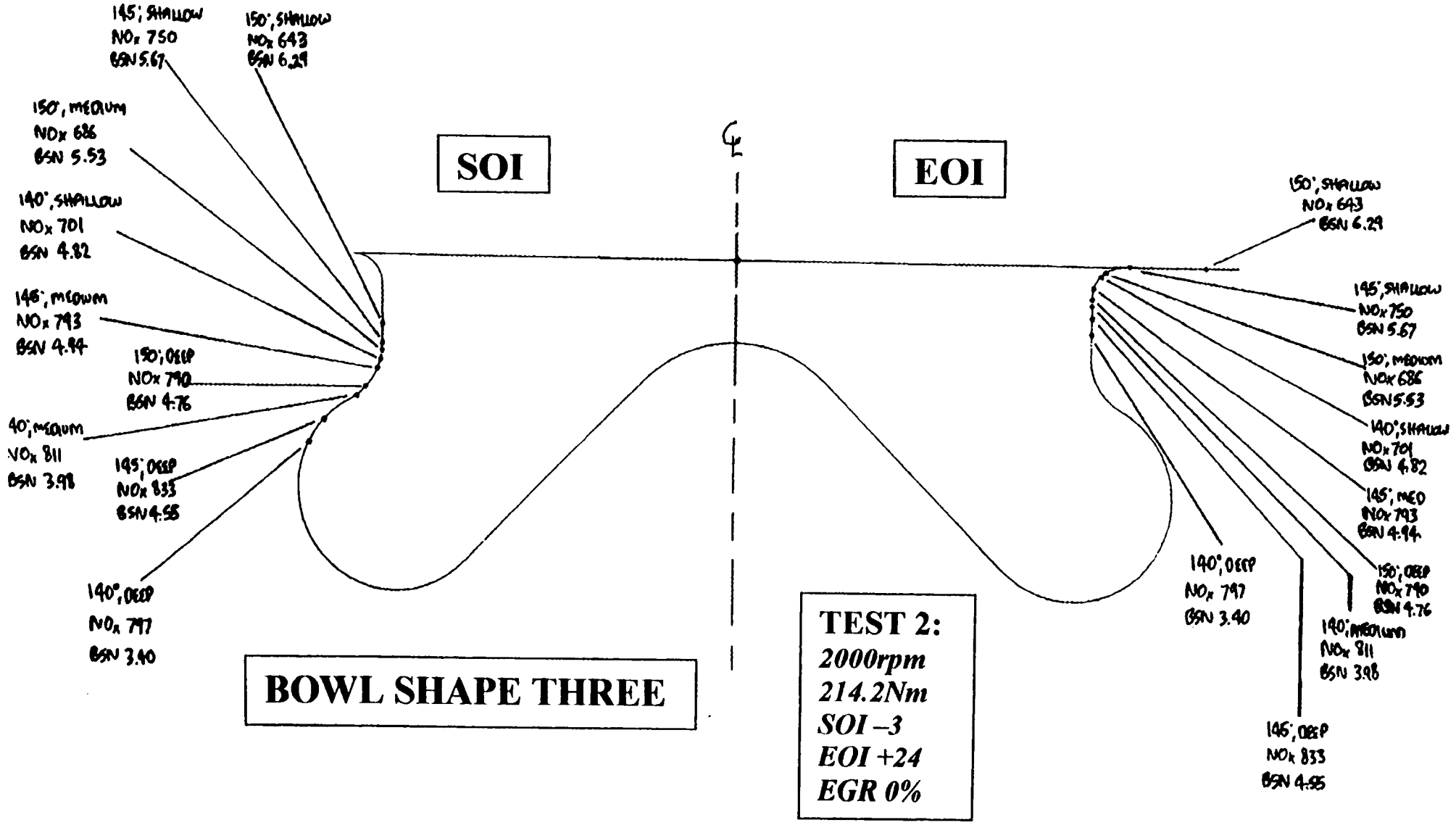

Figure 5.23 Test 2, bowl shape THREE showing the points of impingement at SOI and (3 degrees BTDC) and EOI (24 degrees ATDC), with the engine-out emissions.

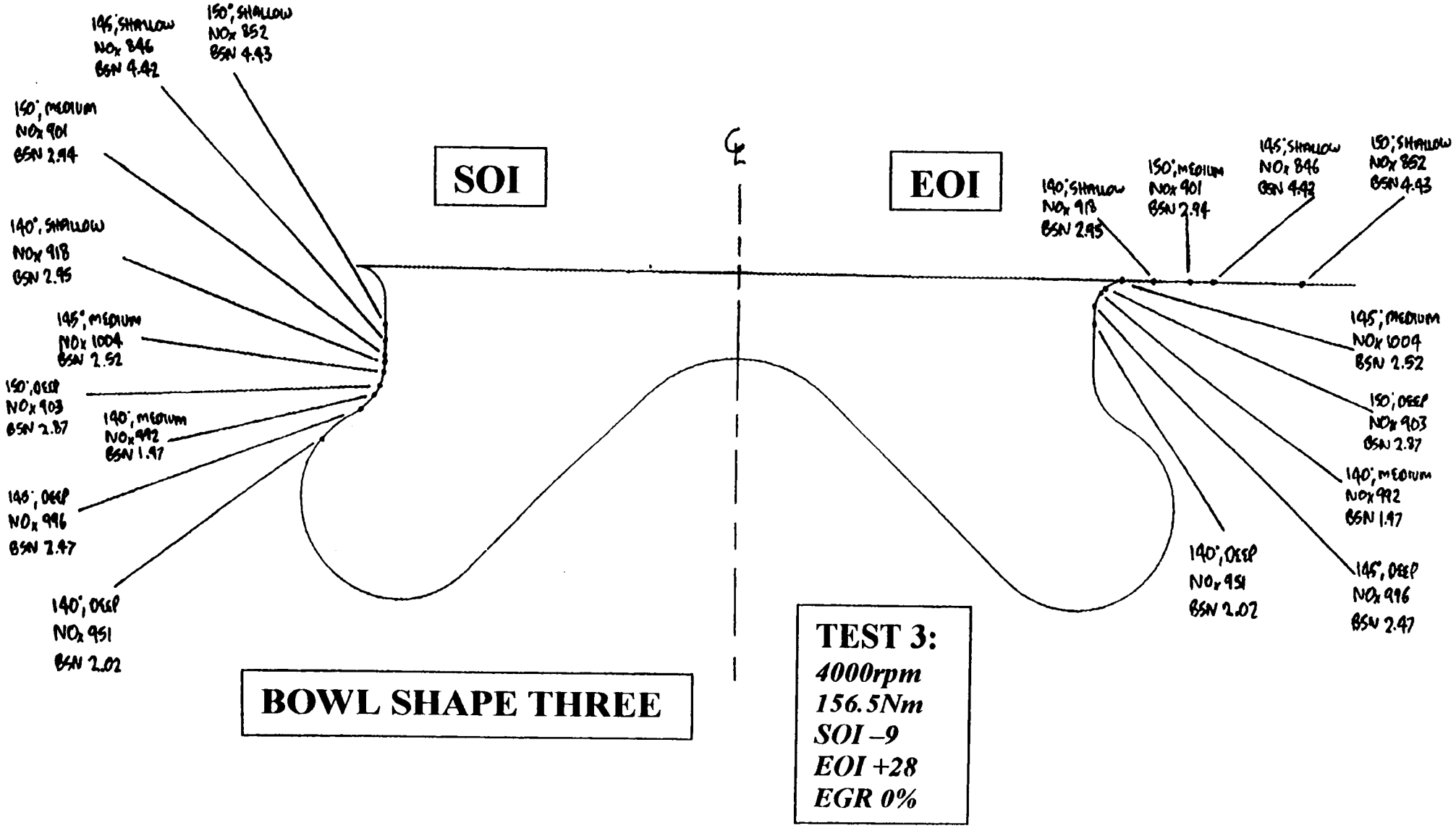

Figure 5.24 Test 3, bowl shape THREE showing the points of impingement at SOI and (9 degrees BTDC) and EOI (28 degrees ATDC), with the engine-out emissions.

Piston bowl shape THREE was designed knowing the realisation of the importance of the point of fuel impingement on performance and emissions (revealed by the test results from bowls ONE and TWO). The primary change of bowl THREE over bowls STD, ONE, and TWO was to increase the impingement lip area. This enabled fuel impingement to be contained within the impingement area if desired, by changing the injector depth and cone-angle. Injector optimisation tests confirmed fuel impingement should be largely confined within the impingement area (ie. the bowl lip).

Particulates versus NOx trade-offs

Figures 5.25 to 5.27 show the trade-offs between particulates and NOx for the three full-load engine test conditions (1, 2, and 3 in table 5.2). Engine test conditions 1 and 2 did not exhibit clear trade-offs in the production of particulates and NOx. Rather, the middle and low impingement point conditions performed best, producing low emissions of both species.

The insensitivity of NOx emission to the point of impingement implied that the peak cylinder temperature remained of similar levels, most likely controlled by the pre-mixed combustion and early diffusion burning resulting from fuel prepared after impingement on the bowl lip. However, the widely different emission levels for particulates suggests large disparities in the mixing-controlled late combustion phase.

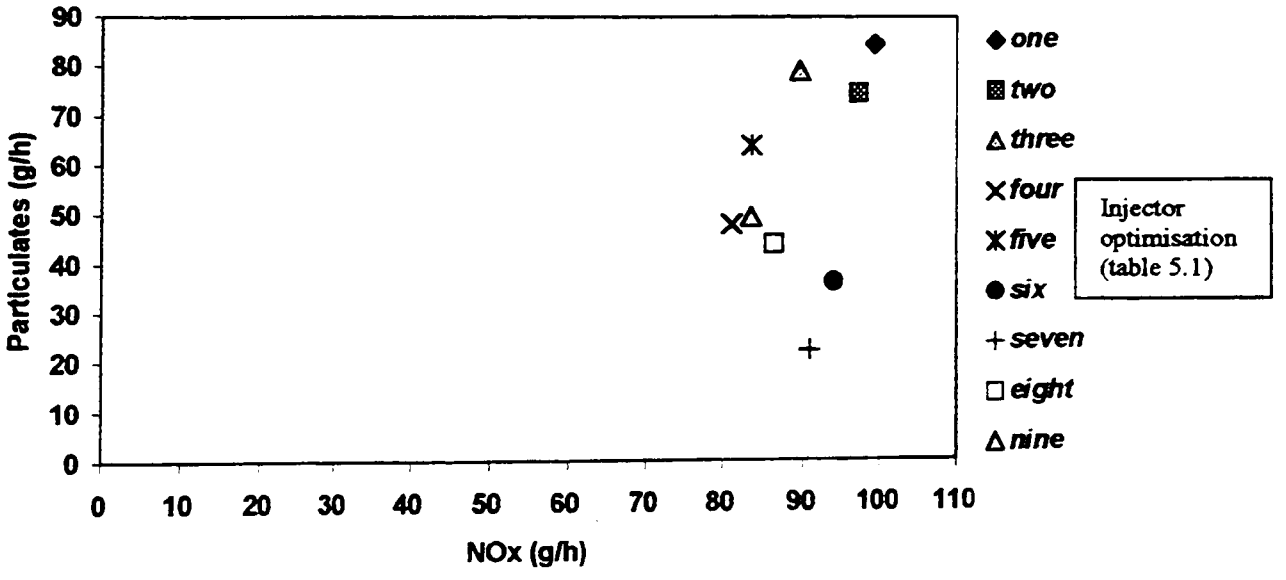

Figure 5.25 Particulates versus NOx trade-off for injector depth and cone angle optimisation at engine test condition 1 (1500rpm, full-load (166.4Nm), SOI 2 degrees BTDC, EGR 0%).

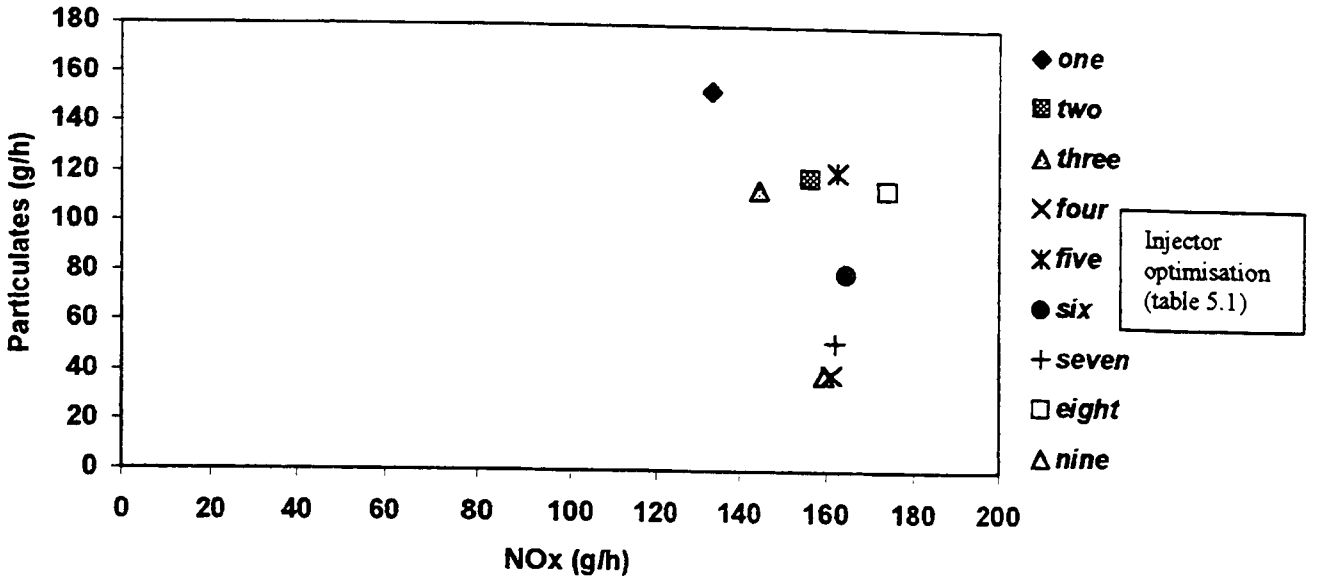

Figure 5.26 Particulates versus NOx trade-off for injector depth and cone angle optimisation at engine test condition 2 (2000rpm, full-load (214.2 Nm), SOI 3 degrees BTDC, EGR 0%).

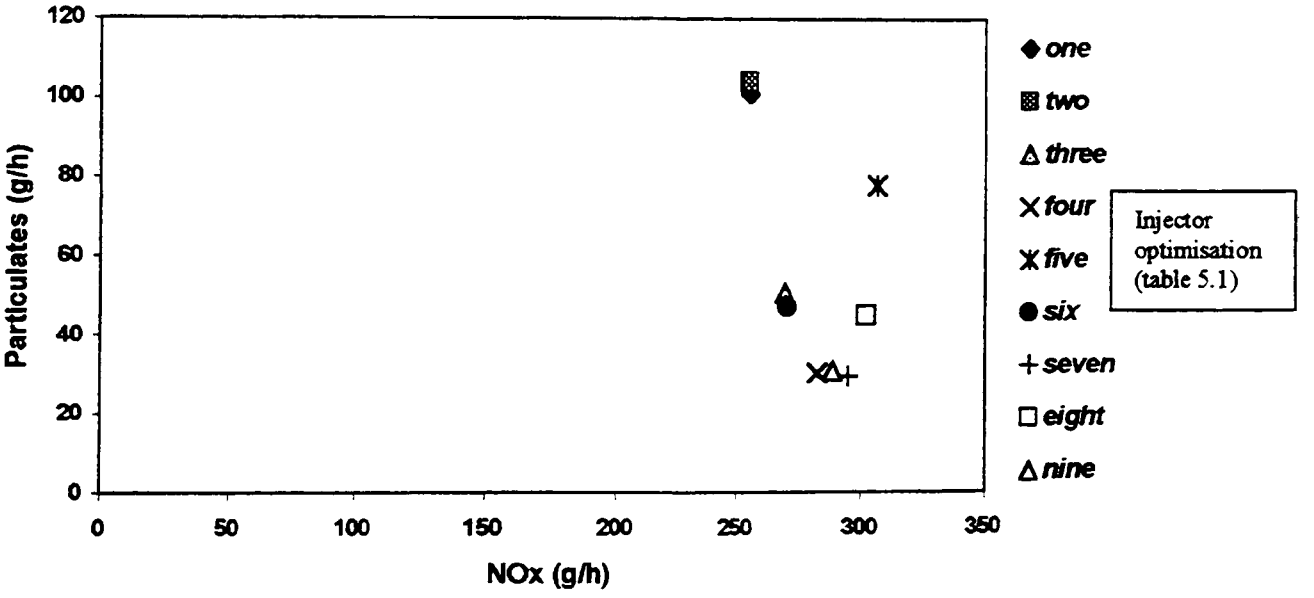

Figure 5.27 Particulates versus NOx trade-off for injector depth and cone angle optimisation at engine test condition 3 (4000rpm, full-load (156.4 Nm), SOI 9 degrees BTDC, EGR 0%).

Test condition 3 showed an unusual trend, in which the variation of particulates with NOx formed a 'U' shaped hook curve. However, in reality the differences in the emission of NOx were relatively small compared to the large changes in particluates. Here again, injector combinations generating middle to low impingement points performed best.

Other performance parameters

The variation of BSFC with different injector configurations (spray cone angle / washer thickness combinations) for the full set of five engine test conditions is shown in the contour map in figure 5.28.

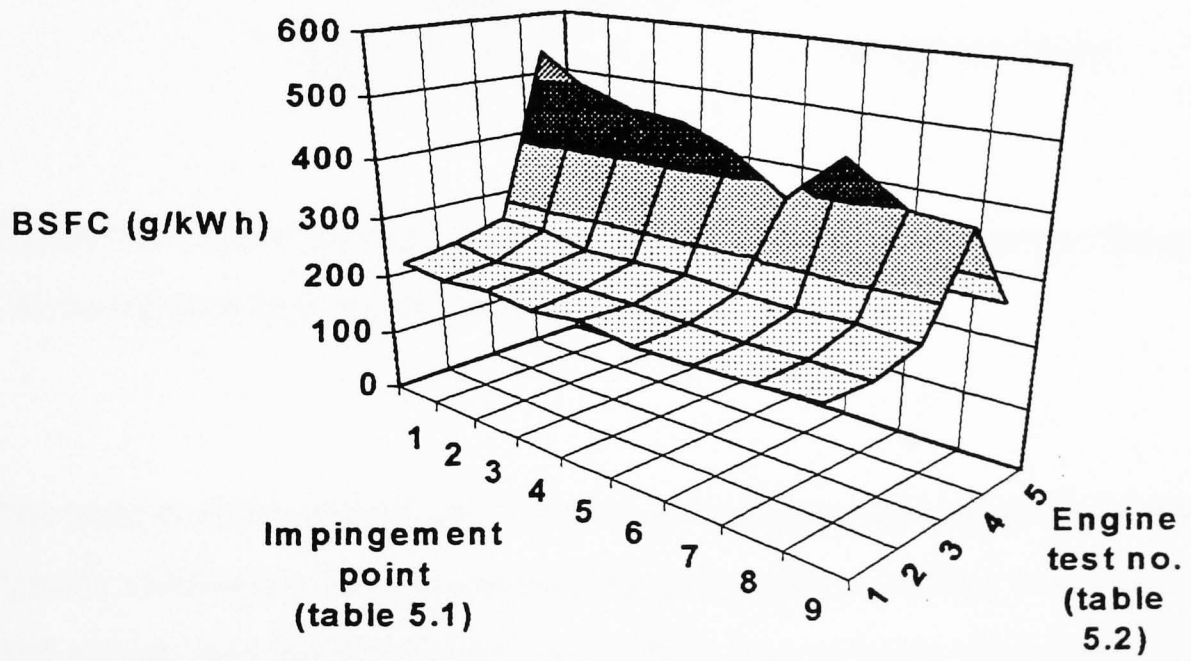

Figure 5.28 Variation of BSFC with injector configuration (impingement point) for the full set of five engine test conditions.

BSFC increased with speed in the three full-load engine test conditions. Figure 5.28 also shows that there was only a slight reduction in BSFC as the impingement point was lowered. However, part-load engine test condition 4 (condition 5 is masked from view in this contour map) showed poor fuel economy when the injector configuration resulted in the highest points of spray impingement (ie. close to the bowl lip). Test condition four had the most retarded ignition timing of all engine test points. It was likely that over penetration of fuel injected late onto the piston face caused the poor fuel economy observed with high impingement configurations.

The emission of carbon monoxide (CO) during part-load operation confirmed the need for an injector combination giving a medium to deep impingement point. Figure 5.29 shows the variation of CO with injector configuration (impingement point) for the two part-load engine test conditions.

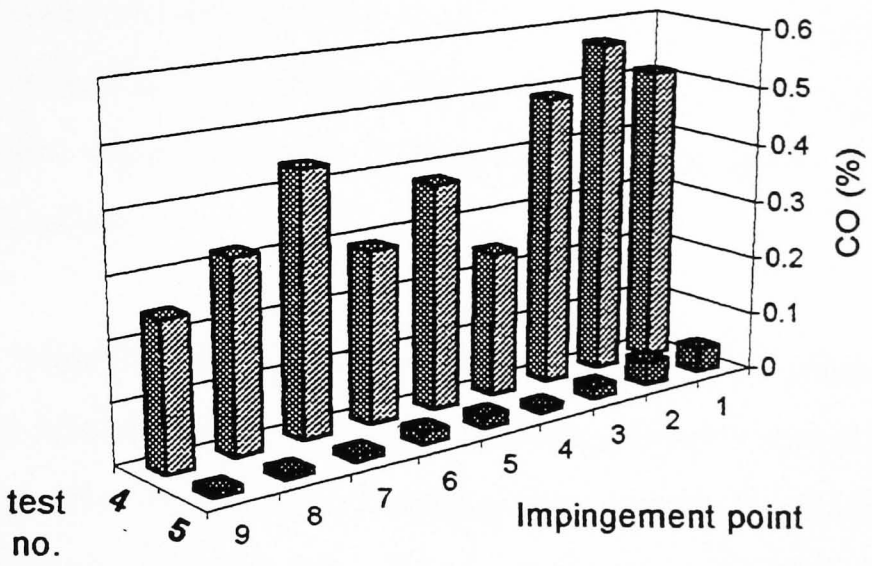

Figure 5.29 Effect of injector configuration (impingement point) on the emission of CO during part-load engine test operation.

The trend in CO mirrored that of BSFC, as efficient combustion resulted in reductions of both parameters. Engine test condition five produced much lower emissions of CO than engine test condition four, most likely due to better tolerance of the engine to EGR, and considerably more advanced SOI, at six degrees before TDC.

Injector depth and cone angle chosen for bowl THREE

An injector washer depth of 4.0 mm, and injector cone angle of 140 degrees was chosen primarily because of its NOx and smoke performance at full-load, in particular at 2000 rpm, full-load. However, the increase in the length of the impingement area for piston bowl shape three, resulted in a bowl that was less sensitive to injector configuration. A range of injector configurations with impingement points half way down the impingement region, performed well in terms of particulates versus NOx trade-offs.

5.4 Discussion of the effect of the point of impingement on performance and emissions

Modern HSDI diesel combustion system design is focused on low emissions. For a low emission combustion system to succeed, it should have a short ignition delay and retarded injection timing to minimise NOx emission. A fast rate of burning (and hence fuel/air mixing) is essential to offset the accompanying loss of cycle efficiency, and deterioration of soot emission. Fuel impingement on the bowl walls modifies combustion and emissions.

Results from the injector optimisation showed a clear link between the point of impingement of the injected fuel spray, and engine performance and emissions. This section discusses the effect of the point of impingement in more detail, and how it was used for the development of piston bowl design, in the quest for reduced drive-cycle emission test results.

5.4.1 Effect of fuel impingement on heat release

The validity of the cylinder pressure measurements taken, and thus of the heat release analysis, was confirmed by calculating and then checking the polytropic index of compression and expansion curves of the engine four-stroke cycle. Typically, the compression polytropic index was found to be 1.3 throughout the compression process, only deviating from this value during combustion. An illustration of the cylinder pressure data is shown in figure 5.30, where the natural log of cylinder pressure is plotted against cylinder volume. The polytropic index was defined by the slope of the compression curve.

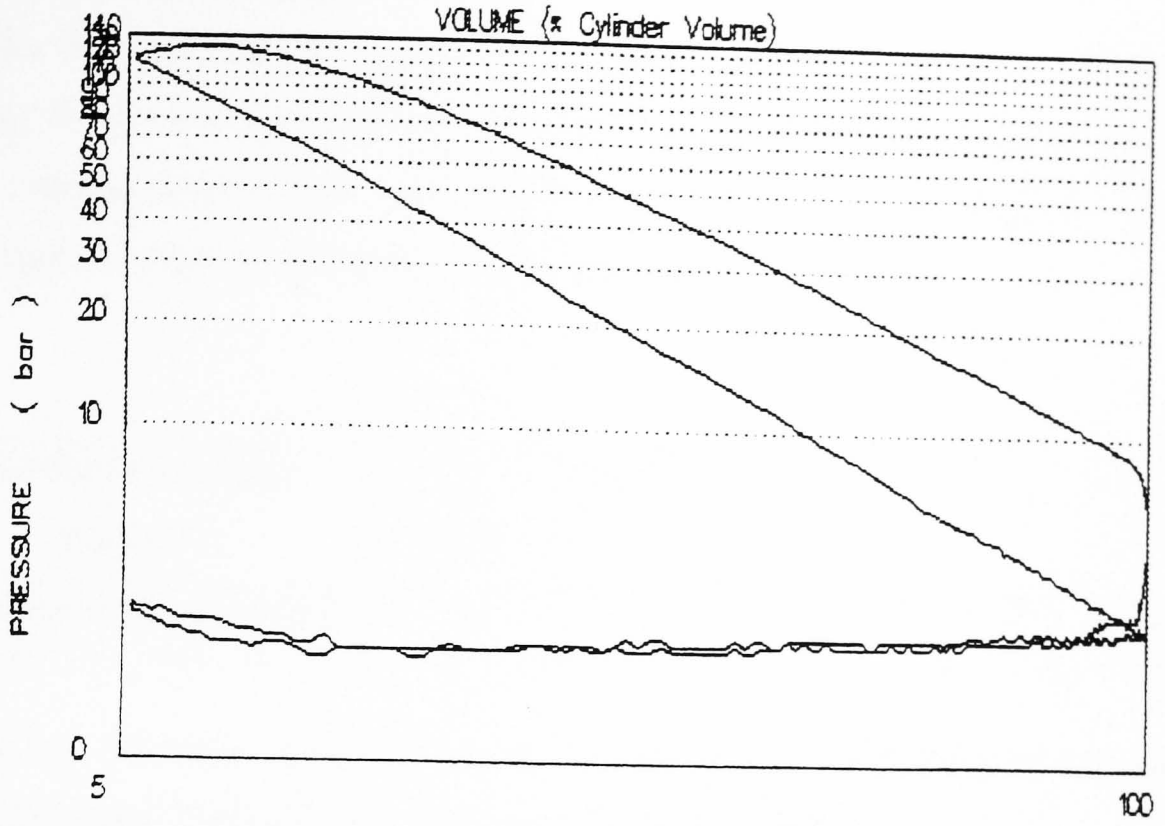

Figure 5.30 Variation of cylinder pressure (natural log scale) with cylinder volume (expressed as a fraction (%) of the swept volume). Gradient of the compression and expansion lines defines the polytropic index of each stroke.

5.4.1.1 Effect of the point of impingement on ignition delay

Ignition delay determined the quantity of fuel prepared for combustion during the pre-mixed burning phase. Depending on its length, the ignition delay period affected peak cylinder temperature and pressure, and thus the emission of NOx.

Ignition delay was obtained by analysing the rate of change (ie. the first derivative) of the cylinder pressure. A point of inflection present in the pressure-trace, produces a minimum in the rate of pressure rise corresponding to the start of combustion. The difference between the start of injection and the start of combustion gave the ignition delay period, in engine crank-angle degrees.

Results for ignition delay

Results for ignition delay versus impingement point from piston bowl shape TWO, during full-load testing at 2000 rpm (which showed a wide variation of emissions with impingement point) are shown in table 5.3. The variation of NOx with impingement point is shown below in figure 5.31 for comparison.

Impingement point (table 5.1)	1 (highest)	2	3	4	5	6	7	8	9 (lowest)
Ignition delay (degrees)	2	2	1	1	2	1	1	1	1

Table 5.3 Variation of ignition delay with the point of impingement (see table 5.1) for bowl shape TWO. Engine operating at 2000 rpm, full-load.

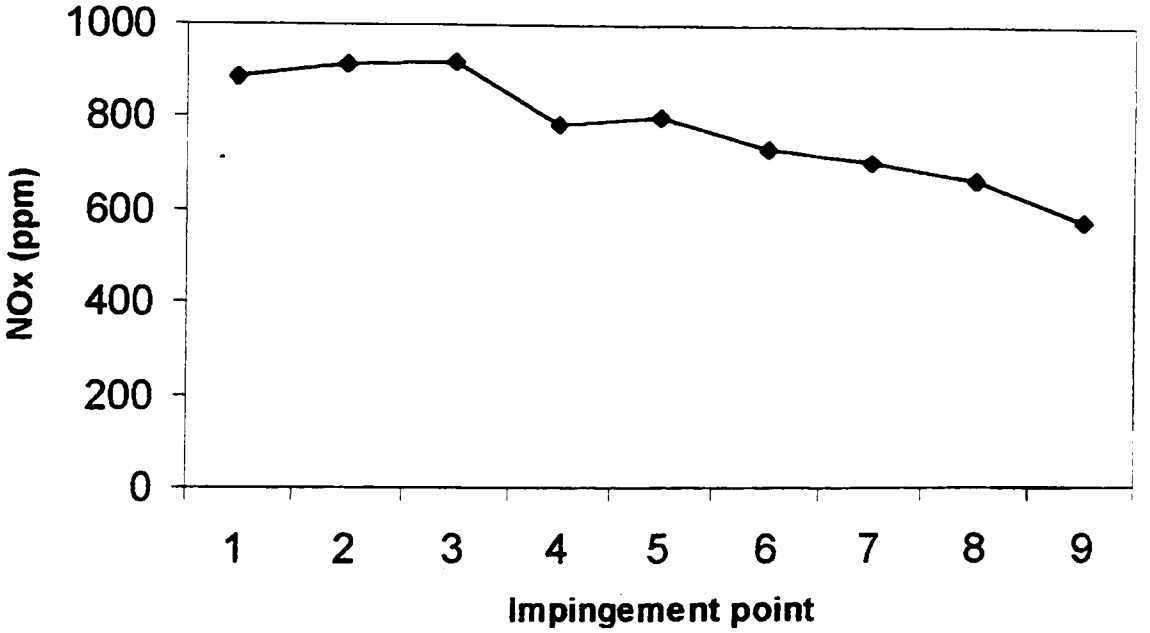

Figure 5.31 Variation of the emission of NOx with impingement point (table 5.1) from bowl shape TWO. Engine operating at 2000 rpm, full-load.

Discussion of ignition delay

The ignition delay period was very short. This was probably due to high in-cylinder air temperature at fuel injection, resulting from high turbocharger boost pressure,

advanced injection timing, and high heat transfer from the combustion chamber surfaces to the intake-air at full-load.

Ignition delay was slightly longer when fuel impingement was high up the bowl (nearer the bowl lip). However, NOx emission changed considerably, exhibiting a clear trend with the point of impingement. The relatively constant but short ignition delay suggested that NOx formation was more dependent on the later stages of combustion, rather than fuel prepared for combustion during the ignition delay period. This indicated that the peak gas temperature was not reached during pre-mixed combustion, resulting from fuel prepared during the ignition delay period. Results from other full-load test conditions and different bowl shapes showed similar trends.

It seems likely that changes in NOx emission could not be attributed to differences in the ignition delay period. Some other mechanisms, or combination of mechanisms, were responsible for changes in NOx emission when the point of impingement was altered.

5.4.1.2 Effect of fuel impingement on pre-mixed combustion

Although it seems likely that the point of impingement had only a small influence on the ignition delay period, it may have affected pre-mixed combustion in other ways. These included the quality of pre-mixed charge prepared during the delay period, and the location of ignition sites within the combustion chamber.

Calculation to determine whether fuel impingement was likely before the start of combustion

If the point of impingement of injected fuel was to have an effect on pre-mixed combustion, then fuel spray must have impinged on the bowl sides before the start of combustion. An approximate estimation of the injection rate through each of the six nozzle holes was obtained using equation 5.8 below, assuming quasi-steady, incompressible, one-dimensional flow.

$$\dot{m}_f = C_D A_n \sqrt{2\rho_f \Delta p}$$

Equation 5.8 Where $\dot{m}_f$ is the fuel mass flow rate, C_D is the nozzle discharge coefficient, A_n is the nozzle area, ρ_f is the fuel density and Δp is the pressure difference across the injector nozzle [Heywood, 1988].

For example, full-load testing at 1500 rpm resulted in the parameter values listed in table 5.4 below.

Parameter	Nozzle area (m^2)	Discharge Coefficient	Fuel Density (kg/m^3)	Fuel line Pressure (Bar)	Cylinder pressure (Bar)	Pressure drop Across injector (Bar)
Value	1.81×10^{-8}	0.80	854	880	60	820

Table 5.4 List of engine and fuel injection parameters at 1500 rpm, full-load, used for calculation of approximate fuel injection velocity.

The discharge coefficient was estimated using equation 5.8, and a known injector fuel flow rate of $800cc^3$ at 100 bar. A full list of fuel properties is given in appendix E.

By dividing the mass flow rate estimated above, by the fuel density and nozzle area, A_n, an approximation of the fuel injection velocity was obtained. At 1500rpm, full-load, the injection velocity was calculated to be 229 m/s. Given that the ignition delay at this condition was only one degree crank angle, and that occupied a duration of only 1.11×10^{-4} seconds, the distance travelled by the tip of the spray in this time (assuming no momentum loss due to interaction with the airflow) was estimated to be 25.4 mm.

Hence, because the path length between the injector and piston bowl impingement area was between 18.0 and 19.8mm (depending on the bowl shape), the injected spray

was likely to have impinged before the start of combustion. It is, therefore, likely that the impingement of the spray on the bowl wall and subsequent spreading along the wall, influenced significantly the secondary (ie. off the wall) mixing of fuel and air.

This secondary mixing off the bowl walls may have become more significant at higher engine speeds, when the spray impinged on the bowl walls even earlier during the ignition delay period. This occurs because at higher engine speeds, the fuel injection pressure rises, increasing jet velocity, and reducing the time taken for the fuel jet to impinge on the piston bowl sides. However, because the ignition delay is primarily controlled by chemical reaction kinetics and not mixing rates, it is possible that a greater quantity of fuel would have been prepared for pre-mixed combustion at higher engine speeds.

Ignition sites

The location of ignition sites was difficult to estimate. At low engine speeds and high loads, fuel the injection velocity was low, but the combustion chamber temperature was high. It was possible that initial ignition sites occurred near the injector, by fuel injected early. Fuel jet growth and entrainment of air in the spray may have been important at low speeds, and a significant factor controlling the amount of fuel prepared for pre-mixed combustion.

However, at higher engine speeds, ignition sites were most likely to be provided by dispersed spray downstream of the impingement points. In this situation, initial jet growth and initial spray quality were less important, but the position of the point of impingement was more critical in determining pre-mixed fuel mixture quality. For example, at the extreme highest points of impingement, the fuel may have spilled over the bowl top onto the relatively cool, large piston surface area.

Fuel causing wall-wetting will most likely have burnt in a diffusion burning mode, controlled by the rate of evaporation from the piston bowl surfaces. When compared to a lower point of impingement, it was probable that a reduced quantity of fuel would be prepared for pre-mixed combustion, which may have helped to reduce NOx at high loads, but could cause quenching and high HC emissions at low loads.

Discussion of fuel prepared for pre-mixed combustion

By simply dividing the duration of the ignition delay period by the total fuel injection period, an approximation of the proportion of fuel prepared for pre-mixed combustion was found. At 1500 rpm, full-load, only about 5.6% of the total fuel injected occured during the ignition delay period, and thus was available for pre-mixed combustion. In practice, the proportion of fuel that had time to prepare for pre-mixed combustion would have been less than 5.6%.

These estimates were confirmed by analysis of heat release diagrams obtained at full-load. Figure 5.32 shows an example of the heat release as a function of engine crank angle for piston bowl shape THREE (engine operating at 2000 rpm, full-load).

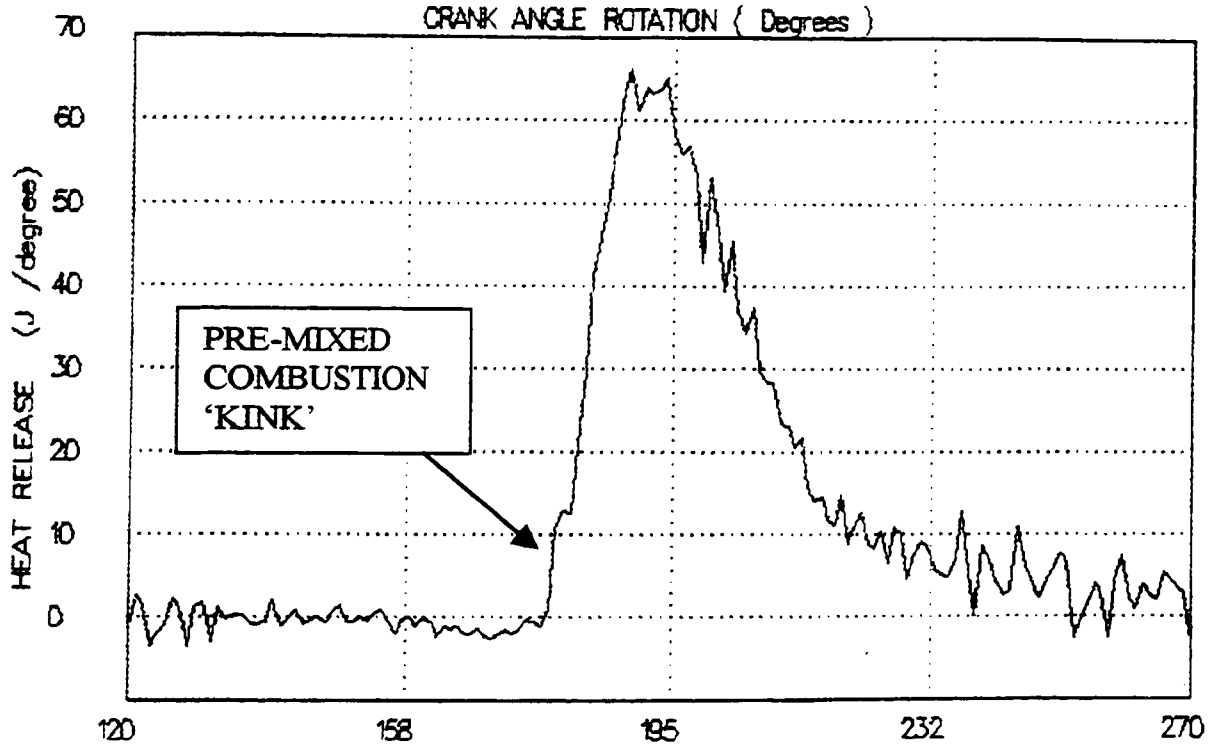

Figure 5.32 Rate of heat release as a function of crank-angle for piston bowl shape THREE (engine operating at 2000 rpm, full-load).

The small fraction of the total heat released during pre-mixed combustion was given by the area under the 'kink' in the graph, as shown above. These results correlated well with the observed trend in the production of NOx, discussed in the ignition delay sub-section. As NOx production was very temperature sensitive, the small amount of

heat release during pre-mixed combustion in these full-load tests had little effect on the results of NOx emission.

5.4.1.3 Effect of fuel impingement on diffusion controlled burning

Once combustion of the pre-mixed charge had occurred (very rapid), combustion continued by diffusion burning. Diffusion burning accounted for the majority of heat released during combustion. Although the heat release rate profiles from full-load testing for different injector configurations were similar, there were some subtle differences which may, in part, help to explain some of the emissions results trends observed.

Comparison of heat release results from various impingement points

The initial rate of heat release rose quickly to a maximum for all impingement points (as shown in figures 5.33 and 5.34 overleaf). Although there were differences in the peak rate of heat release between different injector combinations, the signal was noisy and no trend in peak heat release was noticeable.

Differences did exist in the overall shape of the heat release curve, and the duration around the peak heat release rate. Figures 5.33 and 5.34 show heat release profiles from full-load testing at 2000 rpm, of piston bowl shape THREE, at impingement point numbers 1 and 7 (the injector configuration finally chosen for this bowl shape) respectively.

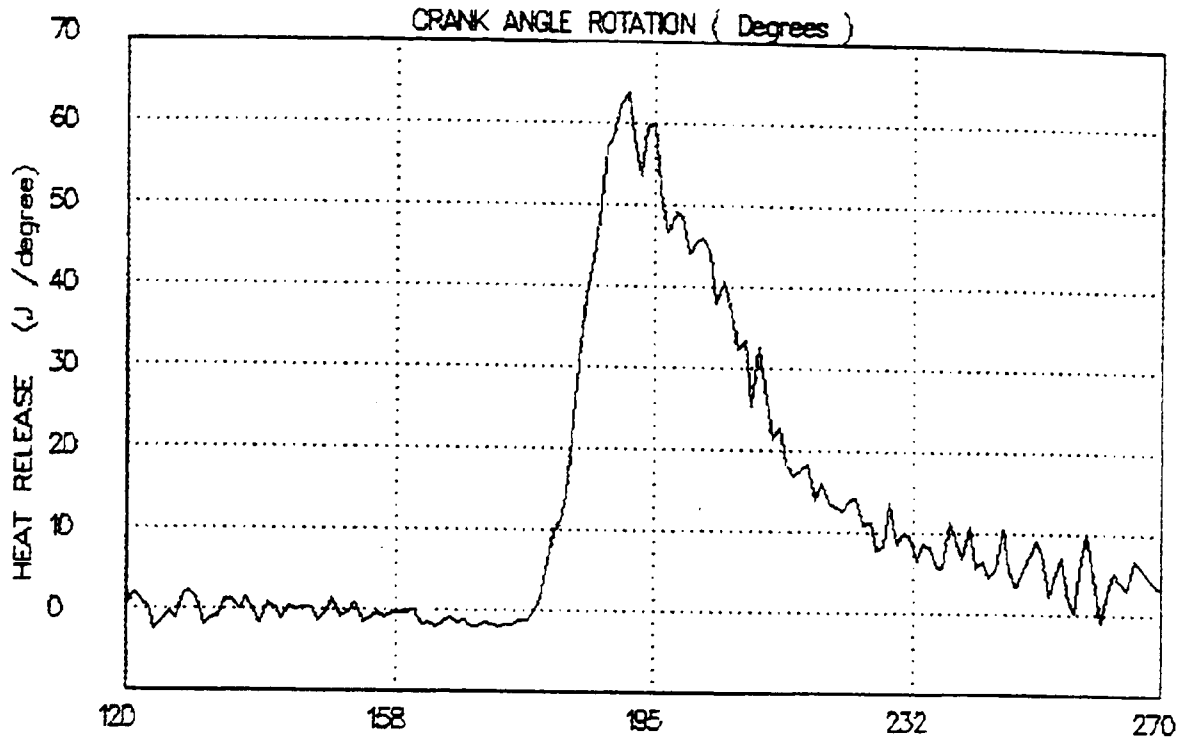

Figure 5.33 Rate of heat release as a function of crank-angle for piston bowl shape THREE (engine operating at 2000 rpm, full-load). Injector configuration of 150-degree cone angle, 5.5mm washer thickness (point 1 in table 5.1).

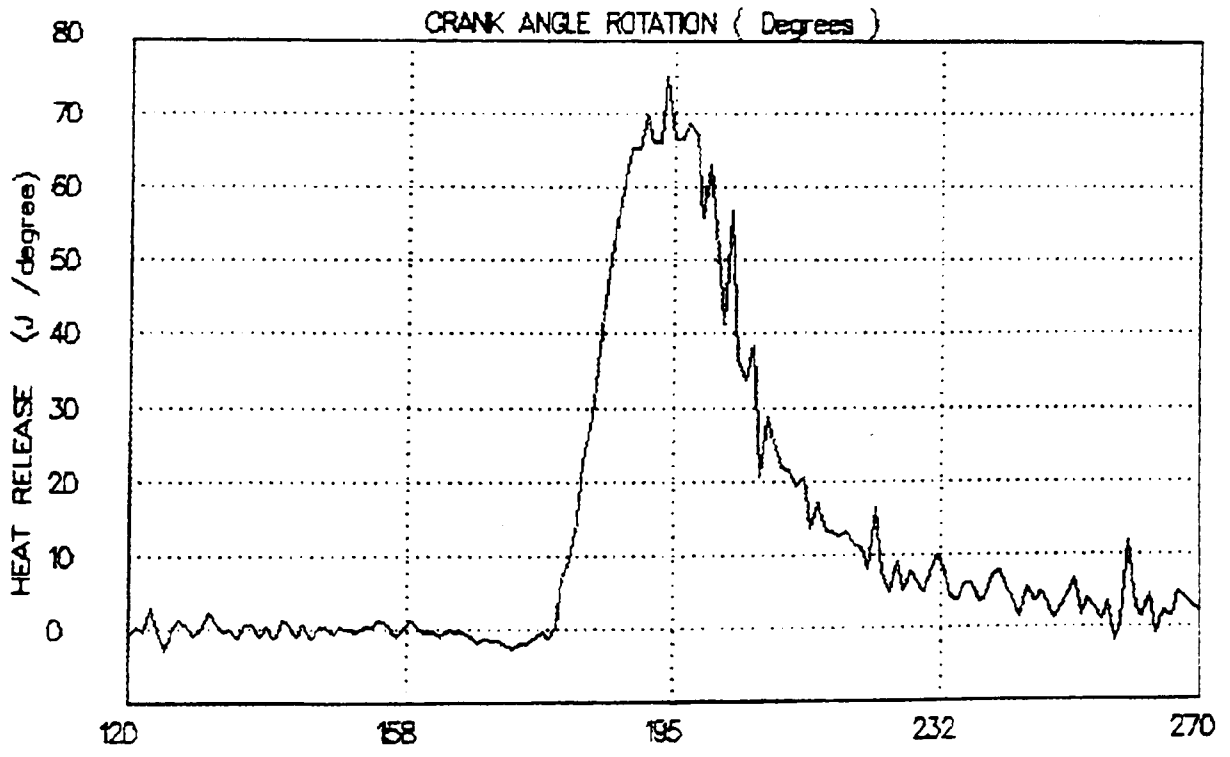

Figure 5.34 Rate of heat release as a function of crank-angle for piston bowl shape THREE (operating at 2000 rpm, full-load). Injector combination of 140-degree cone angle, 4.0mm washer depth (point 7 in table 5.1).

For the highest point of impingement shown in figure 5.33 (ie. no. 1 in table 5.1), the peak heat release rate was sustained for a very short time period, and then the heat release rate decayed slowly towards its final value. In contrast, the chosen injector combination shown in figure 5.34 (no. 7 in table 5.1), maintained its peak heat release rate for longer, but then decayed rapidly towards the end of combustion. This trend was supported by heat release profiles of the other impingement points.

Possible reasons for the difference in the heat release profiles between these two points of impingement became apparent by examining figure 5.23, section 5.3.5 (engine test condition: 2000 rpm, full-load, bowl shape THREE).

The chosen injector combination (impingement point 7) maintained the fuel impingement point within the 'impingement area' of the bowl wall lip at all times during fuel injection. This might have enabled good initial mixture formation, due to the impacting fuel spray on the bowl walls entraining in the vigorous airflow. The process of fuel impingement may have also increased local air turbulence, and increased the rate of mixing still further.

Initially, a similar situation could have occurred with the highest point of impingement (no. 1, table 5.1), and may explain the similar initial rise in the rate of heat release profile. However, as fuel injection proceeded, the highest impingement point no longer impacted on the bowl sides but, instead, spilled over onto the piston top face. Here, the fuel would probably have been cooled by the relatively cold piston face, and may have caused wall wetting over a large surface area because of the shallower angle of impingement. Increased wall wetting as the angle of impingement is decreased has been shown by Naber and Reitz (1988), in flat plate impingement experiments (see figure 2.42, chapter 2).

It was unlikely that fuel formed in a wall jet would be entrained by the vigorous airflow in the piston bowl to form a premixed mixture. More likely, it would have burned in a diffusion mode, at a rate defined by the rate of evaporation of fuel from the piston face. The result was a reduced rate of heat release for a prolonged period, which was observed from the heat release analysis.

Comparison of peak gas temperature and NOx at various impingement points

As a result of the small contribution to heat release of pre-mixed combustion, the peak gas temperature occurred during the diffusion burning phase. This was confirmed, by plotting the variation of gas temperature against engine crank angle, obtained from heat release analysis, as shown in figure 5.35.

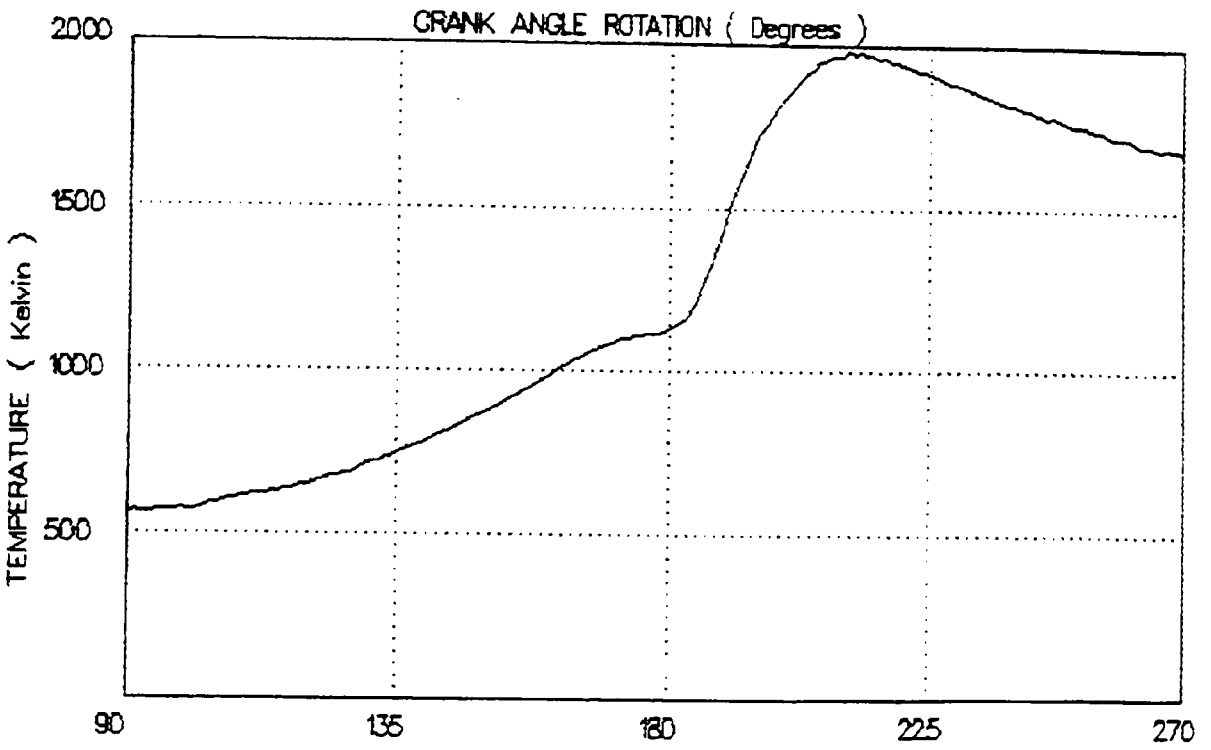

Figure 5.35 Variation of cylinder-averaged gas temperature with engine crank-angle for piston bowl shape THREE (engine operating at 2000 rpm, full-load).

The gas temperature was calculated from the instantaneous cylinder pressure and volume, and thus represented an average cylinder gas temperature at any particular crank angle. Of course, in the diesel engine, heterogeneous combustion created large temperature gradients across the combustion chamber, which could not easily be measured.

As the formation of NOx was closely related to peak gas temperature, some correlation between these parameters might be expected. Figure 5.36 shows the variation of peak gas temperature (cylinder averaged) and NOx emission at each impingement point for piston bowl shape THREE, operating at 2000rpm, full-load.

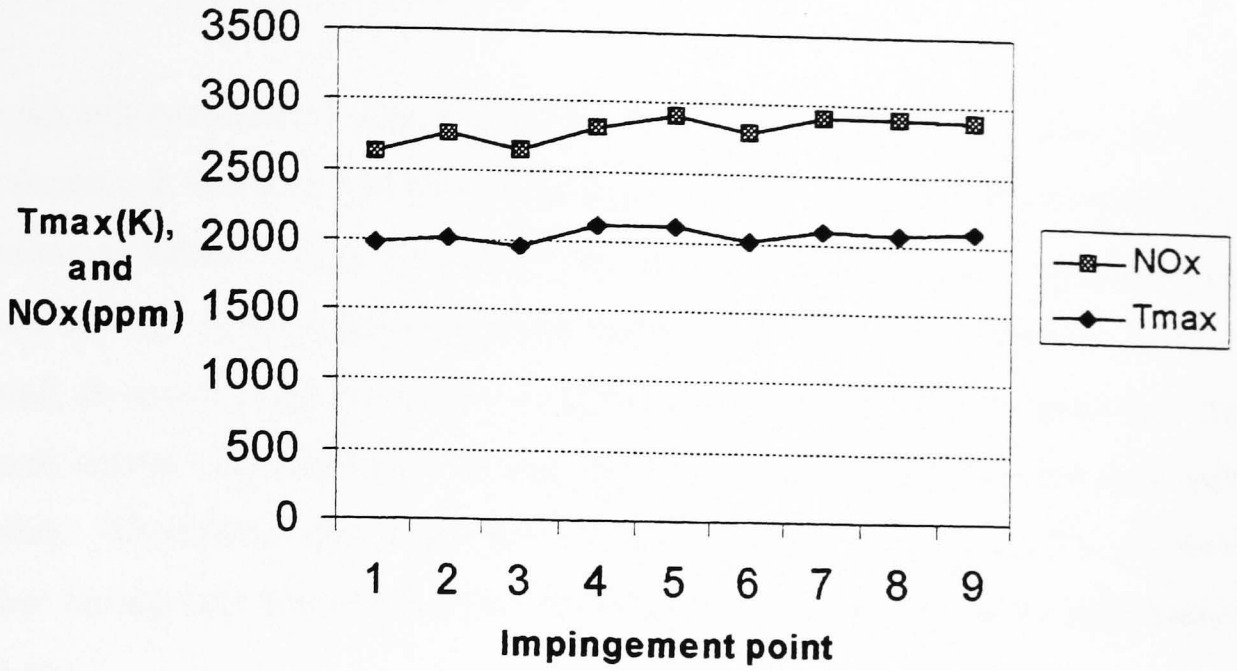

Figure 5.36 Comparison between the formation of NOx, and maximum gas temperature, with the point of fuel impingement (see table 5.1) from piston bowl shape THREE (engine operating at 2000 rpm, full-load).

The emission of NOx was least at the lowest peak cylinder temperatures, and reasonable correlation existed at the higher temperatures as well. Heat release profiles had shown the initial rise in the rate of heat release to be similar for all injector configurations. However, the length of time that the peak heat release rate was sustained, was different for the various injectors. Configurations leading to sustained peak heat release (such as point 7), may have caused early burnt gas to be compressed more than other cases, by the subsequent expanding hot gases. This would raise the peak temperature as illustrated in figure 5.36, and increase the rate of NOx formation.

The lack of a perfect correlation between the emission of NOx and peak cylinder temperature (in figure 5.36) could be due to the NOx formation being dependant on *local* gas temperature, and not average cylinder temperature. Although there was reasonable correlation between NOx formation and the point of impingement, it was likely that a combination of factors, and interaction of the impacted spray with the bulk in-cylinder airflow may have been important.

5.4.1.4 Effect of fuel impingement on late combustion

Although late combustion only accounted for a relatively small proportion of the total heat released, it was likely to have been significant in terms of engine-out smoke and particulate emissions. Soot formed early during combustion was probably rapidly oxidised by hot, vigorous air motion and partially burned gases. However, soot which persisted, or was formed late in the combustion process, would have been surrounded by much cooler expanded gas, having low oxygen concentration and poor mixing capability. Therefore, the proportion of fuel and its position in the combustion chamber during late combustion may be related to engine-out smoke and particulate emissions.

Figure 5.37 (a) and (b) shows a comparison of the cumulative heat release profiles from impingement points 1 and 7 respectively, of piston bowl shape THREE, operating at 2000rpm, full-load.

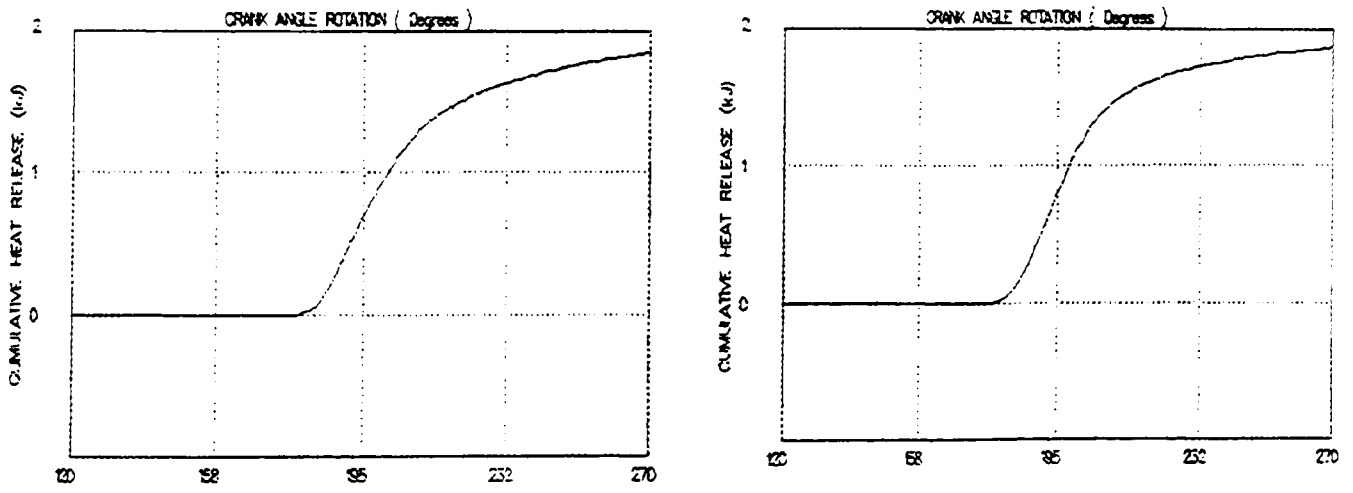

(a) (b)

Figure 5.37 Comparison of the cumlulative heat release profiles from piston bowl shape THREE, operating at 2000 rpm, full-load. Injector configurations (a) 150-degree, 5.5mm washer thickness, and (b) 140-degree, 4.0mm washer thickness.

The start of combustion and initial heat release remained similar for both impingement points, as did the total amount of heat released, but the proportion of

heat released during late combustion was significantly greater in the highest impingement point condition (150-degree, 5.5mm washer thickness).

As stated earlier, the most likely cause of a greater proportion of fuel burning in the late combustion phase was wall wetting of the piston top face, with the rate of combustion being controlled by evaporation of fuel from this surface. Figure 5.38 illustrates the effect of the highest points of impingement (points 1, 2, and 3) on late combustion. The figure plots the variation of engine-out smoke emission with impingement point from piston bowl shape THREE, at 2000 rpm, full-load.

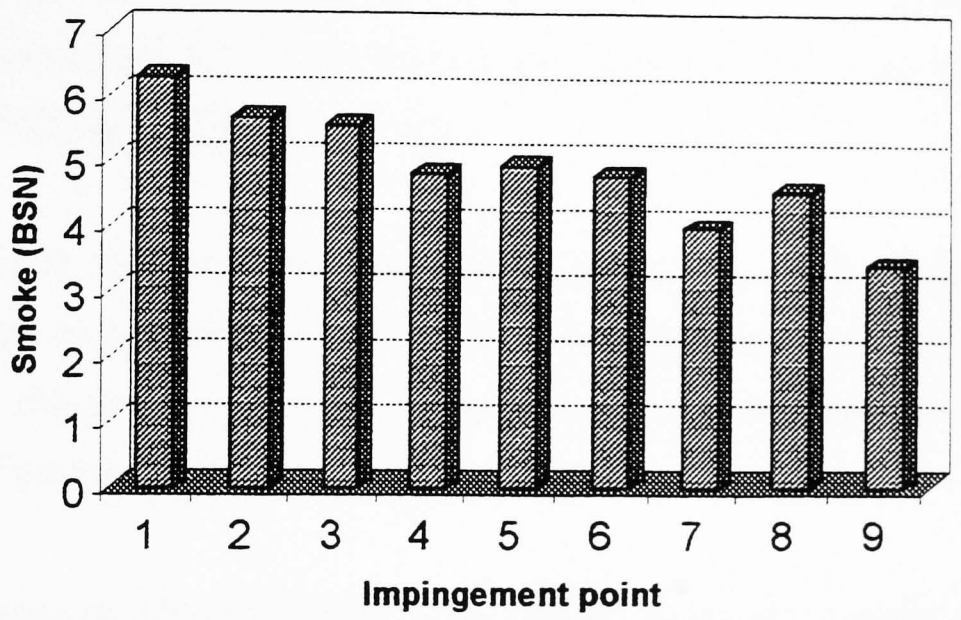

Figure 5.38 Variation of the emission of smoke with the point of fuel impingement (see table 5.1). Results from piston bowl shape THREE (engine operating at 2000 rpm, full-load).

The highest levels of smoke were recorded at the highest three impingement points (1, 2, and 3). These high levels appear to have been caused by late heat release (combustion) of fuel which had over penetrated on to the cool upper surface of the piston.

As long as the duration of injection occupies a significant number of crank-angle degrees (eg. at full-load), there will continue to be a conflict between the requirement for a high point of initial fuel impingement to provide rapid brake-up of the spray, and

the requirement for a low enough impingement point to avoid over-penetration and the production of smoke. It is possible that the introduction of common-rail fuel injection systems with much higher fuel injection pressures would allow greater optimisation of impingement point, especially at high loads where the duration of injection was longest.

5.4.2 Influence of other factors on the optimum point of fuel impingement

Significance of the path of fuel injection

The actual path of fuel injection across the combustion chamber appears to have been relatively un-important. It was the *point* of impingement which had most effect on emissions of NOx and smoke in particular.

The difference in the path length between high and low impingement points was relatively small, especially when the high speed of the fuel jet was considered. It was unlikely that changes in the path length would have any measurable effect on emissions and performance.

Fuel impingement at different angles to the piston surface (for a given impingement point) was possible because of the range of injector washer depths and injector cone angles available. This may have affected formation of the wall jet, and subsequent rate of fuel evaporation, although it was difficult to quantify from the results presented.

Effect of the point of impingement on wall wetting

The effect of wall wetting has already been identified as a likely cause of late heat release and high smoke emission, due to over penetration of fuel onto the piston face. However, there was also evidence from piston bowl shape TWO to suggest that fuel wetting at the base of the bowl resulted in increased emission of smoke. Figure 5.39 illustrates the two most likely areas for wall wetting as a result of fuel impingement on the bowl wall.

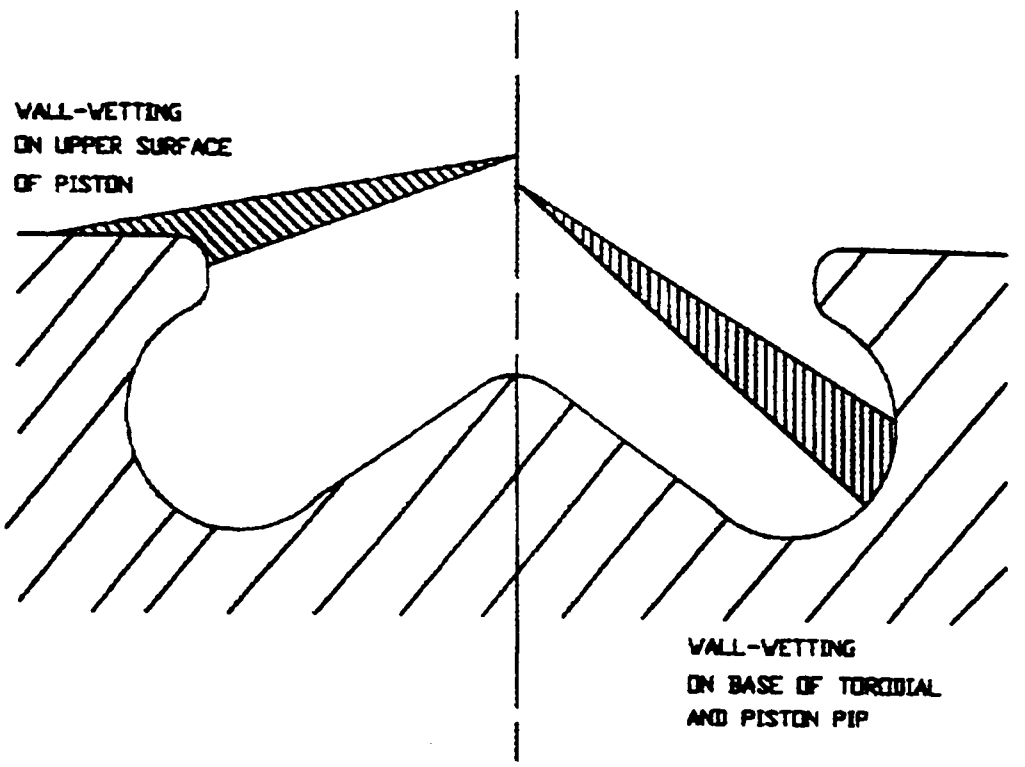

Figure 5.39 Illustration of wall-wetting, caused by over penetrated fuel onto the piston top, and fuel impingement low in the torodial radius.

Results of smoke emission from piston bowl shape TWO at an engine operating condition of 2000rpm, full-load, are shown in figure 5.40 below.

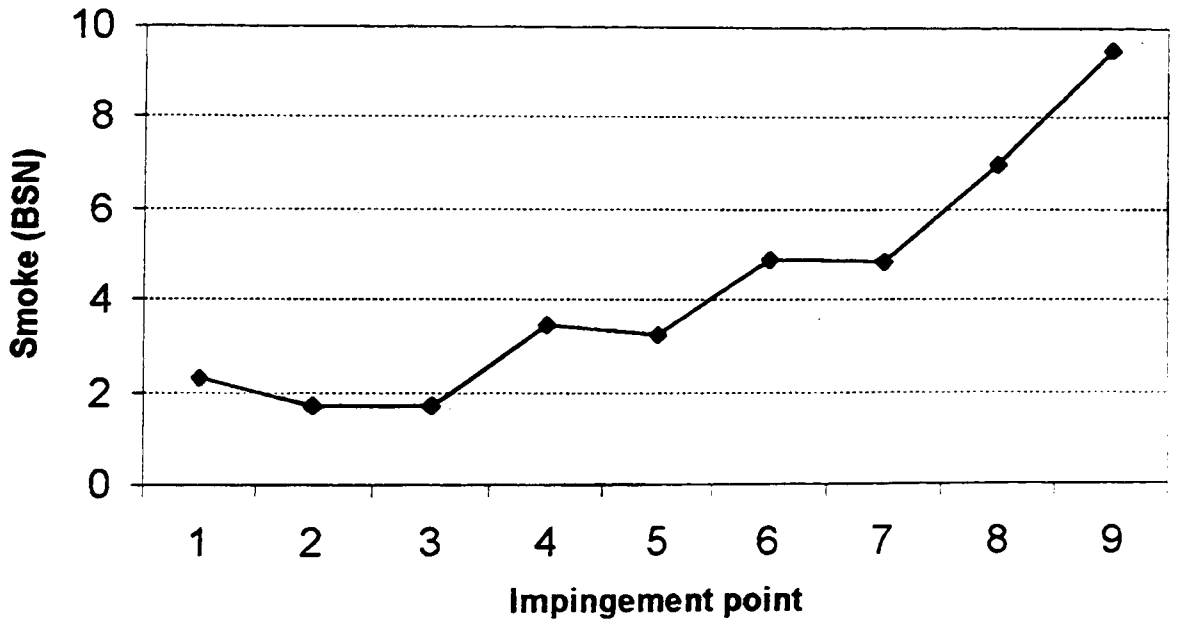

Figure 5.40 Variation of the emission of smoke at different points of impingement (table 5.1), for piston bowl shape TWO, engine operating condition 2000 rpm, full-load.

The sharp increase in the emission of smoke may, at least in part, have been due to severe wall wetting of the lower surface of the bowl. In extreme cases, it might have been possible for the wall jet to be driven up towards the central pip, where airflow was less vigorous and less likely to promote evaporation of the wall jet. CFD simulation of piston bowl shape TWO (presented in a subsequent chapter) supported the probability of wall wetting low down in the bowl, and late heat release when gas temperature and air flow velocity had dropped.

5.4.3 Effect of piston bowl shape on optimum impingement point

The effect of the point of impingement has been discussed in relation to the trend in the production of emissions recorded. The optimum point of impingement was found from tests, and thus from the lowest combination of smoke and NOx emissions. However, the optimum point of impingement also gave clues about the most significant features of bowl design and airflow required. The optimum injector configurations, and resultant optimum points of impingement, are illustrated on templates of the four bowl shapes tested, in figure 5.41 on the following page.

In each case, the line of the fuel spray centre is shown with the piston positioned at TDC, using the injector optimum configurations for each bowl shape (detailed in an earlier section). In all cases, the optimum point of impingement at TDC resulted from injector optimisation tests. The optimum injector configuration was predominantly described by the full-load tests. It can be seen from figure 5.41, that the optimum impingement point at TDC in the case of these four shapes was below or at the bottom of the impingement region.

Piston bowl shape ONE had a slightly lower point of impingement relative to the bowl lip than other bowl designs, although interestingly the point of impingement was in a similar position relative to the bulk airflow, as for bowl shapes STD and THREE which shared a similar aspect ratio (the ratio of bowl width to its depth).

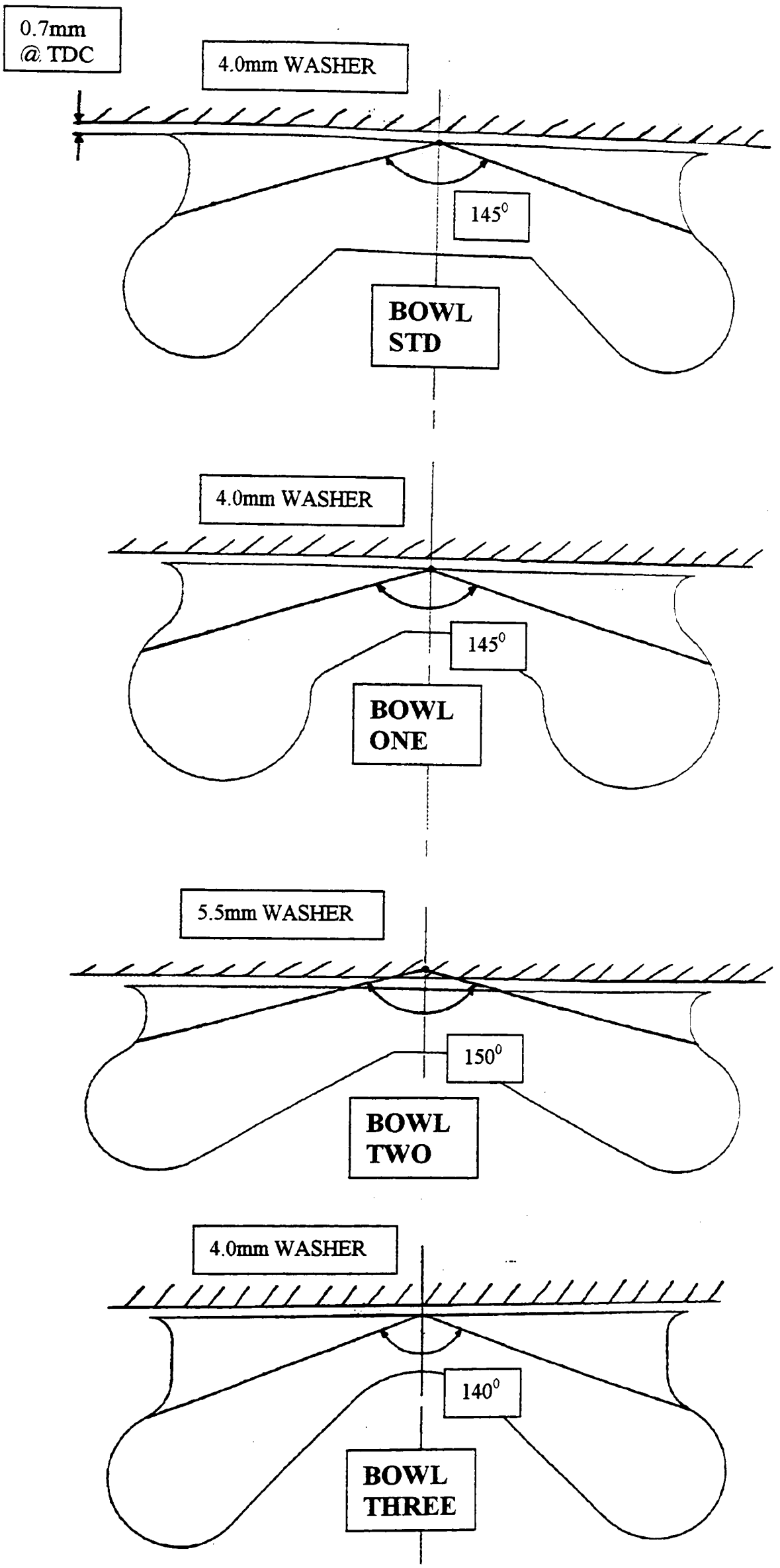

Figure 5.41 Optimum injector configurations and optimum impingement points for the four bowl shapes tested. Piston positioned at TDC.

It was probable that three main factors controlled the optimum point of impingement for a particular piston bowl design. These were:

(a) the point of impingement should be located on the side of the re-entrant bowl lip (the 'impingement area', see figure 4.6, chapter 4) to generate turbulence and disperse the spray upon impact;

(b) the point of impingement should be located such that at the start of injection or end of injection, the spray does not migrate to cause wall wetting low in the bowl or wall wetting of the piston top face due to over penetration;

(c) the point of impingement should be located such that spray generated upon fuel impingement would be entrained in the bulk airflow for the duration of fuel injection.

These factors were considered in the generation of the final bowl design, with the aim of exploiting the benefits of fuel impingement to reduce emissions. Some success was achieved, in that the optimum position of fuel impingement was found to be contained within the impingement area, but overall emissions were not reduced significantly.

This was most likely because of other bowl design-changes affecting airflow undesirably compared with the base piston design (STD). A more comprehensive comparison of bulk airflow between different bowl designs, and the effect bulk airflow on emission and performance results is the subject of a chapter 7.

5.5 Conclusions

Injector optimisation tests

Injector optimisation tests identified the best vertical position of the injector nozzle, and the best injector cone angle for each piston bowl shape. This was done prior to bowl comparison testing.

Full-load tests showed the greatest differences in the injector configuration, because of the high heat input (producing considerable NOx emission), and the premium on mixing at full-load promoting smoke formation. The optimum injector configuration was judged primarily on its particulates versus NOx performance, as the best indicator of overall bowl emissions performance.

Effect of the point of fuel impingement

The injector cone angle, and washer thickness (and thus the point of fuel impingement on the bowl sides) did not influence the ignition delay period measurably. This was because of the dependence of ignition delay on chemical reaction kinetics, and not the rate of mixing of fuel and air.

An estimation of the fuel injection velocity showed that fuel impingement was likely before the start of combustion (SOC). Thus it was possible that the point of fuel impingement may have affected premixed combustion, by affecting the quality of fuel/air mixture prepared for combustion. However, it was not possible to verify this from the experimental results, because of the small faction of fuel injected during the ignition delay period (approximately 5.6%, at 1500 rpm, full-load).

The point of fuel impingement was however, shown to influence the process of diffusion burning. The optimum injector configurations from each piston bowl shape resulted in sustained peak heat release, and a sharp reduction of heat release at the end of combustion. This indicated that the optimum injector configurations rapidly mixed fuel and air into a combustible mixture. The worst performing injector configurations

produced substantial late heat release, increasing the emission of smoke and particulates. It was likely in these cases that 'over-spill' on the piston crown, or wall wetting of the lower bowl surface, reduced the rate of fuel entrainment in the air-stream until late in the expansion stroke, when gas temperature and velocity would have been lower.

The standard (STD) bowl shape

Piston bowl shape STD produced low smoke at all of the full-load conditions. The chosen injector configuration (point 5, table 5.1) resulted in the point of fuel impingement being contained within the impingement lip area (no over-spill onto the piston top crown by the EOI, or low impingement to cause wall-wetting of the lower bowl surface).

Bowl shape ONE

As for the standard bowl shape, the optimum injector configuration (point 5, table 5.1) was found to contain fuel impingement in the bowl lip region. However, higher smoke emissions were found when testing at the lowest point of impingement (point 9, table 5.1). This was most likely caused by wall-wetting of the lower bowl surface, enhanced by the reduced depth of the bowl-lip region in this bowl design.

Bowl shape TWO

Results of injector optimisation for bowl shape TWO were dominated by the poor air utilisation of this bowl shape. Emission of smoke and particulates was very high, especially at test condition 1 (engine operating condition: 1500 rpm, full-load). Impingement points closest to the bowl lip performed best (injector configuration chosen was point 1, table 5.1), even though by the EOI it was probable that 'over-spill' onto the piston crown had occurred.

Bowl shape THREE

Piston bowl shape THREE was designed to exploit the benefits of the point of impingement, by increasing the impingement lip length to contain fuel impingement within this area throughout fuel injection. This resulted in a piston bowl which was less sensitive to the vertical position of injector nozzle, and injector cone angle. The optimum injector configuration for this bowl was point 7 (see table 5.1), although many of the mid-range impingement points performed well.

Chapter 6:

CFD simulation of in-cylinder combustion

Chapter 6: CFD simulation of in-cylinder combustion

6.1 Introduction

Computational fluid dynamics (CFD) modelling of in-cylinder combustion was performed on selected operating conditions of piston bowl shape TWO. The simulation was performed by the Ford motor company specially in order to support the experimental testing undertaken at Brunel university. Following the mesh generation and run of the CFD simulation, the results were stored on CD ROM. Analysing of the results was performed by the author of this thesis using the 'Fieldview' post processing software package, at Brunel University.

CFD combustion simulation results presented

Combustion simulation was undertaken to allow greater understanding of the effect of piston bowl shape, and the influence of the point of fuel impingement on emissions. Testing of piston bowl shape TWO had shown a wide variation in engine performance and emissions, when using different injector configurations having different points of impingement. In particular, the emission of smoke at an engine operating condition of 1500 rpm, full-load, was greatly affected by the point of fuel impingement, as figure 6.1 illustrates.

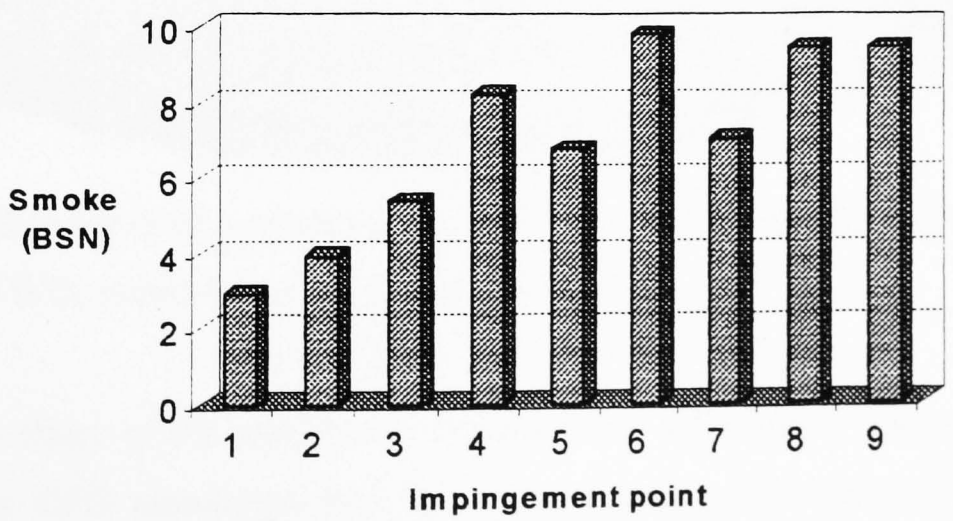

Figure 6.1 Variation of the emission of smoke with impingement point (see table 5.1) for piston bowl shape TWO, engine operating at 1500 rpm, full-load.

The discussion of CFD combustion simulation results presented here is focused on explaining the reasons for the large variations in smoke emissions with the point of fuel impingement. In particular, impingement points 1 (150 degree cone angle, 5.5mm washer thickness) and 9 (140 degree cone angle, 2.5mm washer thickness), having the extreme emissions of smoke, were chosen for comparison.

6.2 Description of combustion simulation program

The 'KIVA 2', CFD three-dimensional computational code was used for simulation of combustion in the engine cylinder. An input file containing the combustion chamber boundary (which changed with piston position), piston bowl geometric profile (input as a series of discrete co-ordinates), initial cylinder gas and fluid properties was provided for each simulation run. The computational grid, generated from a discrete series of points describing the piston bowl profile is shown in figure 6.2.

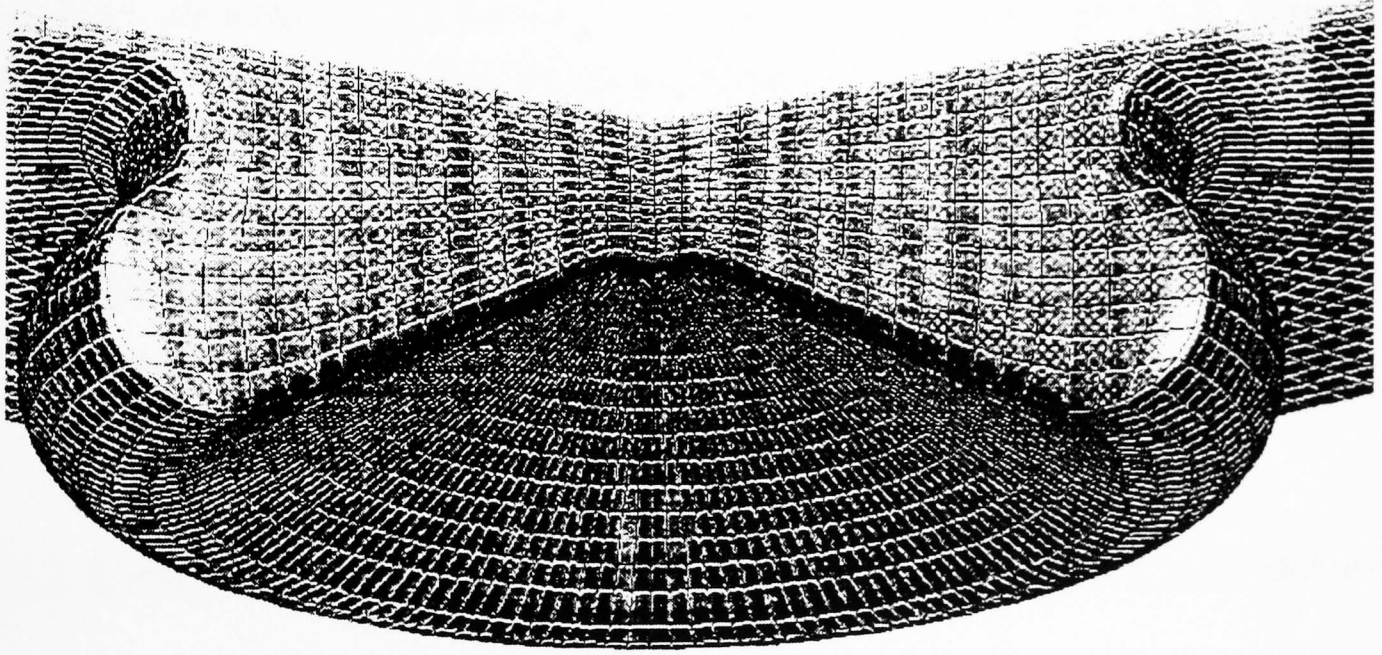

Figure 6.2 Illustration of a section of the KIVA 2, CFD, computational grid of piston bowl shape TWO, viewed from the beneath the bowl.

The physical shape of the combustion chamber was axisymetric (about piston axis). However, the CFD simulation was three dimensional, since the extreme air swirl added a strong three-dimensional influence on combustion, in addition to the strong two-dimensional influence of bowl geometry.

Simulation was limited to the range of compression and expansion, encompassing compression of the intake charge, fuel injection, ignition delay, pre-mixed combustion, and diffusion burning. The run was haulted about half-way down the expansion stroke, at a time when the combustion reactions were considered to be 'frozen', and thus engine out emissions finalised.

An output file of data was produced containing parameters previously specified in the input file. A limited range of parameters were simulated to reduce the run time to a minimum. Typical run time for each injector optimisation condition was 2-3 days on an HP 9000 workstation. The output file was viewed using the 'Fieldview' post-processing software package. A plot was created by importing the selected output data set, produced by the KIVA CFD code at a particular engine crank angle of interest. Once the data had been loaded, a computational surface or surfaces were defined, upon which the bowl geometry and parameters of interest were displayed.

For example, a computational surface through the plane of fuel injection was used to illustrate air velocity disturbance due to fuel injection (see figure 6.3). Selected parameters were displayed to illustrate differences in airflow and the sequence of emission formation.
Once the desired parameters were displayed, and the angle of perspective optimised using the 'transform controls', the picture was saved for later analysis or for use in a movie sequence of successive engine crank angles.

6.3 Comparison of in-cylinder airflow and initial combustion

6.3.1 Format of airflow and combustion plots

The best injector optimisation case of piston bowl shape TWO (150 degree cone angle, 5.5 mm washer thickness) was compared directly with the worst case (140 degree cone angle, 2.5 mm washer thickness) on the same figure. One-sixth of the piston bowl shape was displayed for each of the injector configurations, with the best

case on the right-hand side of the figure. An example illustrating the format of computational surfaces (used in subsequent plots) is shown in figure 6.3.

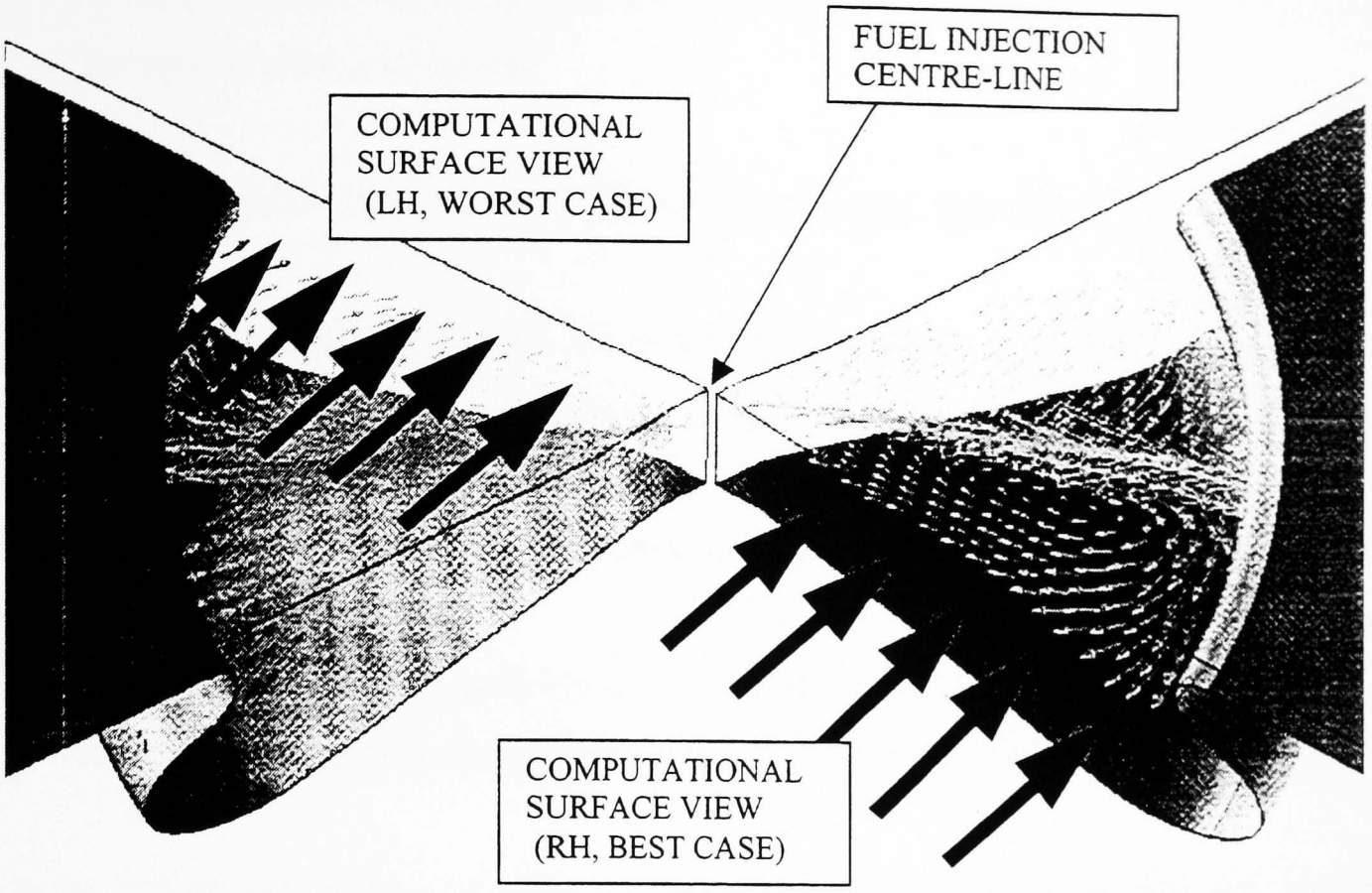

Figure 6.3 Illustration of the computational surfaces used to present results of airflow through a particular plane for bowl shape TWO. Labels on the diagram indicate the computational surface views used in subsequent figures (LH = Left Hand, RH = Right Hand).

Several factors are worthy of note to appreciate subsequent figures of CFD results for bowl shape TWO:

(a) the right-hand (RH) piston bowl section shows results from the best injector optimisation case (150 degree cone angle, 5.5 mm washer thickness), and the left-hand (LH) section from the worst case (140 degree cone angle, 2.5 mm washer thickness), as illustrated in figure 6.4,

(b) fuel injection was from the centre-line of the axisymetric bowl profile (in the middle of figure 6.3 and other airflow figures), but

(c) the vertical position of the start of injection in the combustion chamber differed by 3.0 mm between the best (RH) and worst (LH) cases, because of the difference in the injector washer thickness,

(d) swirl was clockwise in the piston bowl when viewed from above,

(e) in subsequent airflow figures, the computational surface is viewed from one side of each wedge-shaped bowl section, furthest away from the fuel spray path. This is to minimise distortion of the airflow by fuel injection, and more accurately represent the bulk airflow (the two planes of view are marked on figure 6.3),

(f) the two computational surfaces of view used in subsequent airflow figures are identical, because they are both downstream of the path of the fuel spray, and

(g) to enable comparison of widely different airflow velocities at different engine crank angle positions, a velocity vector scale is introduced at the base of each figure (see figure 6.4). This indicates the relative vector scale between figures, although the vector scale is always the same for RH and LH bowl sections on the same figure.

(h) in some airflow figures, gas temperature is represented qualitatively as a scalar value, represented by the greyscale darkness of the vector arrow head. The darkest greyscale corresponds to the highest gas temperature.

6.3.2 Airflow just prior to fuel injection

Figure 6.4 shows the airflow in the piston bowl, for the best (RH) and worst (LH) injector optimisation cases. The piston had closely approached the cylinder head, at two degrees before TDC.

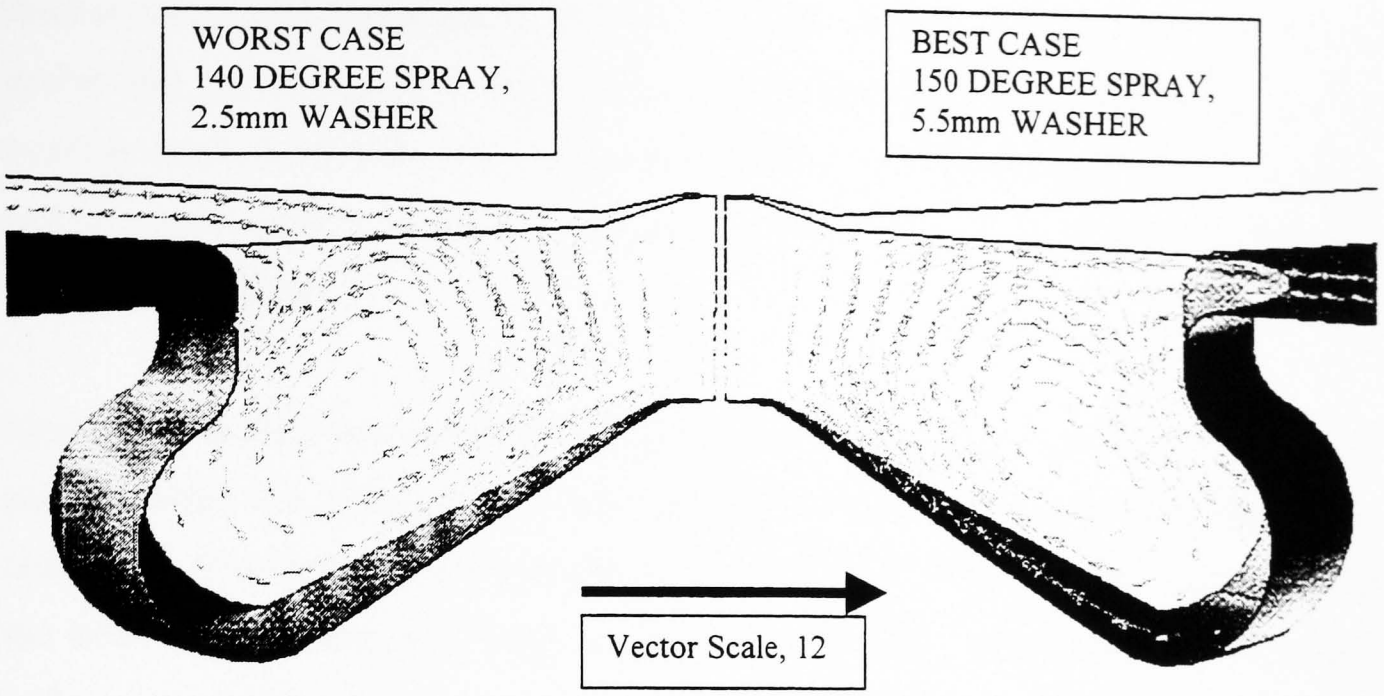

Figure 6.4 Comparison of airflow velocity across a computational surface at the end of compression at 2 degrees before TDC, between the best (RH) injector optimisation case, and the worst (LH) case. Vector scaling factor was 12. Bowl shape TWO; engine speed 1500 rpm, full-load (see table 5.2).

Prior to fuel injection, and given that the intake air initial conditions were the same for both the best and worst injector optimisation conditions, the airflow was identical as expected. The air near the end of compression was at approximately 1100 degrees Kelvin, and had a uniform temperature distribution across the combustion chamber. Note that in the real engine, differences in the combustion efficiency for the best and worst cases would change the turbocharger operating condition slightly, which may have affected the inlet-air initial conditions.

The airflow into the bowl during compression created a swirling torodial motion (viewed from the computational surfaces chosen, see figure 6.4), which had its centre of rotation close to the main torodial radius centre. Note that there were two types of swirl present in the airflow; the bulk swirl viewed from above the piston, and the torodial swirl viewed though the piston section. Together, they formed particle motion akin to the "winding on a ring-wound dynamo" [Fitzgeorge, 1962].

The centrifugal action of the bulk swirling airflow during compression caused the squish jet, formed later towards TDC, to be driven down towards the bowl walls.

Similar findings by Naber and Reitz (1988), Wojik (1990), and Bertodo (1975), have shown that the changeover from squish dominated airflow (a clockwise torodial swirling motion), to bulk swirl dominated airflow (anti-clockwise torodial swirling airflow), occurred at a low bulk swirl ratio, and may have even changed with engine operating condition.

Squish velocity increased from the cylinder edges towards the bowl lip, as the 'curtain area' between the piston crown and cylinder head decreased towards the piston centre-line. Maximum airflow velocity occurred at the base of the piston bowl, and on the sides of the piston pip. Here, air flowed unhindered towards the bowl centre, where air velocity was at a minimum (in fact, because the simulation model was formed as a revolution of symmetry, airflow at the centre-line of the piston would be zero).

6.3.3 Airflow just prior to the start of combustion

Although the piston position had changed very little, and combustion had not yet started, the airflow velocity distribution was significantly modified by fuel injection. Figure 6.5 shows the airflow distribution in the piston bowl, but the vector scale has been reduced by a factor of two to accommodate the increased air velocity.

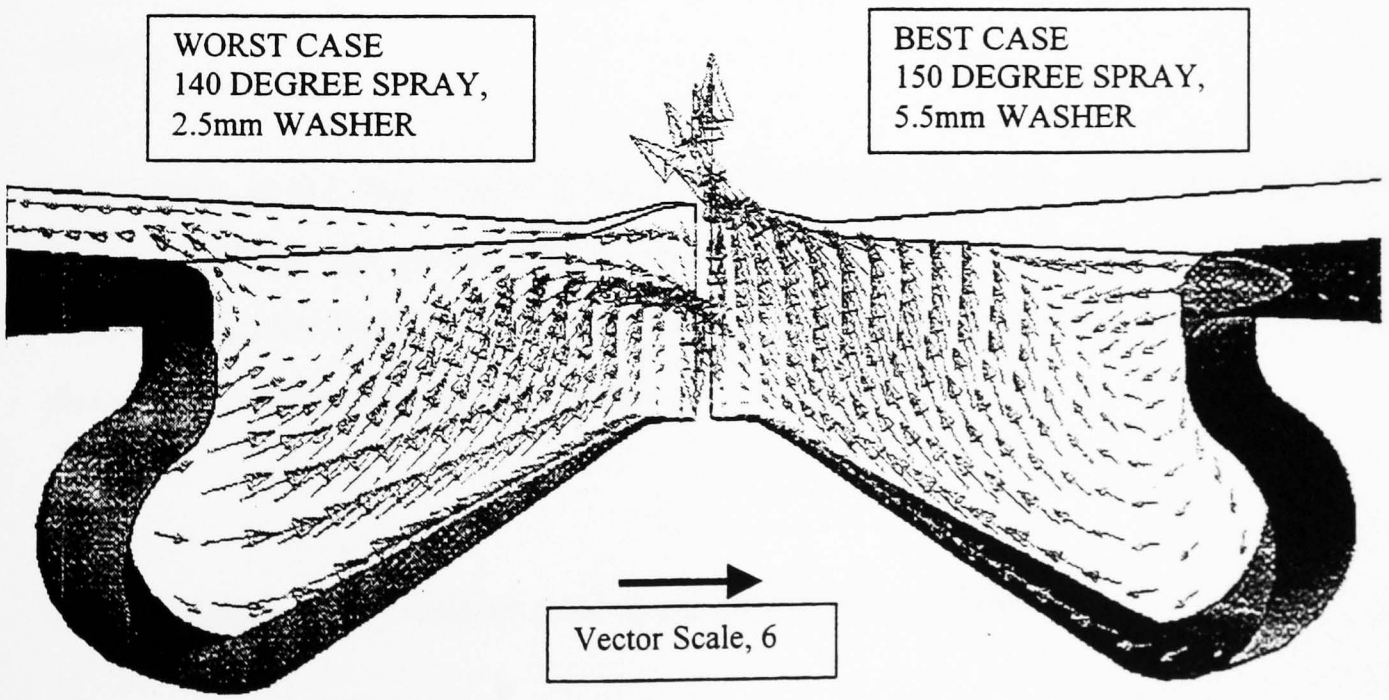

Figure 6.5 Comparison of airflow velocity across a computational surface during fuel injection at 4 degrees after TDC, between the best (RH) injector optimisation case,

and the worst (LH) case. Vector scaling factor was 6. Bowl shape TWO; engine speed 1500 rpm, full-load (see table 5.2).

Airflow velocity induced by fuel injection was many times greater than the bulk airflow velocity generated by swirl and squish. It was likely that turbulence in the airflow, induced by fuel injection, would have significantly increased the rate of mixing and combustion.

Airflow velocity vectors were in the opposite direction to that of the fuel spray. This was because the computational surface view, was, in effect, between two fuel sprays. The injected fuel displaced air, causing it to flow towards spaces between the spray envelopes. Airflow velocity in the best case (150 degrees, 5.5mm washer) case was very strong towards the injector tip. This may have helped to entrain air into subsequent injected fuel, and keep this normally stagnant area of the combustion chamber free from soot deposits.

Also of note was the direction of squish flow between the two cases. In the worst case, it appeared that fuel injected low into the combustion chamber had caused the mean air motion to be lifted up into the middle area of the bowl. This had displaced air in the main torodial radius volume, forcing air out of the bowl in a reverse squish motion.

Conversely, in the best case situation it seemed likely that fuel which had spilled-over in the middle of the piston section shown (inline with the injection centre-line) had displaced air, forcing it towards the bowl centre, despite the slowly falling piston (the piston is now four degrees after TDC).

6.3.4 Initial combustion and modification to airflow

Once combustion of pre-mixed charge had commenced, the velocity of the air and gas (comprising of unburned and partially burned mixture, and combustion products) rose

by many times. The vector scaling factor was reduced three-fold to allow presentation of gas velocity in the normal format. Figure 6.6 shows gas velocity as the vector quantity, and gas temperature as the scalar greyscale value (the darkest arrowheads correspond to the hottest temperatures) for the first sign of combustion at five degrees after TDC.

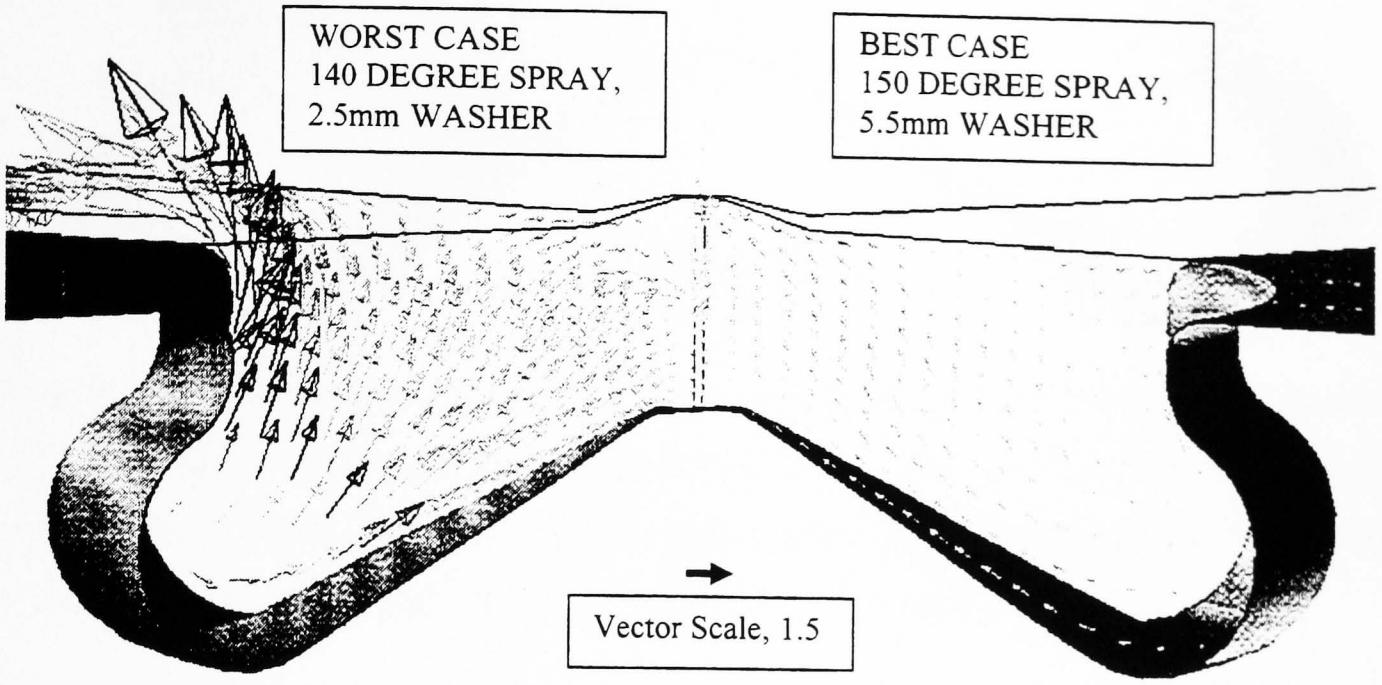

Figure 6.6 Airflow velocity across a computational surface, at the start of combustion for the worst (LH) case (5 degrees after TDC). The best (RH) case had not yet commenced combustion. Vector scaling factor was 1.5. Bowl shape TWO; engine speed 1500 rpm, full-load (see table 5.2).

Figure 6.6 may help to explain why the ignition delay for piston bowl shape TWO was significantly greater than for other bowl designs tested, results of which were presented earlier in chapter 5. This could have been due to a combination of longer fuel path length before impingement, cooler impingement area temperature, a reduction in airflow velocity and turbulence resulting from the wide and shallow piston design, or increased fuel wetting of the two extreme impingement point conditions presented here.

Start of combustion was first observed (see figure 6.6) in the worst impingement point case. Start of combustion in the best case occurred one-degree crank angle later, as shown in figure 6.7.

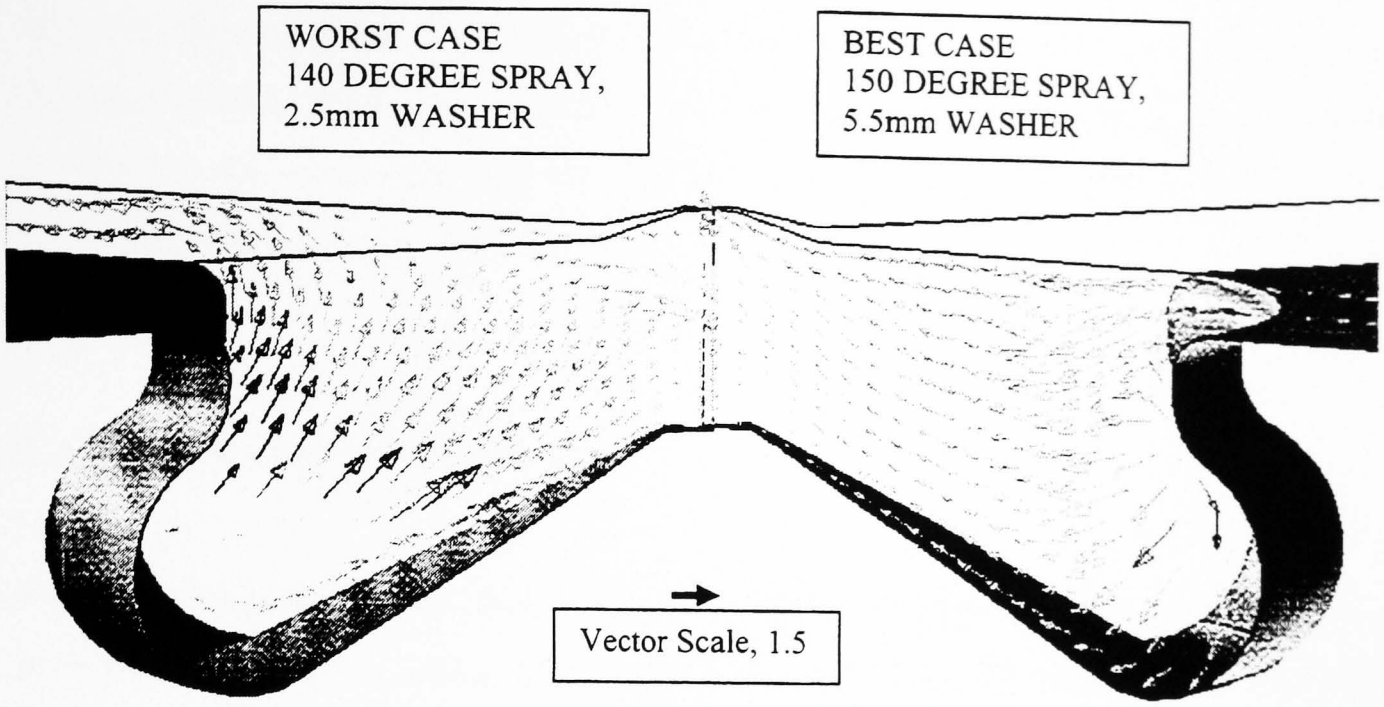

Figure 6.7 Comparison of airflow velocity across a computational surface, between the best (RH) injector optimisation case, and the worst (LH) case, at the start of combustion for the best (RH) case (6 degrees after TDC). Vector scaling factor was 1.5. Bowl shape TWO; engine speed 1500 rpm, full-load (see table 5.2).

The widely different airflow pattern between the best (RH) and worst (LH) cases in figure 6.7, was primarily due to the difference between the crank-angle at which combustion started for the two cases. As combustion proceeded, this anomaly became less important, and more meaningful comparison between the airflow structure at the same engine crank-angle, and its effect on combustion could be made.

It was possible that the impingement lip area was cooled by the strong squish flow, and by conduction from the cool piston face (see figure 6.7). Fuel impingement high-up on the impingement area (towards the bowl lip) in the best case, might have encountered less heat transfer from the piston surface, and a corresponding increase in the ignition delay period.

Gas temperature (represented by the greyscale scalar values, the darkest arrowheads being the hottest) gave an indication of the initial ignition sites, and rate of combustion by comparing successive frames. Initial combustion sites occurred much higher up the bowl towards the bowl lip with the best (highest) impingement point

case, as might be expected. However, the rate of change of the scalar temperature values in the worst case was very large, and driven by combustion from the base of the main torodial radius. This indicated fuel concentration was greatest at the base of the bowl in the worst case, and combustion-induced gas motion may have prevented entrainment of fresh air in this region.

6.3.5 Main heat release stages

Gas velocities decreased from their pre-mixed combustion peaks, as diffusion controlled combustion continued. Fuel injection did not stop until 16 degrees after TDC. Figure 6.8 shows combustion at nine degrees after TDC, typical of the diffusion burning phase.

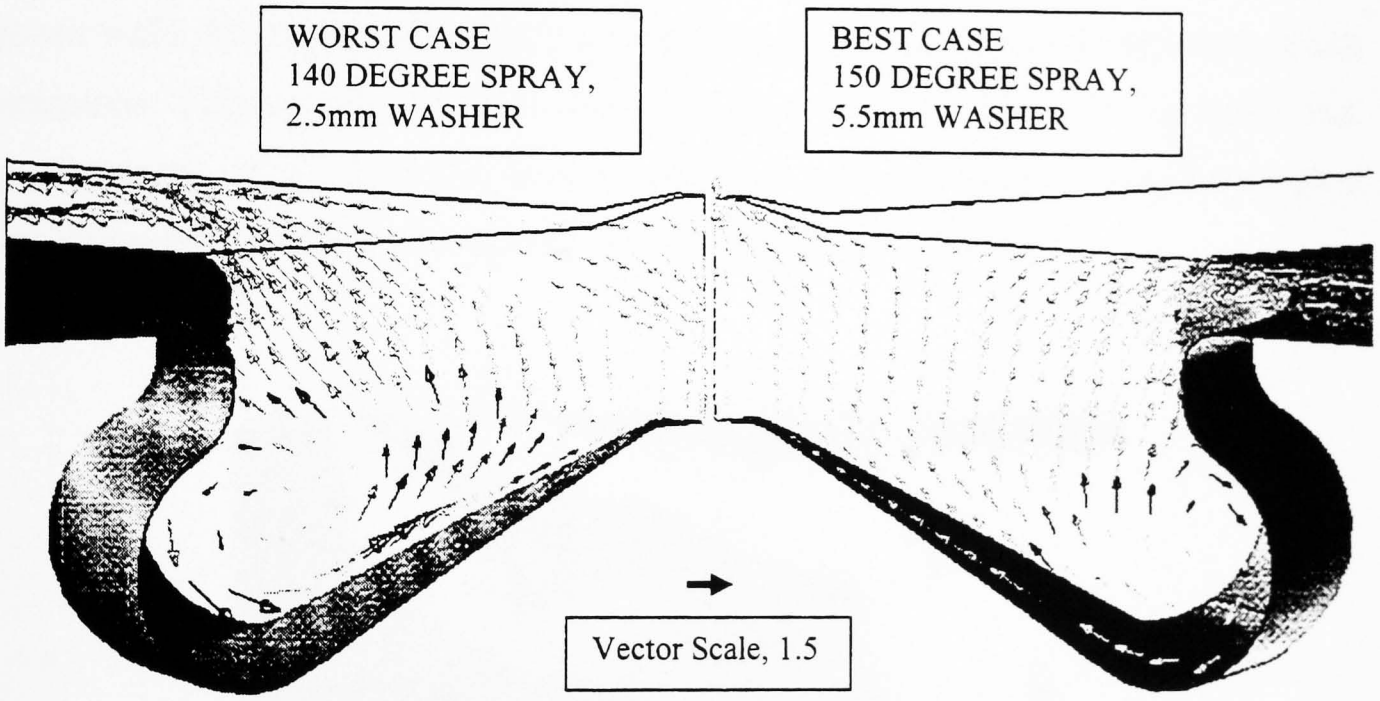

Figure 6.8 Comparison of airflow velocity across a computational surface during diffusion burning at 9 degrees after TDC, between the best (RH) injector configuration case, and the worst (LH) case. Vector scaling factor was 1.5. Bowl shape TWO; engine speed 1500 rpm, full-load (see table 5.2).

The predominant difference in combustion between the best and worst cases was the distribution of temperature of the burning gas, and thus the distribution of local equivalence ratio. The best case, having fuel impingement high up on the bowl lip, had higher temperature and velocity, reverse squish flow. Conversely, combustion in

the worst case was towards the base of the main torodial radius, and moved towards the piston pip into a region of relatively stagnant airflow. This may have had implications for the oxidisation of soot, with high soot concentration possible at the bowl centre.

6.4 In-cylinder fuel distribution

6.4.1 Initial fuel impingement

The fuel distribution within the cylinder changed significantly with the point of fuel impingement. Although there was some spray growth before fuel impingement, the majority of combustible mixture formed was a result of fuel impingement on the piston walls. Fuel distribution and in-cylinder airflow control engine performance and emissions. Figures 6.9 and 6.10 show the liquid fuel envelope at the initial fuel impingement, of the best and worst injector optimisation cases (viewed through a two-dimensional section of one-half of piston bowl shape TWO).

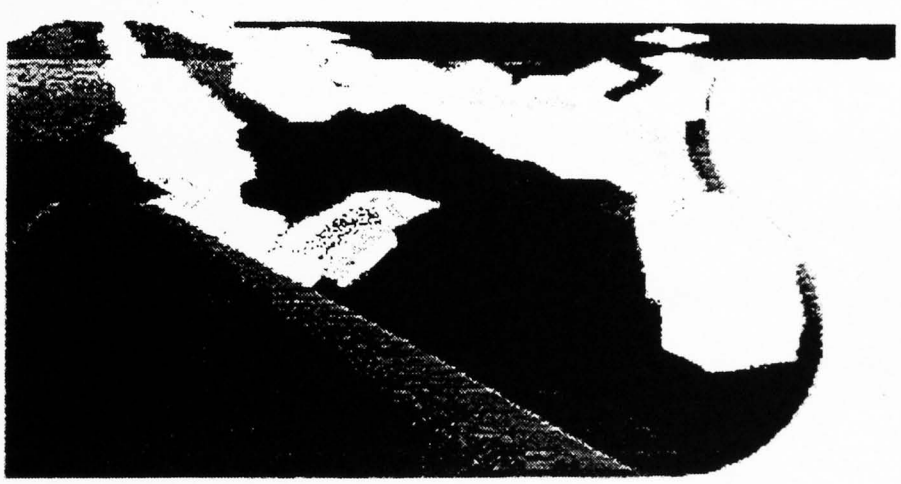

Figure 6.9 Two dimensional section of one-half of piston bowl shape TWO, showing the liquid fuel envelope. Initial fuel impingement at 2 degrees after TDC, of the best injector configuration case (150 degree cone angle, 5.5mm washer depth). Engine speed 1500 rpm, full-load (see table 5.2).

Figure 6.10 Two dimensional section of one-half of piston bowl shape TWO, showing the liquid fuel envelope. Initial fuel impingement at 2 degrees after TDC, of the worst injector optimisation case (140 degree cone angle, 2.5mm washer depth). Engine speed 1500 rpm, full-load (see table 5.2).

The best injector optimisation case resulted in fuel impingement on the side of the piston lip region, which caused the spray to be dispersed in all directions. Conversely, fuel impingement low into the main torodial radius during the worst case, caused little dispersion of liquid fuel. It was likely that better distribution of fuel and air entrainment occurred in the best case, with a more even distribution of equivalence ratios within the bowl.

A small quantity of fuel which had impinged high up on the piston sides (in the best case), spilled-over into the clearance volume region between the piston crown top face and the cylinder head. This over penetrated fuel was dispersed and cooled, such that it did not form one of the initial sites of ignition, but was later consumed during diffusion burning.

The difference in fuel mixture preparation, and the influence of bulk airflow was better illustrated by the three-dimensional pictures in figures 6.11 and 6.12, shown at the same engine crank angle as the two-dimensional plots (figures 6.9 and 6.10).

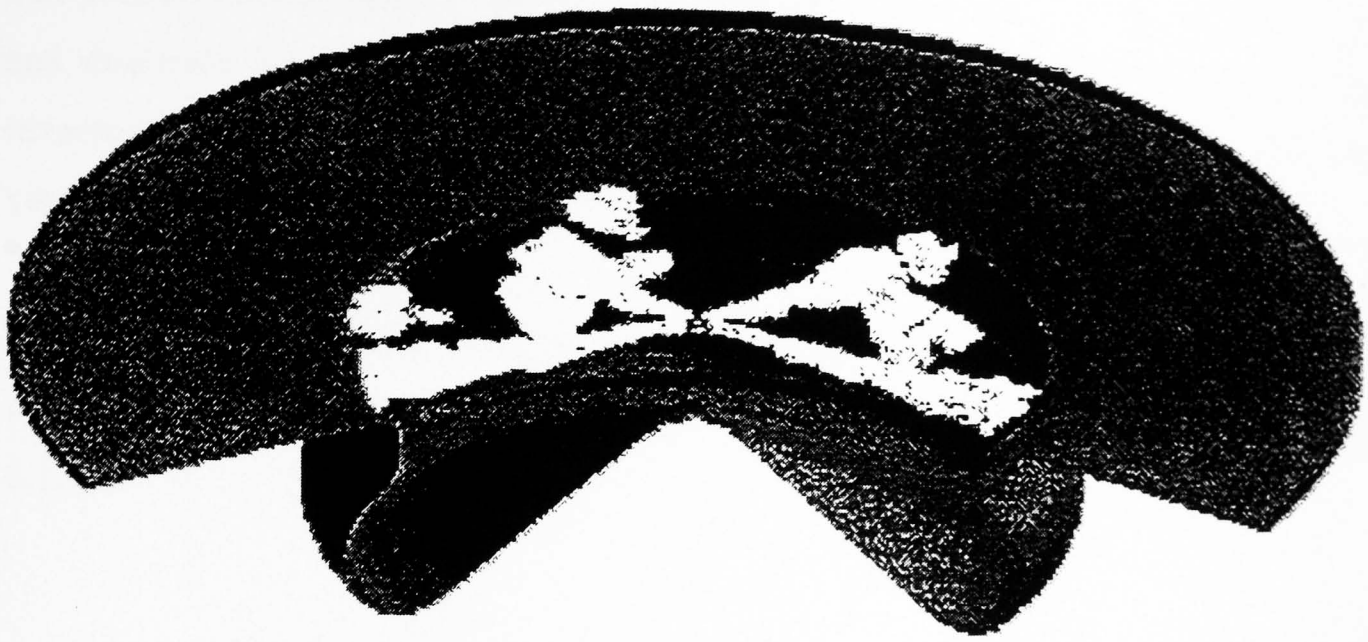

Figure 6.11 Three dimensional perspective view of a section of two-thirds of piston bowl shape TWO, showing the liquid fuel envelope. Initial fuel impingement at 2 degrees after TDC, of the best injector configuration case (150 degree cone angle, 5.5mm washer thickness). Engine speed 1500 rpm, full-load (see table 5.2).

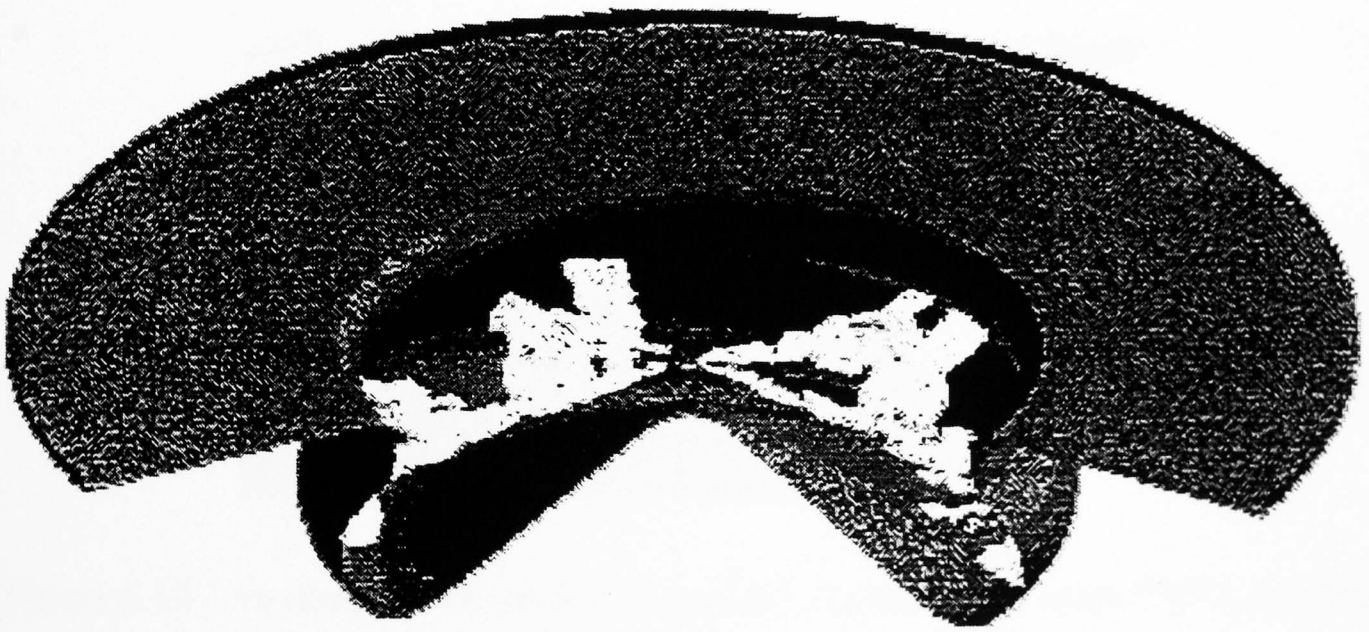

Figure 6.12 Three dimensional perspective view of a section of two-thirds of piston bowl shape TWO, showing the liquid fuel envelope. Initial fuel impingement at 2 degrees after TDC, of the worst injector configuration case (140 degree cone angle, 2.5mm washer thickness). Engine speed 1500 rpm, full-load (see table 5.2).

The pockets of over-penetrated fuel in the best case were broken up into smaller ones, and dispersed by the action of air-swirl. There was little influence from squish or reverse-squish at this time, as the piston had reached TDC, but combustion had not yet commenced.

Large amounts of fuel were concentrated at the base of the worst injector configuration case, resulting in considerable wall wetting of this area (see figure 6.12).

6.4.2 Comparison of wall-wetting just before the start of combustion

Comparison of wall wetting just before the start of combustion is illustrated in the 2D sections of one-half of piston bowl shape TWO, at an engine crank angle of 3 degrees after TDC, as shown in figures 6.13 and 6.14.

Figure 6.13 Two dimensional section of one-half of piston bowl shape TWO, showing the liquid fuel envelope and wall-wetting just before the start of combustion at 3 degrees after TDC, of the best injector configuration case (150 degree cone angle, 5.5mm washer thickness). Engine speed 1500 rpm, full-load (see table 5.2).

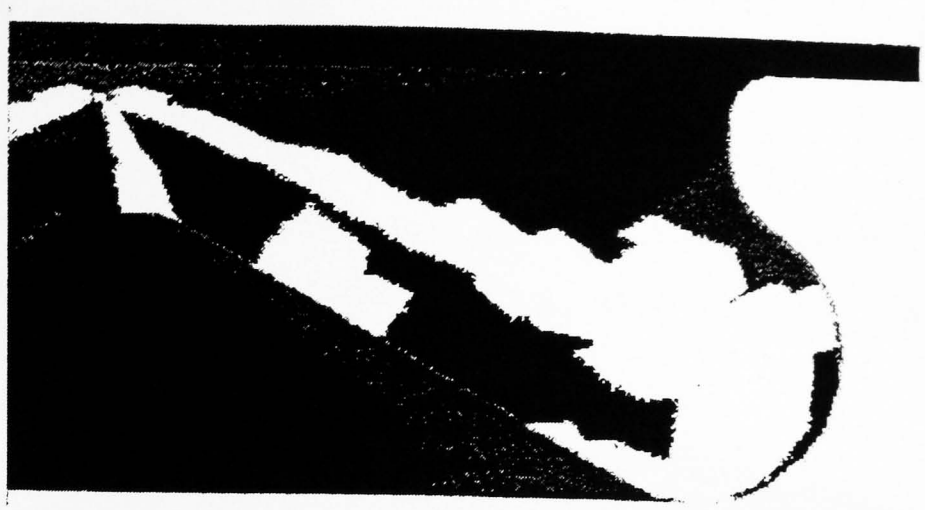

Figure 6.14 Two dimensional section of one-half of piston bowl shape TWO, showing the liquid fuel envelope and wall-wetting just before the start of combustion at 3 degrees after TDC, of the worst injector configuration case (140 degree cone angle, 2.5mm washer thickness). Engine speed 1500 rpm, full-load (see table 5.2).

Liquid fuel was swept clockwise up towards the piston pip in the worst injector optimisation case (see figure 6.14), away from highly turbulent airflow. This may have reduced the subsequent rate of air entrainment, and resulted in a greater proportion of fuel being burnt late in the diffusion burning process. The direction of airflow (described in previous sections) drew fuel mixture around the main torodial radius in a clock-wise motion, as viewed from this half of the piston bowl section.

Conversely, the best injector configuration (see figure 6.13) resulted in fuel which had impinged on the bowl lip region being split-up, promoting fuel flow up and down the bowl. It was likely that this aided fuel/air mixing, and the subsequent rate of combustion (discussed in a later section).

6.4.3 Initial ignition sites

Initial ignition sites were located in the regions of fuel/air mixture formed by fuel injected early. Fuel injected early had the longest time for the self-ignition, chemical reactions to proceed, and thus for the initial sites of ignition to form. Initial ignition sites in the worst case occurred around the periphery of the impinged fuel spray. Here,

the dense fuel spray was surrounded by lower momentum mixture, which had mixed, over time, to within combustible limits.

Initial sites of ignition in the best case were located some distance from the spray centre. Figure 6.15 illustrates the initial sites of ignition for the best injector configuration case.

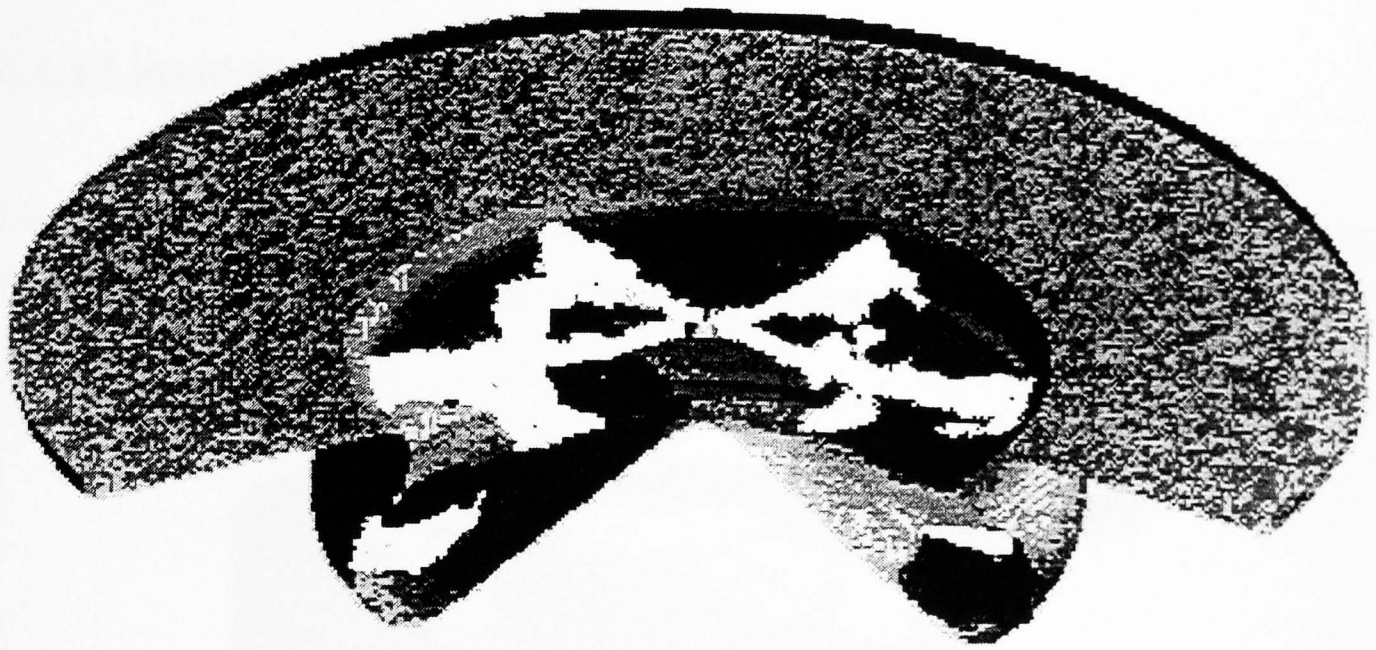

Figure 6.15 Three dimensional perspective view of a section of two-thirds of piston bowl shape TWO, showing the liquid fuel envelope and the initial sites of ignition, as dark regions of the fuel spray. Start of combustion occured at 6 degrees after TDC, for the best injector configuration case (140 degree cone angle, 2.5mm washer thickness). Engine speed 1500 rpm, full-load (see table 5.2).

Fuel injected early impinged on the bowl walls first, and was dispersed by the action of bulk-swirl around the bowl, and squish induced 'torodial' swirl (superimposed on the bulk swirl motion) in the main torodial radius. The first fuel mixture to ignite was located downstream of the point of impingement, near the base of the bowl see figure 6.15). Combustion spread rapidly back towards the point of impingement. A few engine crank-angle degrees later, the low momentum fuel surrounding the injected spray was engulfed in flames.

Combustion was much more vigorous in the worst impingement case (not shown), with liquid fuel continuously being injected into the main combustion area at the base

of the torodial radius. This differed from the best impingement point case (figure 6.15), where burning continued downstream of the impingement point, consuming mixture dispersed by impingement. This high temperature, fuel-rich region in the worst injector configuration case may be one of the factors contributing to the exceptionally high smoke emission recorded.

6.4.4 Liquid fuel remaining at the end of injection

Liquid fuel remaining in the combustion chamber at the end of injection is shown in figures 6.16 and 6.17, for the best and worst impingement cases respectively.

Figure 6.16 Two dimensional section of one-half of piston bowl shape TWO, showing the liquid fuel envelope and the liquid fuel which remained in the combustion chamber at the end of injection, at 12 degrees after TDC, of the best injector configuration case (150 degree cone angle, 5.5mm washer thickness). Engine speed 1500 rpm, full-load (see table 5.2).

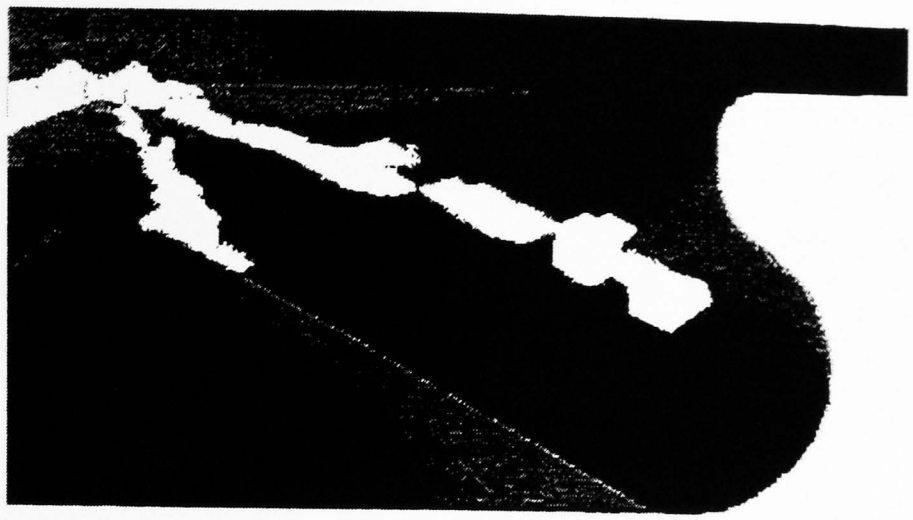

Figure 6.17 Two dimensional section of one-half of piston bowl shape TWO, showing the liquid fuel envelope and the liquid fuel which remained in the combustion chamber at the end of injection, at 12 degrees after TDC, of the worst injector configuration case (140 degree cone angle, 2.5mm washer thickness). Engine speed 1500 rpm, full-load (see table 5.2).

Fuel which was transported as a wall jet to the base of the piston bowl in the best injector optimisation case remained after the end of injection (see figure 6.16). This was surprising, considering the relative smoke emissions of each configuration, but soot formation and oxidation analysis (described in a later section) indicated that this fuel was rapidly consumed in complete combustion, and did not contribute to the emission of smoke. It was possible that the highly turbulent region of the piston bowl where the fuel resided, caused break-up and entrainment of the fuel in the bulk airflow.

6.5 In-cylinder soot formation and oxidation during combustion

Soot formation and oxidation was represented by plotting three-dimensional surfaces of constant soot concentration. The darkest 'greyscale' soot iso-surfaces represented the highest concentration of soot in the combustion chamber, whilst the lightest/white 'greyscale' iso-surfaces represented the lowest soot concentration.

Soot formation and oxidation was considered over a wider range of engine crank-angles than was the case for the liquid fuel distribution. The last frame presented is at 80 degrees after TDC, when combustion reactions were considered to have frozen, and the mean soot concentration in the combustion chamber was similar to that which might have been sampled in the exhaust.

6.5.1 Initial soot distribution

Figures 6.18 and 6.19 show soot iso-concentration surfaces of the best and worst injector configuration cases respectively, just after the start of combustion at 10 degrees after TDC.

Figure 6.18 Three dimensional perspective view of a section of two-thirds of piston bowl shape TWO, illustrating iso-concentration surfaces of soot, formed at 10 degrees after TDC, of the best injector configuration case (150 degree cone angle, 5.5mm washer thickness). Engine speed 1500 rpm, full-load (see table 5.2).

Figure 6.19 Three dimensional perspective view of a section of two-thirds of piston bowl shape TWO, illustrating iso-concentration surfaces of soot, formed at 10 degrees after TDC, of the worst injector configuration case (140 degree cone angle, 2.5mm washer thickness). Engine speed 1500 rpm, full-load (see table 5.2).

Although in the worst case (figure 6.19), a greater total formation of soot had occurred at this stage, combustion had started one engine crank-angle degree earlier. Of more significance was the distribution of soot within the combustion chamber.

The best injector optimisation case (figure 6.18) produced low concentrations of soot, which surrounded the initial sites of ignition, downstream from the point of impingement (discussed in a previous section). Conversely, the worst case formed high concentrations of soot at the base of the piston bowl, where temperatures were high from initial combustion, and considerable wall-wetting had occurred. The soot formed a blanket which was driven clockwise up and outwards, towards the piston pip, by the expanding, combusting gases.

6.5.2 Development of soot distribution during combustion

Development of the soot iso-surfaces is illustrated in figures 6.20 and 6.21, of combustion at 15 degrees after TDC.

Figure 6.20 Three dimensional perspective view of a section of two-thirds of piston bowl shape TWO, illustrating iso-concentration surfaces of soot, formed at 15 degrees after TDC, of the best injector configuration case (150 degree cone angle, 5.5mm washer thickness). Engine speed 1500 rpm, full-load (see table 5.2).

Figure 6.21 Three dimensional perspective view of a section of two-thirds of piston bowl shape TWO, illustrating iso-concentration surfaces of soot, formed at 15 degrees after TDC, of the worst injector configuration case (140 degree cone angle, 2.5mm washer thickness). Engine speed 1500 rpm, full-load (see table 5.2).

Comparison of the best injector configuration iso-soot surfaces at 15 degrees after TDC (figure 6.20), and soot surfaces of the worst case at 10 degrees after TDC (figure 6.19) showed them to be similar in appearance. However, there were significant differences. Firstly, the gradient of soot concentration across the combustion zone was

more gradual in the best case. This may have been a result of greater entrainment of air into the combustion zone, and hence a faster rate of soot oxidation. Secondly, the highest concentration surfaces of soot in the best case became detached from the base of the bowl torodial radius, and moved up towards the piston pip. Later, the highest concentration iso-soot surfaces became detached from the piston base completely, and were subsequently entrained and oxidised in fresh air.

The worst injector optimisation case, at 15 degrees after TDC (see figure 6.21), indicated the formation of a cylindrical volume of very soot-rich mixture, which spanned from the base of the piston up to the cylinder head (note that if two iso-concentration soot surfaces opposed each other, the interim material may be considered to be of equivalent concentration).

Fuel injection ceased at 16 degrees after TDC. The soot surface structure had fully formed by the end of injection, but was modified by combustion-induced airflow and expansion of gas into the cylinder volume as the piston descended.

Figures 6.22 and 6.23 illustrate iso-concentration soot surfaces towards the end of combustion, at 30 degrees after TDC. The iso-soot surfaces have expanded into the cylinder volume, as hot rich mixture was driven out of the piston bowl volume.

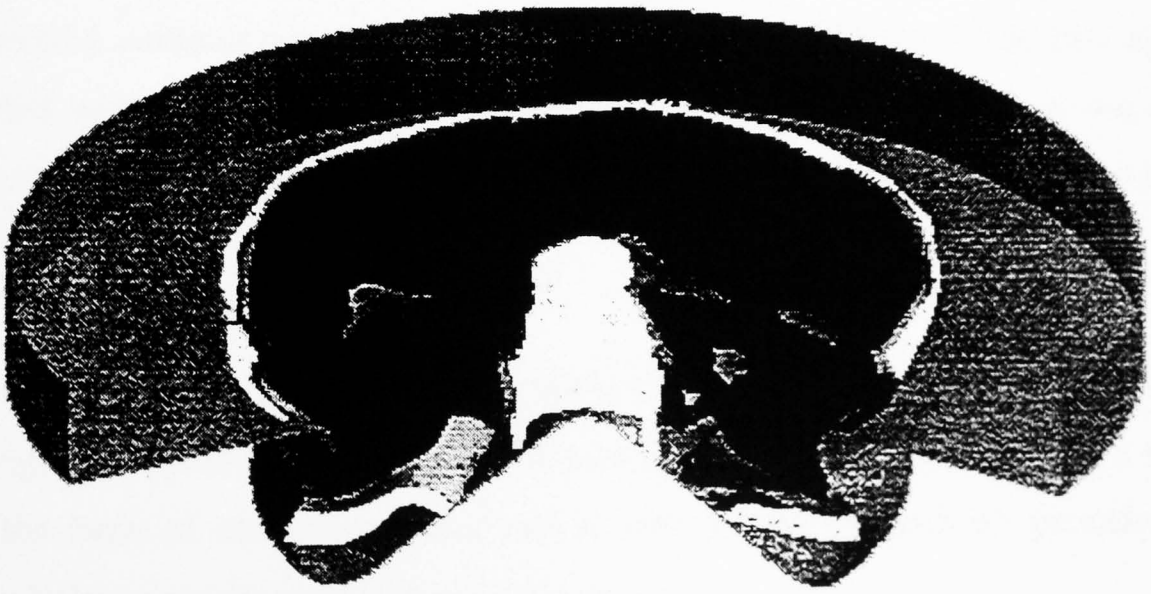

Figure 6.22 Three dimensional perspective view of a section of two-thirds of piston bowl shape TWO, illustrating iso-concentration surfaces of soot, formed at 30 degrees

after TDC, of the best injector configuration case (150 degree cone angle, 5.5mm washer thickness). Engine speed 1500 rpm, full-load (see table 5.2).

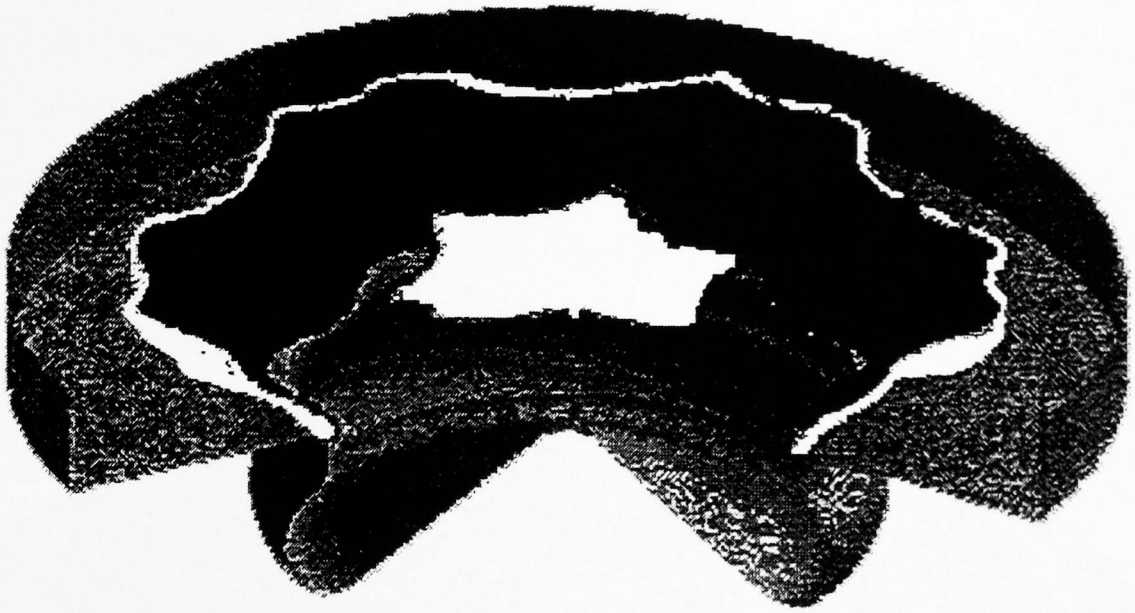

Figure 6.23 Three dimensional perspective view of a section of two-thirds of piston bowl shape TWO, illustrating iso-concentration surfaces of soot, formed at 30 degrees after TDC, of the worst injector configuration case (140 degree cone angle, 2.5mm washer thickness). Engine speed 1500 rpm, full-load (see table 5.2).

The soot-filled torodial volume formed in the worst injector optimisation case (figure 6.23), now nearly completely filled the piston bowl volume in a cylindrical shape, which extended to the cylinder head. Combustion had driven the uppermost edges of the iso-soot surfaces out towards the cylinder walls. Evidence of the fuel spray still persisted well after the end of injection, visible as distortion of the iso-soot surface into a star-like shape, in figure 6.23 (only four injector sprays were shown in this two-thirds bowl section drawing).

The best injector optimisation case (figure 6.22) indicated a possible reason for the low engine-out emission of smoke. The soot rich region became completely detached from the base of the piston bowl, and a central core of fresh air persisted in the relatively low velocity region above the piston pip.

6.5.3 Soot distribution at the end of combustion

As combustion and expansion proceeded, the soot-rich region formed into a mushroom-like shape, forced out by hot expanding gases from the piston bowl. Figures 6.24 and 6.25 show iso-concentration soot surfaces at 80 degrees after TDC, when combustion reactions were considered to have been frozen, and soot concentration fixed to that of engine-out exhaust measurements.

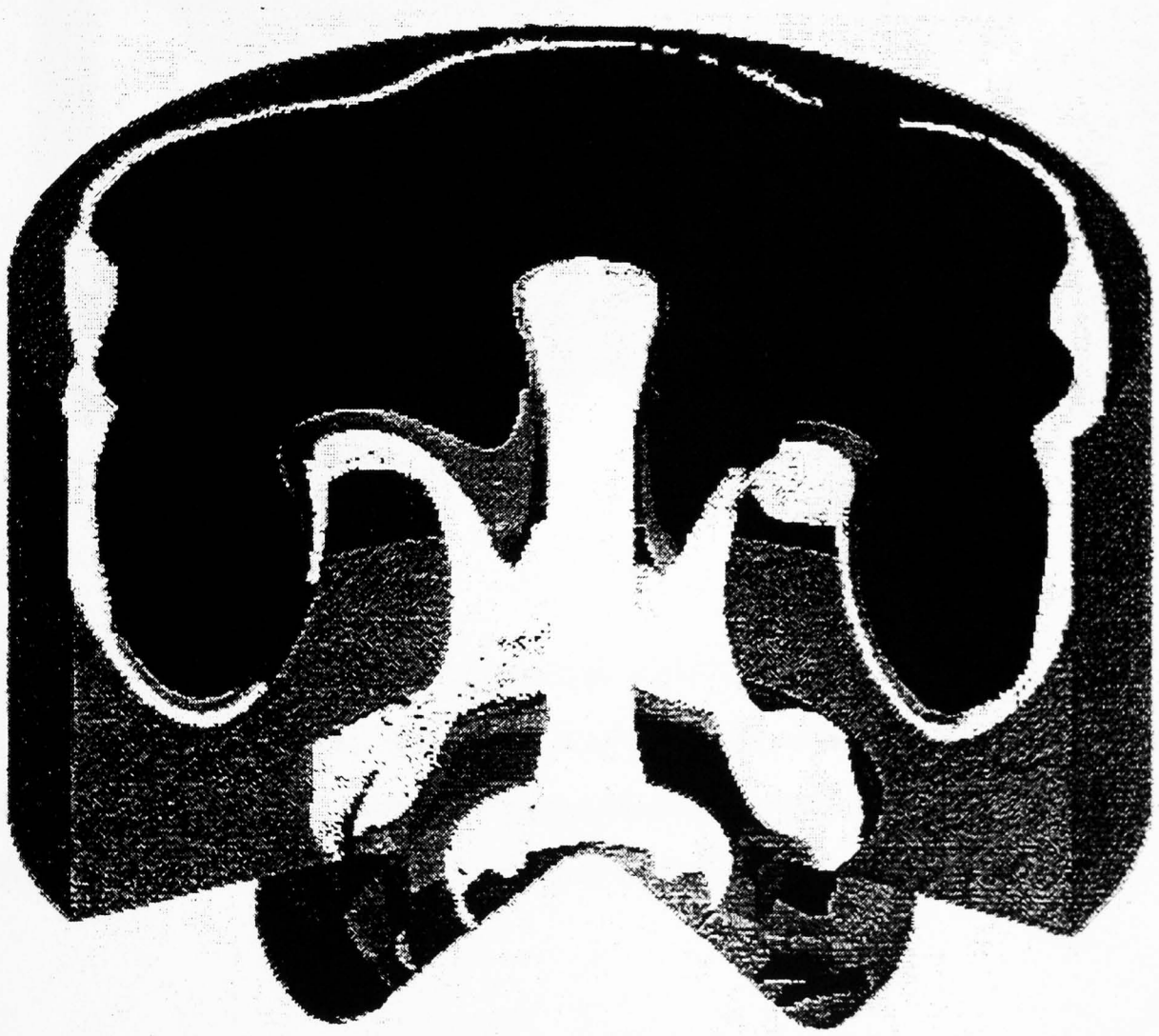

Figure 6.24 Three dimensional perspective view of a section of two-thirds of piston bowl shape TWO, illustrating iso-concentration surfaces of soot, formed at 80 degrees after TDC, of the best injector configuration case (150 degree cone angle, 5.5mm washer thickness). Engine speed 1500 rpm, full-load (see table 5.2).

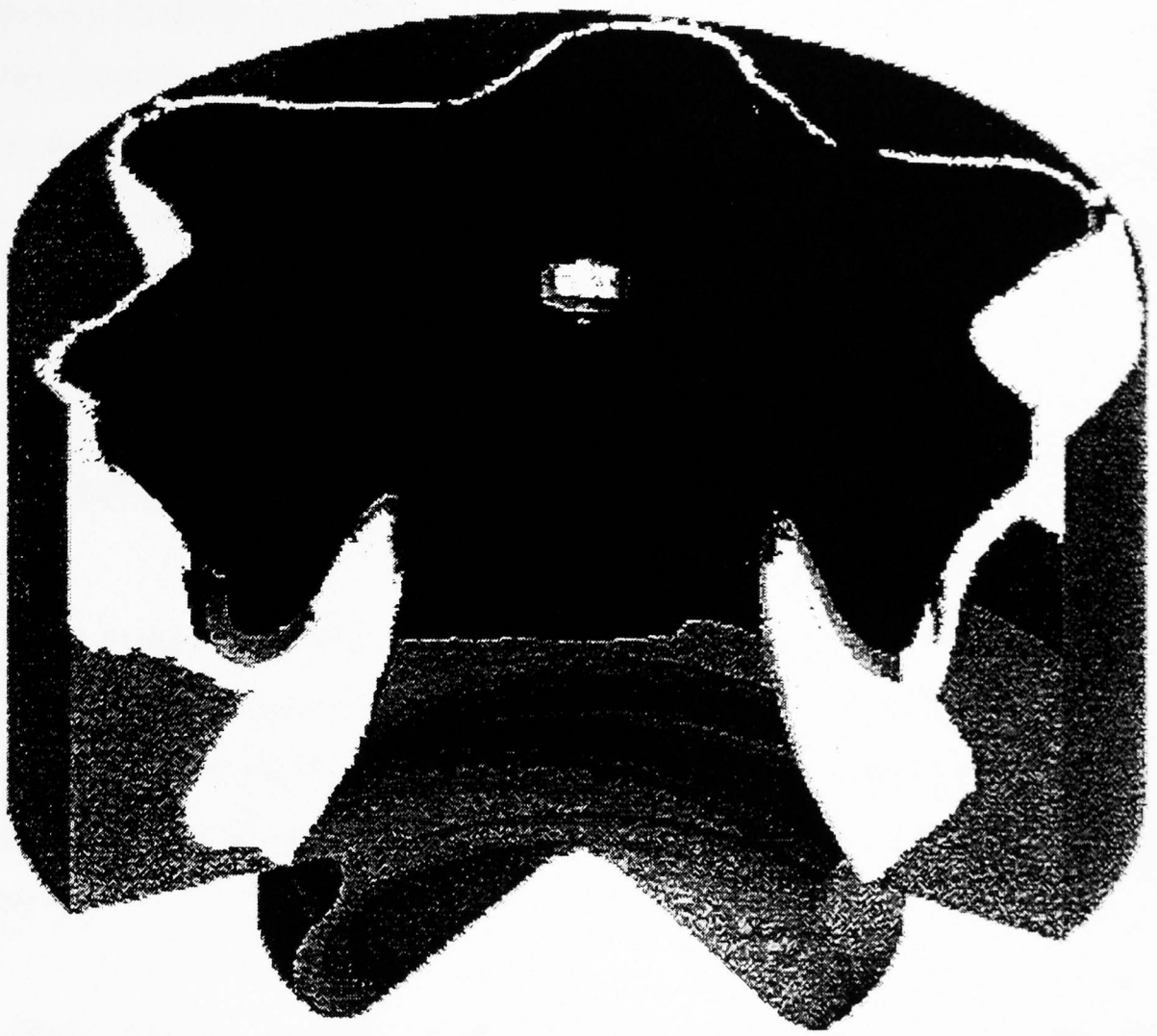

Figure 6.25 Three dimensional perspective view of a section of two-thirds of piston bowl shape TWO, illustrating iso-concentration surfaces of soot, formed at 80 degrees after TDC, of the worst injector configuration case (140 degree cone angle, 2.5mm washer thickness). Engine speed 1500 rpm, full-load (see table 5.2).

Fuel injection deep into the base of the bowl in the worst injector optimisation case (figure 6.25) resulted in the majority of the combustion volume being filled with a high concentration of soot. Although considerable amount of soot remained in the combustion chamber in the best injector configuration (figure 6.24) case also, it occupied a much smaller percentage of the combustion chamber volume. Very little soot remained in the base of the piston bowl in the best case, and the gradient of soot concentration was quite gradual, which may have helped late soot oxidation when the cylinder contents were exiting past the hot exhaust valve.

It would seem that fuel impingement designed to disperse the spray high up in the combustion chamber, combined with the action of swirl and squish to create a wide variation of equivalence ratio's across the combustion chamber, may have helped in the process of soot oxidation, and in creating the right conditions for soot rich regions to be driven out from within the piston bowl. The result was good full-load soot performance with the best injector configuration.

6.6 Conclusions

The three-dimensional CFD combustion simulation provided an invaluable insight into the airflow, combustion and emissions in the HSDI diesel engine. In particular, the work supported many of the conclusions obtained by experimental analysis of the effect of the point of fuel impingement on combustion and emissions (presented in chapter 5).

The initial airflow structure was observed to be the same for both the best (impingement point 1, see table 5.1) and worst (impingement point 9, table 5.1) injector configuration cases, from full-load testing at 1500 rpm of piston bowl shape TWO. This was expected, since fuel injection had not yet occurred, and the initial airflow conditions were the same for both cases, specified after inlet valve closure.

Once fuel injection had commenced, the airflow velocity rose by many times over that produced by swirl and squish. The different vertical position of the injector in the piston bowl between the best (using 5.5 mm washer thickness) and the worst (using 2.5 mm washer thickness) injector configurations, created large differences in the airflow pattern.

Initial sites of combustion were located in the early injected fuel, and resulted in a further large increase in gas velocity. Initial sites of ignition were located downstream of the point of impingement in the best case, but deep at the base of the bowl in the worst injector configuration case.

Fuel impingement high up on the bowl lip in the best case caused wide dispersion of fuel spray, encouraging fuel/air mixing, resulting in rapid combustion. Conversely, fuel impingement in the worst injector configuration case was low in the piston bowl, creating very rich regions at high temperature, promoting soot formation. Soot rich regions were driven up towards the bowl pip in the worst case, into a region of low airflow velocity, and reduced entrainment of fresh air.

By the end of combustion, soot had almost completely filled the bowl-in-piston in the worst injector configuration case (point 9, table 5.1). This had resulted from a combination of high initial soot production from fuel-rich regions at high temperature, and then combustion induced gas flow, which forced the soot rich regions towards the centre of the bowl, where airflow velocity and thus mixing was low. Conversely, the best injector configuration case, resulted in all of the soot rich regions being driven out of the bowl by the combustion induced airflow.

Chapter 7:

Overall comparison of piston bowl shapes

Chapter 7: Overall comparison of piston bowl shapes

7.1 Introduction

Following injector optimisation of each piston bowl shape, a series of tests were carried out to determine the overall performance of each piston bowl at a variety of engine speed/load combinations. Piston bowl shapes were compared primarily by the emission of particulates and NOx, resulting from EGR loops of test conditions chosen to represent typical driving demand. A weighted sum of emissions at each engine test condition (corresponding to the influence of that test condition on the drive cycle total emission) was used to form an overall bowl comparison.

7.2 Selected even mode test conditions from 14-mode test cycle

The 14-mode test encompassed a wide range of engine speed and load requirements, considered by the automotive industry to be representative of the vehicle drive-cycle test requirements for EEC type approval. The injection timing specified at each mode was determined by Ford for the standard piston bowl shape, and retained for subsequent testing of new piston bowl shapes. It was anticipated that the range of injection timings used would give a good indication of the overall piston bowl shape emissions performance. However, it was appreciated that optimisation of injection timing at each mode for each new bowl shape may have improved emission results.

To reduce engine testing time, even-numbered mode test conditions were selected for testing at Brunel university. This did not compromise the range of engine speeds and loads used, and still represented the drive-cycle test requirements. Table 7.1 shows the selected seven, even-mode test conditions.

mode no	speed (rpm)	load (Nm)	SOI (deg)	weighting
1	800	0	25	27.69
2	**1000**	**14**	**2**	**4.04**
3	1150	61.4	25	2.66
4	**1500**	**55.8**	**4.5**	**2.38**
5	1800	11.2	4	8.98
6	**1800**	**27.9**	**4**	**6.02**
7	1800	41.9	5	8.89
8	**1900**	**81**	**4**	**4.24**
9	2150	56.6	5	2.55
10	**2300**	**83.7**	**-2**	**3.3**
11	2400	12.6	2	12.88
12	**2600**	**54.4**	**2**	**3.39**
13	2700	111.7	-5	2.03
14	**3200**	**69.8**	**-6**	**0.85**

Table 7.1 The selected seven, even-numbered mode, test conditions (shown in bold type) from the 14-mode test which were used for overall piston bowl shape comparison.

The weighting factor indicated the contribution of each mode, towards total drive-cycle emissions. The weighting factor was used to calculate a weighted sum of emissions, used in the overall bowl comparison results.

At each mode test condition, an EGR sweep was performed by increasing the amount of EGR progressively by 10%, up to a maximum of 50% EGR if possible. At some mode test conditions, the tolerance to EGR was such that miss-fire occurred before reaching 50% EGR.

7.3 Results of EGR loops at each even mode test condition

At each mode test condition, the level of EGR was increased in discrete steps, whilst maintaining the required engine speed and load. In general, as the level of EGR was increased, the emission of NOx reduced but the emission of particulates increased. The trade-off between particulates and NOx was the best method of defining the performance of a bowl shape, and gave an indication of the sensitivity of the piston bowl to different EGR levels. Particulates versus NOx trade-offs from each test condition are presented in the figures below (note that the level of EGR in the intake charge increases from right to left in steps of 10%, starting from 0% EGR).

7.3.1 Particulates / NOx trade-off from test mode 2

Results of particulates and NOx from an EGR sweep at test mode 2 are shown in figure 7.1 below.

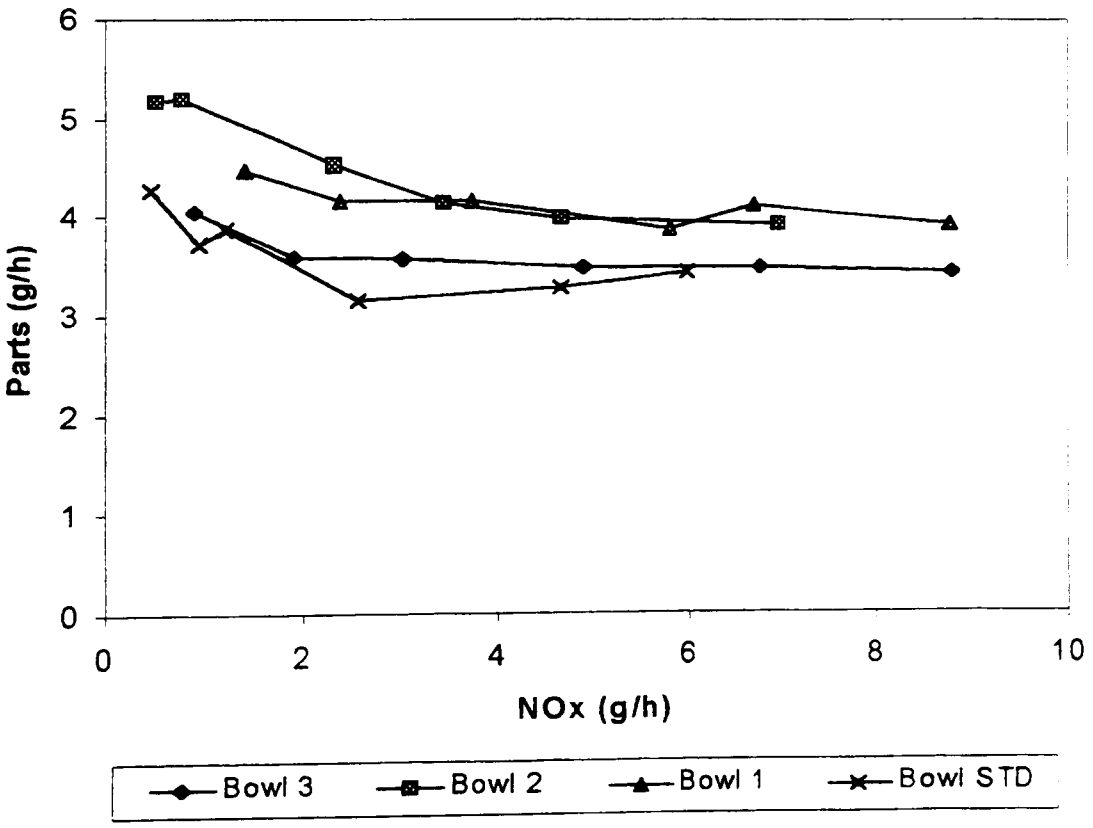

Figure 7.1 Variation of particulates and NOx during an EGR sweep of mode 2, for the four piston bowl shapes tested (1000 rpm, 14 Nm, SOI 2 degrees ATDC). EGR in the intake charge increases from right to left in steps of 10%, starting from 0% EGR.

Test mode 2 required the engine speed to be maintained at just 1000rpm, and at a very light load of 14 Nm. Only a very small quantity of fuel was injected into the engine cylinder in this condition, resulting in an air/fuel ratio of approximately 70:1. Piston bowl shapes STD, ONE and THREE showed very little trade-off in the emission of particulates with NOx. In these cases, NOx was reduced substantially when the level of EGR was increased, but without the penalty of increased particulates emission. This was due to the large amount of excess air in the combustion chamber, preventing soot rich regions from developing as EGR was increased, but yet reducing combustion gas temperature and, thereby, NOx formation. The relatively poor performance of piston bowl shape TWO was most likely due to the poor air utilisation associated with this bowl shape (as was identified during injector optimisation analysis).

7.3.2 Particulates / NOx trade-off from test mode 4

Results of particulates and NOx from an EGR sweep at test condition mode 4 are shown in figure 7.2 below.

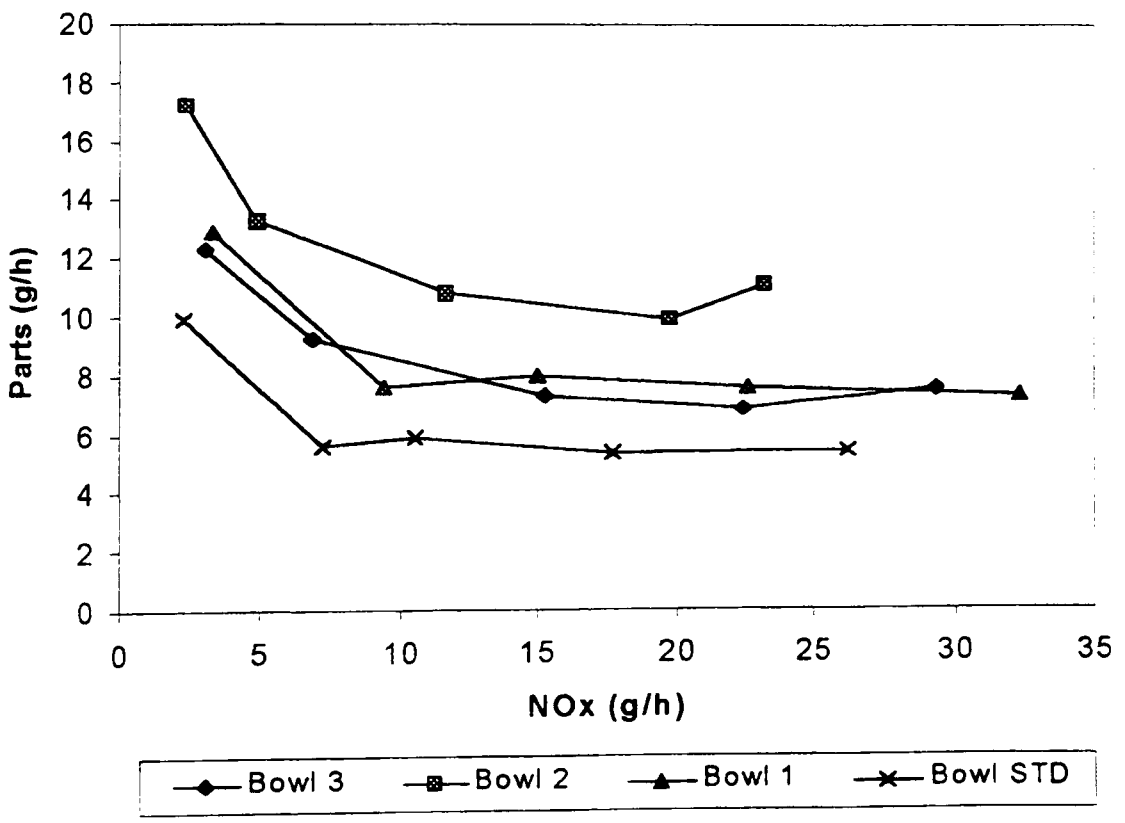

Figure 7.2 Variation of particulates and NOx during an EGR sweep of mode 4, for the four piston bowl shapes tested (1500 rpm, 55.8 Nm, SOI 4.5 degrees ATDC).

At the higher engine load of 55.8 Nm, of test condition mode 4, the air/fuel ratio was typically 38:1 without any EGR, but dropped to 22:1 at an EGR level of 40%. Higher levels of EGR could not be tolerated due to engine miss-fire and excessive HC emission.

The overall emission of particulates and NOx was much higher than for test mode 2, because of the increased load resulting in higher combustion temperature, and increased fuel/air ratio for production of particulates.

The lower air/fuel ratio at this test condition was reflected in a more prominent particulates / NOx trade-off, as mixing of fuel with clean air became difficult at high levels of EGR. A distinct 'cut-off' point of EGR level was observed (see figure 7.2) with piston bowl shapes STD and ONE, above which an increase in the level of EGR produced excessive particultes.

Piston bowl shape STD performed best when operating at test condition mode 4, whilst bowl shape TWO showed a marked particultes versus NOx trade-off, and poor overall performance.

7.3.3 Particulates / NOx trade-off from test mode 6

Results of particulates and NOx from an EGR sweep at test mode 6 are shown in figure 7.3 below.

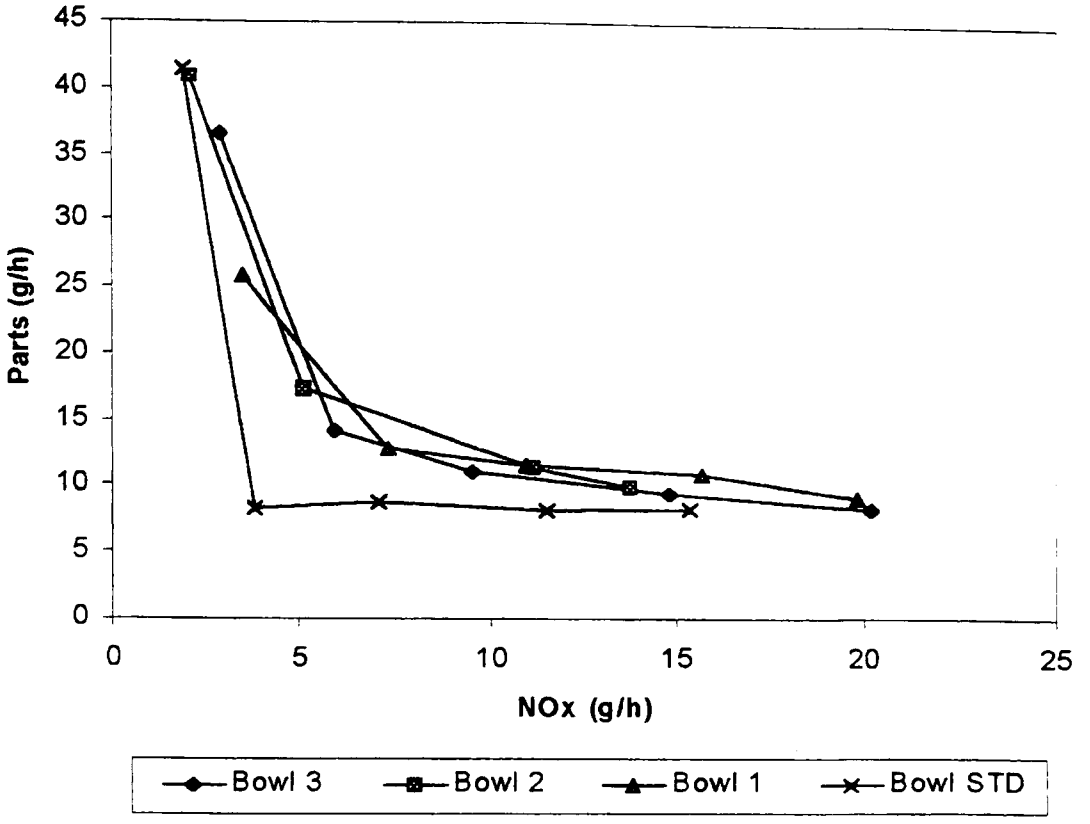

Figure 7.3 Variation of particulates and NOx during an EGR sweep of mode 6, for the four piston bowl shapes tested (1800 rpm, 27.9 Nm, SOI 4 degrees ATDC).

Test condition mode 6 exhibited a sharp 'cut-off' point of the level of EGR that was tolerable, above which the emission of particlutates increased many times. However, closer inspection of the full set of results showed the sharp increase in particulates to be due to an increase in the emission of HC, rather than an increase in smoke which had been observed in previous test conditions. Figure 7.4 shows the variation of the emission of HC with increasing EGR, for test mode 6.

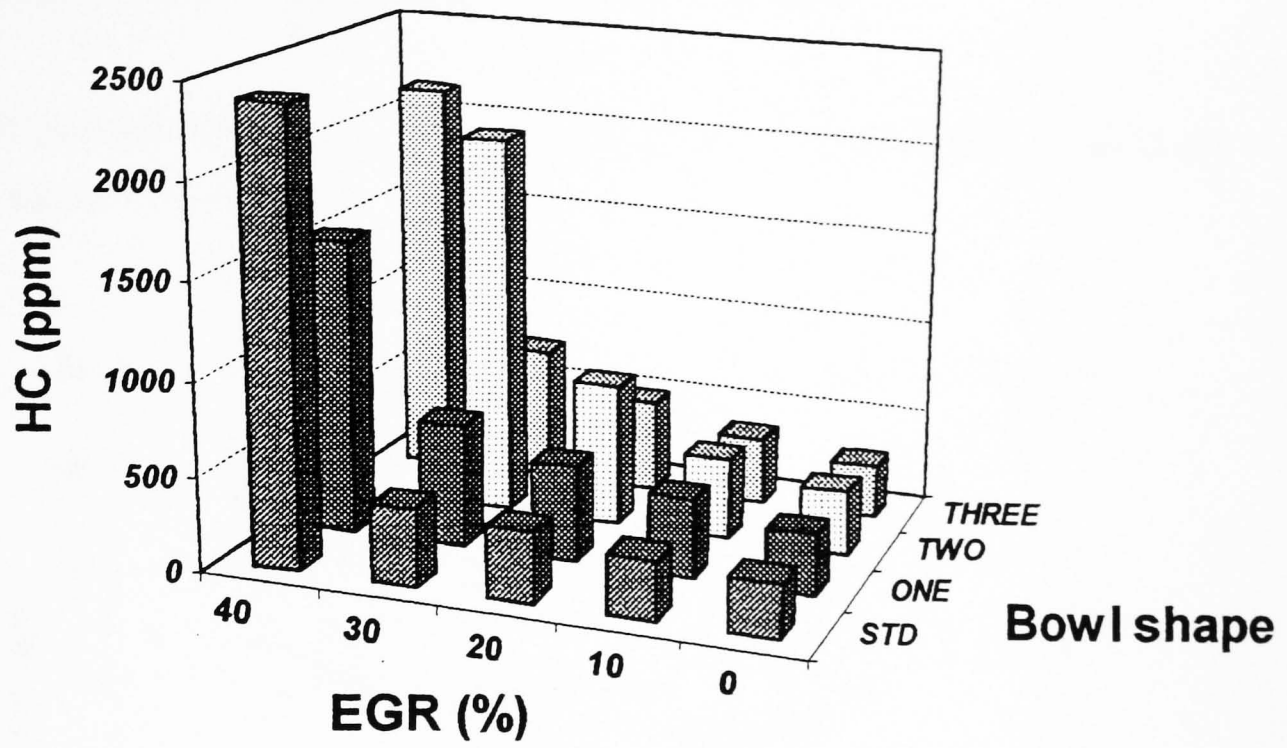

Figure 7.4 Variation of HC emission with increasing EGR level for test mode 6. Note that 40 % EGR was not achievable for piston bowl shape TWO, because of un-tolerable combustion instability.

Whilst the emission of smoke actually slightly *decreased* for the majority of bowl shapes as EGR was increased (at mode test 6), the contribution of HC emission to particulate mass far outweighed this. This unexpected trend in smoke emissions was possibly due to the low engine load, combined with reduced turbocharger boost, causing excessively cool combustion chamber surfaces when operating without EGR.

The late injection timing used at mode 6 (4 degrees after TDC) would have caused a greater proportion of fuel to be over-penetrated onto the cool upper-surface of the piston crown, and may have been responsible for the engine missfire, and subsequent high HC emissions. Lack of combustion and low in-cylinder temperature was also the most likely cause for the overall low smoke emission at this test mode (6), and high CO emission.

7.3.4 Particulates / NOx trade-off from test mode 8

Results of particulates and NOx from an EGR sweep at test condition mode 8 are shown in figure 7.5 below.

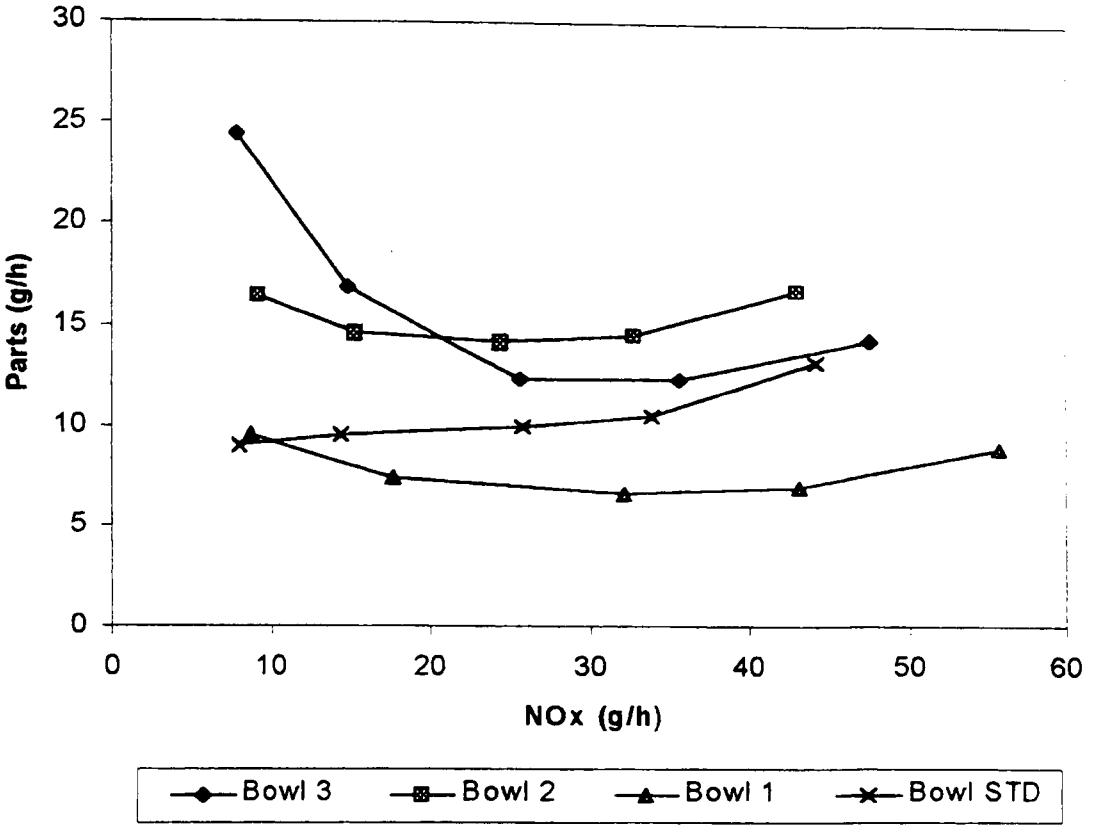

Figure 7.5 Variation of particulates and NOx during an EGR sweep of mode 8, for the four piston bowl shapes tested (1900 rpm, 81 Nm, SOI 4 degrees ATDC).

Test condition mode 8 showed some unusual trends in the variation of particulates with NOx. In many cases, an increase in the level of EGR (moving from right to left in the graphs) resulted in an initial decrease in the emission of particulates as well as NOx. This may have been due to a reduction in the ignition delay period as the level of EGR was increased, because of the higher initial charge temperature at fuel injection. This would have advanced the start of combustion (which was quite retarded because of the late start of injection), promoting better oxidation of soot by avoiding late combustion. Offsetting this, would be a reduction in the proportion of pre-mixed combustion of the total heat released, from which there is very little soot emission.

The reduction in NOx could be attributed to reduced local flame temperature, resulting from the addition of EGR, despite the more advanced start of combustion.

7.3.5 Particulates / NOx trade-off from test mode 10

Results of particulates and NOx from an EGR sweep at test condition mode 10 are shown in figure 7.6 below.

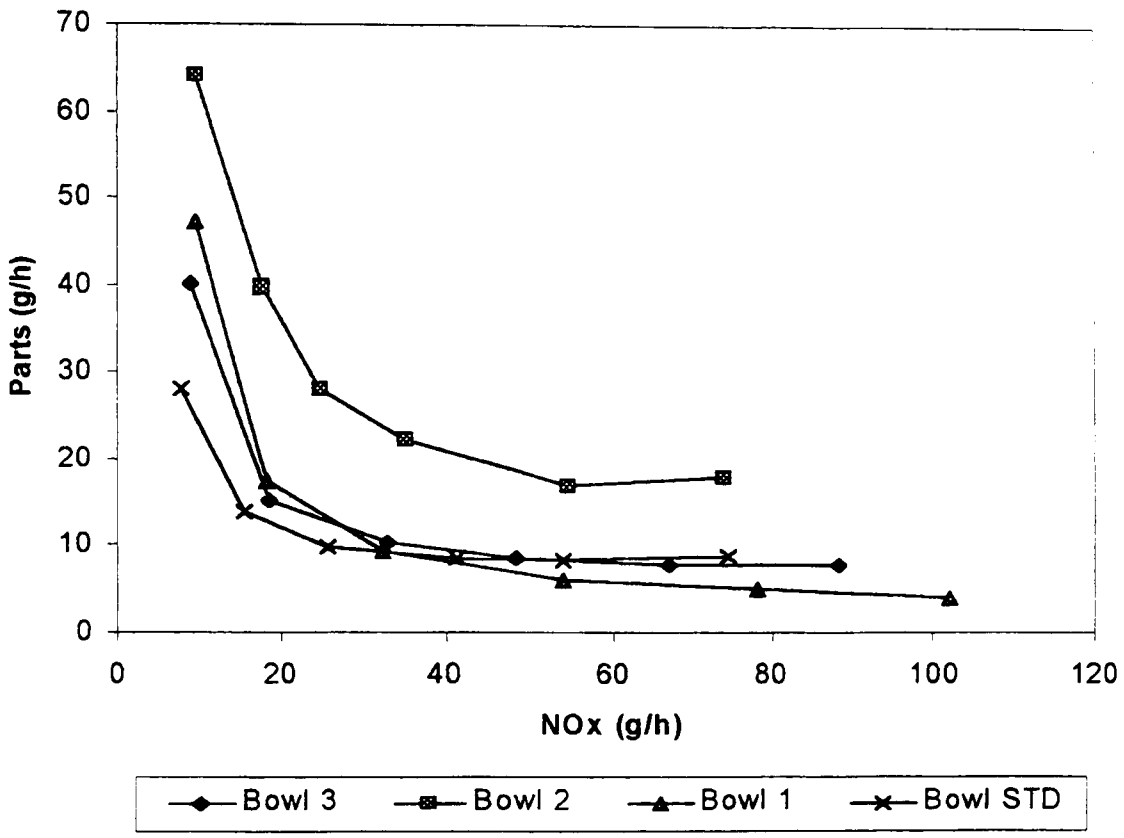

Figure 7.6 Variation of particulates and NOx during an EGR sweep of mode 10, for the four piston bowl shapes tested (2300 rpm, 83.7 Nm, SOI 2 degrees BTDC).

Test condition mode 10 exhibited the classic particulates versus NOx shape. This was because of the high engine load (83.7 Nm), creating demands on fuel/air mixing and air-utilisation. Also the moderately advanced injection timing of 2 degrees before TDC, avoided effects from changes in the ignition delay period as the level of EGR was increased. The overall level of emissions was high compared to other mode conditions, because of the high in-cylinder temperature and low air/fuel ratio of approximately 38:1 before the addition of EGR.

Piston bowl shapes STD, ONE and THREE all performed similarly at this test condition, although bowl shape TWO again demonstrated its poor air utilisation capability with increased particulates and NOx across the whole range of EGR levels.

7.3.6 Particulates / NOx trade-off from test mode 12

Results of particulates and NOx from an EGR sweep at test mode 12 are shown in figure 7.7 below.

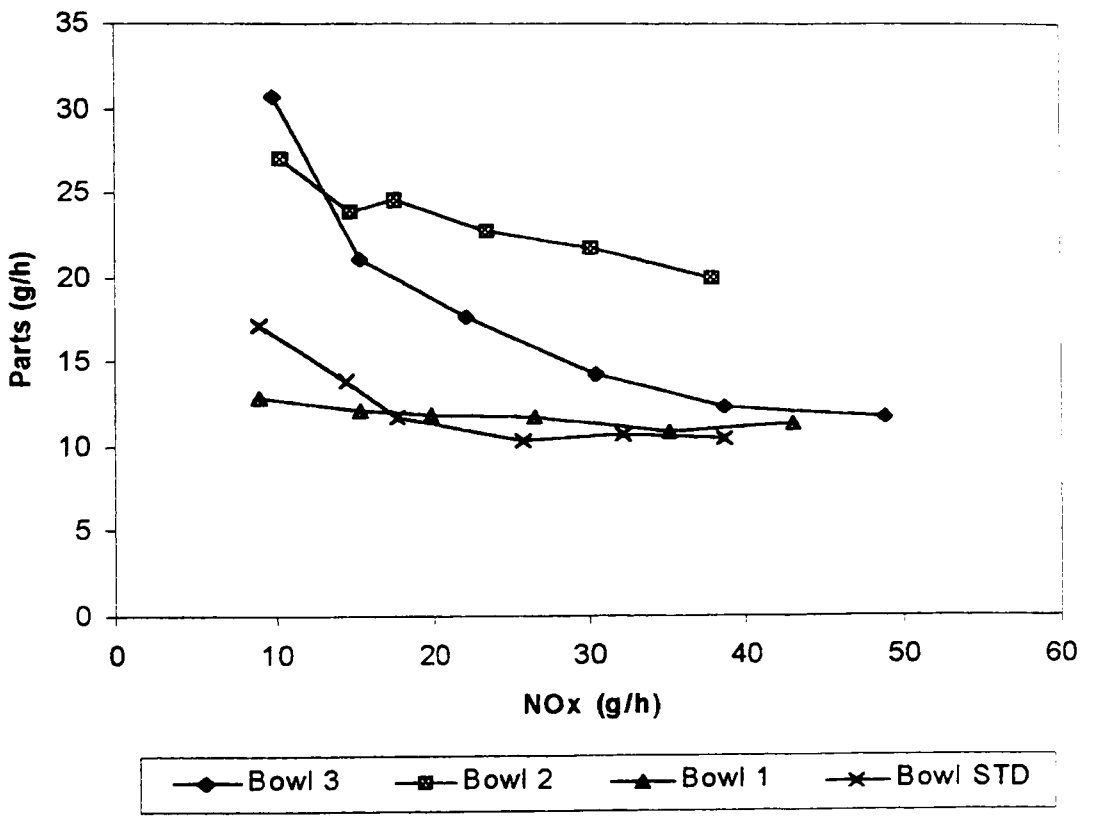

Figure 7.7 Variation of particulates and NOx during an EGR sweep of mode 12, for the four piston bowl shapes tested (2600 rpm, 54.4 Nm, SOI 2 degrees ATDC).

Piston bowl shapes STD and ONE performed well at this test mode, but bowl shape TWO suffered from high particulates at all levels of EGR. Piston bowl shape THREE had low particulates without EGR, but then showed poor tolerance to EGR as the emission of particulates increased rapidly with increasing EGR level. It was difficult to identify why the tolerance to EGR level should have differed greatly between piston bowl shapes THREE and STD, which shared similar basic dimensions. It was possible that changes in the pip shape and minor radii had a significant effect on airflow and subsequent mixing late in the combustion phase, contributing to excessive smoke production from bowl shape THREE.

7.3.7 Particulates / NOx trade-off from test mode 14

Results of particulates and NOx from an EGR sweep at test mode 14 are shown in figure 7.8 below.

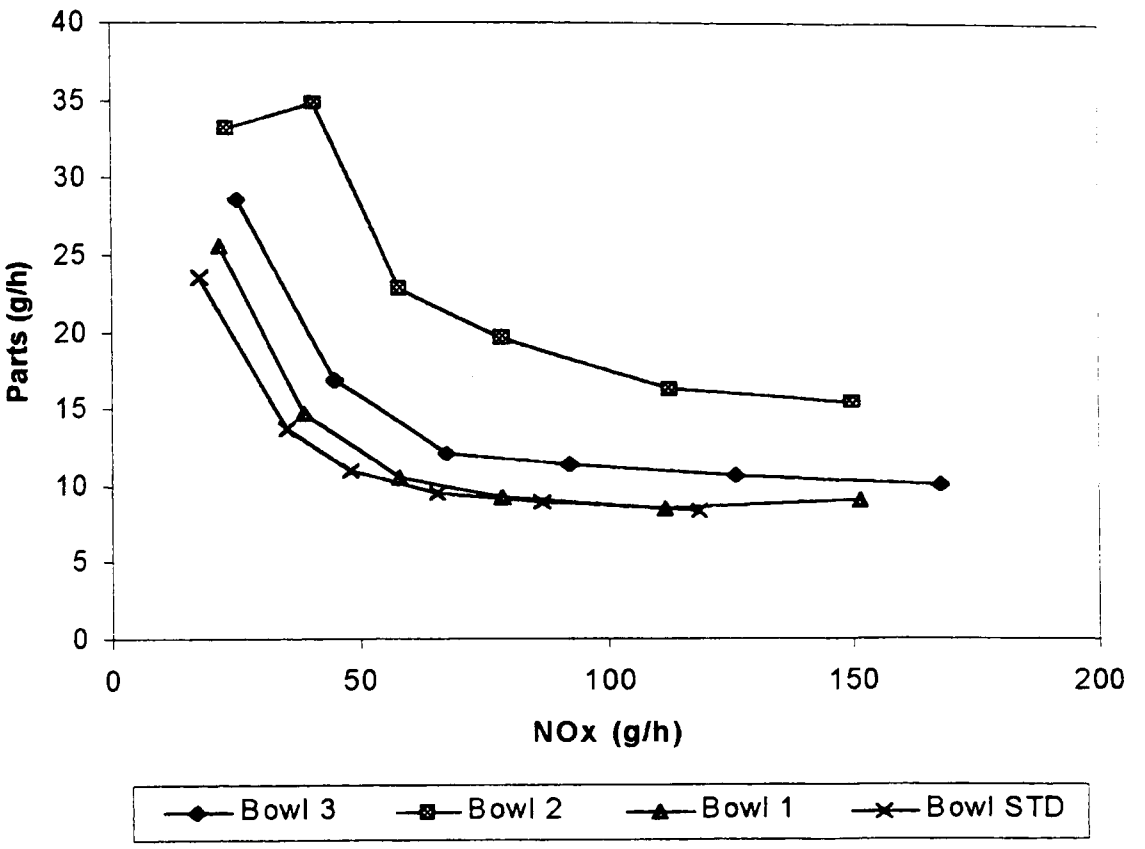

Figure 7.8 Variation of particulates and NOx during an EGR sweep of mode 14, for the four piston bowl shapes tested (3200 rpm, 69.8 Nm, SOI 6 degrees BTDC).

Test mode 14 had the highest initial levels of NOx emission. This was a result of the high engine speed and load raising the combustion temperature. EGR was very effective at reducing the emission of NOx, without a significant penalty in the emission of particulates, up to moderate EGR levels. This was probably because the turbo-charger boost pressure was high (although the engine load was also high - about 50% of full-load), which increased the air/fuel ratio to about 45:1. Hence, a significant quantity of excess air was available for replacement by EGR to reduce NOx formation, without a substantial lack of air to cause smoke formation.

Particulate formation was also minimised at test mode14, because of the advanced injection timing used, reducing the proportion of fuel involved in late combustion when the in-cylinder temperature was lower.

7.4 Overall piston bowl comparison

Piston bowl shapes were compared according to their particulates versus NOx performance at each mode test condition. A weighting was applied to each mode test condition to represent its contribution to the total emissions of the drive-cycle test.

7.4.1 Generation of *overall* particulates versus NOx variation, for each piston bowl shape

Increasing EGR at each test mode produced a particulates versus NOx trade-off, as discussed in section 7.3. Each trade-off curve exhibited an optimum operating condition, and maximum and minimum particulate emission conditions (subject to a limiting smoke value of 3 BSN). An example of these operating conditions is shown in figure 7.9, showing the particulates versus NOx performance for piston bowl shape THREE, operating at test mode 10.

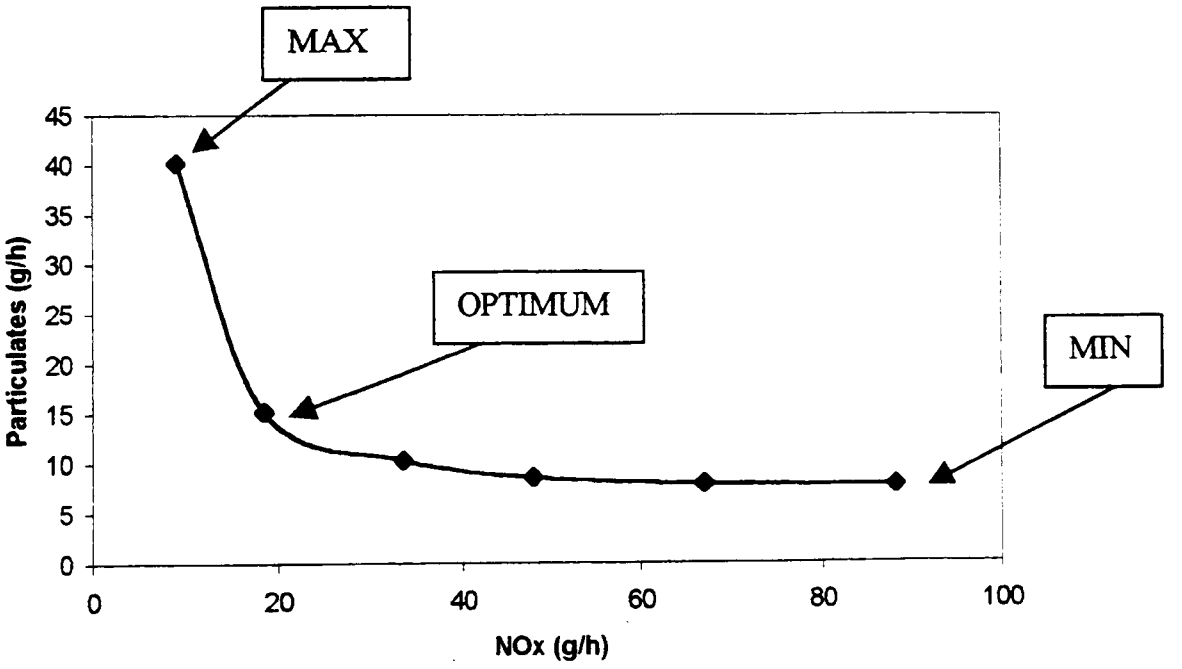

Figure 7.9 Variation of particulates and NOx for piston bowl THREE during an EGR loop at test mode 10. Optimum, maximum, and minimum particulate emission conditions are indicated on the diagram.

The three point conditions were extracted from each test mode (as shown in figure 7.9), and a weighted sum for all test modes calculated (weights used were according to the contribution of that mode to the total cycle emissions test). The unusual trends observed from testing at mode 8 were not included in the total bowl comparison, as they tended to mask the underlying trend in results and distort comparison between piston bowls. The selected optimum, maximum, and minimum points from each mode test are presented in tables 7.2 to 7.13 on the next few pages.

The overall emissions trade-off for each bowl, based on the relative weighted sum of emissions, was obtained using equation 7.1 below.

$$P_0 = \sum_{m=2}^{m=14} P_{0m} \frac{w_m}{W}$$

Equation 7.1 where P_0 is the overall particulate emission (weighted average over 14 modes – even modes only) using the optimum EGR level for each mode; m is the mode number (even modes only used); P_{om} is the particulates for mode m at the optimum EGR level for that mode; w_m is the weight given to mode m; and W is the sum of the relative weights for the seven even modes (W = 19.98).

Similar overall sums were obtained for the minimum and maximum EGR points shown in figure 7.9 to produce figures 7.10 to 7.13 for each bowl shape. This process of calculation was repeated for the NOx emissions at the minimum, maximum, and optimum EGR levels defined by the particulates versus NOx trade-offs.

Calculation of the overall sum of weighted emissions from piston bowl shape STD

Table 7.2 MINIMUM PARTICULATES

mode no	NOx (g/hr)	Parts (g/hr)	Mode weight	weighted NOx (g/hr)	weighted Parts (g/hr)
2	2.6	3.15	4.04	10.50	12.73
4	17.7	5.35	2.38	42.13	12.73
6	11.48	8.18	6.02	69.11	49.24
8				0.00	0.00
10	53.78	8.27	3.30	177.47	27.29
12	25.86	10.42	3.39	87.67	35.32
14	118.28	8.32	0.85	100.54	7.07
			19.98	487.42	144.39
		overall sum of weigthed emission =		24.40	7.23

Table 7.3 MAXIMUM PARTICULATES

mode no	NOx (g/hr)	Parts (g/hr)	Mode weight	weighted NOx (g/hr)	weighted Parts (g/hr)
2	0.45	4.27	4.04	1.82	17.25
4	2.27	9.93	2.38	5.40	23.63
6	1.93	41.5	6.02	11.62	249.83
8				0.00	0.00
10	7.75	28.03	3.30	25.58	92.50
12	8.95	17.18	3.39	30.34	58.24
14	17.82	23.48	0.85	15.15	19.96
			19.98	89.90	461.41
		overall sum of weigthed emission =		4.50	23.09

Table 7.4 OPTIMUM PARTICULATES

mode no	NOx (g/hr)	Parts (g/hr)	Mode weight	weighted NOx (g/hr)	weighted Parts (g/hr)
2	0.94	3.72	4.04	3.80	15.03
4	7.16	5.62	2.38	17.04	13.38
6	3.85	8.34	6.02	23.18	50.21
8				0.00	0.00
10	15.6	13.79	3.30	51.48	45.51
12	17.71	11.72	3.39	60.04	39.73
14	35.26	13.67	0.85	29.97	11.62
			19.98	185.50	175.47
		overall sum of weigthed emission =		9.28	8.78

OVERALL SUM NOx	OVERALL SUM PARTS
24.40	7.23
9.28	8.78
4.50	23.09

Figure 7.10 Overall weigthed sum of particulate and NOx emission for bowl STD

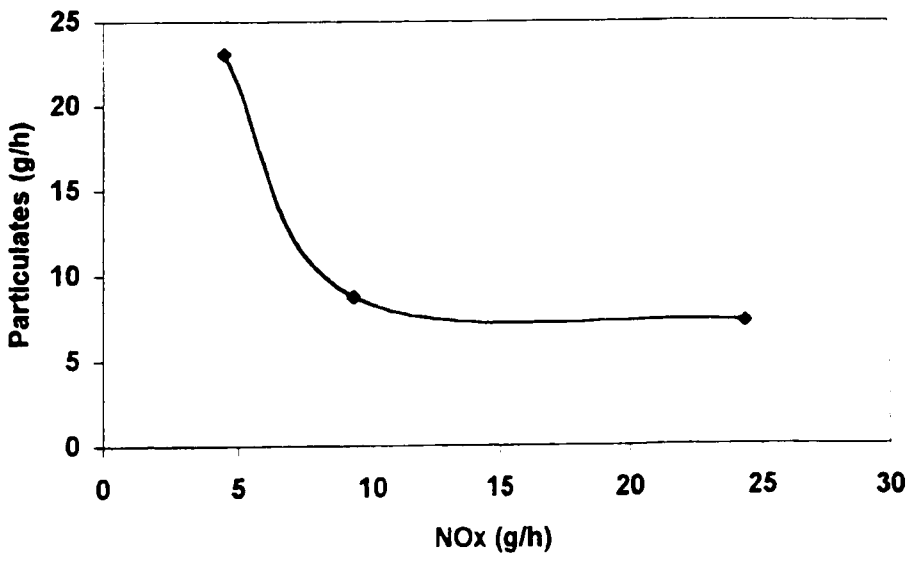

Calculation of the overall sum of weighted emissions from piston bowl shape ONE

Table 7.5 MINIMUM PARTICULATES

mode no	NOx (g/hr)	Parts (g/hr)	Mode weight	weighted NOx (g/hr)	weighted Parts (g/hr)
2	5.77	3.87	4.04	23.31	15.63
4	32.3	7.33	2.38	76.87	17.45
6	19.81	9.09	6.02	119.26	54.72
8				0.00	0.00
10	102.03	4.03	3.30	336.70	13.30
12	35.08	10.92	3.39	118.92	37.02
14	111.27	8.55	0.85	94.58	7.27
			19.98	769.64	145.39
		overall sum of weigthed emission =		38.52	7.28

Table 7.6 MAXIMUM PARTICULATES

mode no	NOx (g/hr)	Parts (g/hr)	Mode weight	weighted NOx (g/hr)	weighted Parts (g/hr)
2	1.4	4.46	4.04	5.66	18.02
4	3.3	12.88	2.38	7.85	30.65
6	3.51	25.91	6.02	21.13	155.98
8				0.00	0.00
10	9.45	47.33	3.30	31.19	156.19
12	8.97	12.84	3.39	30.41	43.53
14	21.83	25.55	0.85	18.56	21.72
			19.98	114.79	426.09
		overall sum of weigthed emission =		5.75	21.33

Table 7.7 OPTIMUM PARTICULATES

mode no	NOx (g/hr)	Parts (g/hr)	Mode weight	weighted NOx (g/hr)	weighted Parts (g/hr)
2	2.39	4.15	4.04	9.66	16.77
4	9.4	7.59	2.38	22.37	18.06
6	7.33	12.85	6.02	44.13	77.36
8				0.00	0.00
10	32.69	9.34	3.30	107.88	30.82
12	15.23	12.19	3.39	51.63	41.32
14	57.76	10.52	0.85	49.10	8.94
			19.98	284.76	193.28
		overall sum of weigthed emission =		14.25	9.67

OVERALL SUM NOx	OVERALL SUM PARTS
38.52	7.28
14.25	9.67
5.75	21.33

Figure 7.11 Overall weigthed sum of particulate and NOx emission for bowl ONE

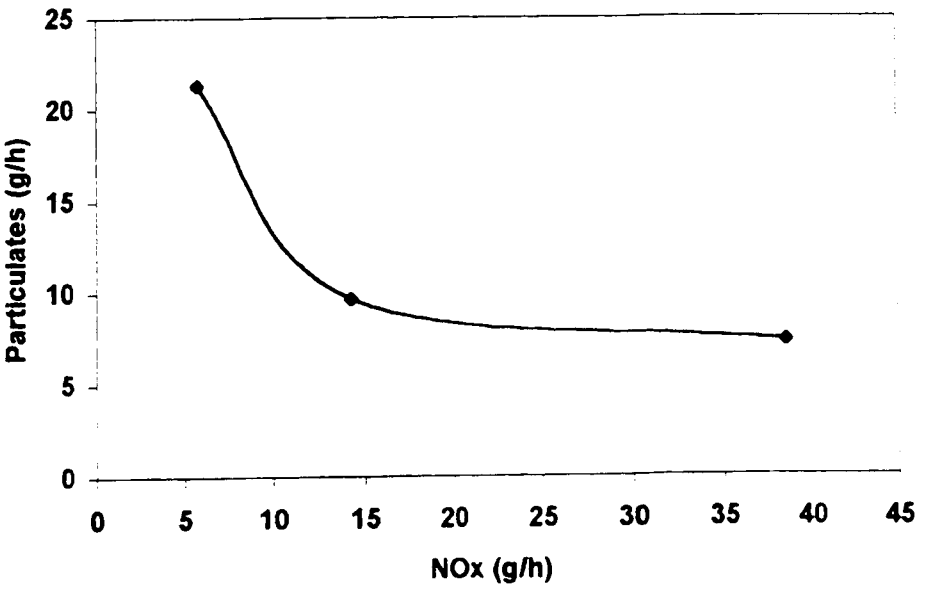

Calculation of the overall sum of weighted emissions from piston bowl shape TWO

Table 7.8 MINIMUM PARTICULATES

mode no	NOx (g/hr)	Parts (g/hr)	Mode weight	weighted NOx (g/hr)	weighted Parts (g/hr)
2	6.95	3.91	4.04	28.08	15.80
4	19.76	9.93	2.38	47.03	23.63
6	13.73	9.98	6.02	82.65	60.08
8				0.00	0.00
10	54.37	16.88	3.30	179.42	55.70
12	37.88	19.94	3.39	128.41	67.60
14	150.37	15.49	0.85	127.81	13.17
			19.98	593.41	235.98
	overall sum of weigthed emission =			29.70	11.81

Table 7.9 MAXIMUM PARTICULATES

mode no	NOx (g/hr)	Parts (g/hr)	Mode weight	weighted NOx (g/hr)	weighted Parts (g/hr)
2	0.48	5.71	4.04	1.94	23.07
4	2.37	17.27	2.38	5.64	41.10
6	2.09	40.74	6.02	12.58	245.25
8				0.00	0.00
10	24.87	28.14	3.30	82.07	92.86
12	10.21	26.99	3.39	34.61	91.50
14	40.91	34.82	0.85	34.77	29.60
			19.98	171.62	523.38
	overall sum of weigthed emission =			8.59	26.20

Table 7.10 OPTIMUM PARTICULATES

mode no	NOx (g/hr)	Parts (g/hr)	Mode weight	weighted NOx (g/hr)	weighted Parts (g/hr)
2	2.32	4.53	4.04	9.37	18.30
4	4.89	13.3	2.38	11.64	31.65
6	5.12	17.46	6.02	30.82	105.11
8				0.00	0.00
10	35.18	22.12	3.30	116.09	73.00
12	14.65	23.82	3.39	49.66	80.75
14	57.8	22.83	0.85	49.13	19.41
			19.98	266.72	328.22
	overall sum of weigthed emission =			13.35	16.43

OVERALL SUM NOx	OVERALL SUM PARTS
29.70	11.81
13.35	16.43
8.59	26.20

Figure 7.12 Overall weigthed sum of particulate and NOx emission for bowl TWO

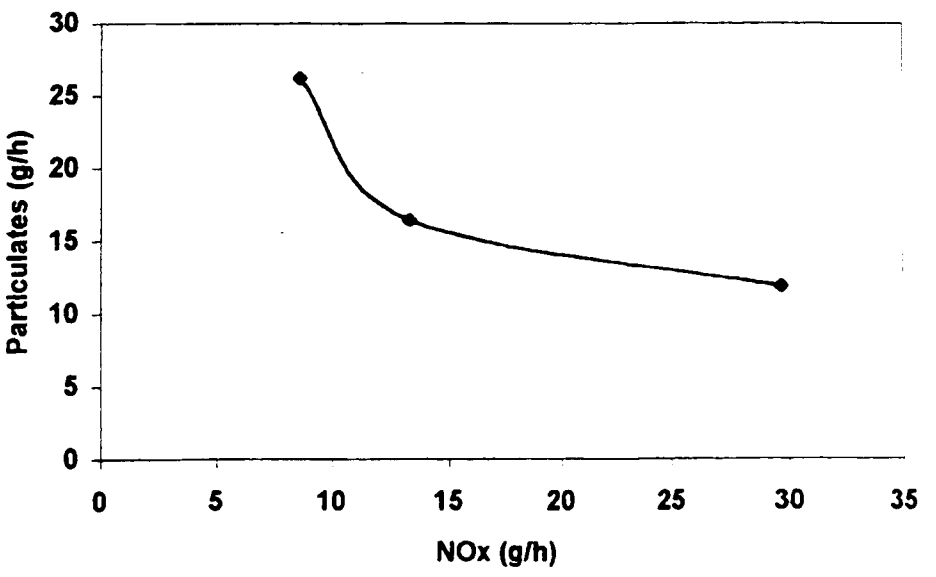

Calculation of the overall sum of weighted emissions from piston bowl shape THREE

Table 7.11 MINIMUM PARTICULATES

mode no	NOx (g/hr)	Parts (g/hr)	Mode weight	weighted NOx (g/hr)	weighted Parts (g/hr)
2	8.77	3.43	4.04	35.43	13.86
4	22.38	6.87	2.38	53.26	16.35
6	20.18	8.23	6.02	121.48	49.54
8	25.58	12.38		0.00	0.00
10	88.33	7.73	3.30	291.49	25.51
12	48.88	11.81	3.39	165.70	40.04
14	167.96	10.14	0.85	142.77	8.62
			19.98	810.14	153.92
		overall sum of weigthed emission =		40.55	7.70

Table 7.12 MAXIMUM PARTICULATES

mode no	NOx (g/hr)	Parts (g/hr)	Mode weight	weighted NOx (g/hr)	weighted Parts (g/hr)
2	0.88	4.05	4.04	3.56	16.36
4	3.04	12.35	2.38	7.24	29.39
6	2.92	36.59	6.02	17.58	220.27
8	7.74	24.53		0.00	0.00
10	8.96	40.18	3.30	29.57	132.59
12	9.74	30.68	3.39	33.02	104.01
14	25.57	28.62	0.85	21.73	24.33
			19.98	112.69	526.95
		overall sum of weigthed emission =		5.64	26.37

Table 7.13 OPTIMUM PARTICULATES

mode no	NOx (g/hr)	Parts (g/hr)	Mode weight	weighted NOx (g/hr)	weighted Parts (g/hr)
2	1.90	3.60	4.04	7.68	14.54
4	6.80	9.26	2.38	16.18	22.04
6	5.95	14.10	6.02	35.82	84.88
8	14.79	16.91		0.00	0.00
10	18.53	15.10	3.30	61.15	49.83
12	15.31	21.06	3.39	51.90	71.39
14	67.74	12.12	0.85	57.58	10.30
			19.98	230.31	252.99
		overall sum of weigthed emission =		11.53	12.66

OVERALL SUM NOx	OVERALL SUM PARTS
40.55	7.70
11.53	12.66
5.64	26.37

Figure 7.13 Overall weigthed sum of particulate and NOx emission for bowl shape THREE

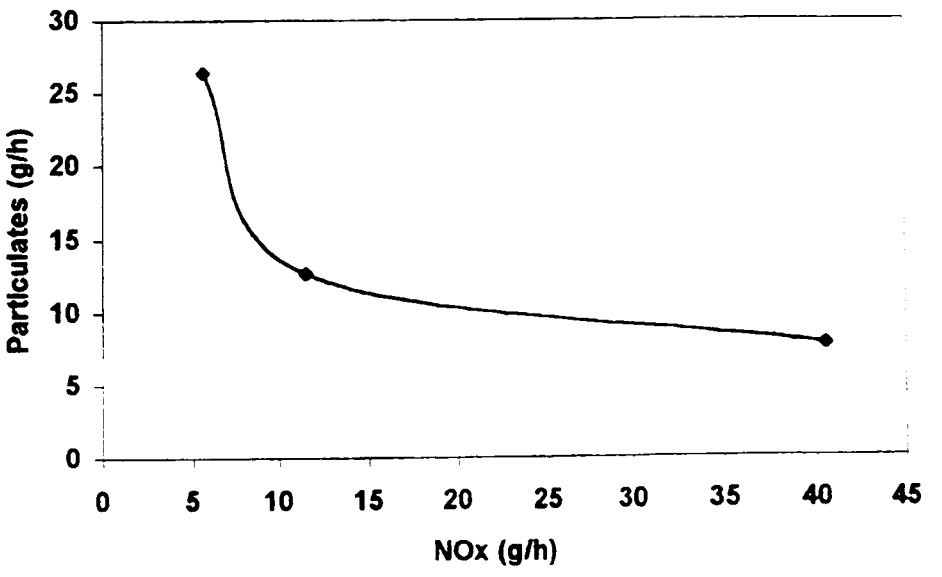

7.4.2 Comparison of overall particulates versus NOx variation, from each piston bowl shape

Figure 7.14 shows the overall particulates versus NOx performance for all four piston bowl shapes tested.

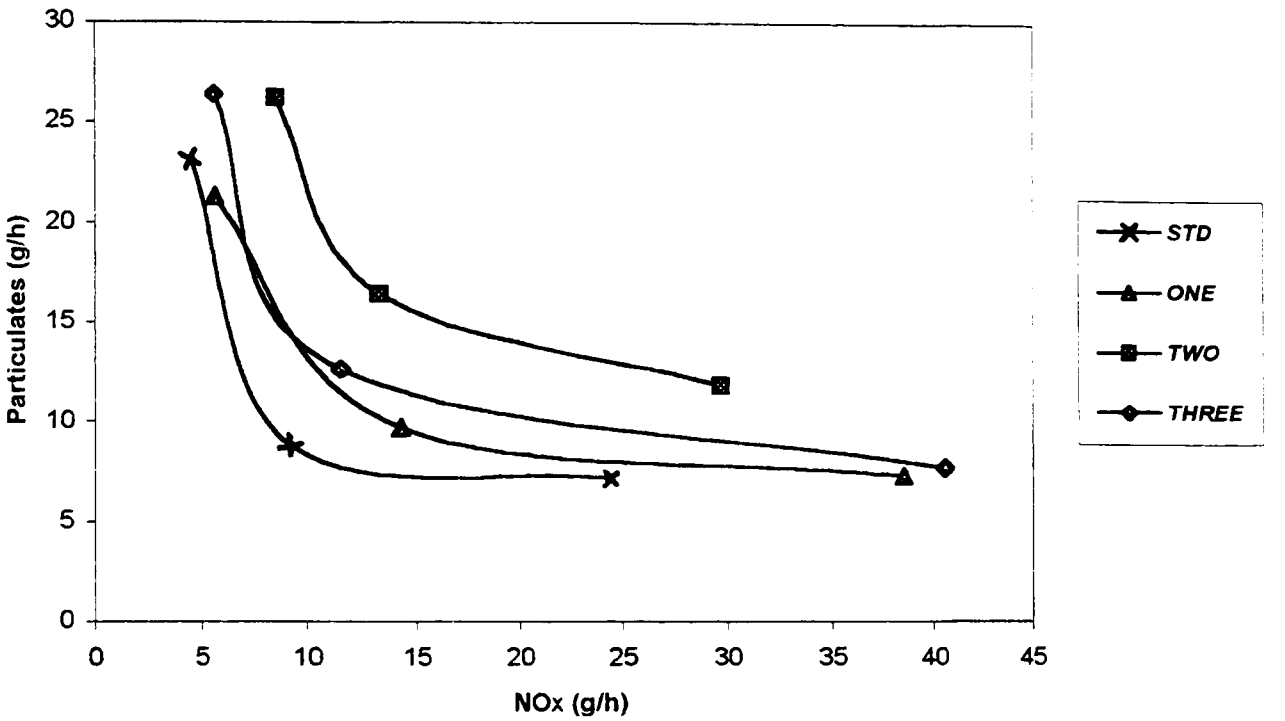

Figure 7.14 Overall piston bowl shape comparison. Weighted averaged particulates versus NOx performance from EGR loops at each mode test condition, but excluding mode 8.

Piston bowl shape TWO had the worst overall particulates versus NOx trade-off of all piston bowl shapes tested. This was expected, given the previous analysis of injector optimisation results had indicated the poor air utilisation of bowl shape TWO.

Piston bowl shape THREE, despite having similar basic dimensions to bowl shape STD, produced poor particulates versus NOx performance. Bowl shape THREE also showed the widest range of emissions results. Small changes in the level of EGR produced large variations in the emission of NOx and particulates. It was possible that the relatively small minor radii, especially around the bowl lip, may have adversely

affected airflow and made the bulk airflow more sensitive to minor changes in EGR level, although it was not possible to verify this in practice.

The best particulates versus NOx performance was obtained using piston bowl shape STD, although the optimum condition required careful control of the level of EGR, in order to avoid excessive particulates at high EGR levels. When the overall shape of the particulates versus NOx graphs were compared, it was evident that as performance was improved, the bowl became more sensitive to EGR level when operating close to the optimum emission point.

Piston bowl shape ONE produced a fairly favourable particulates versus NOx trade-off, despite having a completely different shape to the best performing bowl (bowl STD). It was possible that the good performance of bowl STD and bowl ONE, might be partly attributable to concentrating a greater proportion of their total bowl volume towards the centre of the bowl. This might have reduced the maldistribution of intake charge, caused by the centrifuging action of swirl on the contents of the piston bowl.

7.5 Conclusions

For a given piston bowl shape, the magnitude of particulate and NOx emissions varied significantly between different mode test conditions. This was principally due to the difference in engine speed and load at different modes. Injection timing was also influential, especially for the most retarded mode test conditions, such as mode 8.

The overall comparison of emissions (the weighted sum) between different piston bowl shapes, showed substantial differences in particulate and NOx levels. The standard piston bowl shape (STD) proved to be the best performing bowl shape, although the sensitivity of emissions to the level of EGR around the optimum level was relatively high for this bowl.

The next best performing bowl was shape ONE, whilst the worst performing bowl was bowl shape TWO (having a wide aspect ratio). The poor performance of bowl

shape TWO was identified from injector optimisation tests (chapter 5) to be due to the poor air utilisation of this bowl.

Piston bowl shape THREE, whilst sharing similar basic dimensions to the standard bowl shape, and designed to exploit the benefits of fuel impingement on the bowl lip, did not perform as well as had been expected. Bowl THREE was also the most sensitive to the level of EGR of all bowl shapes tested, with small changes in the level of EGR resulting in large changes in emissions.

Chapter 8:

Effect of in-cylinder swirl on combustion and emissions

Chapter 8: Effect of in-cylinder swirl on combustion and emissions

8.1 Introduction

The effect of in-cylinder swirl on emissions and combustion was investigated. Two different piston bowl shapes were tested at various mode test conditions, with and without EGR. These two bowls had widely different aspect ratios, and therefore, substantially different in-bowl swirl ratios.

In-cylinder swirl variation was made possible by progressively reducing airflow through one of the dual intake ports of each cylinder, until airflow through this port ceased. By progressively reducing the airflow through the most "directed" of the two ports, airflow through the other "helical port" was increased, resulting in an increase in the intake-generated, in-cylinder swirl level. A detailed description and calibration (at steady state) of the port variable-swirl system was presented in chapter 3, section 3.3.3.

Engine performance with an increase in the intake-generated swirl level is reported in this chapter. Included, is also a comparison of the effect of piston bowl shape on the optimum swirl ratio for each engine mode tested. A significant decrease in engine volumetric efficiency when the swirl ratio was increased (especially at high engine speed and loads) often masked the underlying trend in emission results.

8.2 Swirl-test conditions

Piston bowl shapes TWO and THREE were chosen for testing because they differed widely in aspect ratio. This resulted in different in-bowl swirl amplification during compression. Dimensioned sections of piston bowl shapes TWO and THREE were presented in chapter 4, section 4.3, figure 4.9.

For each piston bowl shape, four engine test modes were chosen at which to vary the intake generated swirl level. The tests at these four modes were performed with the level of EGR considered optimum by Ford for bowl shape STD at each mode. Each mode test was also repeated without EGR for comparison. Table 8.1 presents the full set of test conditions used to evaluate the effect of in-cylinder swirl on emissions.

Test No.	Test mode	Speed (rpm)	Load (Nm)	SOI (degrees)	EGR (%)
1	2	1000	14.0	2	0
2	6	1800	27.9	4	0
3	10	2300	83.7	-2	0
4	14	3200	69.8	-6	0
5	2	1000	14.0	2	50
6	6	1800	27.9	4	30
7	10	2300	83.7	-2	30
8	14	3200	69.8	-6	40

Table 8.1 Test conditions used to evaluate the effect of intake-generated swirl on combustion, and exhaust emissions. The tests also identified the effect of piston bowl shape on the optimum swirl ratio (note that tests 5 to 8 were performed at the same mode conditions as tests 1 to 4, but with the addition of EGR).

At each test number (1 to 8 above), intake swirl was increased in discrete steps by closing the port airflow reducing flap mechanism (henceforth referred to as the port "de-activation" mechanism). The first 30 degrees of the port de-activation flap closure actually resulted in a slight decrease in the swirl ratio, possibly due to interaction between the air-flows out of the two separate intake ports. At greater port de-activation flap angles, the intake-generated swirl from the more helical port design dominated, increasing the swirl of the air trapped inside the cylinders at inlet valve closure.

8.3 Effect of in-cylinder swirl on smoke, particulates and NOx performance

The effect of swirl ratio on engine-out emissions depended on the engine test condition, and whether EGR was added. Mostly, the results from piston bowl shape THREE were used to determine the effect of swirl ratio, because the trends for different bowl shapes were found to be qualitatively similar. Differences in the effects of swirl on emissions for different bowl shapes are discussed in section 8.4.

Results from each mode test (with and without EGR), for piston bowl shape THREE, are presented and discussed in the sub-sections below.

8.3.1 Effect of in-cylinder swirl at test mode 2

Figure 8.1 shows the response of NOx to an increase in in-cylinder swirl ratio, at test mode 2 (see table 8.1), with and without EGR.

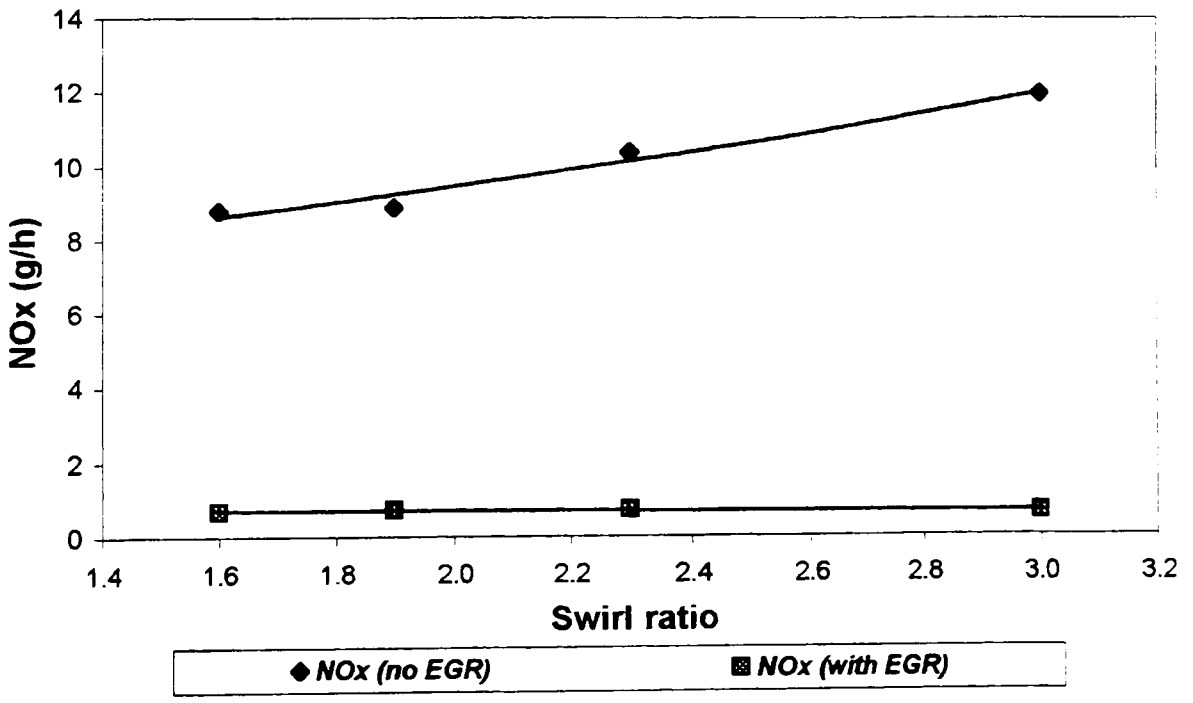

Figure 8.1 Variation of NOx with in-cylinder swirl ratio, for piston bowl THREE, at test mode 2 (1000 rpm, 14.0 Nm, SOI 2 degrees ATDC), with and without 50% EGR.

Test mode 2 illustrated many features which prevailed throughout testing at different mode conditions. Total NOx emission for mode 2 was low, as a result of the very low engine load and speed, despite the high air/fuel ratio (and thus availability of oxygen). However, when the vast excess of air was replaced by 50% EGR, a significant reduction in the emission of NOx resulted. This was most likely a result of reduced flame temperature, as the flame temperature is closely related to oxygen concentration in the intake (Hentschel (1996) and Ladommatos et al (1996) have shown close correlation between oxygen concentration and NOx formation).

An increase in the swirl ratio when testing with EGR (see figure 8.1) did not result in an increase in the formation of NOx, as might have been expected from an increase in the rate of mixing (and thus combustion). This may have been due to the associated reduction in inlet mass airflow as swirl was increased, reducing the effective air/fuel ratio and thus combustion temperature.

A progressive increase in the in-cylinder swirl ratio when testing without EGR, resulted in an almost linear increase in NOx (see figure 8.1). This was probably due to a faster rate of air/fuel mixing and combustion, thus raising the flame temperature. This happened despite a reduction of the engine volumetric efficiency (and thus intake air mass flow rate, reducing oxygen content in the engine cylinder), as a result of the more restricted total inlet tract from closing of the directed port.

The small deviation from the trend of NOx versus swirl ratio for the "without EGR" case (see figure 8.1), at a swirl ratio of 1.9 (fully open directed port), was due to minor differences in airflow compared to the minimum swirl condition. This anomaly was observed throughout the majority of test condition modes, and was most prominent in the without EGR cases.

The response of smoke emission to an increase in swirl ratio is shown in figure 8.2, at test mode 2, with and without EGR.

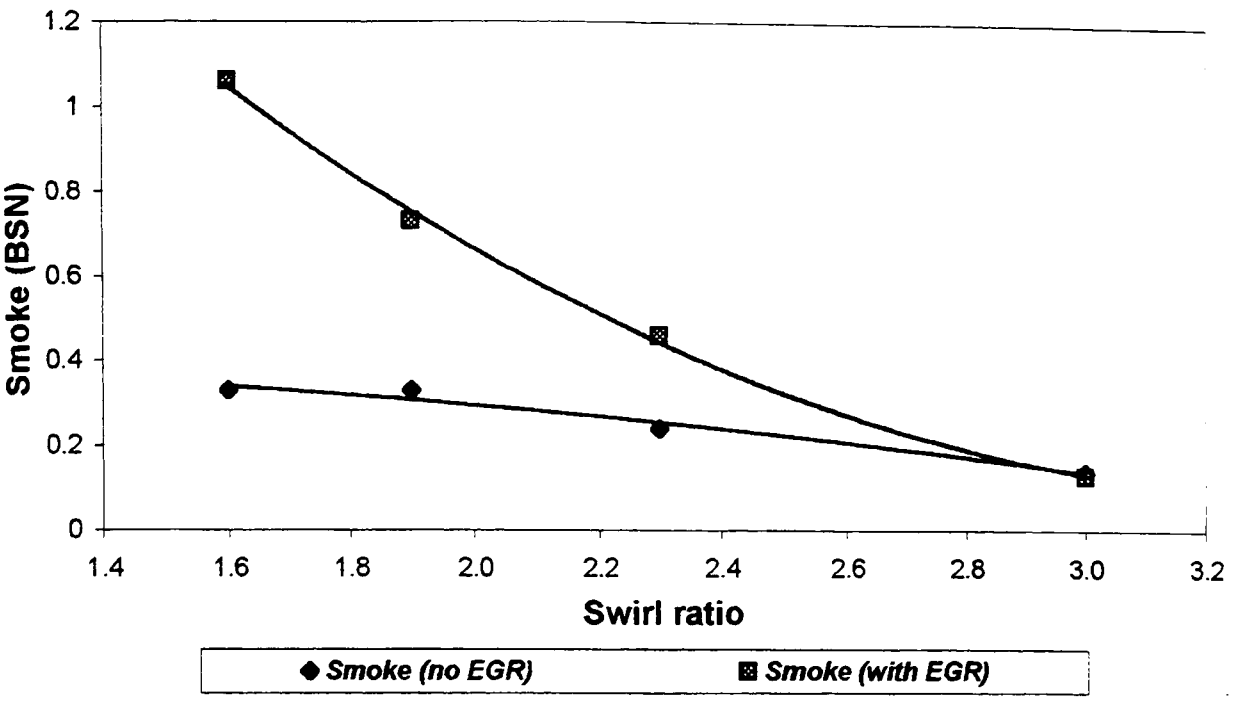

Figure 8.2 Variation of smoke with in-cylinder swirl ratio, for piston bowl THREE, at test mode 2 (1000 rpm, 14.0 Nm, SOI 2 degrees ATDC), with and without 50% EGR.

As was expected, the emission of smoke at the standard swirl ratio (with the directed port full open) was higher when operating with EGR than without EGR. This was most likely due to the reduced availability of oxygen when operating with 50% EGR, creating locally very rich regions, contributing to the emission of smoke. The increase in swirl enabled these rich regions to be broken up, enabling better utilisation of the scarcer oxygen.

When the swirl ratio was increased, the emission of smoke with EGR reduced at a greater rate than without EGR. At a swirl ratio of 3.0, the emission of smoke for both cases was nearly identical. The very large reduction in the emission of smoke with EGR, caused by the increase in swirl, was made possible because of the quantity of excess air still available when operating with 50% EGR at the light load of mode 2 (at very light loads the EGR would itself contain a high proportion of oxygen, and partially oxidised hydrocarbons). An increase in the swirl ratio to 3.0 was just enough to ensure adequate mixing, and reduced the level of smoke emission with EGR down to that of without EGR.

At higher engine load and speed (detailed later), there was in-sufficient oxygen and mixing, when operating with EGR, to reduce the emission of smoke to without EGR conditions, within the range of swirl ratios available.

8.3.2 Effect of in-cylinder swirl at test mode 6

Test mode 6 differed from mode 2, by the engine being operated at a higher speed and load (although the engine load was still relatively low at 27.9 Nm). Injection timing was at 4 degrees after TDC, the most retarded of all the swirl test conditions.

The trend in the formation of NOx with increased swirl (not shown here), was very similar to that of test condition mode 2. The absolute values had increased however, because of the increased fuel energy input, which had resulted from operating at a higher engine load. Operating at a higher engine load had reduced the air/fuel ratio, making the mixing of fuel with fresh air, in order to avoid the production of smoke, more difficult. This was compounded by the late injection timing, which caused a greater proportion of fuel to be burned in the late combustion, soot-forming phase. Figure 8.3 shows the variation of the emission of smoke with in-cylinder swirl ratio, with and without EGR.

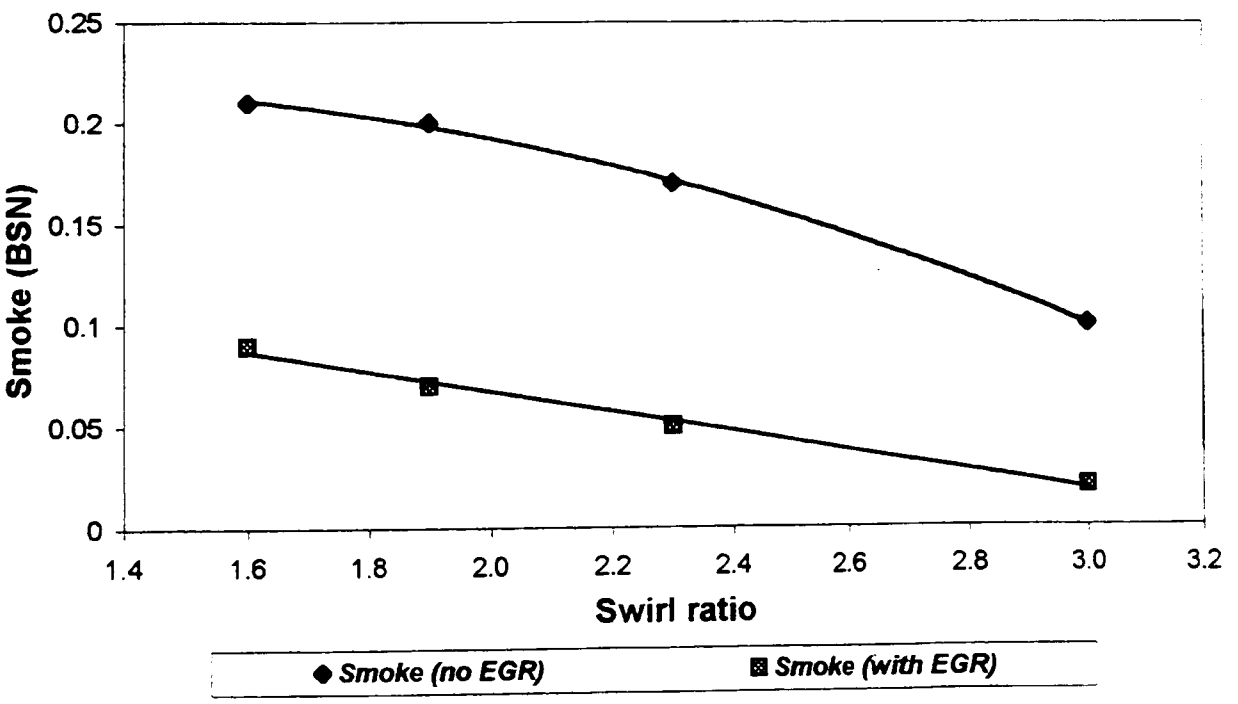

Figure 8.3 Variation of smoke with in-cylinder swirl ratio, for piston bowl THREE, at test mode 6 (1800 rpm, 27.9 Nm, SOI 4 degrees ATDC), with and without 30% EGR.

Initial values of smoke emission, before an increase in the swirl ratio, were much lower than from test mode 2, despite a more retarded injection timing. This may have been due to an increase in the combustion gas temperature, promoting soot oxidation late in the expansion phase.

The results from test mode 6, as shown in figure 8.3 were unusual in that the smoke emission with EGR was actually lower than without EGR, at any given swirl ratio. The same trend was also observed from swirl testing of piston bowl shape TWO. It is probable that an increase in the intake charge temperature, when operating with EGR, caused a reduction in the ignition delay period. This would have moved the start of combustion closer to TDC (the retarded injection timing of mode 6 resulted in a higher proportion of late heat release), and increased the rate of heat release and combustion gas temperature. A reduction in smoke resulted from the more advanced combustion, despite being offset by a reduction in the soot-free pre-mixed combustion phase.

The reduction in the formation of smoke with EGR, when the level of in-cylinder swirl was increased, was limited by the mixing time and the availability of oxygen in the intake charge. This was unlike test mode 2, where a vast excess of air, even when operating with 50% EGR, was available for soot oxidation. However, it was probable that if swirl ratio could have been increased further (without a large penalty in the reduction of engine volumetric efficiency), smoke could have been reduced.

8.3.3 Effect of in-cylinder swirl at test mode 10

Test mode 10 was performed at an engine load of 83.7 Nm, the highest of all swirl test conditions. This resulted in much higher concentrations of NOx in the exhaust, as a result of the higher combustion flame temperature. Figure 8.4 illustrates the variation of NOx with an increase in the level of in-cylinder swirl level, both with and without EGR.

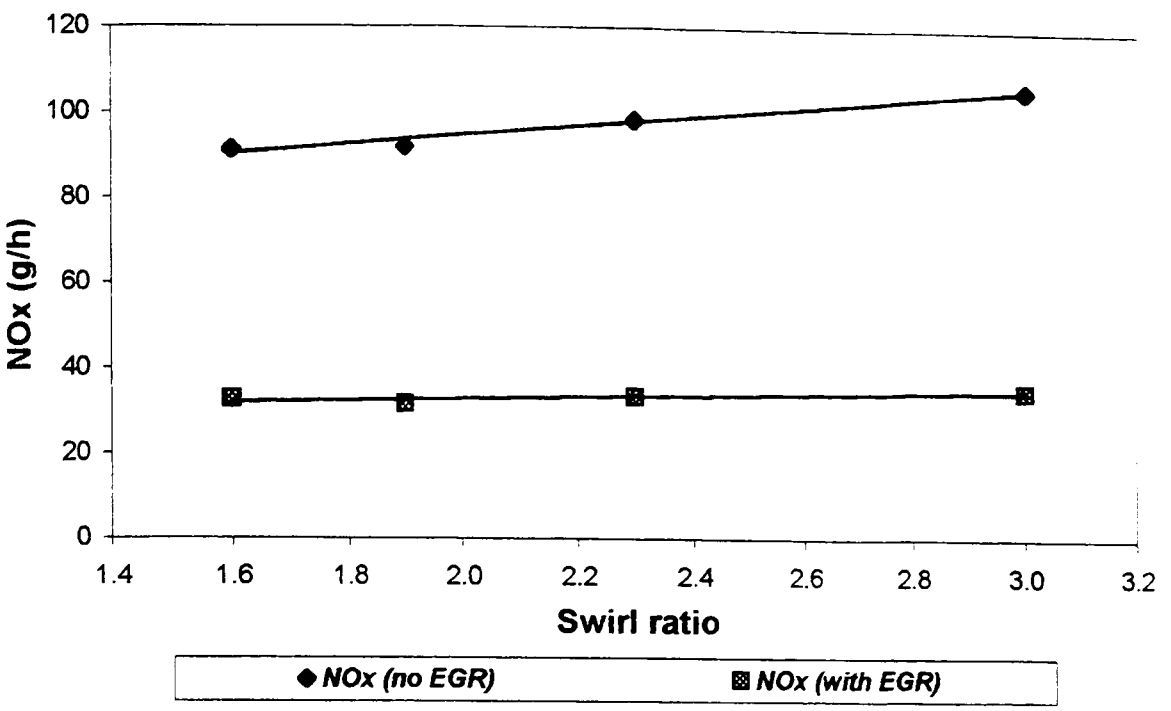

Figure 8.4 Variation of NOx with in-cylinder swirl ratio, for piston bowl THREE, at test mode 10 (2300 rpm, 83.7 Nm, SOI 2 degrees BTDC), with and without 30% EGR.

The most significant difference in the trend for NOx emissions, with an increase in swirl ratio between mode 10 and previous modes, was the relatively small increase in NOx when swirl ratio was nearly doubled. The rate of mixing, and thus combustion, is generally accepted to be directly related to the swirl ratio (Khan et al, 1972; Hiroyasu et al, 1986). It was therefore likely that the increase in NOx was offset by a considerable reduction of engine volumetric efficiency, and thus inlet mass airflow (of 5% when operating without EGR), because of restriction when the directed port was progressively closed. This would have reduced the availability of oxygen in the combustion chamber (the air/fuel ratio was reduced from 40:1 to 35:1), thus reducing the flame temperature and the rate of NOx formation.

Whilst the reduction in engine volumetric efficiency (and associated reduction in air/fuel ratio) seems to have been the dominate factor in NOx production, this would have been offset by the reduced trapped mass (leading to higher cylinder temperature, since the heat released from the same fuel amount is absorbed by a smaller total trapped mass).

At test mode 10, the effect of an increase in the in-cylinder swirl ratio was to *increase* the emission of smoke, for both with and without EGR, as shown in figure 8.5 below.

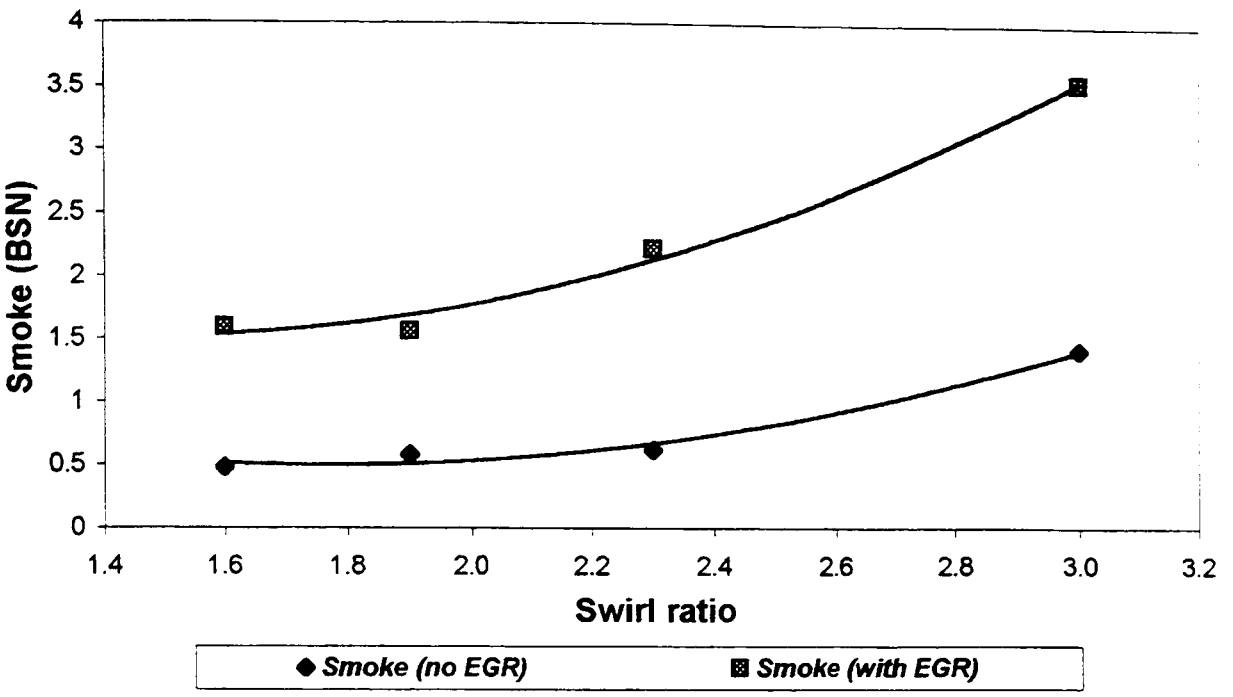

Figure 8.5 Variation of smoke with in-cylinder swirl ratio, for piston bowl shape THREE, at test condition mode 10 (2300 rpm, 83.7 Nm, SOI -2 degrees BTDC), with and without 30% EGR.

The observed increase in the emission of smoke, as the level of in-cylinder swirl was increased, was most likely due to the reduction of intake volumetric efficiency and air mass flow rate, and increase in fuel consumption necessary to maintain the desired engine speed and load. This would have increased the proportion of soot rich regions in the combustion chamber, and made soot oxidation late in the expansion stroke more difficult.

Test mode 10 could probably have benefited from a *reduction* of intake generated swirl (thereby increasing the volumetric efficiency) below the engine design level without port deactivation. In contrast, test modes 2 and 6, have benefited from an increase of in-cylinder swirl to reduce emissions. Therefore, the optimum swirl levels for this engine vary depending on the test mode. High swirl, at the expense of volumetric efficiency is not a viable strategy at test modes involving high engine loads and speeds, and thus lower trapped air/fuel ratios.

8.3.4 Effect of in-cylinder swirl at test mode 14

Figure 8.6 illustrates how the emission of NOx was actually reduced at high in-cylinder swirl levels. This is likely to have arisen as a result of reduced intake air mass flow rate from the considerably restricted intake system, when operating at the high engine speed of 3200 rpm.

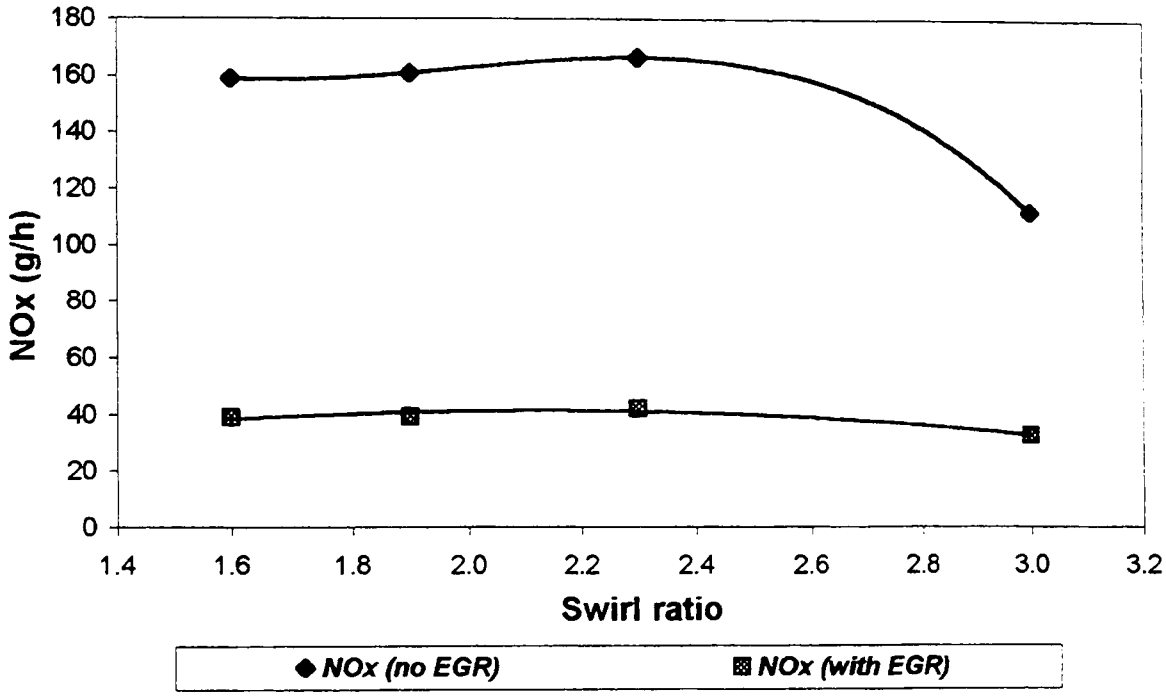

Figure 8.6 Variation of NOx with in-cylinder swirl ratio, for piston bowl shape THREE, at test mode 14 (3200 rpm, 69.8 Nm, SOI 6 degrees BTDC), with and without 40% EGR.

The NOx emission level without EGR was the highest of all mode test conditions. This was because of the high engine speed, and relatively high engine load raising the combustion temperature. Another significant factor in raising flame temperature, and thus NOx production, was the advanced injection timing, 6 degrees before TDC. Furthermore, the high engine speed results in the NO formed around TDC "freezing" at high levels, since less time is available for dissociation of NO during the early stages of the expansion process [Heywood, 1988]. EGR was very effective at reducing the emission of NOx, especially at low in-cylinder swirl levels.

Intake mass airflow was reduced by 41% between the minimum and maximum swirl ratios tested. This combined with an increase in the rate of fuelling, resulted in a significant reduction of the in-cylinder air/fuel ratio and oxygen availability for NOx production, hence reducing engine out NOx emissions. A decrease in NOx occurred despite the reduced air/fuel ratio being offset by reduced trapped mass, and thus higher in-cylinder temperature because less mass was available to absorb the heat released during combustion.

The variation of smoke with in-cylinder swirl ratio showed a similar trend to that of test mode 10. An increase in swirl resulted in an increase in the emission of smoke, despite a probable increase in the rate of mixing. This trend was most likely dominated by the reduction of the engine volumetric efficiency, and thus intake mass airflow rate, as had been observed from many other test conditions.

8.4 Effect of piston bowl shape on the optimum swirl ratio

8.4.1 Primary differences in bowl shapes

Piston bowl shapes TWO and THREE differed mainly in aspect ratio (the ratio of the maximum bowl width to the bowl depth). Piston bowl shape TWO had an aspect ratio of 3.48, whilst piston bowl shape THREE had an aspect ratio of just 2.70. The in-cylinder swirl ratio was amplified during compression by different amounts, as swirling air was forced into the piston bowl volume, as the piston approached TDC. Piston bowl shape THREE would have had a significantly higher in-bowl swirl level at the time of fuel injection, and higher combustion-induced gas flow.

The higher swirl modification properties of piston bowl shape THREE would have also increased heat transfer to the cylinder walls and combustion chamber surfaces, from the hot compressed air during compression, and from subsequent combustion gases. However, heat transfer to the piston bowl would have been offset by the

reduced surface area of piston bowl shape THREE. It was not possible to directly compare this aspect of combustion using heat release analysis, because the differences in heat transfer were too small.

8.4.2 Comparison bowl performance at low-speed mode tests

Comparison of emissions at low speed tests

Comparison of the trend in emissions, from the two piston bowl shapes at certain modes was possible. Figure 8.7 shows the emission of smoke from testing piston bowl TWO, at mode 6, with and without EGR.

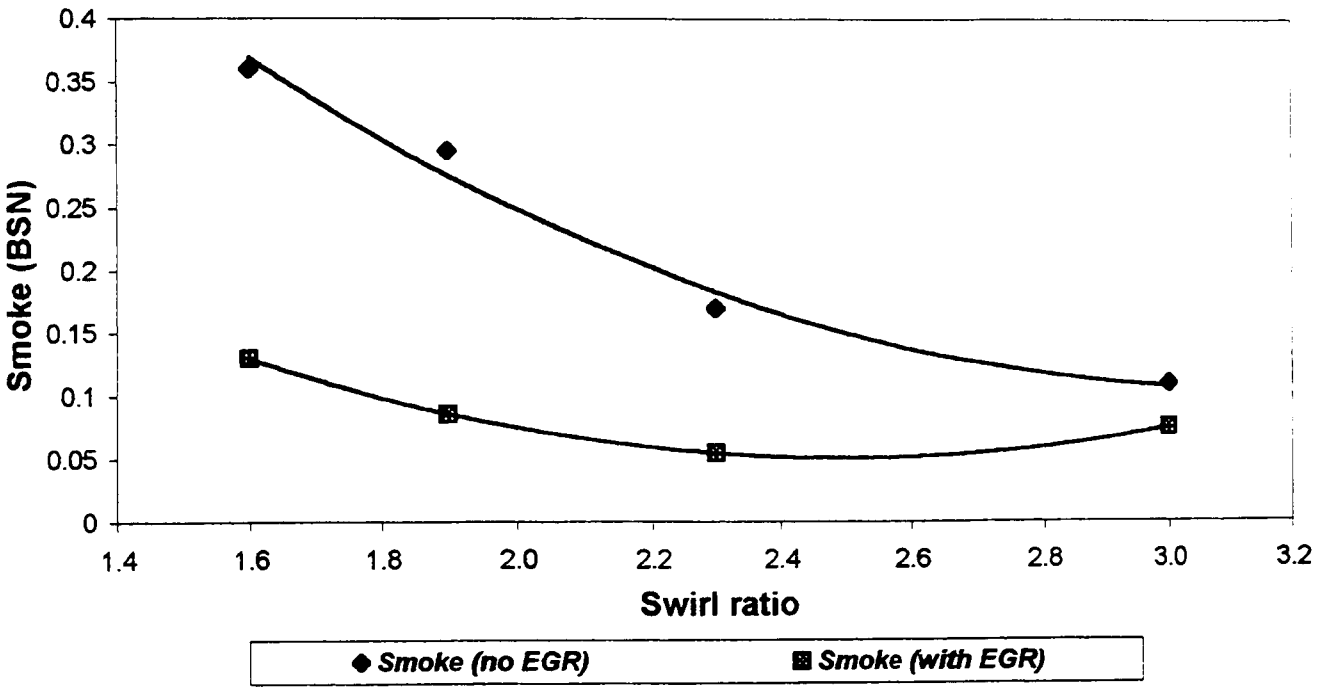

Figure 8.7 Variation of smoke with in-cylinder swirl ratio, for piston bowl TWO, at test mode 6 (1800 rpm, 27.9 Nm, SOI 4 degrees ATDC), with and without 30% EGR.

An increase in the swirl ratio resulted in a sharp decline in the emission of smoke from bowl shape TWO (see figure 8.7), as had been the case for bowl shape THREE but at the lower speed test mode 2 (figure 8.2, section 8.3.1). Piston bowl shape TWO required a higher intake-generated swirl level than bowl THREE for minimum

emissions for the first two, low speed, mode tests (modes 2 and 6). This was necessary to compensate for the reduction of in-bowl swirl amplification from the wider aspect ratio bowl.

Increasing swirl for bowl TWO, when operating at test mode 6 (see figure 8.7), reduced the emission of smoke by improving air/fuel mixing, and reducing the proportion of fuel involved in late (soot forming) combustion.

Comparison of the heat release at low speed tests

Figures 8.8 and 8.9 illustrate how the rate of heat release differed for bowl TWO between the highest and lowest swirl levels, at test mode 6, operating without EGR.

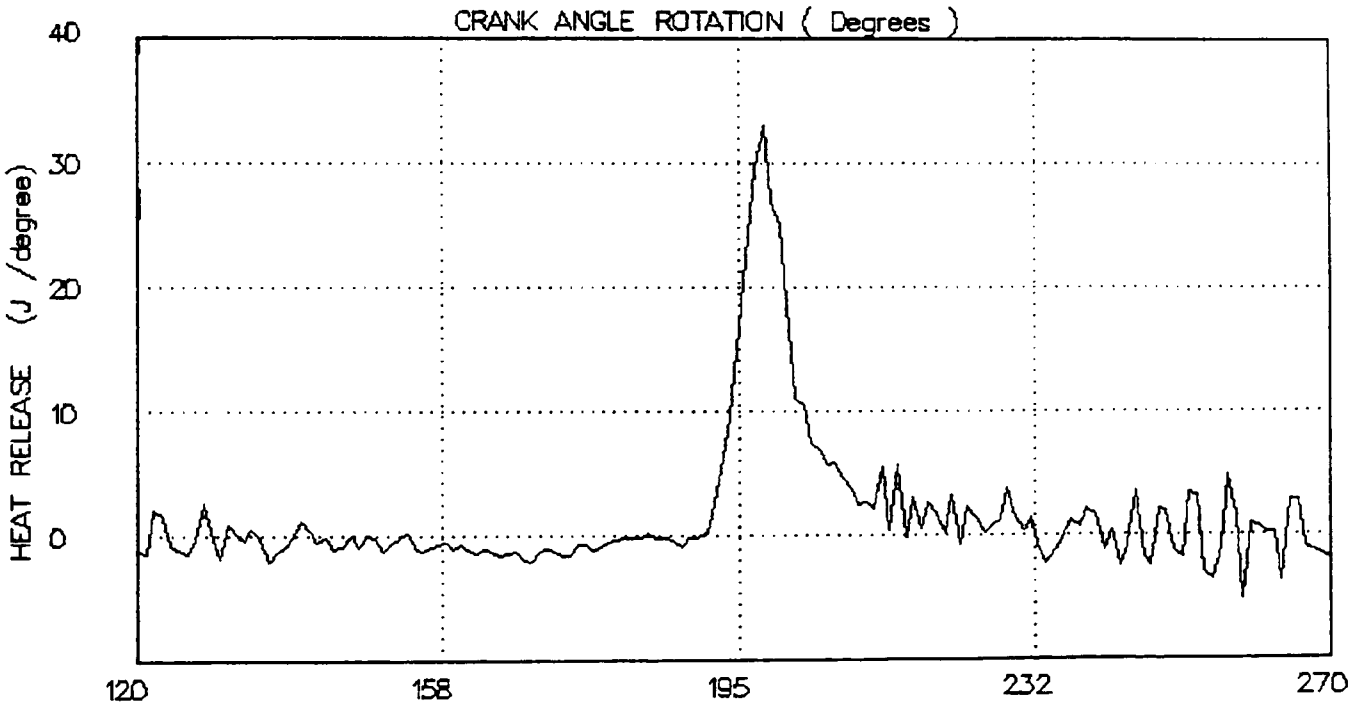

Figure 8.8 Rate of heat release from the minimum swirl experiment (swirl ratio 1.6), for piston bowl shape TWO, at test mode 6, without EGR.

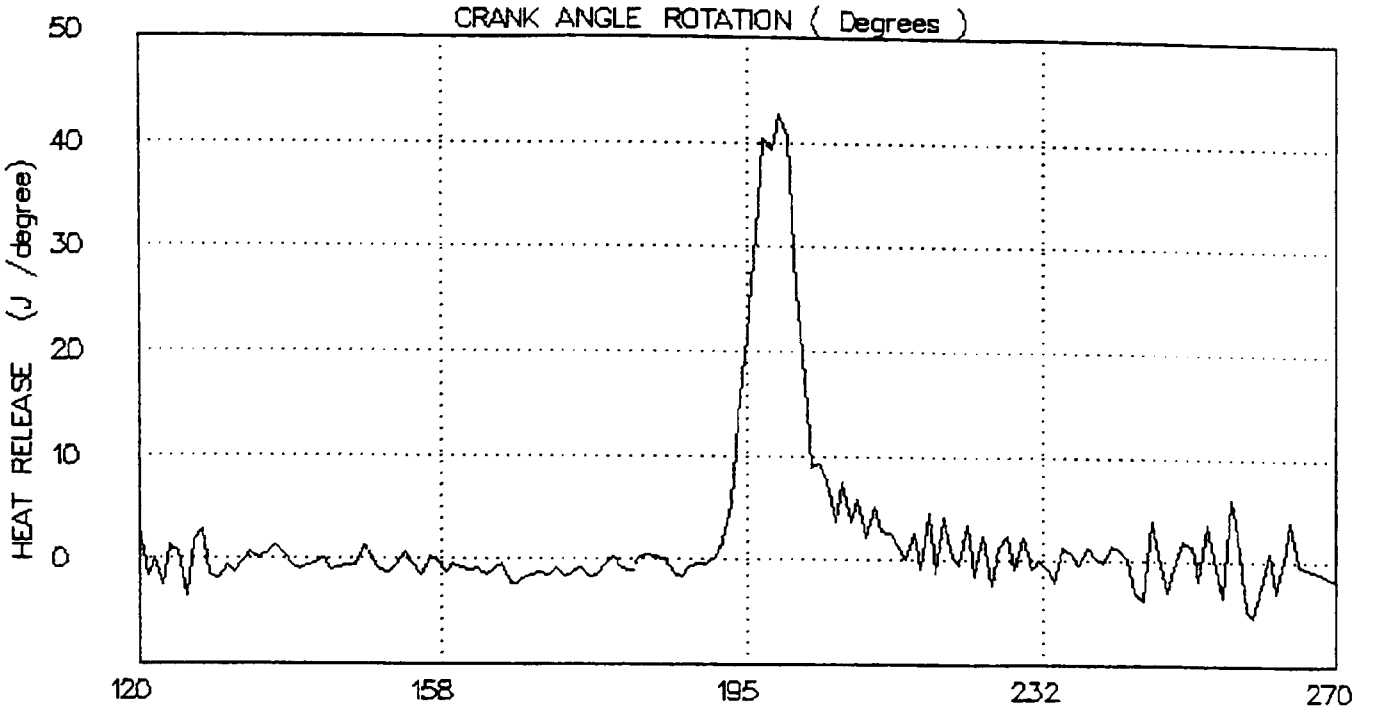

Figure 8.9 Rate of heat release from the maximum swirl experiment (swirl ratio 3.0), for piston bowl shape TWO, at test mode 6, without EGR.

The higher swirl ratio resulted in a much steeper rise in the rate of heat release (figure 8.9), and a higher peak heat release rate. Crucially, the proportion of heat release occurring in late combustion was reduced as the swirl ratio was increased. This was most likely a direct result of the increased rate of mixing and combustion, from an increase in the in-cylinder swirl ratio. Combustion gas temperature also increased significantly throughout the combustion cycle (and during compression as a result of improved turbo-charger performance) aiding soot oxidation.

The same increase in swirl ratio from 1.6 to 3.0 for bowl THREE at mode 6, also result in a marked change in the heat release rate (not shown), similar to bowl TWO. This reduced the emission of smoke (see figure 8.3), although by less than for bowl shape TWO (see figure 8.7). It was likely that the initial in-bowl swirl level in bowl THREE was already high enough to promote mixing and rapid combustion, and so did not suffer from high smoke at low swirl levels.

Production of HC emissions

Whilst an increase in swirl for bowl TWO reduced the emission smoke at the low speed mode tests (modes 2 and 6), the emission of HC did rise significantly, however,

to compensate for the gain in smoke emissions achieved. Figure 8.10 illustrates the change in the emission of HC from testing bowl shape TWO at mode 2, with 50% EGR.

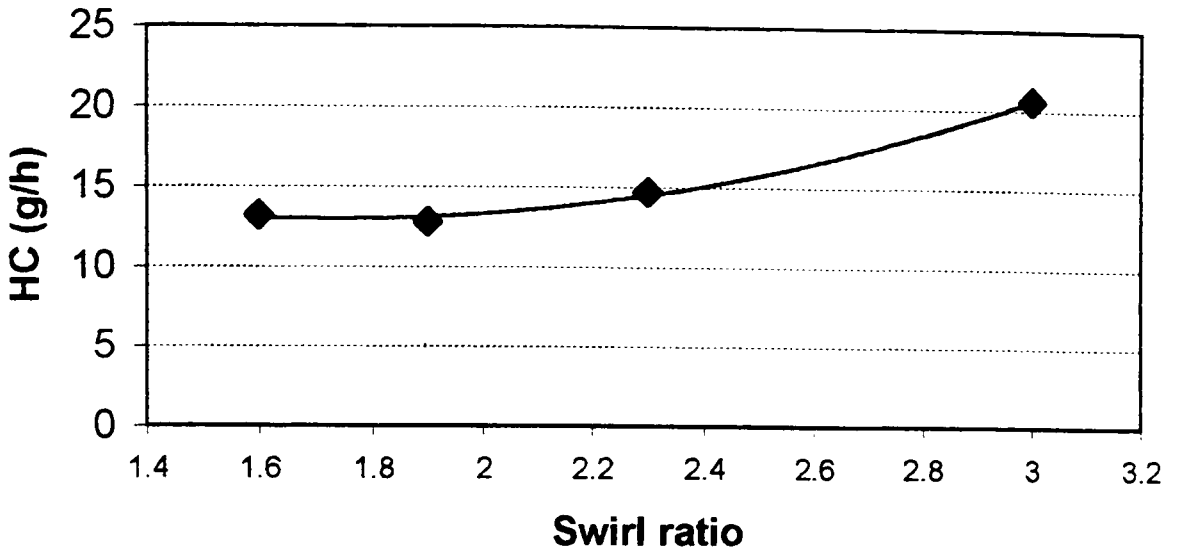

Figure 8.10 Variation of HC emission with an increase in swirl ratio, from testing piston bowl shape TWO at mode 2, with 50% EGR.

The increase in the emission of HC, when swirl was increased at low load test modes, was probably due to quenching and over-mixing of the injected fuel spray, such that it was cooled or became too lean to support combustion. It was possible that increased heat transfer to the combustion chamber surfaces also promoted HC formation. However, the same trend was not observed with bowl shape THREE (not shown), perhaps because of higher gas temperature throughout combustion, due to minimal heat rejection to the piston bowl surfaces.

8.4.3 Comparison bowl performance at high-speed mode tests

Analysis of the effect of swirl ratio on emissions from piston bowl shape THREE (section 8.3), had shown no benefit from an increase in swirl at the high speed mode conditions. Actually, a decrease in the emissions performance, due to throttling of the intake charge by the port deactivation system and associated reduction in engine volumetric efficiency was observed.

Intake system loses were likely to have been similar between the two bowl shapes tested (small differences did exist in the reduction of intake air mass flow rate with an increase in swirl ratio, due to different turbo-charger performance). This resulted in a roughly the same deterioration in volumetric efficiency with port de-activation closure. However, the emission of smoke from testing bowl shape TWO at the high-speed mode tests (modes 10 and 14), did not start to rise until a higher swirl ratio at any given mode test. Figure 8.11 shows a direct comparison between the emission of smoke at test mode 10, for bowls TWO and THREE.

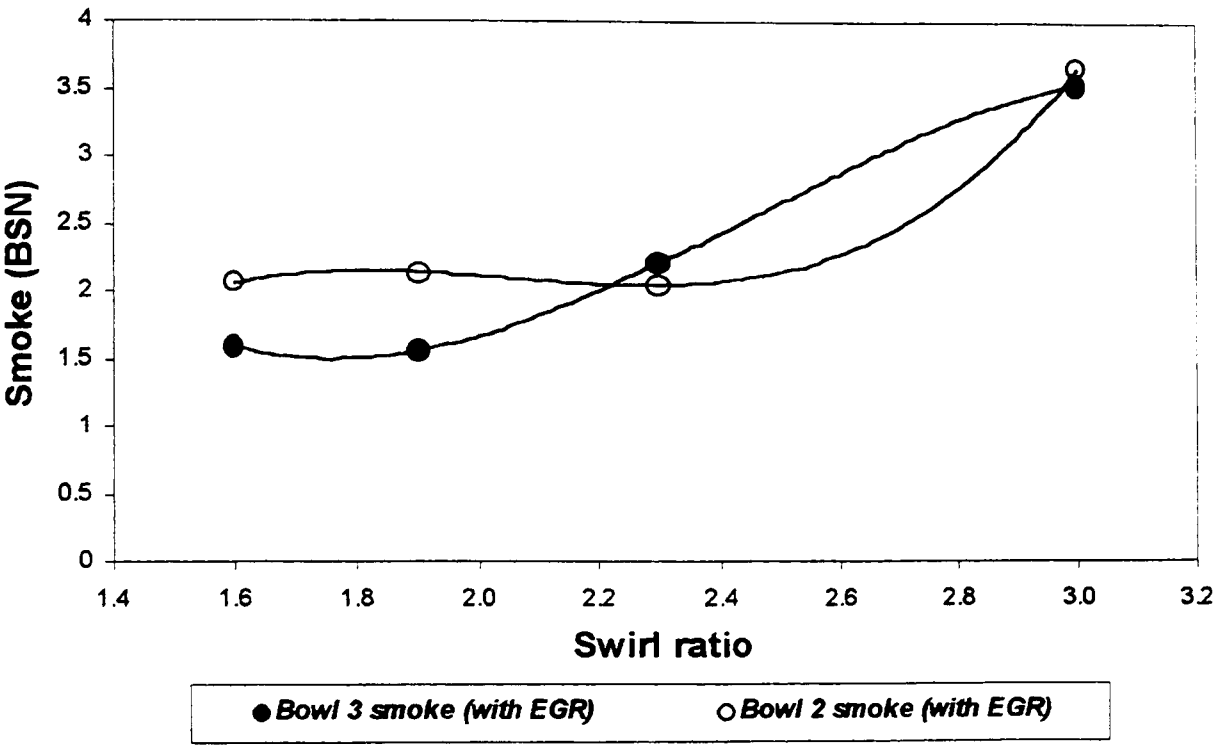

Figure 8.11 Comparison between the emission of smoke for bowls TWO and THREE, at test mode 10 (2300 rpm, 83.7 Nm, SOI 2 degrees BTDC) with 30% EGR.

Typically, bowl shape TWO could tolerate a higher swirl ratio, before the production of excessive smoke (see figure 8.11). Although there were no benefits of using higher swirl ratios when testing bowl shape TWO at high engine speeds, a higher fixed swirl could be used to benefit low speed emissions if no variable emission system was available.

8.5 Conclusions

Testing of two piston bowl shapes of different aspect ratio (and therefore different in-bowl swirl levels), at different engine test conditions, indicated that an optimum swirl ratio existed at each engine operating condition.

The effect of swirl on the production of NOx was small when operating with significant quantities of EGR. However, at low engine speeds, the benefit of swirl to reduce the production of smoke (especially when using EGR) was evident.

At higher engine speeds, piston bowl shape THREE may have benefited from a reduction in the intake generated swirl level, to increase the engine volumetric efficiency. This was because the cylinder head had been designed to operate without a variable swirl system, and a compromise between high and low speed emission performance was desired. Throttling of the intake charge when using the port deactivation system (and associated reduction in volumetric efficiency), often negated possible benefits from an increase in swirl, by decreasing considerably the in-cylinder air/fuel ratio.

The reduction in volumetric efficiency that accompanied the increase in swirl, may have made the results obtained from the swirl tests unrepresentative of the underlying trends. It is likely, that in an alternative swirl-enhancing mechanism, which did not compromise engine volumetric efficiency significantly, would have produced different and more favourable results.

Chapter 9:

Conclusions and recommendations for future work

Chapter 9: Conclusions and recommendations for future work

9.1 Conclusions

9.1.1 Injector optimisation and the effect of fuel impingement

Changes to the position of the spray origin, and spray included-angle were made by varying the injector depth and cone angle respectively. Each injector combination was tested at various full-load and part-load conditions. Full-load tests showed the greatest variation in combustion and emissions performance, because of the premium on air availability and more demanding air/fuel mixing required at high-load test conditions.

The results showed that the point of fuel impingement on the piston bowl walls was the determining factor in the production of NOx and smoke, rather than the path of fuel injection. Ignition delay and pre-mixed combustion were un-affected by changes in the point of fuel impingement, because of the dependence of ignition delay on chemical reaction kinetics, rather than mixing. However, the point of fuel impingement had a profound effect on the processes of diffusion burning and late heat release.

The rate of mixing and heat release increased when the point of impingement promoted spray brake-up and entrainment of air. Over penetration of fuel onto the piston crown top at high points of impingement, and wall wetting of the lower bowl surface at low points of impingement, seem likely to have been responsible for an increase in the proportion of late heat release. This also resulted in an increase in the emission of smoke.

Injector optimisation tests highlighted the poor air-utilisation capability of piston bowl shape TWO, which was the focus of CFD combustion simulation.

9.1.2 Benefits of CFD combustion simulation

CFD combustion simulation supported the results obtained from injector optimisation testing. In particular, it provided further evidence of the importance of the point of fuel impingement in, largely, determining the emission of smoke from piston bowl shape TWO. However, in addition to this, the CFD work provided a valuable insight into the likely airflow structure within the piston bowl.

Results of the liquid fuel envelope and iso-soot surfaces, indicated that for minimum emission of soot, fuel impingement should be positioned to cause wide dispersion of the fuel spray upon impact, high up in the combustion chamber. This promoted fast mixing between injected fuel and airflow induced by swirl and squish, causing rapid oxidation of soot rich regions within the piston bowl. The different combustion airflow structure generated from the optimum point of impingement, caused soot rich regions to be driven out from the bowl into the main combustion chamber.

9.1.3 Overall comparison of piston bowl shapes

Piston bowl shapes were tested by performing EGR loops at even modes of the 14-mode simulated drive cycle test. This encompassed a wide range of engine speeds and loads, and provided a suitable basis upon which to compare the emissions performance of each piston bowl shape.

Significant differences in the trend of particulates and NOx existed between different mode tests. This was principally due to differences in the engine load and speed, affecting the in-cylinder air/fuel ratio and combustion gas temperature. However, injection timing was also significant, particularily at the most retarded test conditions where an increase in the level of EGR probably caused the start of combustion to advance, raising the peak cylinder temperature.

The emissions performance changed significantly between piston bowl designs, both in terms of minimum particulates and NOx emissions, and the sensitivity of each bowl

shape to the level of EGR. Differences between bowl shapes were attributed to changes in the bulk-airflow, caused by different bowl aspect ratios, changes to the pip shape, and detail changes such as the shape of the bowl lip.

Piston bowl shape STD produced the minimum emission of particulates versus NOx trade-off, closely followed by bowl shape ONE. The worst performing bowl was bowl shape TWO, which was identified from injector optimisation testing as being due to the poor air utilisation of this bowl. Bowl shape THREE confirmed the influence of the point of impingement on combustion, but did not result in a reduction of emissions due to adverse changes in the bulk-airflow.

9.1.4 Effect of in-cylinder swirl ratio on combustion and emissions

Two piston bowl shapes (bowls TWO and THREE), having different aspect ratios (and thus in-bowl swirl levels) were tested at selected drive-cycle test conditions, with and without EGR. The results showed that a different level of intake-induced swirl was required for minimum emissions at each test condition, and the optimum swirl ratio at any particular test condition was higher for the wider aspect ratio bowl. This was due to a reduction in swirl amplification during compression from bowl shape TWO.

An increase in the rate of heat release was observed when the swirl level was increased at the low speed test conditions. This resulted in an increase in the emission of NOx, although the addition of EGR reduced the effect of intake-generated swirl. Higher swirl considerably reduced the level of smoke at low-speed test conditions, especially when operating with EGR. On balance, an increase in the level of intake generated swirl was beneficial at low engine speeds.

Engine volumetric efficiency was significantly reduced when swirl was increased at high engine speeds, due to throttling of the intake system. This negated any benefit from an increase in swirl, causing the air/fuel ratio to decrease, and promoting smoke formation.

9.2 Recommendations for future work

Considerable progress was made towards understanding the effect of the point of fuel impingement, and the effect of swirl, on combustion and emissions. However, more work needs to be done to determine the interaction of global airflow within the piston bowl, and the impacted fuel spray. Ultimately, it might then be possible to design an optimum piston bowl shape for each new engine design or advancement (such as for the introduction of a common rail fuel injection system) from fundamental knowledge.

9.2.1 Experimental method and test conditions

The test conditions chosen allowed direct comparison between piston bowl shapes at a variety of engine speeds and loads, representative of the European drive cycle test. However, optimisation of injection timing for each piston bowl shape, at each test condition may have improved the emissions performance of some bowls. An injection timing sweep would also be useful to asses the sensitivity of emissions to injection timing, particularly in the case of particulate and NOx emissions.

The quantity of EGR was determined during experimentation by the reduction in the mass flow rate of intake air. This provided a repeatable parameter to ensure the amount of fresh air in the cylinder, at any given level of EGR, could be controlled. However, changes in exhaust gas temperature between different tests reduced the density of EGR, and thus the mass of EGR in the intake charge. Comparison between EGR loops at different test conditions could be improved by measuring the amount of EGR as a mass fraction of the intake charge. This would make comparison of the level of EGR between different test conditions more meaningful. This would also facilitate comparison of the results with those of other researchers who happened to quote EGR fraction on a mass basis.

9.2.2 Extension of CFD combustion simulation

The CFD combustion simulation of piston bowl shape TWO provided a unique insight into the airflow, initial combustion, and formation of emissions. It also confirmed the knowledge which had been gained from injector optimisation testing.

It would be very beneficial to extend simulation of combustion to piston bowl shapes STD and THREE, which shared similar basic dimensions but differed significantly in the emission of particulates and NOx. The simulation might identify subtle differences in the shape of the piston bowl (for example, sharp radii at the bowl lip), which resulted in major differences in airflow and emissions formation.

9.2.3 Comparison of piston bowl shapes

It was difficult to attribute differences in the emissions performance of each piston bowl shape to key factors in the bowl design, because of the widely different bowl shapes tested. It may be more beneficial to perform a parametric study on the best performing bowl shape (bowl STD), on one area of piston bowl design of interest, such as the depth of impingement area, or angle of impingement area relative to the incoming spray. However, it would be difficult to change one parameter without adversely affecting another. The piston pip, in a region of low airflow velocity and mixing is probably the best region to use for volume compensation, if the compression ratio is to be maintained constant.

Another area which would benefit from further work would be to understand why the excellent full-load performance of piston bowl shape ONE (the best of all bowl shapes tested), was not realised in the part-load EGR conditions from the drive-cycle test. It may be that an injection timing sweep would identify the optimum start of combustion position, which had previously been too advanced because of improved mixing and combustion.

As highlighted previously (section 9.2.1), it might be beneficial to repeat all the bowl comparison tests, having first re-optimised the injection timing at each mode test. This may change the relative performance of different bowl shapes, and would indicate the sensitivity of different bowl design to injection timing at the light-load EGR points of the 14-mode test.

9.2.4 Extension of variable swirl experimentation

Testing at different swirl levels indicated that the emissions performance could be improved at low speed conditions, but throttling of the intake charge at high-speed conditions caused an increase in the emission of smoke. It would be of significant interest to maintain the inlet air mass flow rate constant, when changing in-cylinder swirl level, especially at high engine speeds. This would identify any benefits from an increase in swirl alone, without the complication of a change in the in-cylinder air/fuel ratio. It may then be possible to develop a system to exploit any benefits from swirl, observed throughout the engine speed range.

If the difficulty of maintaining constant intake air mass flow rate, in an engine intended for production was too great, it may be worth investigating the performance of a reduced swirl cylinder head (to increase volumetric efficiency at high engine speeds). A semi-automatic variable swirl mechanism, such as the system used in this project, could be developed to increase swirl at low engine speeds.

References

Abdelhalim S., 'Internal report' Brunel University, 1998.

Abe S., Igashira T., Sakakibara Y., and Kobayashi F., 'Development of Pilot Injection System Equipped with Piezo-Electric Actuator for Diesel Engine' JSAE Review 15, pp201-208, 1994.

Alcock J. F., and Scott W. M., 'Some more Light on Diesel Combustion' Proc. Instn. Mech. Engrs. No.5. 1962-63.

Amann C. A., and Siegla D. C., 'Diesel Particulates – What They Are and Why' Aerosol Sci. Technol., vol.1, pp. 73-103, 1982.

Aorld M. L., Espey C., Litzinger T. A., Santavicca D. A., and Santoro R. J., 'A Study of Non-Swirling and Swirling and their Effects on Spray Flow Fields and Combustion in an Optically-Accessible, D.I. Diesel Engine' SAE Paper 900396, 1990.

Arcoumanis C., Bicen A. F., and Whitelaw J. H., 'Effect of Inlet Parameters on the Flow Characteristics in a Four-Stroke Model Engine' SAE Paper 820750, 1982.

Arcoumanis C., and Chang J-C., 'Spray / Wall Interaction and Implications for Heat Transfer' Seminar of Combustion Engines Group, 14/15 April, Inst. Mech. Engrs., 1992.

Arcoumanis C., and Cutter P. A., 'Flow and Heat Transfer Characteristics of Impinging Diesel Sprays Under Cross-Flow Conditions' SAE Paper 950448, 1995.

Arcoumanis C., Whitelaw J. H., Hentschel W., and Schindler K-P., 'Flow and Combustion in a Transparent 1.9 Litre Direct Injection Diesel Engine' Proc. Instn. Mech. Engrs., Vol. 208, 1994.

Asanuma T., and Obokata T., 'Gas Velocity Measurements of a Motored and Firing Engine by Laser Anemometry' SAE Paper 790096, SAE Trans., vol. 88, 1979.

Belardini P., Bertoli C., Corcione F. E., Police G., and Valentino G., 'The Role of Mean Motion and Turbulence Structure on Gaseous and Particulate Emissions of D.I. Diesel Combustion System' SAE Paper 890839, 1989.

Bertodo R., Brear F., Middlemiss I. D., and Cowling S. J., 'A Method of Direct-Injection Diesel Emmisions Control' Inst. Mech. Engrs., C86/75, 1975.

Bertodo R., Downes T. W. E., Middlemiss I. D., and Brear F., 'Development of the Perkins "Squish Lip" Combustion System' NATO-CCMS 2nd SYMP. On Low Pollution Power, Systems Development, Neuemesse, Dusseldorf, November 1974.

Bopp S., Vafidis C., and Whitelaw J. H., 'The Effect of Engine Speed on the TDC Flowfield in a Motored Reciprocating Engine' SAE Paper 860023, 1986.

Borgnakke C., Davis G. C., and Tabaczynski R. J., 'Predictions of In-Cylinder Swirl Velocity and Turbulence Intensity for an Open Chamber Cup in Piston Engine' SAE Paper 810224, 1981.

Bosch R., 'Internal publication', 1996

Chikahisa T., Konno M., Murayama T., and Kumagai T., 'Analysis of NO Formation Characteristics and its Control Concepts in Diesel Engines from NO reaction Kinetics' JSAE Review 15, pp297-303, 1994.

Dent J. C., and Suliamam S. J., 'Convective and Radiative Heat Transfer in a High Swirl Direct Injection Diesel Engine' SAE Paper 770407, 1977.

Fansler T. D., 'Turbulence Production and Relaxation in Bowl-in-Piston Engines' SAE Paper 930479, 1993.

Ferguson C. R., 'Internal Combustion Engines' Wiley, New York, 1986.

Fitzgeorge D., and Allison J. L., 'Air Swirl in a Road-Vehicle Diesel Engine' Proc. Instn. Mech. Engrs. No.4, 1962-63.

Ford, 'Lynx Upgrade series'0' engine assembly book' 1997.

Fosbery R. A. C., and Gee D. E, 'Some experiments on the measurement of exhaust emissions from diesel engines' MIRA Report 5, 1961.

Fujimoto H., Senda J., Nagae M., and Hashimoto A., 'Characteristics of a Diesel Spray Impinging on a Flat Plate' International Symposium COMODIA 90, pp193-198, 1990.

Gosman A. D., 'Multidimensional Modelling of Cold Flows and Turbulence in Reciprocating Engines' SAE Paper 850344, 1985.

Greeves G., Khan I. M., Wang C. H. T., and Fenne I., 'Origins of Hydrocarbon Emissions from Diesel Engines' SAE Paper 770259, SAE Trans., vol. 86, 1977.

Hawley J. G., Brace C. J., Wallace F. J., and Horrocks R. W., 'Combustion-Related Emissions in CI Engines' Handbook of Air Pollution from Internal Combustion Engines : Pollutant Formation and Control, Academic Press, 1998.

Hentschel W., 'Modern Tools for Diesel Engine Combustion Investigation' Twenty-sixth symposium (International) on Combustion, Naples, Italy, paper no. 107/8, 1996.

Herzog P. L., 'HSDI Diesel Engine Development towards Euro 4' Inst. Mech. Engrs. Seminar publication "Future Engine and System technologies", 1998.

Heywood J. B., 'Fluid Motion Within the Cylinder of Internal Combustion Engines – The 1986 Freeman Scholar Lecture' Journal of Fluids Engineering, Vol. 109/3, March 1987.

Heywood J. B., 'Internal Combustion Engine Fundamentals' McGraw-Hill, New York, 1988.

Heywood J. B., Fay J. A., and Keck J. C., 'Experimental and Theoretical Investigation of Nitric Oxide Formation in Internal Combustion Engines' Comb. Sci. Tech., vol.1, pp313-326, 1970.

Hillard J. C., and Wheeler R. W., 'Nitrogen dioxide in Engine Exhaust' SAE Paper 790691, SAE Trans., vol. 88, 1979.

Hiroyasu H., and Nishida K., 'Fuel Spray Trajectory and Dispersion in a D.I. Diesel Combustion Chamber' SAE Paper 890462, 1989.

Hiroyasu H., Nishida K., Arai M., and Yoshikawa S., 'A Visual Study of D.I. Diesel Combustion from the Under and Lateral Sides of an Engine' SAE Paper 861182, 1986.

Hiroyasu H., Nishida K., and Min J. C., 'Computed Tomographic Study on Internal Structure of a Diesel Spray Impinging on a Flat Wall' International Symposium COMODIA 90, pp193-198, 1990.

Ikegami M., Shioji M., and Nishimoto K., 'Turbulence Intensity and Spatial Integral Scale During Compression and Expansion Strokes in a Four-Cycle Reciprocating Engine' SAE Paper 870372, 1987.

Ishida S., Kihara R., and Furubayashi M., 'Development Status of a Small, Direct-Injection Diesel Engine at Isuzu' SAE Paper 850068, 1985.

Kamimoto T., Takahashi H., Kobayashi H., and Matsuoka S., 'Convective Heat Transfer of an Impinging Diesel Flame in a Rapid Compression Machine' SAE Paper 821035, 1982.

Kamimoto T., and Won Y-H., 'Soot Formation and Related Techniques for its Reduction in Diesel Engines' 2nd Int. Conf. Fluid Mechanics, Combustion and Reliability in Reciprocating Engines, 1992.

Katsura N., Saito M., Senda J., and Fujimoto H., 'Characteristics of a Diesel Spray Impinging on a Flat Wall' SAE Paper 890264, 1989.

Kawamura H., Kihara R., and Kinbara M., 'Isuzu's New 3.27L Small Direct Injection Diesel' SAE Paper 820032, 1982.

Khan I. M., Wang C. H. T., and Langridge B. E., 'Effect of Air Swirl on Smoke and Gaseous Emissions from Direct-Injection Diesel Engines' SAE Paper 720102, 1972.

Kistler, Piezo-instrumentation manual, 1995.

Kistler, Piezo-instrumentation manual, 1997.

Kuo T.-W., Wu K.-J., and Henningsen S., 'Effects of Fuel over Penetration and Overmixing During Ignition–Delay Period on Hydrocarbon Emissions from a Small Open-Chamber Diesel Engine' 11th Annual Energy-sources Technology Conference, Louisiana, American Soc. of Mech. Engrs. 10-13th,1988.

Kuo T., Yu R. C., and Shahed S. M., 'A numerical study of the Transient Evaporating Spray Mixing Process in the Diesel Environment' SAE Trans., vol. 92, 1983.

Ladommatos N., Balian R. A., and Stone R., 'Analysis of Swirl in Unsteady Flow and its Effect on Diesel Combustion' SAE Paper 921643, 1992.

Ladommatos N., Abdelhalim S., Zhao H., and Hu Z., 'The Dilution, Chemical and Thermal Effects of Exhaust Gas Recirculation on Diesel Engine Emissions – Part 1: Effect of Reducing Inlet Charge Oxygen' SAE Paper 961165, 1996(c).

Ladommatos N., Balin R. A., and Horrocks R., 'Investigation of the Benefits of Controlling the Start of Combustion in a Direct Injection Diesel Engine using an Optical Sensor' Proc. Instn. Mech. Engrs. Vol 208, 1994.

Ladommatos N., Balin R., Horrocks R., and Cooper L., 'The Effect of Exhaust Gas Recirculation on Combustion and NOx Emissions in a High-Speed Direct-Injection Diesel Engine' SAE Paper 960840, 1996(a).

Ladommatos N., Balin R., Horrocks R., and Cooper L., 'The Effect of Exhaust Gas Recirculation on Soot Formation in a High-Speed Direct-Injection Diesel Engine' SAE Paper 960841, 1996(b).

Lancaster D. R., 'Effects of Engine Variables on Turbulence in a Spark Ignition Engine' SAE Paper 760159, 1976.

Lida N., 'Surrounding Gas Effects on Soot Formation and Extinction – Observation of Diesel Spray Combustion Using a Rapid Compression Machine' SAE Paper 930603, 1993.

Liou T-M., Hall M., Santavicca D. A., and Bracco F. V., 'Laser doppler velocimetry measurements in valved and ported engines' SAE Paper 840375, 1984.

Maly R. R., 'Progress in Combustion Research' Inst. Mech. Engrs. Combustion Engines Group Prestige Lecture, October 1998.

Matsui Y., and Sugihara K., 'Sources of Hydrocarbon Emissions from a Small Direct Injection Diesel Engine' JSAE Review Vol.7, No.3, October 1986.

McKinley T. L., Primus J. R., O'Rourke P. J., and Butler T. D., 'Comparison of Computed and Measured Air Motion on Circular and Square Piston Cups' SAE Paper 881612, 1988.

Merryman E. L., and Levy A., 'Nitrogen Oxide Formation in Flames: The roles of NO_2 and Fuel Nitrogen' Proceedings of Fifteenth International Symposium on Combustion, pp1073, The Combustion Institute, 1975.

Middlemiss I. D., 'Characteristics of the Perkins 'Squish Lip' Direct Injection Combustion System' SAE Paper 780113, 1978.

Minami T., Takeuchi K., and Shimazaki N., 'Reduction of Diesel Engine NOx using Pilot Injection' SAE Paper 950611, 1995.

Monaghan M. L., and Pettifer H. F., 'Air Motion and its Effect on Diesel Performance and Emissions' SAE Paper 810255, 1981.

Morel T., and Keribar R., 'A Model for Predicting Spatially and Time Resolved Convective Heat Transfer in Bowl-in-Piston Combustion Chambers' SAE Paper 850204, 1985.

Naber J. D., and Reitz R. D., 'Modelling Engine Spray/Wall Impingement' SAE Paper 880107, 1988.

Naohito K., Saito M., Senda J., and Fujimoto H., 'Characteristics of a Diesel Spray Impinging on a Flat Wall' SAE Paper 890264, 1989.

Neitz A., and D'Alfonso N., 'The M.A.N. Combustion System with Controlled Direct Injection for Passenger Car Diesel Engines' SAE Paper 810479, 1981.

Nishida K., and Hiroyasu H., 'Simplified Three-Dimensional Modelling of Mixture Formation and Combustion in a D.I. Diesel Engine' SAE Paper 890269, 1989.

Ogasawara M., Takagi T., and Fujii K., 'Fundamental Studies on NO and CO Emissions and Their control in Combustion Systems' (2^{nd} Report, Numerical Study on Various Factors Affecting NO Formation and Effectiveness of Emissions Control Systems), Trans. of JSME, vol. 39, No. 327, pp3427-3433, 1973.

Okajima S., and Kumagai S., 'Experimental Investigation of Soot Formation and NOx Reduction by Impinging Spray in a Closed Vessel' Twenty–Third Symposium (International) on Combustion / The combustion Institute, 1990.

Packer J. P., Wallace F. J., Adler D., and Karimi E. R., 'Diesel fuel jet mixing under high swirl conditions' Inst. Mech. Engrs., C80/83, 1983.

Packer J. P., Wallace F. J., Idoum A., and Charlton S. J., 'An Experimental and Analytical Study of Jet Impingement and Wall Jets in High Swirl D.I. Diesel Engines using the Hydraulic Analogy' SAE Paper 850263, 1985.

Plee S. L., and Ahmad T., 'Relative roles of Premixed and Diffusion Burning in Diesel Combustion' SAE Paper 831733, SAE Trans., vol.92, 1983.

Rao K. K., Winterbone D. E., and Clough E., 'Influence of Swirl on High Pressure Injection in Hydra D.I. Diesel Engine' Inst. Mech. Engrs., 1992(a).

Rao K. K., Winterbone D. E., and Clough E., 'Laser Illuminated Photographic Studies of the Spray and Combustion Phenomena in a small High Speed D.I. Diesel Engine' SAE Paper 922203, 1992 (b).

Reynolds W. C., 'Modelling of Fluid Motions in Engines – An Introductory Overview' Combustion Modelling in Reciprocating Engines, Plenum Press, 1980.

Ricardo H. R., and Hempson J. G. G. 'The High-Speed Internal Combustion Engine' Inst. Mech. Engrs., 5th ed., 1968.

Ricado H. R., 'Engine Air Motion Studies' Advertising Brochure.

Saito T., Daisho Y., Uchida N., and Ikeya N., 'Effects of Combustion Chamber Geometry on Diesel Combustion' SAE Paper 861186, 1986.

Schapertons H., and Thiele F., 'Three Dimensional Computations for Flowfields in D.I. Piston Bowls' SAE Paper 860463, 1986.

Schenck C., 'Instruction manual' eddy-current dynamometer, type W130, 1983.

Shigemori M., Tsuruoka S., and Shimoda M., 'Development of a System for a Light Duty D.I. Diesel Engine' SAE Paper 831296, 1983.

Shimada T., Sakai K., and Kurihara S., 'Variable Swirl Inlet System and its Effect on Diesel Performance and Emissions' SAE Paper 861185, 1986.

Shimoda M., Shigemori M., and Tsuruoka S., 'Effect of Combustion Chamber Configuration on In-Cylinder Air Motion and Combustion Characteristics of D.I. Diesel Engines' SAE Paper 850070, 1985.

Spicher U., and Dresen-Rausch J., 'Investigation of Ignition and Flame Propagation in a Direct Injection Diesel Engine by Optical Fiber Diagnostics' American Soc. Mech. Engrs., 13th Annual Energy-sources Technology Conference, Louisiana, Jan 14-18th, 1990.

Spicher U., Velji A., Huynh N. H., and Kruse F., 'An Experimental Study of Combustion and Fluid Flow in Diesel Engines' SAE Paper 872060, 1987.

Stone R., 'Introduction to Internal Combustion Engines' 2nd ed, Macmillan, London, 1992.

Stone R., and Ladommatos N., 'The Measurement and Analysis of Swirl in Steady Flow' SAE Paper 921642, 1992.

Suzuki T., 'Development and Perspective of the Diesel Combustion System for Commercial Vehicles' Inst. Mech. Engrs., Prestige Lecture, 22nd May 1997.

Suzuki M., Nishida K., and Hiroyasu H., 'Simultaneous Concentration Measurement of Vapor and Liquid in an Evaporating Diesel Spray' SAE Paper 930863, 1993.

Taylor C. F., 'The Internal Combustion Engine in Theory and Practice, Volume 2: Combustion, Fuels, Materials, Design' MIT Press, London, 1968.

Tindal M. J., Brown P. G., and Kyriakides S. C., 'An Investigation of Swirl and Turbulence in the Cylinders of Direct Injection Diesel Engines' Inst. Mech. Engrs., C127/82, 1982.

Ueda T., Enomoto T., and Kanetsuki M., 'Heat Transfer Characteristics and Dynamic Behaviour of Saturated Droplets Impinging on a Heated Vertical Surface' Bulletin of the JSME, Vol. 22, No. 167, May 1979.

Van Gerpen J. H., Huang C., and Borman G. L., 'The Effects of Swirl and Injection Parameters on Diesel Combustion and Heat Transfer' SAE Paper 850265, 1985.

Vioculescu I. A., and Borman G. L., 'An Experimental Study of Diesel Engine Cylinder Averaged NOx Histories' SAE Paper 780228, SAE Trans., vol. 87, 1978.

Wakuri Y., Takasaki K., and Yang Y., 'Studies on the Fuel-Spray Combustion Characteristic in a Diesel Engine by the aid of Photographic Visualization' Proceedings of the 18th International Congress on Combustion Engines, D18, 157, 1989.

Wang Y., Shu G., Yang C., Ju Y., and Zhao K., 'Combustion Process of Diesel Spray in High Temperature Air' SAE Paper 950856, 1995.

Werlberger P., and Cartellieri W. P., 'Fuel Injection and Combustion Phenomena in a High Speed D.I. Diesel Engine Observed by Means of Endoscopic High Speed Photography' SAE Paper 870097, 1987.

Winterbone D. E., Sun J., and Yates D. A., 'A Study of Diesel Flame Movement by Using the Cross Correlation Method' SAE Paper 930979, 1993.

Wojik K., 'Improvement of combustion Systems of High Speed Diesel Engines with respect to Pollution' American Soc. Mech. Engrs., 13th Annual Energy-sources Technology Conference, Louisiana, January 14-18th, 1990.

Yoshikawa S., Furusawa R., Arai M., and Hiroyasu H., 'Optimizing Spray Behaviour to Improve Engine Performance and to Reduce Exhaust Emissions in Small D.I. Diesel Engine' SAE Paper 890463, 1989.

Yu R. C., Wong V. W., and Shahed S. M., 'Sources of Hydrocarbon Emissions from Direct Injection Diesel Engines' SAE Paper 800048, 1980.

Yu R. C., and Shahed S. M., 'Effects of Injection Timing and Exhaust Gas Recirculation on Emissions from a D.I. Diesel Engine' SAE Paper 811234, SAE Trans., vol. 90, 1981.

Zhang L., Minami T., Takatsuki T., and Yokota K., 'An Analysis of the Combustion of a D.I. Diesel Engine by Photograph Processing' SAE Paper 930594, 1993.

Zhao H., Lowry G., and Ladommatos N., 'Time-Resolved Measurements and Analysis of In-cylinder Gases and Particulates in Compression-Ignition Engines' SAE Paper 961168, 1996.

Zolver M., Griard C., and Herriot S., '3D Modelling Applied to the Development of a DI Diesel Engine: Effect of Piston Bowl Shape' SAE Paper 971599, 1997.

Appendix 'A'

Appendix 'A': Engine specification

Base engine data

Number of cylinders	4
Block material	Cast iron
Cylinder bore	82.50 mm
Crankshaft stroke	85.00 mm
Compression ratio	19.6:1
Maximum cylinder pressure	140 Bar
Piston design	Central bowl in piston
Piston material	Aluminium alloy
Nominal bowl volume	17.18 cc
Oil temperature	110 degrees C
Oil type	15W40
Water temperature	90 degrees C

Cylinder head data

Cylinder head material		Aluminium alloy
Valves per cylinder		4
Valve timing:	inlet opens	9 degrees BTDC
	inlet closes	37 degrees ABDC
	exhaust opens	49 degrees BBDC
	exhaust closes	9 degrees ATDC

Fuel injection system data

Fuel injection pump	Bosch VP30 PSG 5 PCU
Recommended fuel supply pressure	20 kPa
Recommended fuel inlet temperature	35 degrees C
Fuel injectors	Bosch 17mm Minisac, 2 spring
1st nozzle opening pressure	200 Bar
2nd nozzle opening pressure	360 Bar

1st lift	0.02 mm
2nd lift	0.35mm
Number of holes	6
Nominal hole diameter	0.152mm

Appendix 'B'

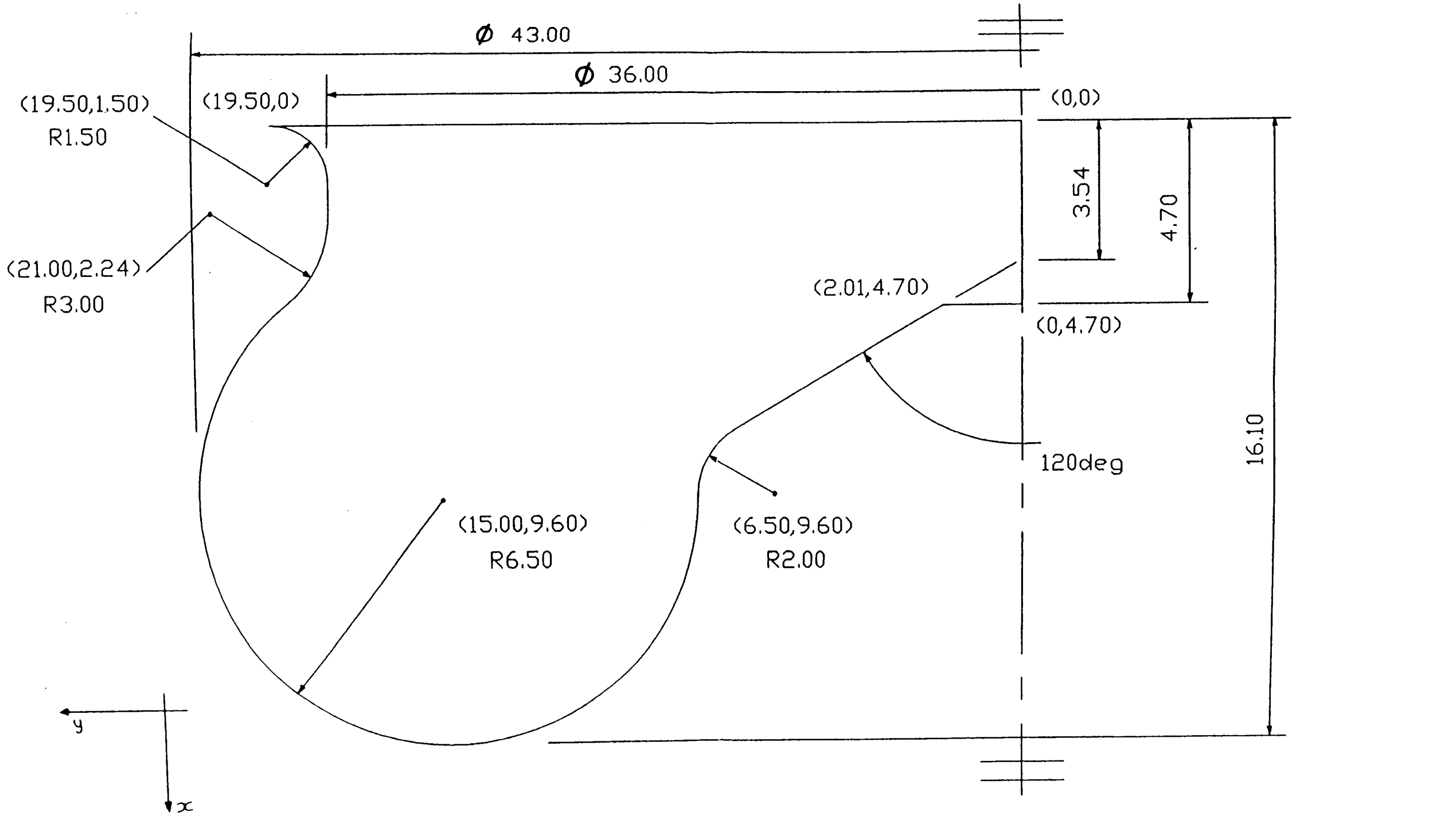

FINISH	TOLERANCE	MATERIAL	PROJECTION		SCALE	ALL DIMENSIONS IN mm	
AS CAST/MACHINED OR ✓ WHERE STATED	DIMENSIONAL +/- 0.1mm ANGULAR +/- 1deg UNLESS OTHERWISE STATED	ALUMINIUM ALLOY AS SUPPLIED		DRAWN MRE DATE 06/09/97 CHECKED DATE	NTS	LYNX UPGRADE PISTON 1	DRG NO. 2

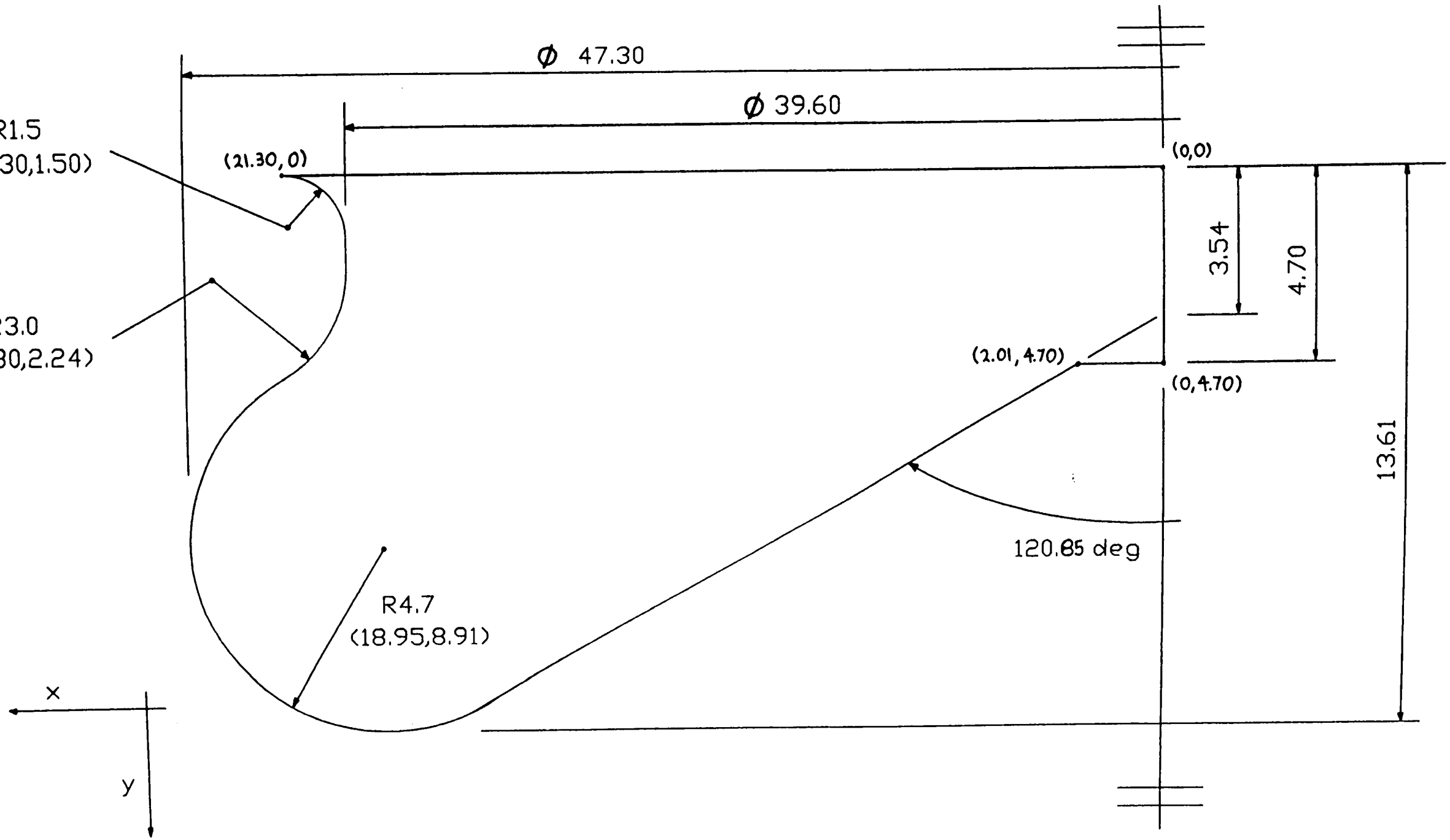

FINISH AS CAST/MACHINED OR 0.4 WHERE STATED	TOLERANCE DIMENSIONAL +/-0.05mm ANGULAR +/-0.1deg UNLESS OTHERWISE STATED	MATERIAL ALUMINIUM ALLOY AS SUPPLIED	PROJECTION	DRAWN MRE DATE 21/04/98 CHECKED DATE	SCALE NTS	ALL DIMENSIONS IN mm LYNX UPGRADE PISTON SHAPE 2 / DRG NO. 1

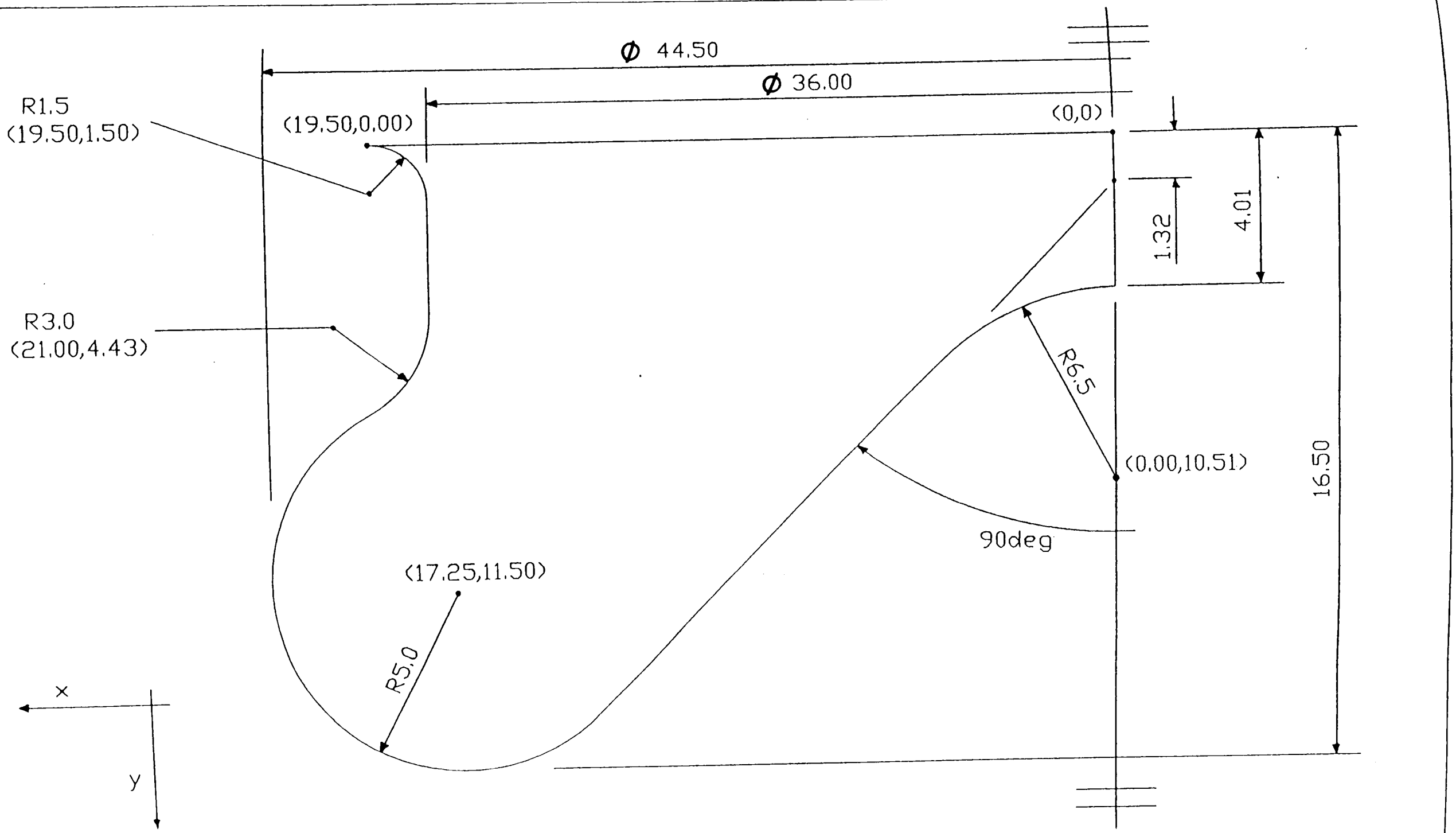

FINISH AS CAST/MACHINED OR ~~9~~ √ WHERE STATED	TOLERANCE DIMENSIONAL +/- 0.05mm ANGULAR +/- 0.1deg UNLESS OTHERWISE STATED	MATERIAL ALUMINIUM ALLOY AS SUPPLIED	PROJECTION	DRAWN MRE DATE 21/12/98 CHECKED DATE	SCALE NTS	ALL DIMENSIONS IN mm LYNX UPGRADE PISTON SHAPE 3	DRG NO. 1

Appendix 'C'

Appendix 'C': Power correction factor

Engine power was corrected to standard temperature and pressure according to the EEC directive 88/195. The power correction factor, α_d, was the coefficient used to determine what the engine power would have been under the standard atmospheric conditions, listed below:

Standard temperature, $T_0 = 298$ K (25 degrees C)

Standard dry pressure, $P_{s0} = 99$ kPa (dry pressure is based on a total pressure of 100 kPa and a water pressure of 1 kPa)

Corrected power was given by $P_0 = \alpha_d P$

where P was the measured power.

For the above equation to be valid, atmospheric conditions at the time of the experiment must have been between 283 K $\leq$ T $\leq$ 313 K, and 80 kPa $\leq$ P_s $\leq$ 110 kPa for compression ignition engines.

The power correction factor, α_d, for compression ignition engines at a constant fuel rate was given by:

$$\alpha_d = (f_a)^{f_m}$$

where f_a = atmospheric factor, and f_m = characteristic parameter for each engine type and adjustment.

For turbo-charged engines, f_a is given by:

$$f_a = \left(\frac{99}{P_s}\right)^{0.7} \left(\frac{T}{298}\right)^{1.5}$$

where P_s and T are measured atmospheric pressure and temperature respectively, and f_m is a function of q_c (corrected fuel flow):

$$f_m = 0.036 \times q_c - 1.14$$

where q_c = q/r, valid between 40 mg/litre/cycle to 65 mg/litre/cycle,

q = fuel flow (mg/cycle/litre swept volume),

r = pressure ratio of compressor outlet to compressor inlet.

Appendix 'D'

Appendix D: Matrix of NOx and smoke emissions from injector optimisation of piston bowl shapes

Piston bowl shape STD

Results of NOx and smoke emissions from the standard bowl injector configuration are shown for comparison in table D1.

NOx(ppm)/BSN	Test 1 1500rpm, full-load	Test 2 2000rpm, full-load	Test 3 4000rpm, full-load	Test 4 1800rpm, part-load	Test 5 3200rpm, part-load
4.0mm, 145degrees	842/2.65	906/2.54	923/1.81	51/0.05	209/2.99

Table D1 NOx and smoke emissions from the standard injector configuration.

Piston bowl shape ONE

Results of NOx and smoke emissions, from varying injector depth only are shown in table D2. Injector cone angle was 145 degrees in all cases.

NOx(ppm)/BSN	Test 1 1500rpm, full-load	Test 2 2000rpm, full-load	Test 3 4000rpm, full-load	Test 4 1800rpm, part-load	Test 5 3200rpm, part-load
2.5mm, Deep	689/5.47	758/1.54	811/1.33	63/0.06	214/1.09
4.0mm, Medium	703/2.52	791/1.04	766/0.96	69/0.03	192/1.38
5.5mm, Shallow	754/2.17	789/1.68	729/2.42	47/0.04	186/2.16

Table D2 Injector depth optimisation results at five engine test conditions.

Piston bowl shape TWO

Results of NOx and smoke emissions, from varying injector depth and cone angle are shown in tables D3 to D7. Each table is a matrix of injector optimisation at one of five engine test conditions.

NOx(ppm)/BSN	140 degrees	145 degrees	150 degrees
2.5mm, Deep	550/9.46	596/9.46	710/9.18
4.0mm, Medium	668/7.03	728/6.75	758/5.38
5.5mm, Shallow	686/8.22	832/3.96	902/2.92

Table D3 Test 1, 1500 rpm, full-load (166.4 Nm), SOI –2 degCA, EGR 0%

NOx(ppm)/BSN	140 degrees	145 degrees	150 degrees
2.5mm, Deep	579/9.48	667/6.99	735/4.87
4.0mm, Medium	706/4.81	804/3.23	932/1.73
5.5mm, Shallow	784/3.44	914/1.71	888/2.30

Table D4 Test 2, 2000 rpm, full-load (214.2 Nm), SOI –3 degCA, EGR 0%

NOx(ppm)/BSN	140 degrees	145 degrees	150 degrees
2.5mm, Deep	574/9.33	861/4.50	908/2.81
4.0mm, Medium	936/1.48	892/2.24	988/1.32
5.5mm, Shallow	924/2.00	887/2.24	874/2.52

Table D5 Test 3, 4000 rpm, full-load (156.5 Nm), SOI –9 degCA, EGR 0%

NOx(ppm)/BSN	140 degrees	145 degrees	150 degrees
2.5mm, Deep	87/0.66	71/0.41	87/0.24
4.0mm, Medium	73/0.39	66/0.18	64/0.09
5.5mm, Shallow	93/0.20	57/0.06	61/0.07

Table D6 Test 4, 1800 rpm, part-load (27.9 Nm), SOI +5 degCA, EGR 30%

NOx(ppm)/BSN	140 degrees	145 degrees	150 degrees
2.5mm, Deep	222/2.91	235/2.12	264/1.89
4.0mm, Medium	161/2.08	232/1.81	242/1.63
5.5mm, Shallow	183/2.42	210/1.87	190/2.29

Table D7 Test 5, 3200 rpm, part-load (69.8 Nm), SOI -6 degCA, EGR 40%

Piston bowl shape THREE

Results of NOx and smoke emissions, from varying injector depth and cone angle are shown in tables D8 to D12. Each table is a matrix of injector optimisation at one of five engine test conditions.

NOx(ppm)/BSN	140 degrees	145 degrees	150 degrees
2.5mm, Deep	757/5.12	771/4.77	850/4.37
4.0mm, Medium	862/3.48	767/5.68	808/6.15
5.5mm, Shallow	832/4.41	883/6.03	915/6.33

Table D8 Test 1, 1500 rpm, full-load (166.4 Nm), SOI –2 degCA, EGR 0%

NOx(ppm)/BSN	140 degrees	145 degrees	150 degrees
2.5mm, Deep	797/3.40	833/4.55	790/4.76
4.0mm, Medium	811/3.98	793/4.94	686/5.53
5.5mm, Shallow	701/4.82	750/5.67	643/6.29

Table D9 Test 2, 2000 rpm, full-load (214.2 Nm), SOI –3 degCA, EGR 0%

NOx(ppm)/BSN	140 degrees	145 degrees	150 degrees
2.5mm, Deep	951/2.02	996/2.47	903/2.87
4.0mm, Medium	992/1.97	1004/2.52	901/2.94
5.5mm, Shallow	918/2.95	846/4.42	852/4.43

Table D10 Test 3, 4000 rpm, full-load (156.5 Nm), SOI –9 degCA, EGR 0%

NOx(ppm)/BSN	140 degrees	145 degrees	150 degrees
2.5mm, Deep	64/0.04	52/0.02	62/0.01
4.0mm, Medium	49/0.03	47/0.04	44/0.06
5.5mm, Shallow	44/0.04	41/0.13	40/0.30

Table D11 Test 4, 1800 rpm, part-load (27.9 Nm), SOI +5 degCA, EGR 30%

NOx(ppm)/BSN	140 degrees	145 degrees	150 degrees
2.5mm, Deep	212/2.12	209/2.14	200/2.41
4.0mm, Medium	195/2.28	167/2.81	172/3.06
5.5mm, Shallow	175/3.19	164/3.90	172/4.23

Table D12 Test 5, 3200 rpm, part-load (69.8 Nm), SOI -6 degCA, EGR 40%

Appendix 'E'

BRUNEL UNIVERSITY (ENGINE LABORATORIES)
DIESEL FUEL ANALYSIS
March 1997

TEST	METHOD	SPECIFICATION	RESULTS
Sample No :			Composite
Appearance	Visual	Report	Slight Hazy
Colour	Visual	Report	Red
Water & Sediment, % (V/V)	Visual	Report	Nil
Flash Point , °C	IP 34	55 min	71
Carbon Residue on 10% Residue, % (m/m)	IP 14	0.30 max	0.20
Ash Content, % (m/m)	IP 4	0.01 max	<0.005
Water Content, (mg/kg)	ASTM D1744	200 max	61
Particulates, (mg/kg)	DIN 51419	24 max	13
Cu Corrosion, 3hr @ 50°C	IP 154	1max	1
Oxidation Stability, (g/m³)	ASTM D2274	25 max	14
Sulphur, % (m/m)	IP 336	0.20 max	0.19
CFPP, °C	IP 309	-15 max Winter -5 max Summer	-11
Density @ 15°C, (kg/m³)	ASTM D4052	820 - 860	853.8
Cetane Number	ASTM D613	49 min	49.1
Cetane Index	ISO 4264	46 min	47.3
Distillation	IP 123		–
Initial Boiling Point °C			169.0
10% Vol Rec @ °C			213.5
50% Vol Rec @ °C			279.0
90% Vol Rec @ °C			343.0
Final Boiling Point °C			371.5
% (V/V) Rec @ 250°C		65 max	30.0
% (V/V) Rec @ 350°C		85 min	92.5
% (V/V) Rec @ 370°C		95 min	97
Carbon % (m/m)	ASTM D5291		86.2
Hydrogen % (m/m)	ASTM D5291		13.4
Aromatics % (V/V)	IP 156		25.1
Olefins % (V/V)	IP 156		2.5
Saturates % (V/V)	IP 156		72.4